Geochemical and mineralogical analysis of Mars analogue materials and the creation of the International Space Analogue Rock Store (ISAR)

Nicolas Bost

UNIVERSITÉ D'ORLÉANS

ÉCOLE DOCTORALE SCIENCES ET TECHNOLOGIES

CENTRE DE BIOPHYSIQUE MOLECULAIRE
INSTITUT DES SCIENCES DE LA TERRE D'ORLEANS

THÈSE présentée par :

Nicolas BOST

Soutenue le : **21 juin 2012**

pour obtenir le grade de : **Docteur de l'université d'Orléans**
Discipline : Géoscience et Environnement

Geochemical and mineralogical analysis of Mars analogue materials and the creation of the International Space Analogue Rock Store (ISAR)

THÈSE dirigée par :
Dr. Frances WESTALL Directrice de recherche, CNRS, CBM, Orléans
Dr. Claire RAMBOZ Chargée de recherche, CNRS, ISTO, Orléans

RAPPORTEURS :
Pr. Hap McSWEEN Distinguished Professor, Univ. de Tennessee (USA)
Pr. Fernando RULL-PEREZ Professeur, Université de Valladolid (Espagne)

JURY :

Pr. Michel FAURE	Professeur, Université d'Orléans, Président
Dr. Frances WESTALL	Directrice de recherche, CNRS, CBM, Orléans
Dr. Claire RAMBOZ	Chargée de recherche, CNRS, ISTO, Orléans
Pr. Hap McSWEEN	Distinguished Professeur, Univ. de Tennessee
Pr. Fernando RULL-PEREZ	Professeur, Université de Valladolid
M. Michel VISO	Responsable de la Thématique Exobiologie, Centre National d'Etudes Spatiales
Dr. Jorge VAGO	ExoMars Project Scientist, Agence Spatiale Européenne

Remerciements

Je souhaite avant toute chose remercier Jean-Claude Beloeil, ancien Directeur du Centre de Biophysique Moléculaire ; Eva Jakab-Toth, actuelle Directrice; Ary Bruand, ancien Directeur de l'Institut des Sciences de la Terre et Bruno Scaillet, actuel Directeur, pour m'avoir permis d'effectuer ce travail de recherche au sein des deux laboratoires dans des conditions optimales.

Je souhaite bien évidement remercier mes deux directrices de thèse, Frances Westall et Claire Ramboz sans qui rien n'aurait été possible. Elles m'ont formé au travail de recherche et transmis leurs connaissances avec passion. Je remercie tout spécialement Frances Westall qui m'a initié à une autre géologie, en m'emmenant à la découverte des roches très anciennes et même d'une autre planète. Je la remercie pour m'avoir « jetée » dans le grand bain de la science en me permettant de participer à de nombreux congrès internationaux où j'ai pu m'exprimer dans un parfait franglais. Enfin, je remercie mes directrices de thèse pour m'avoir laissé une grande autonomie tout au long de ces trois dernières années.

Cette thèse n'aurait pas pu être ce qu'elle est sans le soutien indéfectible de Frédéric Foucher, qui m'a formé à la spectrométrie Raman mais aussi à rédiger de façon claire et précise mes travaux scientifiques.

Je remercie les membres du jury ; Hap McSween et Fernando Rull-Perez qui m'ont fait l'honneur de rapporter mon travail de thèse, Michel Faure, Jorge Vago et Michel Viso qui ont accepté d'examiner ce travail. Je souhaite aussi remercier Michel Viso pour ses remarques et ses conseils qui m'ont permis de mener à bien ce travail de thèse.

Je souhaite bien évidement remercier les membres de l'équipe d'Exobiologie du CBM : Marylène Bertrand, Annie Chabin et André Brack qui m'ont accueilli et m'ont enrichi d'un savoir qui m'a toujours échappé : la chimie !

Je souhaite aussi remercier tous les gens qui m'ont aidé à faire des analyses sur les nombreux instruments que j'ai utilisés, et qui ont participé de près ou de loin à ces travaux de recherche: Fabrice Gaillard, Olivier Rouer, Ida Di Carlo, Phillipe Penhoud, Sabine Petit, Alain Meunier, Claude Fontaine et Iris Fleischer

Je remercie également l'ensemble des accompagnants administratifs et particulièrement Patricia Legland, qui a jonglé avec mes nombreux ordres de mission.

Enfin, je remercie, mes camarades, Damien, Nicolas, Mathieu, Antoine, Mickaël, Anaëlle, pour les bons moments et les bonnes tranches de rire de ces trois dernières années. Je leur suis reconnaissant d'avoir pu mettre en place avec eux l'échelle géologique de Meymac !

Je souhaite remercier Caroline pour son soutien et ses relectures.

Pour terminer, je souhaite évidement remercier ma grand-mère, Jacqueline Clavaud, mes parents, Evelyne et Pierre Bost, qui m'ont toujours soutenu pendant mes études, qui, avec la fin de ce travail de thèse, touchent à leurs fins. Enfin, j'ai une pensée pour tous les êtres chers qui nous ont quittés pendant ces trois dernières années.

Et comme rien ne peut être réalisé sans support financier, je remercie sincèrement le Centre National d'Etudes Spatiales (CNES) et la Région Centre pour leur contribution.

Foreword

The official language for theses in France is French under the French law 94-665 of 4 August 1994 on the use the French language. A letter from the chief of Research and Technology of the 10 April 1995 states: "The awarding of a doctorate to a French national is that it be written and defended in French [...]". Thus, unless otherwise accepted by the University of Orleans, all theses presented to the *Ecole Doctorale Science et Technologie* must be written in French.

This thesis has been written in English because it is tightly related to ongoing and future space missions flown by the European Space Agency (ESA) and the National Aeronautics Space Administration (NASA) and is therefore of high international interest. Thus, in order for the information produced in the course of the thesis project to be available for those working on the Mars missions for which this study was undertaken, this thesis has been written in English with the permission of the University of Orléans. Also, in accordance with the requirements of the University of Orleans, each chapter of this manuscript is followed by a French summary. In addition, all figures have captions in both English and French.

Avant Propos

La langue de rédaction de la thèse est le français. Ceci est l'obligation liée à la loi 94-665 du 4 août 1994 relative à l'emploi de la langue française. Une lettre du directeur général de la Recherche et de la Technologie du 10 avril 1995 précise: « La thèse conduisant à la délivrance d'un diplôme national français, il est de règle qu'elle soit rédigée et soutenue en français [...] ». Donc sauf accord ponctuel des conseils de l'université d'Orléans, les thèses présentées dans le cadre de l'Ecole Doctorale Science et Technologie doivent être rédigées en Français.

Cette thèse est rédigée en Anglais car elle est associée aux futures missions spatiales de l'Agence Spatiale Européenne (ESA) et de la National Aeronautics Space Administration (NASA) dans un contexte international fort. Afin de permettre aux différents acteurs des missions d'utiliser ce travail, cette thèse est rédigée en Anglais avec la permission de l'Université d'Orléans. Conformément aux exigences de l'université d'Orléans, chaque chapitre de ce manuscrit est suivi d'un résumé en français. De plus l'ensemble des figures sont doubles légendées en Anglais et en Français.

Table of Contents

Introduction

Mars has been observed and studied for a long time; the Egyptians observed *Hor-Desher* and the Babylonians venerated *Nirgal*. Since the 1970's, this interest for the red planet was particularly driven by the hope of finding extraterrestrial life. The exploration of the Martian surface and of its geology really began in the second part of the twentieth century with the conquest of space. The first probe to Mars, *Marsnick*, was launched by the Russian Soviet Union (USSR) in 1960 but never arrived. In 1964, the American probe *Mariner 4* was thus the first to observe the surface of Mars. It also measured the atmospheric pressure and it was concluded that liquid water could not exist on the surface of Mars. Since liquid water is essential for life, this finding dashed hopes of discovering Martian organisms. Since then, more than 40 missions have been launched to Mars with only ~50% success. The most important missions dedicated to the search for life and to Martian geology were *Vikings 1* and *2* in 1975, sent by the American National Aeronautics and Space Administration (NASA), the *Mars Exploration Rovers* (MER) with *Spirit* and *Opportunity* that have been in operation since 2003 (NASA), *Mars Express* also in operation since 2004, sent by the European Space Agency (ESA), *Mars Reconaissance Orbiter* in operation since 2006 (NASA), and *Phoenix* in 2008 (NASA). These missions provided extensive information about the composition and temperature of the atmosphere and the composition and mineralogy of outcropping rocks. To date, no evidence of past or present life has been detected and the question of whether life ever arose on the planet is still open. The last NASA mission *Mars Science Laboratory* (MSL), with the rover *Curiosity*, was launched the 26th November 2011. The spacecraft should land on Mars in early August 2012. More details about the Mars exploration by space probes is presented in insert 1. The

different abbreviations concerning the space craft used in this manuscript are also described in insert 1.

The European Space Agency exploration of Mars

In 2001, ESA initiated the *Aurora* programme, a long-term plan for robotic and human exploration of the solar system, in particular of Mars, and for the search for extraterrestrial life. The first step of this exploration is the *ExoMars* mission. *ExoMars* had been redefined several times since the beginning of the project, in particular for financial reasons. In its present version, the mission will be financed jointly by ESA and Roscosmos, the Russian space agency. This 2018 mission to Mars has a number of scientific objectives, which are listed below by order of priority (*European Space Agency, 2010*):

(1) the search for possible biosignatures of past or present life;

(2) the characterisation of water and its geochemical distribution as a function of depth in the shallow subsurface;

(3) the study of the surface environment;

(4) the investigation of the planet's subsurface and deep interior in order to better understand the evolution and habitability of Mars;

(5) the achievement of incremental steps ultimately culminating in a sample return flight.

The first part of the mission will be the launch of the *Trace Gas Orbiter* (TGO) and of the *Descent and Landing Demonstrator Module* (EDL) in 2016 (Fig. 0.1). The TGO objective is to analyse the atmospheric composition, in particular the presence of methane that may possibly be associated with life processes. Methane was detected by *Mumma et al. (2009)*, with observations made from Earth but they have been subject to criticism (e.g. *Lefèvre and Forget, 2009*). This probe will also act as a telecom relay for the 2018 *in situ* mission.

Insert 1: Martian space missions.

More than 40 missions have been launched to explore Mars. After *Viking 1* and *2*, launched by the NASA in 1975, scientists had to wait a long time for new observations of the geology of Mars. In this insert, I list previous missions and instrumentation used to study the Martian geology and the data of which are the basis of this thesis. The missions to Mars consist of two types: orbital and surface missions.

The orbital missions provide global mineralogical information. In 1996, the first probe after *Viking* to be launched to Mars was *Mars Global Surveyor* (MGS). This NASA-Jet Propulsion Laboratory (JPL) orbiter contains the Mars Orbiter Camera (MOC), the Mars Orbiter Laser Altimeter (MOLA) and the Thermal Emission Spectrometer (TES). This mission was essential for obtaining topographic maps of Mars. In 2001, NASA launched the *2001 Mars Odyssey* mission. This orbiter contains a Thermal Emission Imaging System (THEMIS) and a Gamma Ray Spectrometer (GRS). The next mission named *Mars Express* was launched by ESA on the 2nd June 2003. This probe contains a stereoscopic camera (the High Resolution Stereo Camera, HRSC), an infrared spectrometer (the Planetary Fourier Spectrometer, PFS), and an IR-spectro-imager OMEGA (Observatoire pour la Minéralogie, l'Eau, les Glaces et l'Activité). The last orbital mission was the *Mars Reconnaissance Orbiter* (MRO) launched in 2005 by NASA. This orbiter has a High Resolution Imaging Science Experiment (HIRISE), a Mars Color Imager (MARCI) for imaging the surface, and a Compact Reconnaissance Imaging Spectrometer to Mars (CRISM). To date, only *Mars Express* and MRO are still working.

The surface missions include two types of space vehicles: landers and rovers. On the 4th July 1997, the first rover, Sojourner from the *Mars Pathfinder mission* launched by NASA landed on the Martian surface. This small rover explored the landing site Ares Vallis and studied rocks, such as "Yoggi", "Scooby Doo" and "Moe", using cameras and analysed their elemental compositions using the alpha Proton X-ray Spectrometer (APXS). The next mission developed by the NASA was the *Mars Exploration Rover* (MER) launched in two phases in the summer of 2003. This mission had two rovers, Spirit and Opportunity. Spirit landed in Gusev crater and Opportunity in Meridiani Planum in January 2004. The twin rovers have a mast with two cameras including a panoramic camera, an arm with a Rock Abrasive Tool (RAT), an APXS, a Mössbauer and a Microscope Imager (MI) for rocks and minerals interpretation. An infrared spectrometer was placed on the top of the mast. The *Phoenix* mission (NASA) was landed in Vastitas Borealis at the North Pole in 2008, where the lander observed traces of water ice and carbonates. The last mission to be launched on the 26th November 2011 by NASA is the *Mars Science Laboratory* (MSL) with the rover Curiosity which will land on Mars in the middle of the 2012 summer (~06.08). This rover is really a geologist on wheels! It is equiped with different cameras (MastCam on the mast, and a microscopic camera Mars Hand Lens Imager –MAHLI-, on the arm) and various mineralogical and geological instruments, such as a Laser Induced Breakdown Spectroscopy (LIBS, on ChemCam), X-ray diffraction and fluorescence (XRD and XRF), an APXS and a Sample Analysis at Mars (SAM) for analyzing organic molecules. Details are given on MSL-NASA website: http://mars.jpl.nasa.gov/msl/. All these probes, except *Phoenix*, landed in the equatorial regions.

◄ *Figure I1. Artist's conceptions of the different Martian probes. In the top to the bottom: Mars Global Surveyor, Mars Odyssey, Mars Express, Mars Reconnaissance Orbiter, Sojourner -Pathfinder, Mars Exploration Rover, and Phoenix.*

Credits: NASA, JPL, ESA.

Figure 1: Elements of the ESA *ExoMars* programme 2016-2018. On the left TGO and the EDM, to be launched in 2016, and on the right the rover equipped with a drill (in black in front of the rover), to be launched in 2018. The NASA Rover part of the project was deleted in February 2012. Credit ESA.

Figure 1: Eléments du programme ExoMars de l'ESA pour 2016-2018. A gauche, Traces Gases Orbiter (TGO), qui sera lancé en 2016, et à droite le rover avec la foreuse (en noir à l'avant du rover), qui sera lancé en 2018. Le projet de rover de la NASA a été annulé en février 2012. Crédit image ESA.

The EDM will be a static lander with the objective of demonstrating ESA's ability to land on Mars. It will also study the dust in the atmosphere during descent and make several meteorological measurements on the surface.The second part of the mission will be the launch of a rover in 2018. The particularity of this rover will be its drill capable of drilling up to 2 meters in depth (Fig. 0.1). Before the definition of a joint mission, the ESA ExoMars rover weighed approximately 260 kg with only 16.5 kg of

instruments: the Pasteur payload, consisting of nine instruments located inside an analytical laboratory as well as outside the rover. As of writing, although it is planned to add new Russian instruments, all the Pasteur instruments will be maintained in the new joint mission. Since submission of the thesis, two of the ExoMars instruments have been deleted, the Mars-XRD and the Life Marker Chip owing to weight constraints.

The creation of a collection of Mars analogue rocks and minerals which is the main objective of this thesis will also take into account the Mars Science Laboratory mission (MSL, NASA), as well as the ExoMars mission.

Creating a rock library for the exploration of Mars

The *in situ* exploration of planets and other extraterrestrial bodies is limited by the weight and energy consumption of the scientific payload. This intrinsic characteristic of space missions necessitates extensive instrument preparation, including instrument calibration. In order to be relevant, instrument calibration should ideally use material representative of the object to be explored. The Mars 2018 mission will not escape this important phase. However, no sample has yet been returned from Mars and the only samples from Mars in hand are ~85 kg of Martian meteorites. Obviously, due to the scarcity of these samples, it is not realistic to use these rocks to calibrate the instruments. Also, meteorites are not necessarily representative of the rocks that will be analyzed at the landing site.

My doctoral project was undertaken in the Exobiology Group of the *Centre de Biophysique Moléculaire* (CBM), in Orléans (France), and forms part of the activities of the *Observatoire des Sciences de l'Univers en Région Centre* (OSUC). This group was founded by André Brack and is regonized for its expertise in Astrobiology since 1990. The Exobiology Group, and in particular its actual director, Frances Westall, is widely involved in the definition of the new payload and the development of the instruments (CLUPI, PanCam and MicrOmega in particular) for ExoMars.The goal of my work was thus to create a collection of Mars analogue rocks and minerals in order to provide suitable samples for the calibration of the Mars 2018 mission instruments. These same samples are also being used for CheMin and SAM on MSL. This study forms part of a larger project of space analogue rock collection in Orléans, called ISAR (for International Space Analogue Rockstore) and is based on the previous GSPARC (Geological Specimen Archive) collection developed by Derek Pullan in the course of his PhD thesis (*Pullan, 2008*).

The technical objective of this thesis is to offer to the Martian community a collection of fully characterized Mars analogue rocks and minerals, based on a comprehensive and a sound scientific analysis of Martian geology (e.g. volcanic, hydrothermal, alteration processes…). The main question is to define the criteria for the selection of analogues, in this case their similarity to Martian materials, thus optimizing preparation future space missions.

To begin with, an explanation of the collection project, the characterization methodology, and the International Space Analogue Rockstore (ISAR) database and website, which will be presented in the first chapter. I will also present here the instruments used to characterize the rocks in this collection, and also the scientific constraints. In the second chapter, the Martian geology and habitability conditions will be described. This information is essential for a scientific approach to build up the collection. Chapter three explains the choice of the samples selected for the first set of analogues and will give details of their geological characteristics in terms of structures, textures, mineralogy and elemental compositions. In this section, I have essentially concentrated on the diversity of rocks and some of the minerals observed in the Martian surface. In Appendix B, an example of detailed sample characterization is proposed, all the results are also available in a CD (3^{th} cover page). The use of analogue terrestrial field sites is also pertinent to Martian exploration. For the reasons outlined in Chapter IV, I proposed a new site in Cyprus, where hydrothermal, metasomatic and meteoric water alteration of basalts has geological characteristics relevant for early Mars. I can therefore offer a comprehensive study of a suite of rock samples that come from one locality. This approach allows more individual samples from a specifically geologically relevant site to be collected, thus enabling study of context and direct relationships between samples that can help understand past environments on Mars. In the course of my studies, it became however apparent that there are limitations in the analogy between terrestrial and Martian rocks, specifically with respect to basalt compositions and their Fe- and Mg-contents. I therefore prepared artificial Martian basalts based on the data provided by the Spirit rover in Gusev Crater. This preparation is discussed and explained in the fifth chapter. Finally, in conclusion, I show the characterization of the analogue samples using some of the ExoMars instruments. I also present the results of a blind test carried out to check the capability of ExoMars instruments to identify and characterize a rock. I conclude with future perspectives for this kind of study that includes a choice of other samples to complete the ISAR collection and possible artificial weathering experiments to compare with Cyprus samples.

One of the objectives of my doctoral studies was also the development of a future flight instrument, cathodoluminescence in spectroscopy and imagery mode. For the purposes of readability and clarity of this manuscript, the description of this study will be presented in Appendice A.

Introduction (Résumé Français)

Mars est une planète observée et étudiée depuis très longtemps. A partir des années 80, l'étude de Mars se focalise principalement sur la recherche d'une vie extraterrestre. Depuis 1960, une longue série de sondes spatiales a été lancée pour mieux comprendre Mars et peut être y trouver la vie ou des traces d'une vie ancienne. Cette exploration débute sur un échec avec Marsnick (Russie, 1960). Les Etats-Unis, plus chanceux, avec les sondes Viking 1 et 2 lancées en 1975 (NASA), vont être les premiers à se poser sur Mars. Cette réussite sera suivie par l'envoi de rovers, en particulier, des Mars Exploration Rover (MER) avec Spirit et Opportunity, en 2003 (NASA) et Mars Express en 2004 par l'Agence Spatiale Européenne (ESA). Le 26 novembre 2011, la mission Mars Science Laboratory (MSL, NASA) avec son astromobile Curiosity a été lancée pour étudier la géologie de Mars.

Depuis 2001, l'ESA développe son propre programme d'exploration du système solaire : le programme Aurora. En collaboration avec l'agence spatiale Russe (Roscosmos), l'ESA propose deux missions d'exploration de Mars dont les objectifs sont de chercher une vie actuelle ou passée, d'étudier les caractéristiques géochimiques (en particulier l'eau), de mieux comprendre les conditions d'habitabilité de Mars et de préparer un retour d'échantillons martiens sur Terre. La première partie de la mission est la sonde Trace Gase Orbiter (TGO, Fig.1) avec un module de descente atmosphérique (EDL). Le but est d'étudier la composition de l'atmosphère martienne. Son lancement est prévu pour 2016. La seconde partie de la mission, qui doit être lancée en 2018, contient un véhicule appelée Pasteur (Fig. 1).

L'objectif principal de ma thèse est de créer une collection de roches pour préparer les futures missions martiennes. En effet, l'exploration in situ des planètes et des corps célestes est limitée par le poids et l'énergie utile aux instruments scientifiques embarqués. Pour la calibration, il est important d'avoir à disposition une collection d'échantillons parfaitement caractérisés. Nous ne pouvons pas utiliser les météorites car elles sont trop précieuses et parfois, non pertinentes. Il est donc nécessaire de faire un travail de sélection de roches terrestres. Ce travail s'inscrit dans le projet plus vaste de l'International Space Analogue Rockstore (ISAR) qui ne se limite pas à Mars. La collection a pour objectif de proposer des échantillons analogues à une large gamme de corps du système solaire (planètes, astéroïdes, …).

Le premier chapitre sera dédié au projet de l'ISAR, avec la présentation de la méthodologie utilisée et du site web. Le deuxième chapitre s'intéressera à la géologie de Mars. Le troisième chapitre présentera la première sélection de roches analogues. Le quatrième chapitre proposera un site analogue de Mars à Chypre. Enfin, le cinquième chapitre décrira la fabrication de basaltes analogues de Mars.

Ce travail de thèse avait également pour objectif de développer un futur instrument spatial, d'imagerie et de spectroscopie de cathodoluminescence. Dans un souci d'unité et de clarté ce travail est présenté en annexe A

Chapter I
The International Space Analogue Rockstore

This chapter presents the International Space Analogue Rockstore (ISAR) and its associated online database and website, the starting point of this project. The ISAR is a collection of well-characterized rocks and minerals that are analogues of extraterrestrial bodies and that are intended to be used in the testing and calibration of space instrumentation. The ISAR is inspired by and is a continuation of a project first initiated in 2002 by Derek Pullan during his thesis with the Geological Specimen Archive, or GSPARC (*Pullan, 2008*) concerning the creation of a rock collection for calibration of instruments. The GSPARC collection contained "generic" samples sorted by colour, texture, fabric, composition, physical state and size, some of which were analogues of space bodies, such as Mars or the Moon. In contrast, the ISAR is characterized by the fact it contains rocks and minerals that are specifically compositionally similar to those of space bodies in terms of their mineralogy and geochemistry. I need to build up a new database, because the on-line publishing of the data could not be made in an easy way. As described in this chapter, the naming was complicated and did not allow to keep links between samples. Finally, to develop our own site was simpler for the hosting at the CNRS in Orléans (internet safety or server of storage of its data for example)

I.1 The Project

The availability of planetary materials for study in the laboratory is very limited. For instance, there are only 61[1] known meteorites from Mars and only ~500 kg of Moon samples returned during the Apollo and Lunokhot programs (1969-1972). Analysis of these precious samples is particularly problematic if the sample preparation method used is destructive. Moreover, it is unrealistic to use these samples to calibrate and test future space instruments because of the amount of material that would be needed. Furthermore, most Martian meteorites are not compositionally representative of their parent bodies because they are mostly cumulates. The ISAR collection will thus be mainly composed of terrestrial rocks that can be used in calibration exercises. In addition, the rockstore includes an online database where all the textural, structural and compositional characteristics of the rocks are described.

My thesis corresponds to the beginning of this project. Although I have participated in the development of the project and the creation of the database and of the associated website, the main aim of my project is the analysis and study of the ISAR Mars analogue rocks and minerals. The choice of Mars was motivated by the future robotic space missions, in particular the ExoMars-2018 mission as well as MSL described in introduction. These missions also drove the choice of the analytical methods used for the sample characterization.

I.2. Which analyses?

I.2.1 Methodological approach

My methodological approach to the analysis of Mars analogue rocks is essentially based on the investigational strategy of the ExoMars-2018 mission (*European Space Agency, 2010*) and its Pasteur payload. The rover will be equipped with a panoramic camera (PanCam[2]) on the mast to make high-quality 3D imaging. These views will provide information about the geomorphological and global context. A High Resolution Camera (HRC) also on the mast will obtain high quality images of interesting geological targets.

[1] All the Martian meteorites are referenced in the following web site: http://www.imca.cc/mars/Martian-meteorites-list.htm.

[2] http://exploration.esa.int/science-e/www/object/index.cfm?fobjectid=45103&fbodylongid=2127

On the rover, a UHF Radar named WISDOM[3] (for Water Ice and Subsurface Deposit Observation on Mars) will scan the subsurface down to two or three meters. A CLose-UP Imager (CLUPI) placed near the head of the Pasteur drill will be able to observe rock outcrops, the soils, drill fines, and the drill cores before they are ground up for analysis by instruments in the enclosed laboratory. CLUPI is a true colour camera with a very high resolution (7 µm per pixel at 20 cm). The drill will take samples from up to two meters in depth. This will allow analysis of unweathered samples protected from UV radiation and oxidation (*Kminek and Bada, 2006*) in the hopes of detecting hypothetical organic traces of life. The drill will include a miniaturised camera and an infrared (IR) spectrometer named MA_MISS[4] for borehole investigations. The drill will deliver the sample to a crusher in order to obtain a powder with a grain size distribution smaller than 250 µm. The powdered samples will be deposited by a dosing station into a carousel and distributed to different instruments (Fig. 1.1). The first one is a Visible light microscope coupled with a near-IR spectrometer MicrOmega[5]. This instrument will be used to determine interesting targets for the other instruments using an imaging system of 256 x 256 pixels, with a resolution of 20 µm/pixel, and IR spectra ranging from 0.85 to 3.5 µm. The mineralogical phases and any carbon detected by the instrument will be confirmed by spot measurements by Raman spectroscopy. The Raman[6] system will use a green laser excitation (wavelength λ= 532 nm), a spot size of ~50 µm diameter, and the spectra will be accumulated between 200-3800 cm^{-1}, with a resolution of ~6 cm^{-1}. The bulk mineralogy of the sample will be also analysed by X-Ray Diffractometry (XRD) and X-Ray Fluorescence (XRF)[7] with a spot size of ~1 cm diameter. Further details of the organic phases will be provided by the Laser Desorption Mass Spectrometer (LDMS) and the GC-MS, MOMA[8] (Mars Organic Molecule Analyser). Finally, the Life Marker Chip[9] (LMC) will examine soil samples to search for organic molecules deriving from past or present life. Fig. 1.1 shows the arrangement of the different instruments inside the internal Pasteu*r* payload.

[3] http://exploration.esa.int/science-e/www/object/index.cfm?fobjectid=45103&fbodylongid=2128
[4] http://exploration.esa.int/science-e/www/object/index.cfm?fobjectid=45103&fbodylongid=2133
[5] http://exploration.esa.int/science-e/www/object/index.cfm?fobjectid=45103&fbodylongid=2129
[6] http://exploration.esa.int/science-e/www/object/index.cfm?fobjectid=45103&fbodylongid=2130
[7] http://exploration.esa.int/science-e/www/object/index.cfm?fobjectid=45103&fbodylongid=2131
[8] http://exploration.esa.int/science-e/www/object/index.cfm?fobjectid=45103&fbodylongid=2132
[9] http://exploration.esa.int/science-e/www/object/index.cfm?fobjectid=45103&fbodylongid=2193

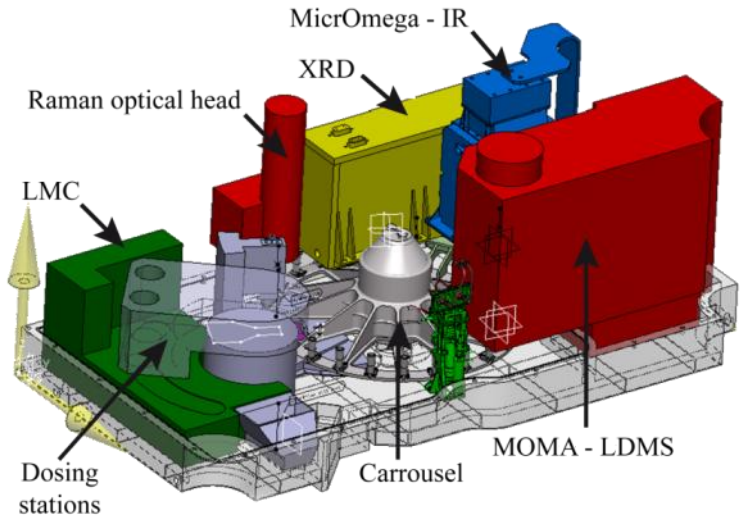

Figure 1.1: The Pasteur internal payload showing the different instruments. *Modified from ESA.*

Figure 1.1: Schéma des différents instruments internes du rover Pasteur. Modifié d'après l'ESA.

Presently, discussions about the Russian participation in the mission may involve additional Russian instruments that migth include an arm equipped with a microscope and other instruments such as an Alpha Particle X-ray Spectrometer (APXS) similar to the one of MSL, a Raman probe, a Mössbauer ...

The instruments on Curiosity (MSL) are also of interest in the preparation of samples for ISAR. These instruments include different cameras: Mast Cam (multispectral true colour camera), MAHLI (mounted to the arm on the rover to acquire microscopic images) and MARDI (descent camera); Chemcam, including a Laser-induced breakdown spectroscopy (LIBS); an Alpha-particle X-ray spectrometer (APXS, such as the instrument on the MERs); and CheMin, for measured chemistry and mineralogy with XRD and XRF. Other instruments are associated to the MSL rover such as Radiation assessment detector (RAD); the Dynamic Albedo of Neutrons (DAN) for measuring hydrogen or ice and water and a meteorological package with Rover environmental monitoring station (REMS).

The instruments used in both missions and the respective equivalent laboratory instruments are given in the Table 1.1.

Measurement type	**ExoMars mission**	**Mars Science Laboratory**	**Laboratory instruments**
Outcrop	Panoramic camera, microscope, High resolution camera.	NavCams, Mast Cam, MAHLI*	Camera
Texture	Panoramic camera, microscope.	Mast Cam, MAHLI*	Camera
Structure	Panoramic camera, microscope.	Mast Cam, MAHLI*	Camera
Mineralogy	Optical microscopy, HR camera Raman IR spectrometer XRD spectrometer	MAHLI* CheMin (XRD)	Optical microscopy Raman WITec IR-Nicolet XRD- INEL
Elemental Composition	XRF	CheMin(XRF) CheCam (LIBS) APXS (combined PIXE- Fluorescence spectrometry)	ICP-AES,MS † ICP-AES,MS † -
Traces of Life	LD- MS Life Marker Chip	SAM (with QMS; GC and TLS)	- -
Complementary instruments			
Texture, Structure, Mineralogy, other			Transmitted light, optical microscopy, SEM + EDX, Microprobe, Mössbauer, spectrometry.
Traces of life			SEM, TEM.

*MAHLI : Mars Hand Lens Imager, ‡ The laboratory miniaturized Mössbauer spectrometer "MIMOS II" . † The analyses were made in the Service d'Analyse des Roches et Minéraux – Centre de Recherches Pétrographiques et Géochimiques (SARM-CRPG), Nancy, France.

Table 1.1: Comparison of the MSL and the ExoMars-2018 payloads and the instrument suites used for laboratory characterisation of the analogue samples.

Tableau 1.1: Comparatif des futurs instruments embarqués sur la charge utile de la Mission ExoMars- 2018, des instruments de MSL avec les instruments de laboratoire utilisés pour la caractérisation des échantillons analogues.

I used high performance laboratory instrumentation to provide the similar analyses to the ones provided by space instruments, as well as analytical methods not used in space, such as optical microscopy of thin sections, scanning electron microscopy (SEM), electron microprobe and cathodoluminescence, and elemental analysis by Inductively Coupled Plasma Atomic Emission and Mass Spectrometer (ICP-AES, MS). To determine the level of oxidation of rock-forming elements, I used Mössbauer spectrometry.

I.2.2. Sample Preparation

The samples were observed and analysed in a number of formats. At the outcrop and hand specimen scale, rough rock surfaces of freshly collected samples and/or of sawn rock samples were used. Rock fragments exhibiting weathered and fresh surfaces were used for Mössbauer spectrometry (MBS). Standard polished thin sections (30 µm-thick) were prepared at CNRS-ISTO-Orléans laboratory, for optical microscopy, Raman spectroscopy, cathodoluminescence, SEM, energy-dispersive X-ray spectroscopy (EDX), and electron microprobe studies. Powdered rock samples (<100 µm grain size) were prepared for Raman spectroscopy, infrared spectroscopy (IR), X-Ray Diffraction (XRD), and ICP analysis with an electrical and then a manual agate mortar. Sieved powders with a grain size <250 µm were also prepared because this will be the powder size produced by the sample preparation system on the ExoMars-2018 mission. A flow diagram of the preparation procedure is displayed in Fig. 1.2.

I.2.3. Instrumentation

- An Olympus E410 camera with characteristics similar to that of CLUPI was used to image the outcrops and the hand samples using various objectives. The outcrops images could be compared with the ones provided by HRC.

- An optical microscope Olympus BX51 was used to analyse the thin sections in transmitted, reflected and polarized-analysed light to distinguish and identify the different minerals and the possible traces of life contained in the sample at the microscopic scale (if they are large enough).

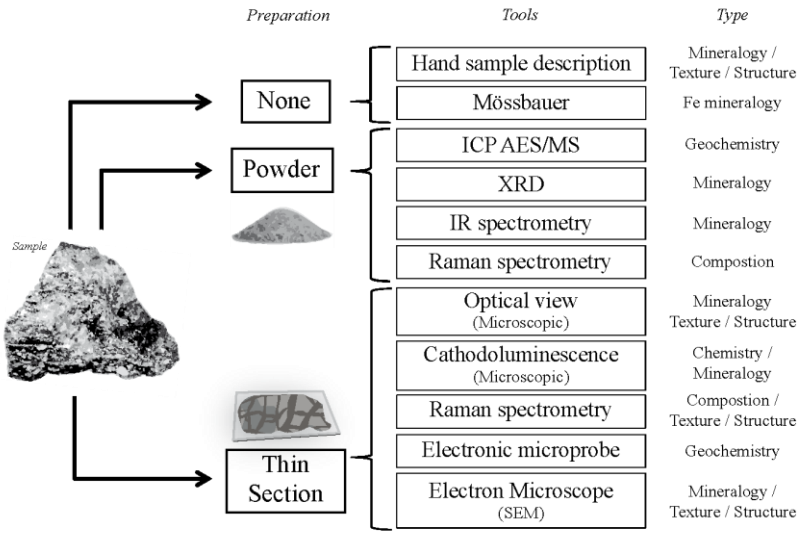

Figure 1.2: Flow diagram summarising the different types of preparations for the different laboratory instruments used for the characterisation of the ISAR samples. Note that *in situ* measurements on Mars are only made on hand specimens and powders.

Figure 1.2: Résumé des différents types de préparations utilisés pour les différents instruments de laboratoire afin de caractériser des échantillons de l'ISAR. A noter que les mesures faites in situ sur Mars sont réalisées seulement à partir d'échantillons massifs et de poudres.

- Two SEMs were used for high resolution and magnification imaging as well as for EDX analyses: a JSM- 6400 JEOL at the CNRS-ISTO laboratory, Orléans and a Hitachi FEG-SEM S4200 at the University of Orléans. These instruments were used in two modes of imaging. Secondary electrons were used to make high resolution imaging (down to few tens of nanometers in resolution) and backscattered electrons were used to distinguish the different component phases at sub-micrometric scale. Both systems were equipped with an EDX detector that allows qualitative elemental analyses.

Insert 2: The Raman instrument and Raman compositional mapping.

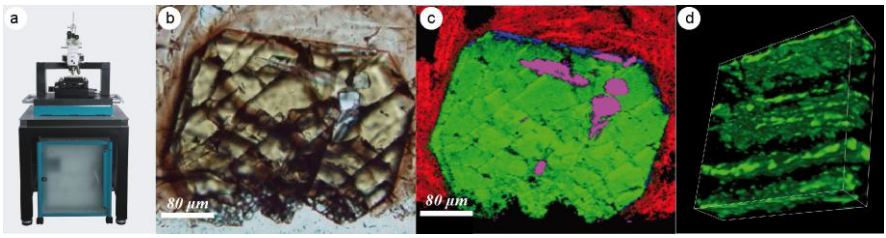

Figure I2 : a- The AFM-Raman Witec Alpha 500 RA instrument in the lab; b- Optical view of amphibole in volcanic sample from Tenerife Spain; c- Compositional map of b, amphibole is in green, and blue (border); apatite in pink and plagioclase in red. d- 3D Raman view of layers kerogen in carbonaceous chert from the Josefsdal Chert (3.3 Ga), Barberton (80x80x20 µm^3).

The WITec Alpha500 RA is a confocal micro-Raman spectrometer coupled with an Atomic Force Microscope (AFM). The micro-Raman probe is focused on the surface of the sample using an optical microscope objective. The confocality of the system allows the collection of information only near the focal plan of the objective using a pinhole and leads to better spatial resolution. The sample is fixed on a piezo-electric scan Table that allows very accurate lateral and vertical displacement (200x200x20 micrometers with a resolution down to few nanometers). This Table is itself fixed on a motorized positioning Table allowing larger displacement of up to 10x15x2 centimeters. It is possible to obtain a hyperspectral image, where each pixel is associated with a spectrum, with a maximum of 160 000 pixels/image by moving the sample below the laser. The spatial resolution is then given by the ratio scan size/number of pixels and is limited by the numerical aperture of the objective, the laser wavelength and the pinhole size; with the 532 nm laser, a 100x objective (N.A. = 0.96) and a pinhole size of 25 µm, the in-plane spatial resolution is about 350 nm and the vertical resolution is about 1 µm.

Raman scattering is a complex phenomenon. The analytical model does not permit identification of a compound from its spectrum. Thus identification is generally made by comparison with spectral databases. For this study, I mainly used the Ruff database through the CrystalSleuth freeware.

Various kinds of maps can be made of the different charachertistics mineral components. Indeed, when a spectrum is associated with a unique compound, the spectrum intensity is directly related to the concentration of that compound, while the peak position may be associated with the stress state, or the peaks ratio to the crystal orientation in the case of a mineral characterized by more than one peak. It is thus possible to map all these characteristics by associating a colour scale to the desired parameter. The most common maps are of concentration and composition obtained by associating a color bar to the intensity and a colour to each component respectively. More information can be found in *Poilblanc and Crasnier, (2006)*.

- A WITec Alpha500 RA Raman spectrometer, CBM, Orléans, working with a green laser (Nd:YAG frequency doubled, λ=532 nm; similar to that used for the ExoMars-2018 mission, *Rull-Pérez and Martinez-Frias, 2006*), was used to obtain mineralogical information. The method is based on the inelastic

Raman scattering allowing identification of a compound from the vibration of its atomic bonds. The identification is made from the diffraction spectrum of the scattered beam given by the CCD camera of the spectrometer, expressed as CCD counts versus wavenumber (in cm^{-1} relative to the incident laser wavenumber). The instrument used allows the sample to be scanned in order to make compositional mapping. Each pixel in a map is associated with a spectrum (hyperspectral data). This is a non destructive method that does not necessitate any sample preparation. Both this instrument and optical microscopy were fundamental techniques for the characterization of the ISAR samples. More details on the instrument are displayed in Insert 2**.**

- A Nicolet IR spectrometer, 400-4000 nm, in transmitted mode at the CNRS-ISTO laboratory, Orléans, and a Nicolet Magna IR 760 spectrometer ESP associated with a Thermo Scientific Integrations Sphere near IR Nicolet 6700 FT-IR, at the University of Poitiers were used for mineralogical identification. IR spectrometry is a key technique in Martian exploration; the Omega instrument of Mars Express (ESA) and CRISM on the Mars Reconnaissance Orbiter (NASA) have provided much information on the mineralogy of the surface of Mars, in particular phyllosilicate mineralogy (e.g. *Poulet et al., 2005; Bibring et al.,2006; Mustard et al., 2009; Ehlmann et al., 2011;*and Chapter II). IR is highly complementary to Raman spectroscopy.

- Two X-ray instruments were used for mineral identification: an INEL XRM3000/CPS120 X-ray diffractometer in transmitted mode, at the CNRS-ISTO laboratory, Orléans, and a Brucker D8 Advance diffractometer in reflected mode, at the Hydrasa laboratory, University of Poitiers. This technique measures the lattice parameters of crystals and thus allows their identification. This technique is mostly used on powdered samples. Powders were analysed, respectively, for the first instrument in a 0.3 mm capillary using a beam emitted by a Co generator and for the second in a powder paste using a Cu generator ($\lambda CoK\alpha$ = 1.78897 Å, $\lambda CuK\alpha$ = 1.541838 Å).

- A laboratory version of the miniaturized Mössbauer spectrometer "MIMOS II", at the Johannes Gutenberg Universität-Mainz, Germany, was used to determine the level of oxidation of minerals in the rocks. Spectra were obtained in backscattered geometry with a field of view of 15 mm. This instrument is part of the payload of the two Mars Exploration Rovers (*Klingelhöfer et al., 2003*).

- A Cameca SX-50 electron microprobe at the ISTO-BRGM laboratory, Orléans, was also used to determine the elemental composition of specific minerals.

- Cathodoluminescence was used to study the presence of trace elements (e.g. Mn in carbonates) and detection of vacancies in minerals (e.g. lattice defects related to electrostatic charging phenomena during electron irradiation). This technique also permits observation of crystal growth microstructures. The instrument used has been developed in Orléans with the aim of developing such an instrument for future space exploration (*Thomas et al., 2009*). One of the objectives of my research was to contribute to the optimization of this instrument. For the clarity of this manuscript, this project and the significant advances made during the last three years are presented in Appendice A.

This list of equipment is not exhaustive but it corresponds to those mostly used. Other types of analyses have and will be made on the ISAR samples.

I.3. Nomenclature and relationship between samples

The GSPARC system, on which the ISAR project is based, attributed a complex name to each sample. Although this system was suitable for the classification of a huge quantity of individual samples, it was not useful for the ISAR collection where the link between samples and subsamples is important. Thus, we decided to use our own nomenclature that takes into account the heredity and the relationship between the samples, in the manner of a family tree.

Fragmentation of the parent sample during preparations produced many smaller pieces, most of which will be probably never studied (the cutting wastes for instance). Moreover, the samples could be sand or gravel. The referencing of each particle or grain would then be unnecessary. The chosen solution has been to define two types of samples: the initial parent samples and the sub-samples. Parent samples correspond to those taken in the field. They may be composed of several pieces of rocks, sand, gravel, etc. They can be seen as “a box” containing all the pieces originating from the same place and taken at the same time (Fig. 1.3). The name of the initial samples consists of two numbers for the year, two letters for the originating country/locality and two numbers for the order of sampling during the field trip. For example: 10SA02 is the second sample taken in 2010 in South Africa. Some parts of the initial samples are then prepared for future analyses in powder form or as thin sections. The prepared samples are labeled by adding a dash and a number to the name of the initial sample, for example: 10SA02-1. The cutting waste is not referenced and is replaced back in the box of the initial sample. Samples can also be split into subsamples. These sub-samples are named by adding a letter at the end of the original sample

reference. They can themselves be further split and the additional subsamples will be named by adding a number at the end. For example: 10SA02-1a then 10SA02-1a1… This relationship between the samples can be represented as the family tree shown in Fig. 1.3.

I.4 The ISAR database

The aim of the ISAR is to propose samples for calibrating space instruments for any *in situ* mission. For this reason, all the sample data and associated analyses are displayed in a web-based database: www.isar.cnrs-orleans.fr. The website was first developed by Frédéric Foucher (CNRS-CBM) in html and php and the associated database was developed in MySQL. The nomenclature of the samples was also chosen in order to facilitate the structure of this database. Finally, the website was improved in terms of ergonomy and design by the company IdWeb[10] in Bourges.

The website includes all the results provided by the different instruments for the samples included in the ISAR collection. The web site consists of a home page which presents the project and different pages presenting the team, the equipment, the rockstore, and missions using the ISAR collection (Fig. 1.4). A newspage gives the main events with which the ISAR members have been associated or present (e.g. congresses, workshops) and the latest team publications. The second and main part of the website is the database, which summarizes all the analytical information obtained with the different instruments for each sample (Fig. 1.4). After logging in, the user can download a pdf file containing all the information and relevant figures, as well as text files with the different spectra and other data. Finally it is possible to borrow a sample using the lending system.

In order to choose samples, it is necessary to know the geology of Mars. The next chapter will thus present the geology of Mars and the possibilities of finding life or traces of fossil life on outcrops. These considerations will allow us to make an appropriate analogue sample selection.

[10] More information's about Idweb in this web site : http://www.idweb.fr/

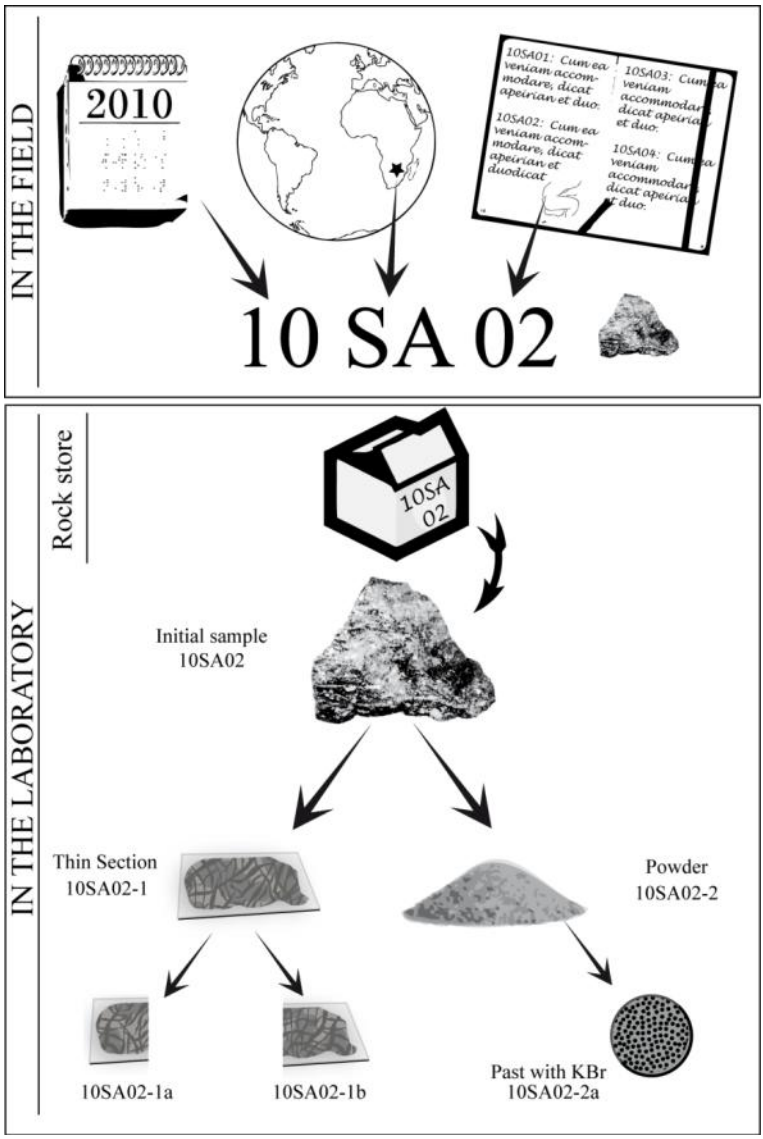

Figure 1.3: Nomenclature used for the ISAR collection and relationship between the samples in the collection.

Figure 1.3: Nomenclature utilisée pour les échantillons de l'ISAR avec les relations entre eux.

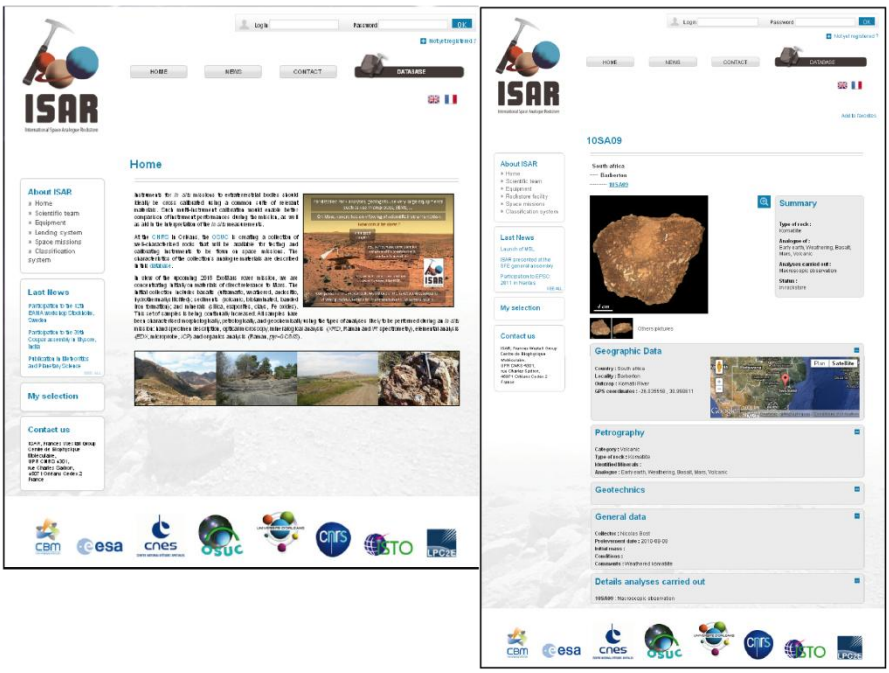

Figure 1.4: Screen capture from the ISAR website: Home page and sample page.

Figure 1.4: Capture d'écran de la page d'accueil et d'une page échantillon.

The ISAR (Résumé Français)

Ce chapitre a pour objectif de présenter l'ISAR, la collection internationale de roches analogues à des objets du système solaire. Cette collection est inspirée par le projet initié par D. Pullan pendant sa thèse en 2008, le « Geological Specimen Archive ». En effet, il est essentiel de pouvoir disposer d'échantillons analogues pour tester de futurs instruments de vols. Des échantillons provenant de l'espace sont disponibles sur Terre, tels que les échantillons lunaires rapportés par les missions Apollo et Lunokhot, ou encore les météorites martiennes. Cependant ces échantillons sont beaucoup trop précieux pour être utilisés dans des tests avec des méthodes destructives.

Mon travail de thèse correspond au début du projet ISAR. J'ai donc participé au développement du projet avec la création de la base de données et du site internet. Mais l'objectif principal est l'analyse et l'étude d'échantillons analogues de Mars. Le choix de Mars est motivé par l'actualité des futures missions robotiques qui s'intéressent essentiellement à Mars, en particulier MSL et le projet ExoMars.

Ce chapitre définit la stratégie d'analyse et le choix des échantillons. Les analyses faites sur les échantillons analogues se basent essentiellement sur la future mission ExoMars et sa charge utile : Pasteur. Ce véhicule est équipé de nombreux instruments comme des caméras (PanCam et HRC). Un radar UHF (WISDOM). Une« loupe » (CLUPI) fixée au sommet de la foreuse pour observer le sol et les échantillons prélevés. La foreuse contient un petit spectromètre IR (MA_MISS). La petite carotte prélevée par la foreuse, sera broyée puis envoyée à l'intérieur du véhicule, dans le laboratoire scientifique (Fig. 1.1). Le laboratoire est composé de DRX, XRF, Raman, IR, Life Marker Chip et LDMS. Ces instruments vont examiner l'échantillon pour le caractériser d'un point de vue pétrologique et organique (recherche de traces de vie fossile ou actuelle). Actuellement, la liste des instruments est en cours de discussion avec l'agence spatiale Russe Roscosmos en vue d'une collaboration pour cette mission. Pour ce travail, nous prendrons aussi en compte les instruments de MSL. La liste des instruments que nous utiliserons est donnée dans le Tableau 1.1.

Pour cette étude et pour la lithothèque ISAR, les échantillons sont préparés de différentes manières : aucune préparation, en poudre ou en lame mince. Notons que les lames minces ne sont pas des préparations utilisées par les futures missions spatiales, mais restent la base du travail du géologue. La procédure de préparation pour chaque instrument est résumée dans la Fig. 1.2.

Pour cette étude, nous utiliserons une large gamme d'instruments comme l'appareil photo, le microscope optique polarisant, le MEB, les spectrométries Raman et IR, la DRX, le Mössbauer, l'ICP-MS/OES des éléments mineurs et majeurs, la microsonde électronique et la cathodoluminescence. Cet instrument, potentiellement spatialisable et utilisé sur Mars fait l'objet d'une description plus précise dans l'annexe A. Le détail de chaque instrument n'est pas repris dans ce résumé, consultez le paragraphe I.2.

Nous utiliserons dans l'ensemble de cette thèse la nomenclature de référencement des échantillons développée pour l'ISAR. Le code de l'échantillon initial se compose de deux chiffres pour l'année (exemple 10 pour l'année 2010) suivi de deux lettres symbolisant le pays (exemple SA pour South Africa soit Afrique du Sud) et de deux chiffres pour l'ordre de prélèvement sur le terrain. Lorsque des échantillons fils sont préparés (comme une lame mince ou une poudre) un chiffre est ajouté puis une lettre puis un chiffre etc…. La nomenclature est reprise sur la Fig. 1.3.

Enfin, la base de données de l'ISAR a été développée à l'origine par Frédéric Foucher puis améliorée par l'entreprise IdWeb et associée au maintien du site web du projet: www.isar.cnrs-orleans.fr. Le détail des informations sur chaque échantillon est disponible en ligne avec plusieurs niveaux de droits d'accès. L'accès sécurisé, réservé aux utilisateurs enregistrés, permet de télécharger l'ensemble des données au format pdf. La Fig. 1.4 correspond à des captures d'écran du site web (page d'accueil et page échantillon).

Chapter II
Mars

The red planet was named after the Roman god of war. Mars is the fourth planet and the farthest of the telluric planets from the Sun in the Solar System. It formed during planet accretion 4.564 billion years ago. Its orbit is eccentric, between 1.38 and 1.66 AU and it has four seasons. Mars is a small planet, only 1/10 of the Earth's mass and its radius is approximately half of the Earth's radius (3380 km of equatorial diameter). Finally, Mars has two small moons with irregular surfaces, Phobos and Deimos.

II.1. Geological setting

The internal structure of Mars is still unknown but orbital measurements of its properties indicate that it has a core and possibly a differentiated mantle (review in *Dehant, 2010*). However, no geological activity has been observed on the planet today (*Carr and Head, 2009*). The Martian surface is characterized by a global dichotomy: in the south, highlands with very large craters (e.g. *Hellas Planitia* crater, 2,200 km in diameter and 9.5 km of depth, it is the largest visible crater in the Solar

system) and in the north, a smoother surface which is 4 km deeper than the southern highlands. The landscape is characterized by very large volcanoes (e.g. *Olympus Mons* at 26 km altitude is the highest volcano in the solar system), large canyons (e.g. *Valles Marineris* is more than 4,000 km-long, 200 km-wide and up to 7 km-deep) and numerous craters. Due to the absence of plate tectonics, almost all impact craters have been preserved through geological time, although it appears that craters in the northern hemisphere have been covered by later lavas flow and sediment deposits (e.g. *Mangold et al., 2009; Le Deit et al., 2011; Dehouck et al., 2010*). The preservation of craters means that their superposition can be used in order to estimate the age of the different regions and thus subdivide the surface into different geological periods (Fig. 2.1). *Hartman and Neukum (2001)* suggested a Noachian period from 4.5 to 3.7 Ga, the Hesperian one from 3.7 to 3.0 Ga and the Amazonian era from 3.0 Ga to the present. *Bibring et al. (2006)* suggested another geological time-scale based on orbiter-analysed surface mineralogy with the Noachian, Hesperian and Amazonian replaced by *Phyllossian*, *Theiikia*n and *Siderikian*, respectively (see Fig. 2.1). In this manuscript, we refer to the former system.

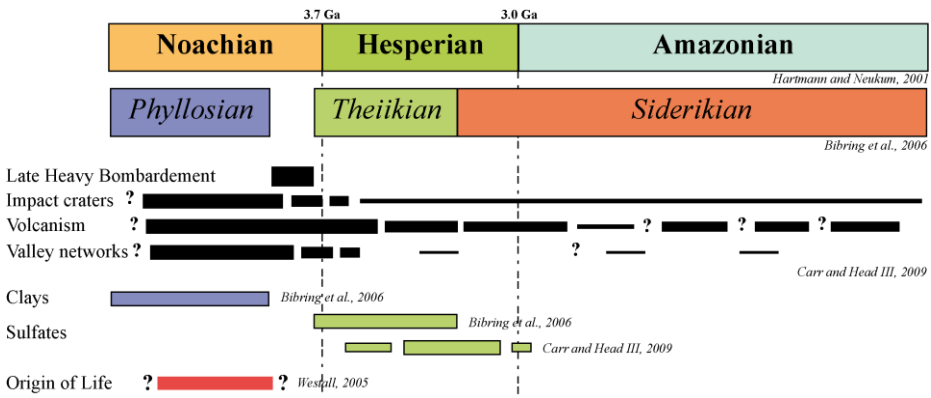

Figure 2.1: Geological time scale of Mars with the two systems of nomenclature (*Hartmann and Neukum, 2001* and *Bibring et al., 2006*) correlated with the different periods of geological, impact and fluvial activity, as well as surface mineral formation.

Figure 2.1: Echelle des temps géologiques martiens basée sur deux nomenclatures (Hartmann and Neukum, 2001 et Bibring et al., 2006). Cette échelle est corrélée avec différents phénomènes géologiques comme les impacts, les activités fluviales ou les formations minéralogiques.

Not all the Martian surface has been observed but it seems to be essentially composed of volcanic rocks associated with different sediments derived from basaltic alteration and weathering. A major part of the surface is covered by several meters of dust and detritus, named regolith. We do not here describe and discuss the regolith. The terrain description is based on the data from the *Mars Global Surveyor* (MGS), *MRO* and *Mars Express* orbiters, the *Phoenix* lander and *Spirit* and *Opportunity* rovers.

II.1.1. Igneous rocks

The data of the Thermal Emission Spectrometer (TES) of MGS was used by *Bandfield (2002)* to propose two major categories of surface mineralogy. The first one consists of plagioclases, high-Ca pyroxenes, sheet silicates/high-Si glass and hematite, suggesting a basaltic composition. The second one also consists of plagioclase, and silicate sheets/high-Si glass but its low content in high-Ca pyroxene is more consistent with andesite. This interpretation was based on measurements made during the Mars Pathfinder mission at the landing site *Chryse Planitia* in *Ares Vallis* in 1997 (*Wänke et al., 2001*). However, the more Si-rich composition has been re-interpreted and explained as being due to measurements made on the altered surface of the basalts, since the top layer of the analyzed rocks was not removed before analysis, as it was done later during the MER missions (*Bandfield et al., 2004; Christensen et al., 2005*).

Analyses of rocks made in the Gusev Crater by Spirit indicate that, although Martian basalts are relatively similar in composition to the terrestrial ones, they have higher MgO (8 to 10 wt%), FeO (15 to 18 wt%) and Cl (>0.70 wt%) (*Gellert et al., 2006*). *McSween et al. (2009)* compared all data from Martian meteorites, rovers (Mars Pathfinder and the MERs) and orbit (TES of MGS and the Gamma Ray Spectrometer (GRS) of Mars Odyssey). In particular they plotted all these compositions within the classical total alkali-silica diagram (TAS) shown in Fig. 2.2a. This diagram plotting silica composition against alkali elements (Na_2O and K_2O) is essential for determining the classification of volcanic rocks. It should be noted that, contrary to *in situ* analyses, basalt compositions measured from orbit correspond to average values made over large areas all over the planet. Moreover, analyses made *in situ* on the ground by the MERs were obtained from the abraded surfaces of massive rocks that were either unaltered or less altered than the weathered rock surfaces studied from orbit and by Mars Pathfinder. This difference explains the offset of the MER data with respect to the others ones (*McSween et al., 2009*). Most MER analyses fall within the

basalt-thephrite-basanite-picrobasalt-komatiite field of the TAS diagram, with a tholeiitic evolution (FeO*/MgO-silica diagram, Fig. 2.2b), according to the classification of *Le Bas et al. (2000)*.

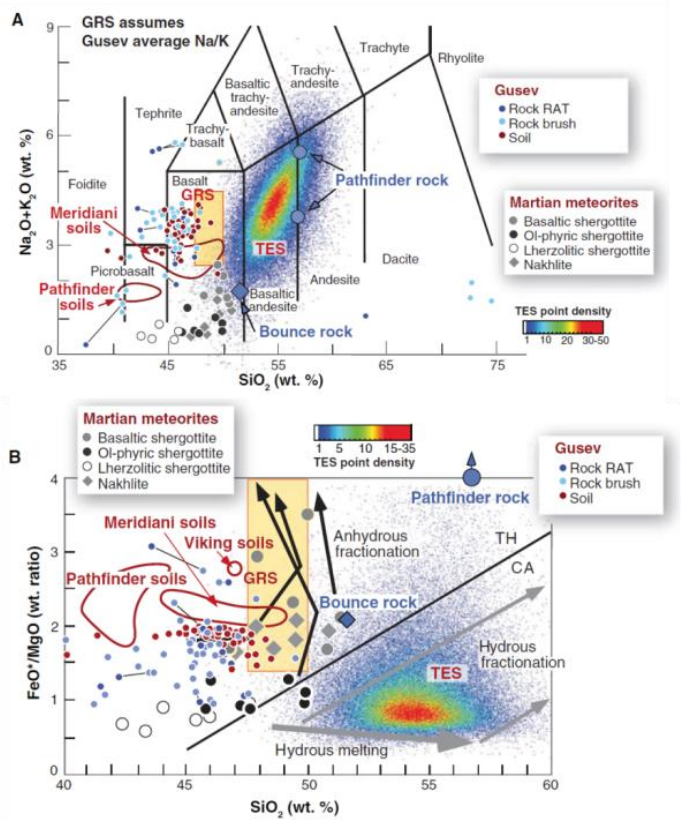

Figure 2.2- a. Composition of volcanic rocks and soils from the Gusev crater plotted in a total alkali-silica (TAS) diagram used for classification of volcanic rocks. b. FeO*/MgO-silica diagram used for distinguishing tholeiitic (TH) and wet calc-alcali (CA) rocks. Data points for the same rocks analysed from RAT-brushed and RAT-ground surfaces are connected by tie-lines. (After *McSween et al., 2009*).

Figure 2.2- a. Composition chimique des roches et des sols volcaniques provenant du cratère Gusev reportées dans le diagramme total alcalins-silice (TAS) habituellement utilisé pour la classification des roches volcaniques. b. Diagramme FeO/MgO-silice utilisé pour distinguer la série tholéitique (TH) de la série calc-alcaline (CA). Les données provenant de la même roche et comportant plusieurs analyses sont reliées par une ligne (d'après McSween et al., 2009).*

Finally, it has been shown that Martian meteorites are stony meteorites that are not really representative of the crust (*McSween et al., 2009*). They have been divided into three groups: *Shergottites*, *Nakhlites*, and *Chassignites*, named after the locations where the first meteorite of each class was discovered. They are collectively referred to as the *SNC group* meteorites. Most meteorites are cumulates; *Chassignites* are dunites, *Nakhlites* and the famous ALH84001 are clinopyroxenites, and a large part of the *Shergottites* are "lherzolitic Shergottites", a variety of peridotite. Only some *Shergottites* are "basaltic Shergottites", for example the Los Angeles meteorite found in 1999 (*Rubin et al., 2000*). Nevertheless, they plot separately from the basalts observed in *Gusev crater* in the TAS diagram in Fig. 2.2a.

The basaltic composition of *Adirondock*, *Humphrey* and *Mazatzal* rocks measured by *Spirit* in the *Gusev Crater* was discussed by *Gellert et al. (2004)* and *McSween et al. (2004)*. It is interpreted in terms of normative anorthite, fayalite-forsterite, diopside, hypersthene and some chromite, magnetite, ilmenite and apatite. On the TAS diagram of volcanic rocks, most of the *Gusev* basalts fall in the silica-poor side of the basaltic field, with rare tephrite samples overlapping the picrobasalt field (Fig. 2.2a). The compositions of the *Gusev* rocks and soils, Martian meteorites, and the *GRS* data, calculated by neglecting the volatile elements, also indicate that the crust is dominated by basalts. These basalts show no evidence of fractionation and are very primitive (*McSween et al., 2009*). There is some evidence of komatiites on the Martian surface (*Reyes and Christensen, 1994; Nna-Mvondo and Martinez-Frias, 2007*).

As noted above, *McSween et al. (2009)* suggested a different interpretation for the andesite detected based on the *TES* data. *Bandfield et al. (2004)* previously interpreted andesitic or basalt-andesitic compositions based on the interpretation of a feldspar, pyroxene and quartz mineral association (SiO_2 concentrations of 62 wt%; see Fig. 2.2). However, data related to iron oxidation were not available at that time (*Taylor et al., 2008*) and, moreover, the original analyses were made on raw rock surfaces. *McSween et al. (2009)* therefore, explained the high silica-content by chemical weathering of the basalts (palagonitisation, *i.e.*, the devitrification of a basaltic glass under the influence of water to form palagonite). This phenomenon was probably relatively common on early Mars, when liquid water was still present.

As cumulates, most Martian meteorites are more representative of the Martian mantle than of its surface. On Earth, typical plutonic rocks include granites but the evidence for granites on Mars is weak (*Taylor et al., 2008*). Although SNC meteorites are mostly pryoxenites and peridotites, they do

contain interstitial acidic glasses and are characterized by isotopic compositions that suggest the existence of components having a composition similar to that of the terrestrial granitic continental crust (*Bonin, 2011; Bonin, 2012*). In the *Tharsis* area, rhythmically layered deposits observed on the flanks of the giant volcanoes, including *Olympus Mons*, evoke alternating basalt flows and acidic pyroclastites (*Bonin, 2011*). Finally, infrared spectra in some impact craters correspond to compositions close to granites and trondhjemites (*Bandfield et al., 2004; Christensen et al., 2005*).

II.1.2. Sedimentary rocks

Although less abundant than basalts, sedimentary rocks have been detected on Mars. Most of the sediments are derived from basaltic precursors, *i.e.* basaltic sands and altered basaltic detritus (*Tosca et al., 2004; Ehlmann et al., 2009*). Water may be responsible for this alteration (e.g. *Bibring et al., 2006; Ehlmann et al., 2009; Viles et al., 2010; Ehlmann et al., 2010*). In particular, the orbital analyses suggest aqueous alteration of the surface materials, first by neutral to alkaline fluids during the pre-Noachian/Noachian period, followed by alteration under more acidic conditions from the Hesperian onwards (*Poulet et al., 2005; Bibring et al., 2006*). These different pH conditions resulted in the formation of different types of phyllosilicates, such as neutral to alkaline Fe-Mg smectites (saponite, nontronite) during the pre-Noachian/Noachian period and Al-rich smectites during the Hesperian/Amazonian. It should be noted, however, that phyllosilicates can be formed by deuteric processes during fractionation within the magmatic chamber (*Meunier al., 2010*) and such an hypothesis has been proposed for unusually thick clay deposits (*Meunier et al, 2012*). *Ehlmann et al. (2011)* have recently reviewed the origin of clays on Mars.

Many very specific types of clays have been interpreted from orbital measurements including chlorite, vermiculite, nontronite and smectite (review in *Ehlmann et al., 2011*). I am somewhat skeptical about these detailed interpretations because the classification of clays is already difficult on Earth using advanced instrumentation and it is therefore even more difficult from orbit. For this reason, I will only use the group clay name in this study.

Other types of sediments occur on Mars. Alteration and silica-enrichment may also be induced by hydrothermal activity. In particular *Ruff et al. (2011)* suggested that the opaline silica identified in laminated and cross-bedded tephra in the Eastern Valley, between Home Plate and the Mitcheltree/ Low Ridge complex by Spirit (*Squyres et al., 2008*), could be interpreted as

hot spring sinter deposits associated with volcanic activity. Silica deposits are visible on the Martian surface and form elongated dykes (*Ruff et al., 2011*) or nodules (*Squyres et al., 2008*). *Miliken et al. (2008)* place their formation during the Hesperian to Amazonian epochs.

Evaporitic deposits including jarosite, gypsum, and other hydrated sulfates associated with hematite have been described in the high latitudes around the polar ice cap, as well as in other locations at the Martian surface (e.g.: in Meridiani Planum, *McLennan et al., 2005*; in Valles Marineris, Margaritifer Sinus, Terra Meridiani, *Gendrin et al., 2005*). Small amounts (~1 wt%) of carbonate minerals have been described from several SNC meteorites (*Gooding, 1992*). In particular, *Borg et al. (1999)* and *Treiman et al. (2002)* described carbonates in the 4.5 billion years old ALH84001 meteorite that *Mc Kay et al. (1996)* and *Thomas-Keptra et al. (2009)* interpreted as mineralogical indications of past life. Carbonate minerals have also been detected from orbit in the Martian dust (<5 wt%; *Bandfield et al., 2003*). Mg-rich carbonates associated with phyllosilicates and olivines were identified in the Nili Fossae by MRO (*Ehlmann et al., 2008*).

►Figure 2.3: Mineral distribution and diversity on Mars. Mineralogical determination was obtained by orbital observation (in particular CRISM and OMEGA) and *in-situ* measurements and superimposed on the MOLA topographic map. After *Bandfield et al., 2002; Hynek et al., 2002; Ehlmann et al., 2008; Boynton et al., 2009; Carter et al., 2010; Michalski and Niles, 2010; Morris et al., 2010; Ehlmann et al., 2011* and NASA online data. The position of the MER rover Opportunity is also plotted on this map.

►*Figure 2.3: Carte de la distribution des minéraux observés sur Mars. La détermination minéralogique est obtenue à partir des observations depuis l'orbite (en particulier avec les instruments CRISM et OMEGA) et in situ. Les données sont superposées sur la carte topographique de Mars MOLA. D'après Bandfield et al., 2002; Hynek et al., 2002; Ehlmann et al., 2008; Boynton et al., 2009; Carter et al., 2010; Michalski and Niles, 2010; Morris et al., 2010; Ehlmann et al., 2011 et les données en ligne de la NASA. La position du rover Opportunity est repérée sur cette carte.*

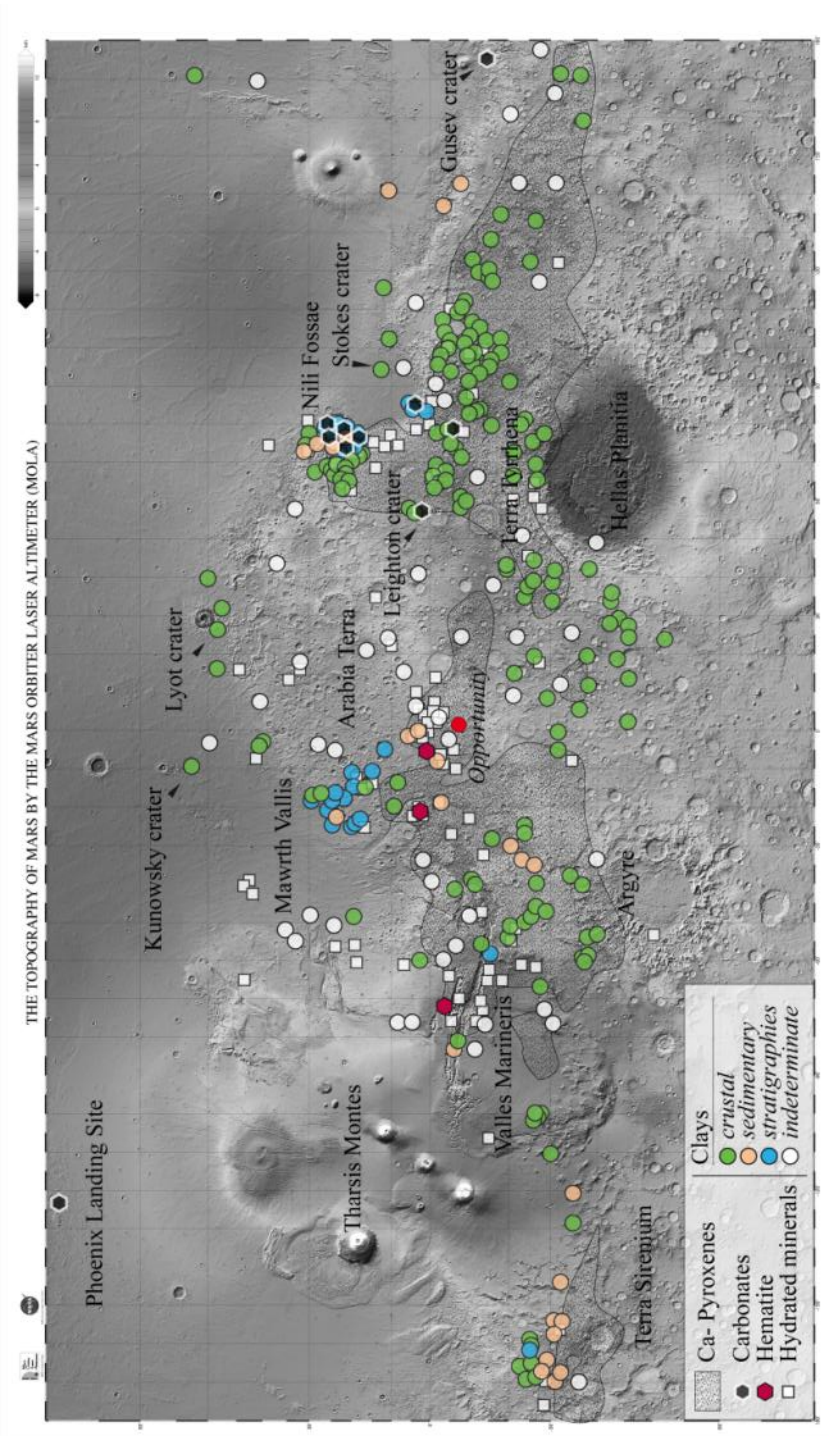
THE TOPOGRAPHY OF MARS BY THE MARS ORBITER LASER ALTIMETER (MOLA)
Phoenix Landing Site
Kunowsky crater
Lyot crater
Mawrth Vallis
Arabia Terra
Nili Fossae
Stokes crater
Leighton crater
Gusev crater
Opportunity
Terra Cimmeria
Hellas Planitia
Tharsis Montes
Valles Marineris
Argyre
Terra Sirenum
Ca- Pyroxenes
Carbonates
Hematite
Hydrated minerals
Clays
crustal
sedimentary
stratigraphies
indeterminate

Not far from Nili Fossae, in Leighton crater, Fe- Mg- carbonates (siderite, magnesite) associated with phyllosilicates (kaolinite group) and Fe- Mg-bearing silicates have also been detected (*Michalski and Niles, 2010*). Three to five percent calcium carbonates were also observed *in situ* in the soil of Mars by the Phoenix lander (*Boynton et al., 2009*). Finally, the most important evidence of carbonates was made by the *Spirit* rover in the end of December 2005 in very old volcaniclastic rocks (Hesperian) of the Comanche outcrop, in the Columbia Hills of Gusev Crater (*Morris et al., 2010*). Using its Mössbauer, Spirit detected approximately 26 wt% of Fe-Mg carbonates in the rock associated with olivine ($Fo_{0.72}$). Using APXS, *Morris et al. (2010)* calculated the mineral composition of this Mg-Fe carbonate as: $Mc_{0.62}Sd_{0.25}Cc_{0.11}Rh_{0.02}$, with Mc = magnesite; Sd= siderite; Cc= calcite and Rh = rhodocrosite.

Figure 2.3 is a non-exhaustive overview of mineral type and locality on Mars based on orbital measurements (essentially from Omega and *C*RISM) and from the *in situ* measurements (the MER Spirit, Opportunity and Phoenix).

II.2 Life on Mars

The main objective of the future Martian mission, in particular the ExoMars mission, is to search for evidence of past or present life. But, what kind of evidence can we expect? In this subsection, we try to give some indications mainly based on possible terrestrial analogues of hypothetical microbial Martian remains.

II.2.1 Mars habitability

A minimal definition of life can be stated by the dynamic interaction between structures having a semi-permeable boundary and macromolecules acting as catalysts and templates (*Ruiz-Mirazo and Moreno, 2011*). Habitability can be simply resumed as the association the necessary ingredients for life in a particular location (*Brack, 2000; Southam and Westall, 2007; Hoelhler and Westall, 2010*), namely: liquid water; endogenic and/or exogenic organic molecules for constructing the macromolecules necessary for cellular life; a source of energy, in the case of Mars chemical energy from redox reactions on reactive mineral surfaces (cf. *Jakosky and Shock, 1998*); and nutrients (H, N, O, P, S, plus transition metals) obtainable on Mars from aqueous/hydrothermal alteration of the volcanic crust. The

important aspect for life, however, is the temporal and spatial scale of the habitable environment which will be different for (1) an origin of life, (2) nurturing established or thriving life, or (3) preserving life in survival/dormant mode (*Westall et al., in prep.*).

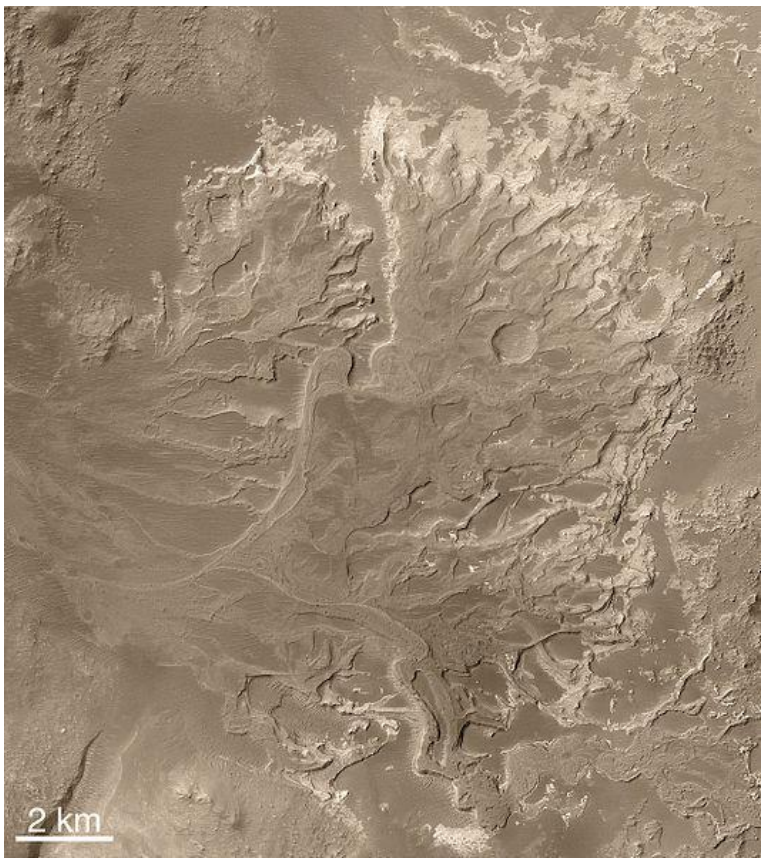

Figure 2.4: Fossilized delta in Eberswalde crater. Image courtesy of NASA.

Figure 2.4: Delta fossile dans le cratère Eberswalde. Image de la NASA.

On Mars, there is both mineralogical and geomorphological evidence for water on the surface and for aqueous/hydrothermal alteration. These minerals include various phyllosilicates (e.g. *Poulet et al., 2005*), sulphates (e.g. *McLennan et al., 2005* and *Gendrin et al., 2005*), carbonates (e.g. *Morris et al., 2010*), hydroxides (e.g. *Christensen et al., 2001* and *Arvidson et al.,*

2006), and amorphous silica (e.g. *Squyres et al., 2008* and *Ruff et al., 2011*). The distribution of the different mineral facies has been correlated to Martian surfaces of different ages. For example, *Bibring et al. (2006)* and *Mustard et al. (2008)* noted a concentration of Fe/Mg phyllosilicates, such as nontronite that formed under alkaline conditions in the oldest terrains, whereas more acidic phases, such as sulphates, are distributed on younger Late Noachian/Early Hesperian surfaces.

Some of the most ancient, altered terrains observed on Mars occur in Mawrth Vallis (e.g. *Loizeau et al., 2007, 2010*) in which a > 200 m-thick layered unit contains a high proportion of aqueous alteration products (as high as 50% after the model from *Poulet et al., 2008*), or in Nili Fossae where the crust has suffered a variety of alteration processes (*Mangold et al., 2007* and *Ehlmann et al., 2009*). The implication is that liquid water should have been stable at, or close to the surface for long periods and over large areas in order to be able to build such a large quantity and variety of hydrated units.

There are also numerous morphological features on Mars that suggest the presence of liquid water at the surface of the planet. Dendritic valleys (indicative of aqueous precipitation and/or sapping) flowed into craters and formed fans and deltas of river-deposited sediments, such as *Subur Vallis*, *Nepenthis Vallis* (*Kleinhans et al., 2010*), or the Eberswalde delta (Fig. 2.4). Layered material in some of the craters may represent, at least partly, sediments deposited in a lake, such as the Gale Crater, the landing site for MSL.

For early Mars, *Ehlmann et al. (2011)* proposed a hydrological regime largely driven by subsurface hydrothermal circulation characterised by ephemeral superficial water which culminated at the end of the Late Noachian while groundwater processes dominated in the Hesperian-Amazonian periods. Both the mineralogical and the morphological evidences indicate a degradation in the surface habitability of Mars from the mid Hesperian onwards (*Bibring et al, 2006* and *Carr and Head, 2009*). Decreased surface temperatures accompanied rarefaction of the atmosphere down to ~6 mbar, with consequent sublimation of at least part of the inventory of liquid water, the rest being trapped in a subsurface cryosphere (*Clifford et al., 2001*). After this period, low-lying areas that were rapidly filled with water, for example by catastrophic outflow channels, would have lost their water very quickly through sublimation in the tenuous atmospheric conditions that prevailed. Crater-lakes, however, if fed by an active hydrothermal system may have lived longer, but this activity still requires the presence of underground water (liquid or ice). Furthermore, recent studies suggest localized hydrothermal activity in impact craters, probably triggered by impact energy, which could

have created favourable environments for the presence of liquid water, even after the end of the presence of perennial liquid water at the surface (*Marzo et al., 2010*). Also there is some geomorphological evidence for short-lived aqueous activity, linked to volcanic activity (e.g. *Fassett and Head, 2007*). In conclusion, Mars appears to have been habitable in its early history but, in the late Noachian to early Hesperian, conditions at the surface radically changed. Habitable conditions became less favorable in the late Hesperian to Amazonian (Fig. 2.5).

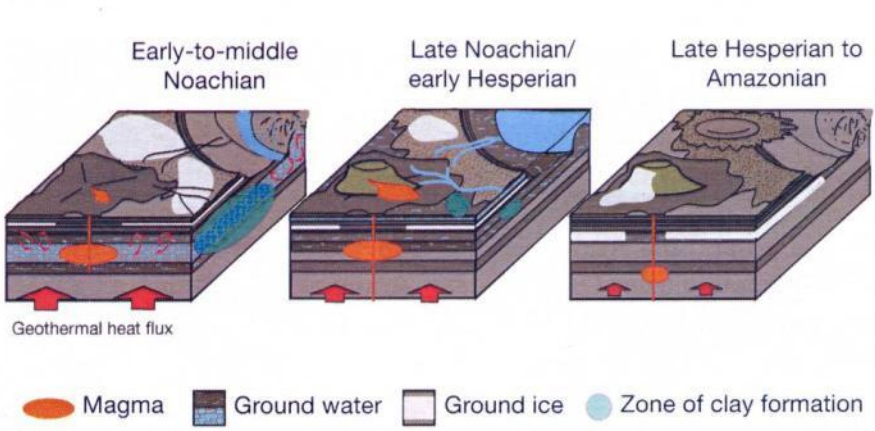

Figure 2.5: Changing habitability on Mars through time. After *Ehlmann et al. (2011)*.

Figure 2.5 : Evolution des conditions d'habitabilité de Mars en fonction du temps. D'après Ehlmann et al. (2011).

II.2.2 The search for traces of life on Mars

If life ever appeared on Mars, it would probably have been based on chemotrophy since the habitable conditions may not have been conducive to the appearance of phototrophy (*McKay, 1996; Westall et al., in prep*.). The lack of continuously habitable conditions may mean that Martian life forms remained at a primitive level of evolution. The first living cells would have had only a minimal number of metabolic and reproductive components and were probably very small. In comparison, on Earth, the oldest morphologically preserved cells (3.45 Gy, *Westall et al., 2006b* and *Westall et al., 2011*) are very small, <1 µm in size, and formed monolayer colonies on volcanic particle surfaces. Even today, subsurface chemotrophic

microorganisms are extremely small with diameters ~0.2 µm and they also form very small mono-layer colonies that are heterogeneously distributed on sediment particle surfaces (*Ciobanu, 2012*). Primitive Martian microorganisms may have had (and may still have, if there is extant life on the planet) similar characteristics.

Biosignatures in rocks are related to various aspects of microorganisms: their morphology, their organic constituents, or their metabolic processes (*Westall, 1999; Westall et al., 2000; Westall and Cavalazzi, 2011; Summons et al., 2011*). Cells, cellular products, such as extracellular polymeric substances, associations of cells, such as colonies, microbial mats, and bio-constructions (e.g. stromatolites, bioherms…) can be preserved through mineralization (fixation of minerals to the organic structures). On Earth, the identification of biosignatures in very ancient rocks is particularly controversial, not only because of the difficulty in correctly identifying the biosignature but also in terms of demonstrating its syngenicity with the formation of the rock (e.g. *Westall and Folk, 2003; Rasmussen et al., 2008*). On Mars, although any evidence of life will be of primary importance, whatever its age and relationship with the host rock, it will be equally important to understand the timing of the formation and emplacement of the biosignature in order to better interpret it. For instance, water-lain sediments may contain biosignatures related to colonies of chemotrophic organisms that inhabited the volcanic sediments and/or associated subaqueous hydrothermal environments, or organic molecules fixed to phyllosilicates. Once lithified, these same sediments and mineral deposits could host endolithic species in cracks or intergrain spaces. Nevertheless, in all of these cases, the organisms would be chemotrophs and the carbon and energy sources would be similar. Note that the volcaniclastic sediments in which the Early Archaean microfossils occur were strongly lithified by silica-saturated seawaters and by widely pervasive hydrothermal silica. They are now termed “cherts”.

II.2.3. Possible analogue samples from Earth

Following previous considerations on Martian habitability, we can consider that Martian life forms that could have appeared during the pre-Noachian/Noachian period would be relatively similar to those observed in Early Archaean sediments on Earth and that the same types of volcaniclastic/hydrothermal sediments with similar carbonaceous remains could be detected. To date, the oldest traces of cellular life on Earth, dating back to 3.45 Gy, have been found in the Kitty’s Gap chert (Pilbara, Australia) (*Westall et al., 2006b* and *Westall et al., 2011*). These traces of life are very

small (≤ 1 µm) and their fossilized expressions (microfossils, organic remains) are subtle. Their observation thus requires the use of sophisticated equipment, such as a SEM as shown in Fig. 2.6. Detection of comparable structures *in situ* on Mars will be impossible due to the limitations of space instrumentation, thus underlining the necessity of missions to return samples from Mars to the Earth for suitable analysis in the laboratory.

Because of the similarities in terms of lithology and microbial life forms, it was deemed important to include samples of the early Archaean cherts (silicified volcaniclastics and hydrothermal sediments) to the ISAR collection. Calibrating instruments with this type of samples is thus important in order to maximise the possibility of life detection (specifically in terms of organic molecules), in particular for the ExoMars mission.

►Figure 2.6: a- SEM micrograph of an irregularly shaped colony of silicified coccoidal microorganisms at the edge of a volcanic clast (HM—hydromuscovite). Slight recrystallisation of the quartz matrix (Q) has occurred at the lower edge of the colony. b- Detail of (a) showing two sizes of coccoidal cells in the colony, 0.4–0.5 µm (small arrow) and 0.7–0.8 µm (large arrow), embedded in film-like EPS. Some of the coccoidal cells exhibit compromise boundaries and appear to be dividing. c- Two sizes of dividing cells. Note their wrinkled surfaces. On the large individual (arrow), one side of the dividing cell is inflated while the other side is deflated, indicating that the latter cell is dead. d- This dividing cell is characterised by a meniscus between the two halves (small arrow) as well as a thin collapsed, wrinkled veil that coats it and appears as a ‘‘ghost’’ at the edges of the cell (large arrow). Modified after *Westall et al. (2011a).*

►*Figure 2.6: a- Images MEB de colonies de microorganismes silicifiés de forme coccoïdale au bord d'un grain d'hydromuscovite (HM). Une légère recristallisation de la matrice de quartz (Q) est observable en bordure de la colonie. b- Détail de (a) montrant des cellules coccoïdales de différentes tailles, 0,4-0,5 µm (petite flèche) et 0,7-0,8 µm (grande flèche), incorporées dans un film de type EPS. Certaines des cellules présentent des parois communes et semblent être en pleine division cellulaire. c- Deux cellules se divisant. On notera leurs surfaces ridées. Sur l'individu du dessus (flèche), un côté de la cellule en division est gonflé alors que l'autre est dégonflé, indiquant la mort de cette cellule. d- Gros plan sur la cellule en division qui se caractérise par un ménisque entre les deux moitiés (petite flèche) ainsi que par un petit effondrement, avec un voile froissé qui apparaît comme une structure « fantôme » sur les bords de la cellule (grande flèche). Modifié d'après Westall et al. (2011a).*

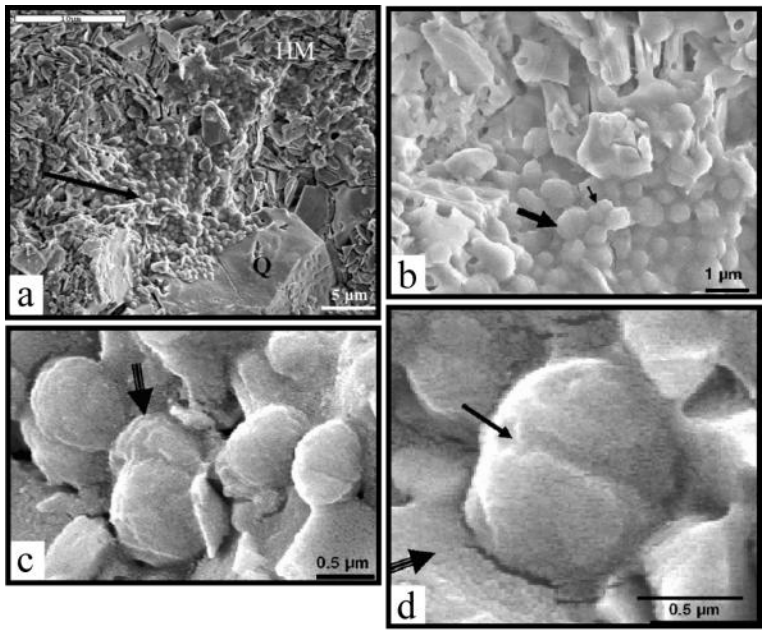

II.3. Earth versus Mars

Although terrestrial rocks are the most readily available ones for such a collection as the ISAR, many of these rock types are distinctly different in geochemical composition to those found on Mars. Even though Mars and the Earth are very similar in terms of origin, planetary formation and had somewhat similar environmental conditions in their early histories (e.g. presence of liquid water in the surface), the surface of Earth is very young due to the crustal recycling (e.g. plate tectonics and sagduction phenomenon). This phenomenon leads to important metamorphism on most of terrestrial rocks. Moreover, the water cycle and the biosphere are responsible for important weathering and alteration of terrestrial rocks throughout the geological history. By comparison with Mars, there are only a few locations on Earth where the rocks are older than 3 Gy, for instance in Greenland, Canada, Australia, South Africa and South America. Mars, on the other hand, is essentially composed by Noachian/Hesperian-aged terrains (Fig. 2.7).

The terrestrial Archaean rocks are essentially composed by magmatic rocks: tonalite, trondghemite and granodiorite (TTG) and volcanic rocks: komatiites, basalts and some andesite- rhyolites. These igneous rocks are associated with sedimentary derivatives that include the silicified

volcaniclastics noted above (cherts) and purely hydrothermal phases, such as hydrothermal chert and Banded Iron Formations (BIF) (the latter may or may not have a partly biogenic origin). All these rocks have undergone metamorphism ranging from low grade (prehnite-pumpellyite) to lowermost greenschistes facies, e.g. parts of the Pilbara in Australia and the Barberton Greenstone Belt in South Africa, Fig. 2.7; c.f. *Hofmann and Bolhar, 2007*) to very high grade conditions (amphibolite- granulite facies, e.g., the ISUA formation in Groenland, Fig. 2.7; e.g., *Rosing et al., 2011*).

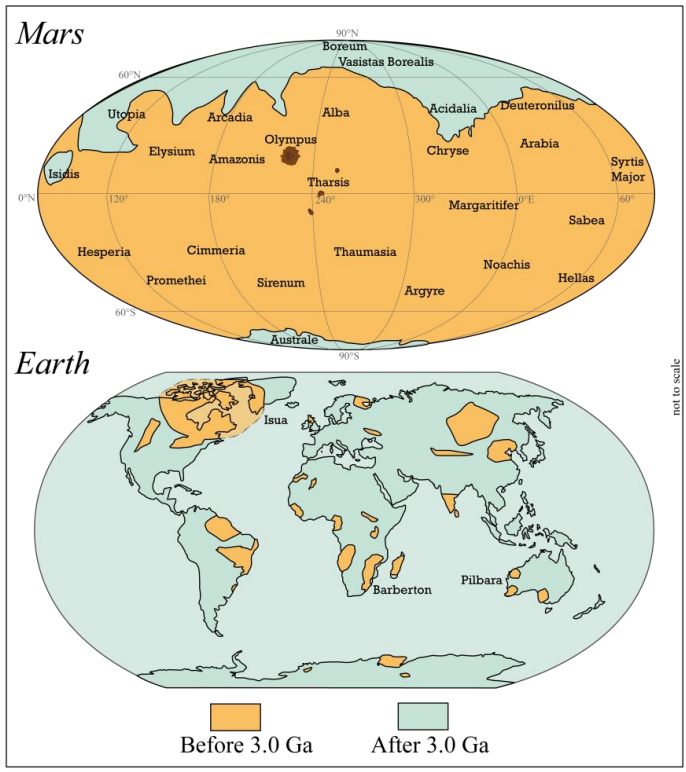

Figure 2.7: Maps comparing the general age of the surfaces of Mars and of the Earth. The surface of Mars is very old in comparison to that of Earth, where young terrains formed by plate tectonics, in particular the oceanic crust (in light blue), dominate. After *Soderblom and Bell III, (2008).*

Figure 2.7: Cartes des âges de la surface de Mars comparées à celle de la Terre. Comparativement à la Terre, la surface de Mars est essentiellement composée de vieux terrains. Cette différence est essentiellement due à la tectonique des plaques active sur Terre qui conduit notamment à la formation de la croûte océanique (en bleu clair). D'après Soderblom and Bell III, (2008).

Based on these considerations, for the preliminary suite of characterized rocks for the ISAR, I have selected a variety of terrestrial materials as Martian analogues. The selection process and the pertinence of this first set of samples for the ISAR will be described in the next chapter.

Mars (Résumé Français)

Mars est la quatrième planète rocheuse à partir du Soleil. Elle s'est formée en même temps que les autres planètes telluriques : il y a 4,564 milliards d'années. Mars est une petite planète dont la masse est seulement 1/10ème de celle de la Terre avec deux petites lunes, Phobos et Deimos, en orbite autour.

La structure interne de Mars est mal connue, mais il semble qu'elle possède un noyau et un manteau différencié. Cependant, aucune activité géologique n'a été observée en surface. La surface de Mars est caractérisée par une dichotomie globale: au Sud, des hautes terres avec de très grands cratères (comme Hellas Planitia) et au Nord, quatre kilomètres en-dessous des hautes terres du Sud, une surface beaucoup plus lisse. Les plus grands volcans du système solaire (e.g. Olympus Mons), de très grands canyons (e.g. Valles Marineris) et de nombreux cratères sont visibles à la surface de Mars. La planète ne montrant pas d'activité tectonique, l'ensemble des cratères est toujours visible ce qui permet de dater l'âge de la surface. Trois éons ont été déterminés : de 4.5 à 3.7 Ga le Noachien, de 3.7 à 3.0 Ga l'Hesperien et de 3.0 à aujourd'hui l'Amazonien. Récemment, les âges ont été redécoupés en fonction de l'analyse minéralogique de la surface en Phyllossian, Theiikina et Siderikian (Fig. 2.1).

Ce chapitre va décrire les différentes roches observées à la surface de Mars. Toute la surface n'a pas encore été cartographiée, mais il semble qu'elle soit essentiellement composée de roches volcaniques associées à différents sédiments issus de l'altération de basaltes. La surface de Mars est largement recouverte d'un régolithe, une épaisse couche de poussière rouge. Nous ne détaillerons pas cette formation en nous intéressant uniquement aux roches.

Les roches ignées observées à la surface de Mars sont essentiellement des matériaux pauvres en silice, composés globalement d'olivine, de pyroxènes et de plagioclases. Ce sont principalement des roches éruptives de type basaltique. Ces roches sont très similaires à leurs analogues terrestres, mais présentent un fort enrichissement en MgO (8 à 10 % poids), FeO (15 à 18% poids) et en Cl (>0,70% poids). Le diagramme TAS (où l'échantillon est représenté en fonction de sa teneur en SiO_2 et en Na_2O+K_2O) et le diagramme FeO/MgO-Silice (Fig. 2.2) reprennent l'ensemble des données obtenues sur les roches volcaniques de Mars. Les données TES sont obtenues à partir de l'orbite et doivent être considérées avec précaution. Quelques observations interprètent la présence d'andésites et de roches plus riches en silice. Faute de confirmation in situ, la question reste ouverte. Cependant il est possible de trouver une explication par l'altération des basaltes par de l'eau liquide qui favoriserait la formation de produits plus riches en silice. Les météorites SNC provenant de Mars (Shergottites, Nakhilites et Chassignites) sont quant à elles plutôt représentatives du manteau et non pas de la surface. Finalement, il n'a toujours pas été observé précisément de granitoïdes à la surface de Mars (Bonin, 2011).*

Les roches les plus abondantes après les basaltes sont les sédiments. Ces sédiments sont essentiellement dérivés de basaltes ou de sables basaltiques. L'eau est un des paramètres essentiels qui contrôle la formation de sédiments. Suivant les

variations de pH en surface, différents types de phyllosilicates se sont formés (ex : saponites, nontronites). Récemment, des travaux ont montré que les phyllosilicates pouvaient être formés sur Mars par des processus tardi-magmatiques comme le deuterisme. L'essentiel des argiles ont été interprétées à partir des mesures orbitales; ce sont des chlorites, vermiculites, saponites, nontronites et smectites. D'autres types de sédiments sont présents sur Mars. D'importants niveaux de silice ont été interprétés comme issus de l'activité hydrothermale, ou comme étant de la silice hydratée microcristalline (opale) déposée avec des tephras. Ce sont certainement des sources chaudes hydrothermales associées à du volcanisme datant de l'Hesperien à l'Amazonien. Des sédiments évaporitiques composés de jarosite de gypse et d'autres sulfates hydratés ont été décrits dans les hautes latitudes autour de la calotte polaire et dans divers endroits à la surface de Mars. Enfin, des traces ténues de carbonates ont été observées, principalement dans les météorites martiennes. La météorite AHL84001 en est un exemple célèbre car elle semble présenter des évidences de traces d'une vie passée provenant de Mars. La dernière preuve de présence de carbonates provient de l'affleurement Comanche vue par Spirit dans le cratère Gusev qui montre des carbonates associés à des olivines. Sur la figure 2.3 sont référencés plusieurs sites où ont été détectés ces roches et des minéraux particulièrement intéressants pour la recherche de vie : les carbonates, les sulfates et les minéraux hydratés.

Un des principaux objectifs des missions vers Mars est la recherche de preuves d'une vie passée ou présente. Quel type d'évidence pouvons-nous trouver ? L'habitabilité de Mars se résume à la capacité des organismes à trouver les ingrédients nécessaires à leur survie, à savoir : l'eau liquide, des molécules endogéniques et/ou exogéniques pour construire les macromolécules nécessaires à la vie cellulaire, une source d'énergie et des nutriments (H, N, O, P, S, et les métaux de transition). Ces deux derniers ingrédients peuvent être facilement obtenus sur Mars par les réactions redox à la surface des minéraux, et par l'altération des roches volcaniques, respectivement. Sur Mars, il existe maintenant de nombreuses preuves minéralogiques et géomorphologiques de la présence d'eau liquide à la surface et d'altérations hydrothermale ou aqueuse. La présence de minéraux hydratés comme les phyllosilicates, les sulfates ou encore les carbonates, les hydroxydes et la silice amorphe indiquent la présence d'eau liquide. L'observation de vallées dendritiques, de chenaux, de delta et de sédiments de rivière (voir Fig. 2.4) montre l'écoulement d'eau liquide en surface. D'après les datations de la surface, l'eau n'aurait coulée sur Mars qu'au Noachien, et avec un régime hydrologique éphémère. A l'Hesperien et à l'Amazonien, l'eau est uniquement présente en faible quantité sous la surface. En conclusion, seule la jeune Mars était habitable, puisqu'à partir de l'Hesperien les conditions deviennent de moins en moins favorables à la vie. L'hypothèse la plus probable est la présence d'une vie (dans les stades les plus évolués) relativement similaire à celle que l'on observe dans les sédiments Archéens (3.8-2.8 Ga) terrestres. Les plus anciennes traces de vie ont été détectées dans des chailles (cherts) de Kitty's Gap, Pilbara, Australie et sont datées à 3.45 Ga. Ces traces fossiles sont extrêmement petites (seulement quelques µm) et seuls des équipements tel que la microscopie à balayage électronique (MEB) sont en mesure de les détecter (voir Fig. 2.6). Pour la

constitution de la collection de l'ISAR, il apparaît essentiel d'ajouter des échantillons de chailles contenant ce type de fossiles.

Le choix des échantillons de la lithothèque doit se faire en prenant en compte la géologie de Mars. La manière la plus simple pour obtenir des échantillons analogues de Mars est de les collecter sur Terre. Cependant, les roches martiennes et terrestres ne sont pas identiques. En effet, si Mars et la Terre sont très similaires par leur origine et leur formation (même composition chimique, présence d'eau à la surface, ...), la surface de la Terre est beaucoup plus jeune à cause du recyclage de la croûte (liée à la tectonique des plaques ou aux phénomènes de sagduction). Par comparaison avec Mars, seuls quelques affleurements sur Terre sont des terrains Archéens (e.g. Abitibi, Canada et Pilbara, Australie) tandis que Mars est essentiellement composée de terrains Noachien et Hesperien (Fig. 2.7). De plus, les anciennes roches terrestres ont subi un métamorphisme important qui n'a pas eu lieu sur Mars.

A partir de ces considérations sur la géologie de Mars comparée à la Terre, je vais présenter la première sélection de roches analogues de Mars de l'ISAR. Le processus de sélection et la pertinence des échantillons seront décrits dans le prochain chapitre.

Chapter III
Selection and analysis of the first group of Mars-analogue samples

In this chapter, I present and describe the selection of the first group of Mars-analogue samples for the ISAR collection and the online data base. The choice of materials is based on the geology of Mars as described in the previous chapter and on the samples already available in the laboratory. The exobiology team of the CBM has a large collection of rocks, especially Archaean volcanic rocks, volcaniclastics and other sediments from South Africa, Australia, Canada, Svarlbard, and Greenland, provided by Frances Westall. Other samples were provided by Nick Arndt (ISTerre, Grenoble, France) and Silvio Rotolo (Universita di Palermo, Italia), and were also obtained during my own field trips to Rio Tinto (Spain), South Africa, the Troodos Ophiolite Complex (Cyprus), and in France (French Massif Central).

This chapter will mainly focus on the selection on the samples and the rationale for analogy to Mars. The emphasis is not on the results of all the samples (which are presented in the Appendice B and are available on the ISAR website), but rather to demonstrate the approach using relevant instrumentation on a few selected samples. The petrology of each sample and the results of the analyses will therefore be only briefly described and the pertinence of the results will be discussed[11]. I chose to present only the detailed results obtained on samples from Svalbard as an example in Appendice B. All the data are available in pdf file in the CD on the third cover page (for the print format) and on the ISAR website (for the numerical

[11]The content of this chapter is in review in PSS (*Bost et al., in review*).

format). Obviously, as the ISAR is an on-going project, new samples and new relevant techniques will be added in the future. The details of geochemical analysis are in Appendice C.

III.1. Analogue sample selection

III.1.1 Volcanic selection

A variety of volcanic rocks forms the core of the first group of rocks in the collection. The preliminary selection was mainly based on the elemental composition of the Martian basalts given by *McSween et al. (2009)* and displayed in Fig. 3.1. A certain number of samples with relevant compositions were already available in the laboratory collection, e.g. from Svalbard, Tenerife and South Africa (09SV15, 09TE08 and 07SA20 respectively).

The Svarlbard sample 09SV15 was chosen because it is associated with dunite xenoliths (09SV02) and carbonates (09SV05) that have been previously described as analogues of the carbonate deposits in the meteorite ALH84001 (*Treiman et al., 2002*). The dunite (09SV02) was also added to the collection as an analogue magmatic rock to the Martian mantle. Sample 09TE08 from Tenerife was chosen because it fits well with the Ca/Si vs. Mg/Si diagram proposed by *Mc Sween et al. (2009)*. This sample could be an analogue of the most altered Martian basalts (*Hurowitz et al., 2006*). Also note that altered volcanic rocks may sometimes contain evidence of life associated with alteration phases (*Furnes et al., 2007; Cavalazzi et al., 2011*). Sample 07SA20 from Barberton in South Africa was chosen because it is representative of alteration processes (silicification) associated with hydrothermal processes observed on the Early Earth. Such processes may have also occurred on Early Mars.

However, as noted above, all the terrestrial basalts are depleted in Fe and Mg. Moreover, sample 09SV15 has slightly higher Na_2O- and K_2O-contents than those of Martian basalts, whereas sample 09TE08 from Tenerife plots outside the limits of the TAS and FeO*/MgO-silica diagrams because of its high Na_2O- and K_2O-content and high FeO*/MgO ratio.

I added one sample from Etna (09ET01) to this collection, a "primitive basalt" that falls in the main Martian basalt field of the TAS diagram (Fig. 3.1). This sample was provided by Sylvio Rotolo (Universita di Palermo, Italia).

Finally, I added komatiites because they have been observed on Mars (see chapter II) and because they are similar in MgO-content to Martian basalts. Komatiites are very primitive lavas erupted at high temperatures, between 1560° and 1600°C (*Arndt, 2003*). These volcanic rocks have a high MgO-content of 18 wt% and a TiO_2-content of < 1 wt%. Komatiites are olivine and pyroxene cumulates characterized by an acicular "spinifex" texture (so named after the spiny grass common in the Pilbara region of Australia where komatiites outcrop). I sampled a highly altered komatiite in the Komatii River, South Africa (10SA09; see Insert 3) and Nick Arndt (ISTerre; University of Grenoble) gave me a relatively fresh komatiite from Dundonald, Canada (11CA02, *Arndt et al., 2004*).

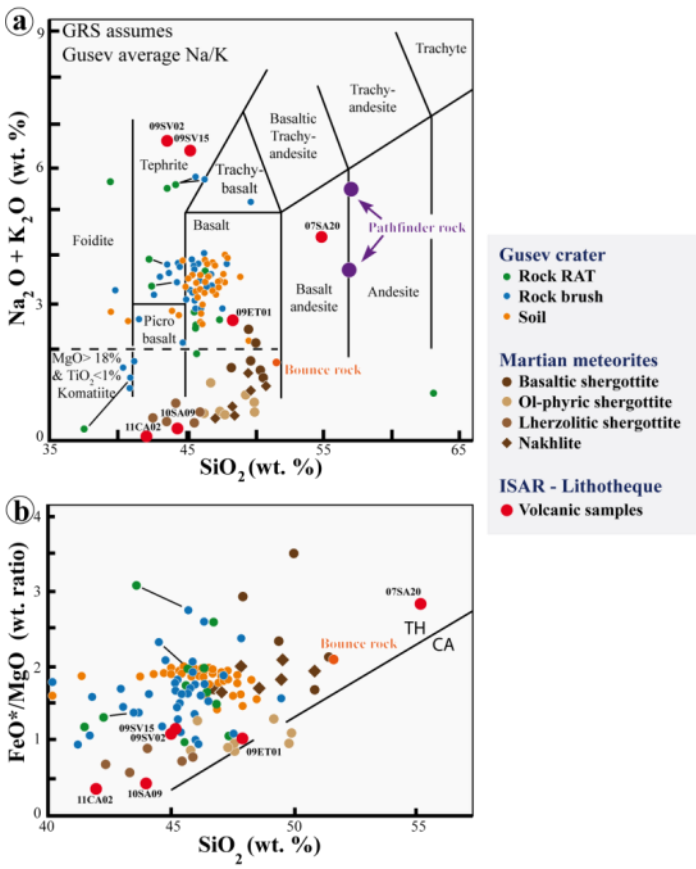

◄Figure 3.1- $Na_2O + K_2O$ oxides and FeO*/MgO ratios versus SiO_2 plots (in wt.%; 3.1a and 3.1b, respectively). The terrestrial volcanic samples presently included in the ISAR collection are also shown (red circles). Bounce rock is the only sample of basaltic origin that was analysed in the Meridiani Planum by the Opportunity rover (*Rieder et al., 2004 and Zipfel et al., 2004*). The FeO*/MgO-silica diagram is used for distinguishing dry tholeiitic (TH) and wet calc-alkaline (CA) rocks. All Martian samples are tholeiitic.

◄*Figure 3.1 Teneur en $Na_2O + K_2O$ et rapport FeO*/MgO en fonction de SiO_2 (en % poids), figures* 3.*1a et* 3.*1b respectivement. Les échantillons volcaniques terrestres de la collection ISAR sont représentés par les ronds rouges. L'échantillon « Bounce rock » est le seul échantillon d'origine basaltique trouvé et analysé sur Meridiani Planum par le rover Opportunity (Rieder et al., 2004 et Zipfel et al., 2004). Le diagramme FeO*/MgO- SiO_2 est utilisé pour distinguer les série tholeiitiques (TH) des séries calco-alcalines (CA). L'ensemble des roches martiennes est issue de la série tholeiitique.*

III.1.2. Sediment selection

Some of the sedimentary analogue rocks were chosen for their astrobiological relevance with respect to future missions to search for past traces of life on Mars. If life ever occurred on Mars, it was probably during the pre-Noachian/Noachian/earliest Hesperian periods, when liquid water was still present on the Martian surface. Remains of this primitive life could potentially be found in sediments and in altered volcanic rocks dating from this period. On Earth, sediments dating back to the same period are very rare due to crustal recycling. Therefore, only a few locations contain Early Archaean age volcanic sands and silts (volcanoclastics) deposited and altered in water. These lithologies have been largely preserved because they were silicified by silica-rich seawater and hydrothermal fluids (*Hofmann and Bohlar, 2007*). They host well preserved silicified mineralogical and organic traces of primitive life that were probably similar to Noachian microbial remains, if life existed on Mars (i.e. chemolithotrophs, cf. Chapter 2; *Westall et al., 2006a, 2011a* and *2011b*). Hydrothermal activity and siliceous fluids related to volcanism on Mars (*Ehlmann et al., 2009*) could have contributed to the preservation of Martian microorganisms (*Westall et al., 2011a*).

Many of the Early Archaean sediments from Australia and South Africa have been previously investigated by Frances Westall (e.g., *Westall et*

al., 2011a and references therein). For this study, we chose a 3.45 Ga old silicified volcanoclastic deposit from the Pilbara craton in NW Australia (00AU05). Early Archaean non-carbonaceous and carbonaceous hydrothermal cherts from the Barberton Greenstone Belt, South Africa (99SA01, 99SA05) and from the Pilbara (00AU04) were also chosen together with a Banded Iron Formation (BIF) sample (06AU01). BIFs have not yet been discovered on Mars but the high Fe-content of Martian rocks (15 to 18 wt%) (*McSween et al., 2009*) and the detection of hydrothermal silica-rich deposits on Mars (*Squyres et al., 2008*) suggest that BIFs may have deposited in aqueous basins in the early Martian history. BIFs consist of alternating Si- and Fe-rich layers formed in water. They were common on Earth during the Archaean and the Proterozoic. They were deposited in basinal settings through the oxidation of reduced Fe which was mostly introduced into the seawater by hydrothermal fluids. The exact origin of these sediments, *i.e.*, the mechanisms responsible for oxidizing the Fe (possibly microbial) and for the layering (seasonal/microbial?), is still highly debated (*Posth et al., 2010*). The selected BIF for this study was a ~ 3.5 Gy old sample from the Pilbara Craton in Australia.

As noted in the previous chapter, carbonates observed on Mars are associated with basalt alteration phases. The carbonate-alteration of basalts in the Comanche outcrop produced Fe-Mg-rich phases (*Morris et al., 2010*). The secondary carbonates observed in the ALH84001 meteorite were also zoned Fe and Mg carbonate phases (*Borg et al., 1999; Treiman et al., 2002*). Thus similary zoned carbonates in terrestrial rocks were chosen. They were deposited by hydrothermal exhalations/fluids (and possibly aqueous alteration during eruption under a glacier) in a recent basalt (≈100 ky) from Svalbard. They were collected by Frances Westall during the 2009 AMASE mission (sample 09SV05; cf. *Treiman et al., 2002; Steele et al., 2007*). In order to complete the carbonate selection, I sampled carbonates in hydrothermal veins (stockwerk) associated with pillow basalts in the Troodos ophiolitic complex in Cyprus (11CY04). Details concerning the Cyprus mission are described in Chapter IV. Table 3.1 lists the samples, their origin and relevance for Mars.

►Table 3.1: List of the analogue samples characterised for the ISAR collection and their proposed Martian equivalents.

►*Tableau 3.1: Liste des échantillons analogues caractérisés pour la collection de l'ISAR et des exemples d'équivalences martiennes.*

Type	ISAR number	Name	Origin	Martian analogue (e.g).
Volcanic rocks	09ET01	Primitive basalt	Etna volcano, Italy	Basalt (Gusev)
	09SV15	Picritic basalt	Svalbard, Norway	Basalt (Gusev)
	09TE08	Altered phonolite	Tenerife, Spain	Soils and altered rock
	07SA20	Altered basalt (silicified)	Barberton, South Africa	hydrothermal activity
	11CA02	Komatiite	Dundonald, Ontario, Canada	Komatiite
	10SA09	Altered Komatiite (silicified and carbonated)	Barberton, South Africa	Altered komatiite
Magmatic rock	09SV02	Dunite (xenoliths)	Svalbard, Norway	Martian mantle
Sedimentary rocks	09SV05	Mg-Fe-rich carbonates (associated with basalt)	Svalbard, Norway	Carbonates (ALH84001meteorite, Comanche outcrop)
	11CY04	Hydrothermal carbonates	*Skouriotissa*, Cyprus	Carbonates (Comanche outcrop)
	99SA01	Carbonaceous hydrothermal chert	Barberton, South Africa	Various hydrothermal silica deposits with possible iron concentrations and opaline silica. Theses rocks can contain traces of early life on Mars (Eastern Valley; Home Plate, Gusev crater; Meridiani Planum (+ Haematite), along Valles Marineris rift).
	99SA05	Hydrothermal chert sill in silicified volcaniclastic sediments	Barberton, South Africa	
	06AU01	BIF	Pilbara, W Australia	
	00AU05	Silicified volcanic sediments (chert)	Kitty's Gap, W Australia	
	00AU04	Hydrothermal Chert vein in pyroclastic volcanic sediments	Kitty's Gap, W Australia	
	10AR01	Nontronite	Artificial Sample	Phyllosilicates associated with altered basalt. (Mawrth Vallis)

III.2 Sample description

III.2.1. Volcanic rocks

III.2.1.1. **09ET01**, a "primitive" basalt.

This sample comes from the Etna volcano, located on the eastern coast of Sicily. Etna is a basaltic stratovolcano renowned for its frequent effusive eruptions. Although the Etna lavas are compositionally picritic, the ISAR sample comes from one particular horizon of Etna lavas characterised by a "primitive", non-fractionated composition. "Primitive" lavas are rare on Earth but must have been common on Mars (e.g. *Mc Sween et al., 2009*). The sample, dated at 3930 ± 60 BP (*Coltelli et al., 2000*), originates from a sub-plinian eruption which created 0.183 km^3 of scoria lapilli with 30 to 60 % of microvesicularity (*Coltelli et al., 2005*). The magma was derived from fractionation products of mantle-derived magmas (*Kamenestsky et al., 2007*) formed in association with subduction activity beneath the Appenines (*Tonarini et al., 2001*).

The sample is a microvesiculated tephra composed of olivine-rich scoria lapilli and rare cognate lithic clasts. The hand specimen surface is brown and an occasional orange crust around individual olivine grains is a sign of oxidation. Large olivine grains (1-2 mm) are present (Fig. 3.2a). In microscopic view, the sample is composed of brown (oxidized) and black (non-oxidized) lapilli <1 cm in diameter. Mineralogically, the rock consists of large blocky olivine (Fo91) crystals and smaller euhedral olivine crystals associated with pyroxenes (diopside, Mg#92.5) in a basaltic glass (Fig. 3.2b). Some small plagioclase crystals occur in the pyroxene matrix. The basalt contains some Cr-spinel grains. The chemical composition of this sample is close to the average Martian basalt composition (Fig. 3.1).

III.2.1.2. **09SV15**, a tephritic basalt

The "tephritic-basalt" sample has the same provenance as the dunite xenolith (09SV02) and one of the carbonate (09SV05) samples. They were obtained from two quaternary stratovolcanoes (≈100 Ky), Sverrefjell (N79°26,255; E013°20,486) and Sigurdjfell (N79°16,119; E013°32,235), on the island of Svarlbard, north of Norway. The two volcanoes are very similar in their magmatic structure and petrography. They were formed by off-ridge

alkali basaltic volcanism associated with the opening of the Artic Basin and the Greenland Sea (*Skelkvåle et al., 1989*). They are primitive and ultramafic basalts containing approximately 20 % xenoliths (mantle dunites, sample 09SV02, and some gneissic crustal elements). The two volcanoes are aligned along the Bockfjord, parallel to an important fault which defines the contact between a major Devonian (416 to 374.5 My) graben, filled with Devonian red-beds (molasse), and Caledonian basement rocks of the Heckla Hoek formation. Quaternary volcanism is subactive and associated with hot springs. (for more information see *Skjelkvåle et al., 1989* and *Fookes, 2008*).

Sample 09SV15 is a massive and highly vesicular basalt with vesicle sizes ranging from 1 to 5 mm. The outer surface of the hand specimen shows some brownish grey bleaching, indicating very minor weathering. The fresh basalt surface is dark grey. Dunite xenoliths up to 2 cm in size and some macroscopic olivine grains (0.5-1 mm size) can be observed in the basalt (Fig. 3.2b). The mineralogy of the primitive basalt is olivine (Fo_{90}) occurring as phenocrysts with pyroxenes ($Mg_{\#57}$) and associated with plagioclase microlites and minor glass (Fig. 3.2c). Secondary minerals include amphibole, oxides and spinels. This sample has the particularity of containing quartz grains, possibly a xenolithic contribution.

The rock has a chemical composition which is relevant for tephrite-type basalts (Fig. 3.1), rich in alkali elements, on Mars. Its textural and mineralogical characteristics, typical for this type of basalt, will be readily identifiable using the instrumentation available for the upcoming Mars missions.

III.2.1.3. **09TE08**, altered phonolite

This is an altered "phonolitic-basalt" from the El Teide volcano (N28°261379; E-16°594848) on the island of Tenerife in the Canaries archipelago off western Africa. Tenerife is the exposed part of a giant volcanic edifice that extends from the floor of the eastern central Atlantic at – 3700 m to + 3718 m at the summit of the volcano. Its subaerial history began in the late Miocene and is associated with mafic to intermediate monogenic cones and fissure systems along the Santiago rift to the NW and the Dorsale rift to the NE. The volcano produces different types of magmas, especially basalts and phonolites (*Ablay and Marti, 2000*).

This sample is a black massive rock with microvesicularity and some vesicles resembling cracks. The weathered surface of the rock is brown (Fig. 3.2e). In thin section, the matrix is composed of elongated plagioclase without

preferential orientation in a matrix containing euhedral and subeuhedral amphibole, apatite, spinels and some quartz grains. The rock is well crystallised, although discrete preferential orientation of the plagioclases could indicate a "paleoflow" lava stage during its formation (Fig. 3.2f). This phonolite contains some amphibole and other hydrous silicates, indicating a water-rich melt. This sample has characteristics that make it a good chemical analogue of weathered Martian basaltic rocks.

III.2.1.4. **07SA20**, silicified basalt

This sample is a silicified basalt from the Kromberg Formation (3.42-3.33 Gy) of the Onverwacht Group in the Barberton greenstone belt in South Africa (S26°02'08"; E30°59'55"). These pillow basalts were erupted under water. High seawater silica-contents and hydrothermal silica enrichment of the Early Archean seawater led to the silicification of the basalts and to interlayred sedimentary deposits (cf. *Hofmann and Bohlar, 2007*). In spite of their archean age, the basalts are well-preserved, having been affected only by lower greenschist metamorphism.

In hand specimen, the sample is a massive green rock with a fine-grained vesicular texture and a weathered brown crust (Fig. 3.2g). The surface of the pillow basalt is characterized by a vitreous crust. *Furnes et al. (2007)* described purported fossil traces of microbial activity in these types of vitreous rinds from similar Barberton basalts. In thin section, the basalt consists of glass with major plagioclase associated with microlites of amphibole and other accessory minerals, such as spinels and clinochlore (Fig. 3.2h). Calcite occurs in the vesicles. The basaltic glass has been altered to chlorite and clays. The ubiquitous presence of quartz shows that the bulk sample is highly silicified. The Early Archaean silicified altered pillow basalt 07SA20 from Barberton could be comparable to pre-Noachian/Noachian Noachian basalts formed in silica-enriched seawater and/or under the influence of silica-dominated hydrothermal activity (on Mars, there were no silica sinks such as siliceous microorganisms).

III.2.1.4. **11CA02**, komatiite

This sample is a relatively fresh komatiite from Dundonald, Ontario in Canada. Dundonald Beach is situated in the Kidd-Munro formation (2,719-2,710 Gy) of the Abitibi Greenstone Belt. The sample, provided by Nick Arndt, was collected from the upper part of a 5 meters vertically zoned

intrusive sill (*Arndt et al., 2004*). It was sampled about 25 cm beneath the upper contact.

The rock is massive and dark-coloured with a thin brownish alteration layer. The polished face shows centimetre long, acicular pyroxenes and altered dark olivines with a spinifex texture (Fig. 3.2i). In thin section, the pyroxene crystals are zoned: their augitic core is replaced by pigeonite in the outer parts (Fig. 3.2j). The olivines are altered to hydrothermal amphibole (tremolite-actinote, formed between ~300°-350°C) that are elongated and often show skeletal overgrowths. They are associated with Ti-spinels and a few sulphides (Ni-Fe).

Insert 3: The Barberton Greenstone Belt and the Komatii River.

In summer 2010, I participated in a field trip organized by A. Hofmann and F. Westall in the South African Barberton Greenstone Belt. Outcrops along the Komatii River belong to the *Hooggenoeg Formation*. This formation consists of pillowed and massive basalts, as well as spinifex-textured komatiitic basalt with thin intercalated silicified sedimentary horizons. At the top of the sequence are dacitic rocks and a thin sedimentary unit. The volcanic rocks have been dated to 3.445 Gy (*Armstrong et al., 1990*). This was the opportunity to collect komatiite samples along the Komatii river (Fig I3) and to include them in the first group of analogue samples for the ISAR. Other samples were also collected but have not yet been studied (various basalts and silicified sediments).

Figure I3: View of the Barberton Mountains and the Komatii river.

III.2.1.5. **10SA09**, altered komatiite

This sample originates from the type locality on the Komatii River in the Barberton Greenstone Belt, South Africa (S26°01'65"; E30°59'35"; Insert 3). The sample comes from the Kromberg formation (3.42-3.33 Gy) in the Onverwacht group. These rocks, similarly to the silicified basalts from Barberton (cf. sample 07SA20 hereabove), have been affected by lower greenschist regional metamorphism. The sample is a silicified komatiitic basalt with a highly altered spinifex texture. The structure and the bulk chemical composition however are still preserved. Silicification aided preservation of the rock although it also induced a marked loss of Ca, Al and Mg.

The weathered surface of the rock shows altered spinifex texture (Fig. 3.2k). In a cut surface, the sample has a textureless, almost glassy appearance. Thin section study documents significant alteration. Although the sample still exhibits the typical olivine spinifex texture, the olivines are totally altered to amphibole and phyllosilicates (Fig. 3.2l). Some talc fibres can be observed. The other major phase, pyroxenes are also altered to talc, micas and phyllosilicates (originally clays, now mica). Some accessory grains of iron oxide, such as hematite, occur together with dolomite.

The komatiite samples 11CA02 and 10SA09 are particularly relevant because they are primitive Mg-rich basic volcanics, typically abundant in the Archean period on Earth and possibly on Mars in Noachian terranes (*Nna-Mvondo and Martinez-Frias, 2007*).

III.2.2. Plutonic rocks

III.2.2.1. Sample **09SV02** : Dunite

Dunite xenoliths occur in the tephritic basalt from Svalbard (sample 09SV15). The dunite is a coarsely crystalline (1-2 mm grain size) green coloured rock (Fig. 3.2m). The rock consists of olivine and pyroxene (enstatite) associated with spinels (Fig. 3.2n). Where altered at their edges, the dunite xenoliths are marked by a reduction in grain size. This sample could be an analogue of possible Martian deep crustal or mantle rocks exposed at the surface due to an impact or an eruption. Similar samples could be identified *in situ* on Mars using the instrumentation available for the 2011 and 2018 missions.

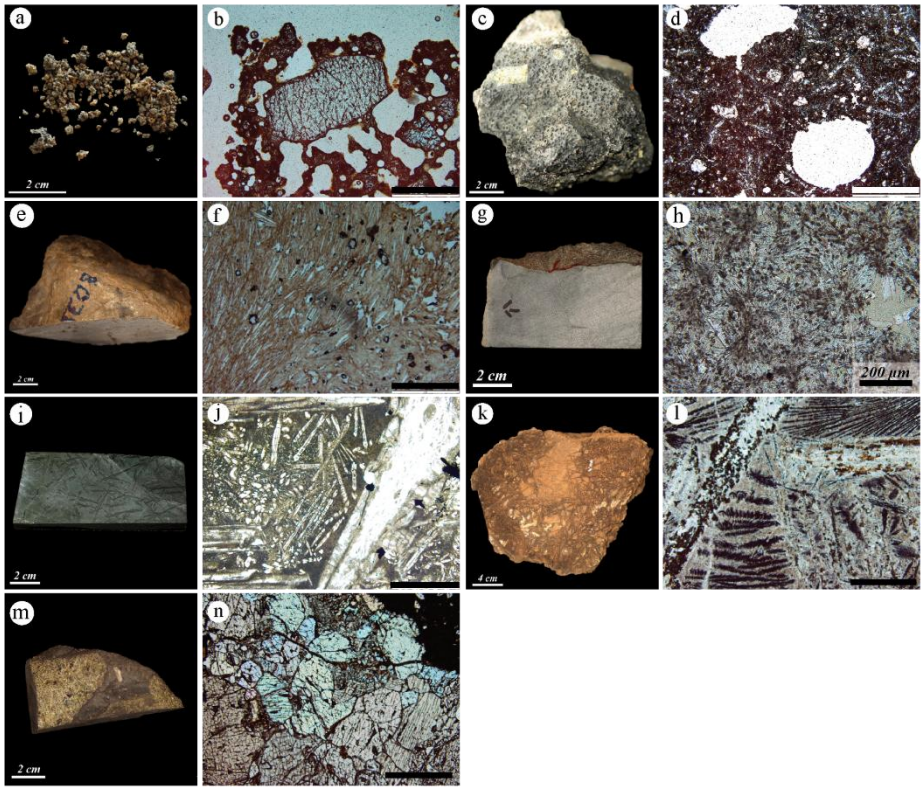

Figure 3.2: Macroscopic (a, c, e, g, i, k and m; scale bar is 2 cm, unless specified) and microscopic views of the volcanic and plutonic Mars analogue samples (b, d, f, h, i, l and n transmitted light microphotographs of thin sections, scale bar is 1 mm unless specified). a, b- primitive basalt 09ET01; c, d- picritic basalt 09SV15; e, f- altered phonolite 09TE08; g, h- altered silicified basalt 07SA20; i, j- komatiite 11CA02; k, l- altered komatiite10SA09 and m, n- xenolithic dunite 09SV02.

Figure 3.2: Photographies (a, c, e, g, i, k et m; barre d'échelle = 2 cm, sauf autre précision) et microphotographies des échantillons volcaniques et plutoniques analogues de Mars (b, d, f, h, i, l and n en lumière polarisée non analysée, barre d'échelle = 1 mm sauf autre précision).). a, b- basalte primitif 09ET01; c, d- picro-basalte 09SV15; e, f- phonolite altérée 09TE08; g, h- basalte silicifié 07SA20; i, j- komatiite 11CA02; k, l- komatiite altérée 10SA09 ; m, n- dunite 09SV02.

III.2.3. Sedimentary samples.

III.2.3.1. **09SV05**, hydrothermal carbonates

This sample is a carbonate crust from a fumarole vent in the tephritic basalts from the Sigurdfjell volcano in Svalbard. These carbonates are associated with low vesicular basalt with dunite xenoliths (samples 09SV15 and 09SV02, respectively). The zoned carbonates were deposited by hydrothermal exhalation or possibly by aqueous alteration during eruption under an ice cap (*Steele et al., 2007; Amundsen et al., 2011*).

This sample is a basaltic breccia cemented by carbonates (Fig. 3.3a). The basalt contains a small vesicular dunite xenolith (<3 mm of diameter). The basalt breccia fragments are coated and cemented with mamillated carbonates having a brown colour (cf. Chapter III.2.1.2. 09SV15). In thin section (Fig. 3.3b), the carbonate crusts are zoned parallel to the basalt fragment surfaces, indicating chemical evolution. The carbonate phase immediately adjacent to the basalt surface is dolomite, followed by ankerite with magnesite representing the outermost layer. Carbonate rosettes also occur within vesicles in the basalt and have been compared to those in the ALH84001 Martian meteorite (*Treiman et al., 2002*).

III.2.3.2. **11CY04**, carbonates in altered pillow basalts

This sample is a hydrothermal carbonate associated with the upper unit of pillow-lavas, which constitutes the top of the Olympos sequence of the Troodos ophiolitic unit, in Cyprus (N35°04756; E32°54583). This ophiolitic sequence dates from the Upper-Cenomanian to Lower-Campanian (*Ministry of Agriculture, natural resources and environment, Government of Cyprus, 1995*). The sample was obtained from a network of carbonated hydrothermal veins (stockwerk).

The hand specimen (Fig. 3.3c) is characterized by a clear carbonated microlitic cement enveloping angular clasts (up to 1 cm) that was sampled from the upper pillow basalt in the ophiolitic series. The carbonate precipitate is banded and highly vesicular (Fig. 3.3d). The partially altered basaltic clasts are composed of orthoclase, augite, phyllosilicates (montmorillonite group)

and minor anatase (determined by Raman). Some rare euhedral calcite-dolomite crystals are also visible.

III.2.3.3. **99SA01**, carbonaceous chert

This sample is a carbonaceous hydrothermal chert vein from the Buck Reef Chert (3.42 Gy), Kromberg Formation of Overwacht Group, Barberton Greenstone Belt, South Africa. It was a feeder vein that follows a syn-sedimentary growth fault cutting across the underlying volcanics and into sedimentary layers that were deposited in a large basinal structure. The fault was probably active during sedimentation and certainly after sedimentation.

The sample is a massive black chert with some white quartz veinlets (Fig.3.3e). In thin section, the chert has a fine-scale granular texture consisting of small carbonaceous particles in a micro-crystalline quartz matrix (Fig.3.3f). Part of the sample consists of brecciated material having the same compositional and textural characters. Small pyrite grains occur as accessory minerals.

III.2.3.4. **99SA05**, hydrothermal chert vein

This sample consists of stratified silicified sediments from the Buck Reef Chert (3.42 Gy), Kromberg Formation of the Overwacht Group of the Barberton Greenstone Belt, South Africa that have been infiltrated parallel to the sediment layers by a hydrothermal chert vein. The infiltration occurred possibly during diagenetic or post diagenetic lithification of the sediments by silicification (a rapid process, cf. *Hofmann and Bohlar, 2007*).

The hand specimen is a laminated black and white chert. The original sedimentary layering and sedimentary textures can still be seen, as well as intrusive layers of hydrothermal chert, parallel to the bedding. Laminae thicknesses range from 2 mm to 2 cm (Fig. 3.3g). The laminated texture and sedimentologic structures are highlighted on the weathered surface of the sample whereas the unweathered surface is uniformly black and the structures are difficult to see. In thin section, the hydrothermal chert layer consists of uniform microcrystalline quartz. Intrusion of the hydrothermal layer into the sediments caused brecciation of the upper contact. Rare carbon-containing inclusions occur within the hydrothermal chert. The host rock consists of layers of volcanic clasts (1-5 mm) that include a horizon of long slivers of silicified, finely laminated carbonaceous clasts (Fig. 3.3h). These may represent fragments of silicified microbial mats (cf. *Tice and Lowe, 2004;*

2006; Tice, 2009). The whole sediment was lithified prior to intrusion of the hydrothermal vein. Such rock could be observed on Mars around hydrothermal vent, in particular associated with impact craters.

III.2.3.5. **06AU01**, Banded Iron Formation (BIF)

This BIF sample originates from the Coppin Gap Greenstone Belt, Pilbara Craton in Australia (E20°53'00'', S120°06'40"). Stratigraphically, it belongs to the Panorama Formation of Warrawoona Group, as does the silicified volcanic sand (00AU05) from the nearby-located Kitty's Gap Chert (see below).

This rock is a fine-grained, red and white laminated chert. The laminae range from 0.5 to 2 cm in thickness (Fig. 3.3i). Fe-stained fractures and fractured layering can be seen on hand specimen. The weathered surface is composed of fine-grained goethite-hematite and other undefined nanophased iron oxides. In thin section, the white layers consist of microcrystalline quartz (Fig. 3.3j). They are extremely finely layered, the laminae having thicknesses of 10-100 µm. The layers are delicately wavy or occur in ~1 mm thick packets of conformable laminae. Soft sediment deformation structures occur. The red layers are rich in fine-grained iron oxides. At the contact between the Fe-poor and Fe-rich layers are large lozenge-shaped crystals of pseudomorphosed dolomite (now Fe oxide). The Fe-rich layers exhibit ghost layering similar to that in the Fe-poor layers. The whole sediment is criss-crossed by fine Fe-rich or Si-rich fractures. Stylolites also occur.

Although BIFs have not been detected on Mars, the high Fe-content of Martian rocks and the evidence for hydrothermal silica suggest that such (bio?)-chemical sediments could be found on Mars.

III.2.3.6. **00AU04**, hydrothermal chert from Kitty's Gap

The sample (S20°53'45"; E120°04'40") belongs to the Panorama Formation of the Warrawoona Group, Pilbara, Australia. The chert vein, sourced in the underlying felsic volcanic, crosscuts the basal sediments of the Kitty's Gap Chert. Intraformational brecciation of the lowermost layers of the sedimentary horizon indicates that the hydrothermal activity was coeval with sediment deposition (3.446 Gy).

This sample is a 2 cm-thick black vein penetrating volcaniclastic sediments and dominently consisting of pumice fragments, 5 mm in size (Fig. 3.3k). In thin section, the microcrystalline quartz vein is basically featureless except for some rare carbon- and anatase-containing inclusions (Fig. 3.3l). Although silicified, the vesiculated pumice fragments are well preserved. Some 0.5 mm-long euhedral crystals having a lozenge-shape and coated with anatase might be ghost zircons (*Orberger et al., 2006*).

III.2.3.7. **00AU05**, Silicified volcanic sediments (Chert) from Kitty's Gap

This sample is a silicified volcanic sand/silt from the 3.446 Gy-old Kitty's Gap Chert which occurs in the Panorama Formation of the Warrawoona Group Pilbara Craton, Australia (*de Vries et al., 2004*). Like the BIF sample described above, it is located in the Coppin Gap Greenstone Belt (S20°53'45"; E120°04'40''). The outcrop consists of laminated black and white chert representing silicified volcanic sands and silts deposited in a mud flat/tidal channel environment. The sedimentary structures, including ripple, channel and flaser bedding, are clearly visible. The sediment contains cryptic mineralogical and carbonaceous traces of life (*Westall et al., 2006b; 2011a; Orberger et al., 2006*).

The sample is characterised by submillimetre- to millimetre-thick black and white laminae (Fig. 3.3m). The laminae are more visible on the weathered rock surface than on the unweathered one. Sedimentary structures include ripple bedding (bimodal), flaser linsen bedding and channel bedding. Layers of small pumice fragments (<0.5 cm diameter) also occur. Thin section analysis shows that the differences in colour between the black and white layers are related to grain size, the darker layers being finer-grained than the white layers (Fig. 3.3n). The sediment consists of volcanic clasts, now replaced by hydromuscovite and Ti-oxide spherules (cf. *Orberger et al., 2006*) in a silica matrix. A chert vein mainly consisting of featurless microcrystalline quartz traverses the silicified sediment. Similar chert veins have also formed bedding parallel intrusion sills. This sample hosts traces of life in the form of microfossils and organic molecules (*Westall et al., 2006a; 2011a*). This type of sample could host similar traces of primitive life on Mars.

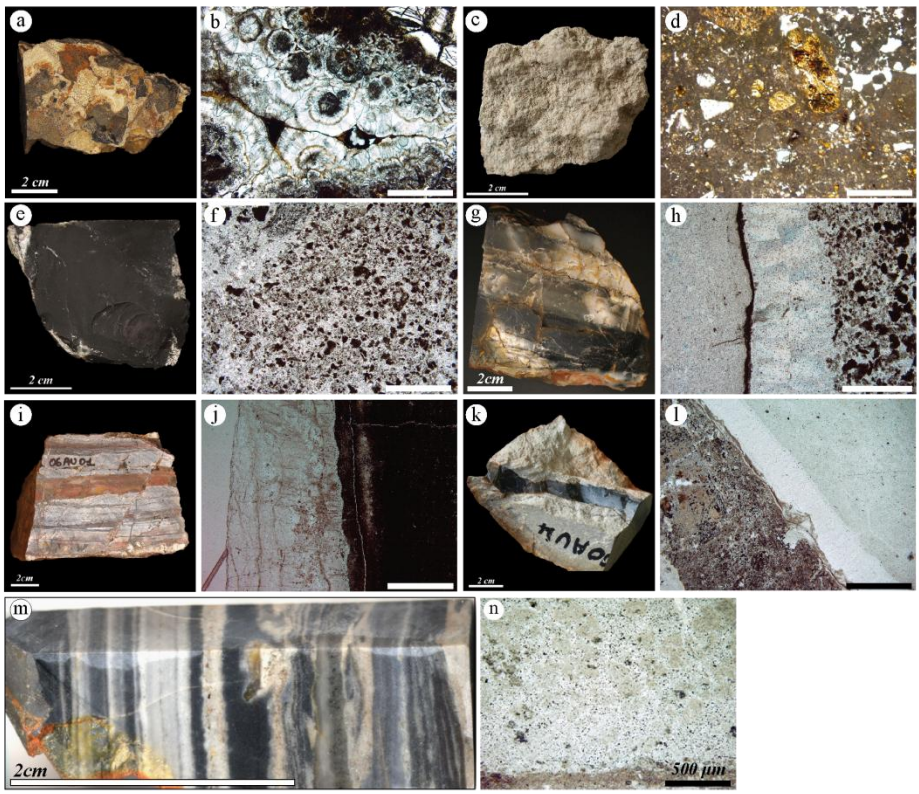

Figure 3.3: Macroscopic (a, c, e, g, i, k, and m scale bar is 2 cm) and microscopic views (transmitted light micrographs of thin sections, scale bar is 1 mm unless specified) of the Martian analogue samples. a, b- carbonates 09SV05; c, d- hydrothermal carbonates 11CY04; e, f- carbonaceous hydrothermal chert 99SA01; g, h- hydrothermal chert 99SA04; i, j- BIF 06AU01; k, l- hydrothermal chert 00AU04 and m, n- silicified altered volcanoclastic sediments 00AU05.

Figure 3.3: Photographies macroscopiques (a, c, e, g, i, k et m; barre d'échelle = 2 cm, sauf autre précision) et microscopiques des échantillons sédimentaires analogues de Mars (b, d, f, h, i, l and n en lumière polarisée non analysée, barre d'échelle = 1 mm sauf autre précision). a, b- carbonates 09SV05; c, d- carbonates hydrothermaux 11CY04; e, f- chaille carbonée hydrothermale 99SA01; g, h- chaille hydrothermale 99SA04; i, j- BIF 06AU01; k, l- chaille hydrothermale 00AU04 et m, n- sédiments volcanoclastiques silicifiés 00AU05.

III.3. Results and discussion

In this section, I summarize the analyses of each sample using laboratory instruments. The analyses were made either on the rough rock surface, on powder preparations or on thin sections with high performance laboratory instruments. When possible, analyses were also made on the weathered surface. All the textural and compositional information is accessible in the ISAR on-line database: http://www.isar.cnrs-orleans.fr.

A qualitative evaluation of the reliability of identification of structure, texture, mineralogy or composition by the individual instruments is given in Tables 3.2 and 3.3 and shown by the following symbles: (++) for unambiguous identification with the instrument, (+) for probably identification, (-) for ambiguous identification, (--) for non-identification.

There are necessarily some differences in the performances of the instruments presently used to characterize the ISAR rocks and those that will be used during the MSL and ExoMars missions. This study demonstrates that, even using laboratory equipment, some common rocks on Mars (for example volcanics) can hardly be unambiguously identify. This is all the more true if the instruments have not been previously calibrated, demonstrating thus the utility of the ISAR.

It is worth noting that some of the experimental settings are not exactly the same between the laboratory and flight instruments. For example, all the XRD analyses were made in a fine capillary with a Co generator, whereas the XRD analyses made during the ExoMars-2018 mission analytical laboratory will be made with a Fe^{50} generator (those made with the ChemMin instrument on MSL will use a Co generator). The IR instrument in the ExoMars rover, MicrOmega, will operate in reflection mode while our analyses were made in transmission mode. Variations in instrumentation settings make it all the more important to test flight instrumentation with the same suite of samples. This study also underlines the importance of using different instruments to facilitate rock identification. In certain circumstances, even the absence of a signal from an instrument can aid interpretation.

The first results demonstrate the limitation of using powder preparations for making geologically-relevant interpretations. Textural and structural information based on macroscopic and microscopic observations, in

association with mineralogy and elemental chemistry, are essential for determining rock type and history and, hence, the relevance of the rock for habitability and its potential for preserving signatures of life. In the laboratory, the Raman, XRD, IR instruments give only partial data on a powder (e.g., in the case of Raman spectroscopy, *Foucher et al. 2011; 2012*). On Mars, where the resolution of the rover instruments will be less than that of the laboratory instruments, we estimate that only about 50% of the minerals used in our study could be undoubtedly identified. On Mars, determination of rock type will depend heavily on the colour panoramic camera together with the colour microscope (acting as the geologist's hand lens). An abrasive tool to obtain a smooth surface for observation and analysis with the microscope will be very important for rock identification and, in the case of the ExoMars mission, for selecting rocks relevant to the search for traces of life. In the future, the combination of Raman spectral mapping enhanced by complementary cathodoluminescence imagery could provide very useful information on mineralogy, texture and structure, as shown in A

►Table 3.2. Comparison of textural, elemental and mineralogical data obtained for the selected volcanic and magmatic rocks using different instruments and different sample preparations (rock surface, powder, thin section). (++) unambiguous identification, (+) probably identification, (-) identification ambiguous, (--) identification impossible. Macro.: Macroscopic view, Micro.: Microscopic view, P.: Powder, W.S. : Weathered surface, T.S.: Thin section - * Raman spectrum only - The hatched area indicates that the measurement is not applicable for a specific instrument.

►*Tableau 3.2. Comparaison de la texture, des données élémentaires et minéralogique des échantillons volcaniques et magmatiques à partir des différents instruments et des différentes préparations (surface brute de la roche, poudre et lame mince). (++) identification certaine, (+) identification probable, (-) indentification ambigüe, (--) identification impossible. Macro : observation macroscopique, Micro: observation microscopique, P : poudre, W.S. surface altérée, T.S. : lame mince - * : seulement spectre Raman- Les zones hachurées indiquent que la mesure n'est pas réalisable avec l'instrument.*

Table 3.2 : Volcanic samples

Sample				Optic			*In situ* measurements						Lab. Comp. measurements.				
				Macro.	Micro.	**TOTAL**	Raman*	XRD	IR	Mössbauer		**TOTAL**	Raman*	EDX	µ probe	CL image	Raman mapping	**TOTAL**
			preparation :	-	-		P.	P.	P.	fresh	W.S		T. S.	T.S.	T.S.	T.S.	T. S.	
09ET01	*Primitive basalt*		Structure	++	++	++										+	+	+
			Texture	+	++	++										+	+	+
		Mineralogy	Olivine	+	++	++	++	++	+		++	++	++	++	++		++	++
			Mg-olivine				+	+	--		-	+	+	++	++		++	++
			Pyroxene	-	++	++	++	++	-		++	++	++					
			Diopside				+	+	--		-	+	+	++	++		++	++
			Feldspath	--	+	+	+	+	--		--	+	++					
			Plagioclase				-	+	--		--	+	+	++	++		+	++
			Other															
			Spinel	--	-	-	-	--	--		-	-	+	++	++		-	++
			Hematite	--	-	-	--	--	--		+	+	--	--	--		--	--
			Rock	++	++	++	+	+	-		+	+	++	++	++		++	++

Table 3.2 (continued): Volcanic samples

Sample				Optic			*In situ* measurements							Lab. Comp. measurements				
				Macro.	Micro.	TOTAL	Raman*	XRD	IR	Mössbauer		TOTAL	Raman*	EDX	µ probe	CL image	Raman mapping	TOTAL
			preparation :	-	-		P.	P.	P.	fresh	W.S		T. S.	T.S.	T.S.	T.S.	T. S.	
09SV15	*Picritic basalt*		Structure	++	+	++										-	-	-
			Texture	++	++	++										+	+	+
		Mineralogy	Olivine	+	++	++	+	++	++	+	+	++	++	++	++	-	++	++
			Mg-olivine				+	+				+	++	++	++		++	++
			Pyroxene	-	++	++	+	++	+	+	+	++	++					
			Augite				-	+	+	+	+	+	++	++	++	-	++	++
			FeldspathFeldspar	-	+	+	--	++	--	--	--	++	++	++	++	+	++	++
			Plagioclase				--	+	--			+	++	++	++	+	++	++
			Other															
			Spinel	--	+	+	--	-	--	-	-	-	++	++	+	-	++	++
			Amphibole	--	+	+	--	-	--	--	--	-	++	++	+	-	++	++
			Oxide	--	+	+	--	-	--	+	+	-	--	-	--	-	-	-
			Rock	++	++	++	+	++	+	+	+	+	++	+	+	-	++	++

Table 3.2 (continued): Volcanic samples

Sample				Optic			*In situ* measurements							Lab. Comp. measurements				
				Macro.	Micro.	TOTAL	Raman*	XRD	IR	Mössbauer		TOTAL	Raman*	EDX	µ probe	CL image	Raman mapping	TOTAL
			preparation :	-	-		P.	P.	P.	fresh	W.S		T. S.	T.S.	T.S.	T.S.	T. S.	
09TE08	*Altered phonolite*		Structure	++	+	++										+	-	-
			Texture	+	++	++										+	+	+
		Mineralogy	Feldspar	--	++	++	++	++	++	--	--	++	++	++	++		++	++
			Plagioclase		+	+	+	++	++			++	++	++	++		++	++
			Amphibole	--	++	++	--	--	--	+	+	+	++	++	++		++	++
			Tremolite							-	-	-	++	++	++		++	++
			Apatite	--	+	+	--	--	--	--	--	--	++	++	++		++	++
			Cl-Apatite										++	++	++		++	++
			Other															
			Spinel	--	+	+	--	--	--	+	+	+	--	++	+		+	++
			Quartz	--	++	++	--	--	--	--	--	--	++	++	++		++	++
			Rock	-	+	+	-	+	+	-	-	+	++	++	++		++	++

Table 3.2 (continued): Volcanic samples

Sample			Optic			*In situ* measurements						Lab. Comp. measurements				
			Macro.	Micro.	TOTAL	Raman*	XRD	IR	Mössbauer		TOTAL	Raman*	EDX	µ probe	CL image	Raman mapping	TOTAL
		preparation :	-	-		P.	P.	P.	fresh	W.S		T. S.	T.S.	T.S.	T.S.	T. S.	
07SA20	*Altered basalt (silicified)*	Structure	++	+	++										+	-	-
		Texture	++	+	++										+	-	-
		Mineralogy: Feldspath	-	++	++		++	++	--	--	++	++	++	++		++	++
		Mineralogy: *Plagioclase*		+	+		++	++			++	++	++	++		++	++
		Mineralogy: Pyroxene	-	++	+		++	--	+	+	++	++	++	++		++	++
		Mineralogy: *Augite*					++		+	+	++	+	++	++		++	++
		Mineralogy: Amphibole	-	++	++		++	++	--	--	++	++	++	++		++	++
		Mineralogy: *Actinolite*						+			+	+	++	++		++	++
		Mineralogy: Other															
		Mineralogy: *Quartz*	-	++	++		++	++	--	--	++	++	++	++		++	++
		Mineralogy: *Spinel*	--	+	+		--	--	+	+	+	--	++	++		++	++
		Mineralogy: *Clinochlore*	--	-	-		--	--	--	--	--	++	+	+		+	+
		Mineralogy: *Titanite*	--	--	--		--	--	--	--	--	++	++	++			++
		Mineralogy: *Chlorite*	--	-	-		++	--	--	--	++	--	+	+		+	+
		Mineralogy: *Clays*	--	++	++		--	--	--	--	--	--	+	+		-	+
		Rock	+	+	+		++	+	-	-	++	+	++	++		+	++

Table 3.2 (continued): Volcanic samples

Sample				Optic			*In situ* measurements						Lab. Comp. measurements				
				Macro.	Micro.	TOTAL	Raman*	XRD	IR	Mössbauer		TOTAL	Raman*	EDX	µ probe	CL image	Raman mapping	TOTAL
			preparation :	-	-		P.	P.	P.	fresh	W.S		T. S.	T.S.	T.S.	T.S.	T. S.	
		Structure		++	++	++										+	++	++
		Texture		++	++	++										+	++	++
11CA02	*Komatiite*	Mineralogy	Amphibole	--	-	-		-					++	++	++		++	++
			Trem-Actinolite				-						+	+	++		+	+
			Pyroxene	+	++	++		-					++	++	++		++	++
			Augite				+						+	+	++		+	+
			Phyllosilicates	--	+	+		+					++	++	++		++	++
			Clays		+	+	-						+	+	++		+	+
			Other															
			Titanite	--	+	+	--	--					+	++	++		+	++
			Sulfures	--	+	+	--	--					-	++	++		-	+
			Rock	+	+	+	-	-				?	+	++	++		++	++

Table 3.2 (continued): Volcanic samples

Sample				Optic			*In situ* measurements						Lab. Comp. measurements				
				Macro.	Micro.	TOTAL	Raman*	XRD	IR	Mössbauer		TOTAL	Raman*	EDX	µ probe	CL image	Raman mapping	TOTAL
			preparation :	-	-		P.	P.	P.	fresh	W.S		T. S.	T.S.	T.S.	T.S.	T. S.	
10SA09	*Altered komatiite*	Structure		++	++	++										+	++	++
		Texture		++	++	++										+	++	++
		Mineralogy	Amphibole	-	++	++		--	++	--	--	++	++	++	++		++	++
			Antigorite						++			++	++	++	++		++	++
			Phylosilicates	-	++	++												
			Micas	-	++	++			++			++	++	++	++		++	++
			Clays	-	++	++		++	--			++	+	+	+		+	+
			Other															
			Hematite	+	+	+		--	--	--	++	++	++	+	+		++	++
			Magnetite	-	+	+		--	--	++	--	++	-	+	+		+	+
			Talc	-	+	+		++	++	--	--	++	-	+	+		+	+
			Dolomite	-	+	+		--	--	--	--	--	+	++	++		+	++
		Rock		+	++	++		-	++	+	+	++	+	++	++		++	++

Table 3.2 (continued): Volcanic samples

Sample				Optic			*In situ* measurements							Lab. Comp. measurements				
				Macro.	Micro.	**TOTAL**	Raman*	XRD	IR	Mössbauer		**TOTAL**	Raman*	EDX	µ probe	CL image	Raman mapping	**TOTAL**
			preparation :	-	-		P.	P.	P.	fresh	W.S		T. S.	T.S.	T.S.	T.S.	T. S.	
		Structure		++	+	++										-	-	-
		Texture		++	++	++										+	+	+
09SV02	*Dunite*	Mineralogy	Olivine	+	++	++	+	++	++	+	+	++	++	++	++	-	++	++
			Mg-olivine				+	+				+	++	++	++		++	++
			Pyroxene	-	++	++	+	++	+	+	+	++	++					
			Enstatite				-	+	+	+	+	+	++	++	++	-	++	++
		Rock		++	++	++	+	++	+	+	+	+	++	+	+	-	++	++

►Table 3.3. Comparison of textural, elemental and mineralogical data from the sedimentary rocks using different instruments and different sample preparations (rock surface, powder, thin section). (++) unambiguous identification, (+) probably identification, (-) identification ambiguous, (--) identification impossible. Macro.: Macroscopic view, Micro.: Microscopic view, P.: Powder, W.S. : Weathered surface, T.S.: Thin section - * only Raman spectrum- The hatched area indicate that the measurement is not applicable for a specific instrument.

►*Tableau 3.3. Comparaison de la texture, des données élémentaires et minéralogiques des échantillons sédimentaires à partir des différents instruments et des différentes préparations (surface brute de la roche, poudre et lame mince). (++) identification certaine, (+) identification probable, (-) identification ambigüe, (--) identification impossible. Macro : observation macroscopique, Micro : observation microscopique, P : poudre, W.S. surface altérée, T.S. : lame mince - * : seulement spectre Raman- Les zones hachurées indiquent que la mesure n'est pas réalisable avec l'instrument.*

Table 3.3: Sedimentary samples

Sample				Optic			*In situ* measurements						Lab. Comp. measurements				
				Macro.	Micro.	TOTAL	Raman*	XRD	IR	Mössbauer		TOTAL	Raman*	EDX	µ probe	CL image	Raman mapping	TOTAL
			preparation :	-	-		P.	P.	P.	fresh	W.S		T. S.	T.S.	T.S.	T.S.	T. S.	
09SV05		Structure		+	++	++										+	+	
		Texture		+	++	++										+	+	
	Carbonates	Mineralogy	Carbonate	+	++	++	++	+	+		++	++	++	++	++	++	++	++
			Dolomite		+	+	+	+	+		--	+	++	+	++	+	++	++
			Ankerite		+	+	+	-	-		+	+	++	+	++	+		
			Magnesite		+	+	+	-	-		--	+	++	+	++	+	++	++
			Other															
			Pyrite	--	-	-	-	--	--		--	-	+	++	++	--	+	++
		Rock		++	++	++	+	-	-		-	+	++	++	++	+	++	++

Table 3.3(continued): Sedimentary samples

Sample				Optic			*In situ* measurements						Lab. Comp. measurements				
				Macro.	Micro.	TOTAL	Raman*	XRD	IR	Mössbauer		TOTAL	Raman*	EDX	µ probe	CL image	Raman mapping	TOTAL
			preparation :	-	-		P.	P.	P.	fresh	W.S		T. S.	T.S.	T.S.	T.S.	T. S.	
11CY04	*Carbonates*		Structure	+	+	+											-	
			Texture	+	+	+											+	
		Mineralogy	Carbonate	+	++	++	+	+	+				++	++	++		++	++
			Dolomite	--	+		+	+	+				++	+	++		+	-
			Other					-	-									
			Orthoclase	--	+	+	+	--	-				++	++	++		++	++
			Anatase	--	+	+	+	--	--				++	+	++		++	++
			Augite	--	+	+	+	--	--				++	++	++		++	++
			Phyllosilicates	--	+	+	+	--	--				+	+	+		+	+
	Rock			++	++	++	+	+	+			+	++	+	++		++	++

Table 3.3(continued): Sedimentary samples

Sample			Optic			*In situ* measurements						Lab. Comp. measurements.				
			Macro.	Micro.	TOTAL	Raman*	XRD	IR	Mössbauer		TOTAL	Raman*	EDX	µ probe	CL image	Raman mapping	TOTAL
		preparation :	-	-		P.	P.	P.	fresh	W.S		T. S.	T.S.	T.S.	T.S.	T. S.	
99SA01	*Hyd. Chert*	Structure	++	+	++											-	-
		Texture	+	++	++											+	+
		Mineralogy: Quartz	+	++	++	++	++	++	--	--	++	++	++	++		++	++
			+	++	+	+					+	++	++	++		++	++
		Carbonaceous	--	++	++	--	--	--	--	--	--	+				++	++
		-matter	+	++	++							++				++	++
		Rock	++	++	++	-	+	+	--	--	+	++	++	++		++	++
06AU01	*B.I.F.*	Structure	++	+	++											+	+
		Texture	++	+	++											+	+
		Min.: Quartz	++	++	++	++	++	++	--	--	++	++	++	++		++	++
		Hematite	-	+	+	-	+	--	++	++	++	++	+	+		++	++
		Goethite	-	+	++	-	+	--	++	++	++	++	+	+		++	++
		Rock	+	+	+		++	+	+	+	++	++	++	++		+	++

Table 3.3(continued): Sedimentary samples

Sample			Optic			*In situ* measurements						Lab. Compl. measurements				
			Macro.	Micro.	TOTAL	Raman*	XRD	IR	Mössbauer		TOTAL	Raman*	EDX	µ probe	CL image	Raman mapping	TOTAL
		preparation :	-	-		P.	P.	P.	fresh	W.S		T. S.	T.S.	T.S.	T.S.	T. S.	
00AU05	*Chert with sed.*	Structure	++	++	++											+	+
		Texture	++	++	++											+	+
		Mineralogy – Quartz	++	++	-	++	++	++			++	++	++	++		++	++
		Mineralogy – *microcrystaline*		++								+	+			++	++
		Mineralogy – Phylosilicates	--	+	++	-	--	--			-	++	++	+		++	++
		Mineralogy – *Hudromuscovite*		-								+	+			+	+
		Mineralogy – Other															
		Mineralogy – *Ti-oxide*	--	-	+	-	--	--				+	++	++		++	++
		Rock	++	++	+	+	+	+			+	+	++	++		++	++

Table 3.3(continued): Sedimentary samples

Sample			Optic			*In situ* measurements						Lab. Comp. measurements.				
			Macro.	Micro.	TOTAL	Raman*	XRD	IR	Mössbauer	TOTAL	Raman*	EDX	µ probe	CL image	Raman mapping	TOTAL
		preparation :	-	-		P.	P.	P.	fresh W.S		T. S.	T.S.	T.S.	T.S.	T. S.	
00AU04	*Hyd. Chert + sed.*	Structure	++	++	++										++	++
		Texture	++	++	++										++	++
		Min. Quartz	++	++	++	++	++	++		++	++	++	++		++	++
		Min. Other														
		Min. *Anatase*	--	+	+	+	--	--		+	++	++	++		++	++
		Rock	+	++	++	+	++	++		++	++	++	++		++	++

III.4. Mineral selection

The minerals chosen for the ISAR collection have been identified on Mars and include calcium carbonates (aragonite and calcite) and a Mg-carbonate (magnesite); silicates including the nesosilicate olivine, the sorosilicate epidote, the cyclosilicate tourmaline (schorl), the inosilicates enstatite, wollastonite and diopside, and the phyllosilicates muscovite and nontronite. Tectosilicates could be represented in the form of quartz from the different cherts described above. Opal was selected as an hydrated silica polymorph (cf. *Squyres et al, 2008* and *Ruff et al., 2011*). A phosphate, apatite, and the sulphates gypsum and barite were also added to the collection. Barite has not yet been observed on Mars, but as a major terrestrial suphate, it could be useful for calibrating instruments. Finally, I selected different Fe- and Ti-oxides to complete this mineral collection (goethite, magnetite, rutile) and a spinel. Lastly, we are using a laboratory-synthesised nontronite (10AR01) as an analogue of phyllosilicates forming in neutral conditions by aqueous alteration of basalts on Mars (*Bibring et al., 2006* and *Meunier et al., 2010*). Naturally-formed nontronites display a wide range of compositions. The Table 3.4 summarizes the selection.

►Table 3.4: List of analogue minerals characterized for the ISAR collection and calculated chemical formulae using electron microprobe analysis (except for the artificial nontronite).

►*Tableau 3.4: Liste des échantillons analogues caractérisés pour la collection de l'ISAR avec les formules structurales obtenues par microsonde électronique (sauf pour la nontronite artificielle).*

Type	ISAR number	Name	Chemical Formula
Carbonate	12FR01	Magnesite	$(Mg_{1,98}Ca_{0,02})_2CO_3$
	12FR02	Aragonite	$CaCO_3$
	12FR03	Aragonite	$CaCO_3$
	12FR04	Aragonite	$CaCO_3$
	12FR05	Calcite	$CaCO_3$
Silicate	12FR11	Schorl	$Na_{0,58}[]_{0,42}(Fe_{1,36}Mg_{1,04}Ca_{0,09}Ti_{0,05}K_{0,01}Mn_{0,01}Al_{0,44})_3$ $Al_6[Si_{5,78}Al_{0,21}O_{18}](BO_3)_3(OH,F)_4$
	12FR12	Wollastonite	$Ca_{0,28}Mg_{0,58}Si_{1,02}O_3$
	12FR13	Muscovite	$(K_{0,91}Na_{0,09})(Al_{1,89}Fe_{0,07}Mg_{0,07}Ti_{0,01})_1(Si_{3,01}Al_{0,99})_4O_{10}(OH)_2$
	10AR01	Nontronite	$(Si_{3.25}Fe^{3+}_{0.75})Fe^{3+}_2O_{10}(OH)_2Na_{0.75}$
	12FR14	Epidote	$Ca_2Al_2(Fe_{0,39}Mn_{0,02}\odot Ti_{0,01}Al0_{,68})Si_3O_{12}(OH)$
	12FR15	Diopside	$(Ca_{1,02}Mg_{0,94}Fe_{0,10})_2(Si_{1,93}Al_{0,03})O_6$
	12FR18	Olivine	$Fe_{0.08}Mg_{1.92}SiO_4$
	12FR19	Enstatite	$(Fe_{0.17}Mg_{1.92})_2Si_{1.94}O_6$
	12FR17	Opal	$Si_{0.95}O_2\ nH_2O$
Phosphate	12FR08	Apatite	$Ca_{4.81}Mn_{0.14}(PO_4)_3(OH,F,Cl)_1$
Oxide	12FR06	Rutile	$Ti_{0.99}Fe_{0.01})O_2$
	12FR07	Goethite	$FeO(OH)$
	12FR09	Magnetite	Fe_3O_4
	12FR10	Spinel	$MgAl_2O_4$
Sulphates	12FR16	Baryte	$Ba_{0,99}Sr_{0,01}SO_4$
	12FR20	Gypsum	$CaSO_4\ 2H_2O$

Figure 3.4: Optical view of the mineral selection, from top to bottom and from left to right, samples 12FR01 to 12FR20.

Figure 3.4: photographies des minéraux sélectionnés pour la collection, de haut en bas et de gauche a droit les échantillons 12FR01 à 12FR20

The minerals were studied without treatment and as polished sections by Raman spectroscopy. The polished sections were also used for SEMobservation and SEM-EDXS and electron microprobe analysis for the elemental composition. The chemical formulae in Table 3.4 were calculated on the basis of a mean value from 40 electronic microprobe measurements.

The pure Fe-nontronite was synthesised at 150°C in the Hydrasa laboratory, Poitiers, by the group of Sabine Petit and Alain Meunier. Cristallographic characterization was performed by *Decarreau et al., (2008).* All details on each sample are listed in the online web site: www.isar.cnrs-orleans.fr.

III.5 Conclusion

We have created a preliminary collection of Mars-analogue rocks and minerals for testing space instrumentation for the upcoming *in situ* missions to Mars. These materials include a variety of basalts, the most common rock type on Mars, as well as volcanic and chemical sediments (carbonates, BIF, cherts) and various minerals. However, the selection of terrestrial analogues of Martian materials is limited by some major geochemical differences in the compositions of, especially, Fe-containing rocks on the two planets. For example, Martian basalts contain much more Fe and Mg than terrestrial basalts. Within this limitation, the rocks we have chosen correspond as closely as possible to Martian materials. The collection of rocks in the ISAR thus provides a relevant selection of materials the structure, texture, and mineralogical and geochemical compositions of which will be useful for testing spaceflight instrumentation and will help to interpret the nature of the rocks on the Martian surface and their potential for containing and preserving traces of life. The relevance of the sample analogy is detailed in Table 3.5. The analogy based on the different characteristics studied: geochemistry, petrology, (include texture and structures) and geotechnical properties are described in Table 3.5 using stars, 1 star to 5 stars representing weak to excellent correspondence to Martian materials. The geotechnical property results are based on the estimation of the resistivity of the samples and the opportunity to find this type of sample morphology on the Martian surface. The minerals are not included in this Table because they are not relevant for geochemistry and petrology.

ISAR number	Geochmistry	Petrology	Geotechnics	Total
09ET01	***	****	*	8/15
09SV15	***	****	***	10/15
09TE08	**	***	***	8/15
07SA20	***	**	***	9/15
11CA02	***	****	***	10/15
10SA09	***	****	***	10/15
09SV02	****	****	**	10/15
09SV05	****	****	**	10/15
11CY04	****	****	***	11/15
99SA01	***	***	***	9/15
99SA05	***	***	***	9/15
06AU01	***	***	***	9/15
00AU05	****	***	***	10/15
00AU04	****	***	***	10/15

Table 3.5. Relevance of the ISAR rock samples as analogues of the Martian surface materials. The number of stars, between 1 to 5, represent weak to excellent correspondence, respectively.

Tableau 3.5. Pertinence des échantillons de la collection ISAR en fonction de leur degré d'analogie avec la surface de Mars. De 1 à 5 étoiles, du plus mauvais au meilleur, respectivement.

In this study, we have used different samples from different locations around the world. It could be interesting to search for a good analogue site in which the different rock types and mineralogy can be seen in context and with direct relation to each other. A site containing fresh basaltic rocks to totally altered basalts composed essentially of phyllosilicates (clays) would be of great relevance for understanding geological processes on early Mars. Such a site is the Troodos Ophiolite Complex in Cyprus, and it will be described in the next Chapter.

Première sélection (Résumé Français)

Ce chapitre présente le premier groupe d'échantillons sélectionnés comme analogues de Mars. Le choix des échantillons est basé sur la géologie de Mars décrite dans le précédent chapitre puis en sélectionnant des échantillons déjà disponibles dans le laboratoire. En effet, l'équipe d'Exobiologie, par l'intermédiaire de F. Westall, a déjà rassemblé une large collection de roches en particulier des roches volcaniques et sédimentaires de l'Archéen. D'autres échantillons ont été envoyés par des spécialistes ou recueillis lors de mes propres missions de terrain à Rio Tinto, en Afrique du Sud, à Chypre et dans le Massif Central Français.

Ce chapitre est centré sur la sélection d'échantillons analogues de Mars. J'ai cherché à évaluer le degré de pertinence de chaque échantillon en utilisant de nombreuses methodes d'analyse à l'aide d'instruments de laboratoire en corrélation avec les instruments spatialisés pour l'exploration martienne. Ce chapitre présente brièvement les données obtenues pour chaque échantillon. Pour plus d'informations, l'annexe B présente les résultats détaillés obtenus sur deux échantillons provenant de Svalbard (Norvège).

Mars étant essentiellement composée de basaltes, je me suis principalement concentré sur l'étude des basaltes. Nous avons choisi comme échantillon un basalte de Svalbard (09SV15) car il a déjà été décrit comme analogue de la météorite martienne ALH84001 et parce qu'il est associé à des carbonates (09SV05) et à une dunite (09SV02). La dunite est une roche caractéristique du manteau terrestre. Nous avons choisi un échantillon de Tenerife (09TE08) car son rapport Ca/Si vs. Mg/Si est très similaire aux roches de Mars. De plus cet échantillon peut être représentatif de basaltes altérés. Il ne faut pas oublier que les basaltes, au cours de leur altération, peuvent contenir des traces de vie. Nous avons choisi l'échantillon de basalte silicifié (07SA20) provenant de Barberton en Afrique du Sud car il est représentatif du processus de silicification associé à de l'hydrothermalisme. Ces phénomènes sont caractéristiques de la Terre primitive. J'ai choisi un basalte primitif de l'Etna (09ET01) car il est géochimiquement très similaire à la moyenne des basaltes martiens (Fig. 3.1). Enfin, j'ai ajouté deux komatiites, dont une peu altérée provenant du Canada (11CA02) et une autre beaucoup plus alterée provenant d'Afrique du Sud (10SA09). Ces roches semblent avoir été observées sur Mars et sont des roches volcaniques typiques de l'Archéen (Terre).

Plusieurs types de roches sédimentaires ont été incorporés dans la première sélection en partie en fonction de leur intérêt exobiologique, en accord avec les objectifs des futures missions vers Mars. Comme nous l'avons vu dans le chapitre précédent, la vie sur Mars n'a pu apparaître qu'entre le Noachien et l'Hespérien, lorsque que l'eau liquide était présente en surface. Les roches similaires à la surface de la Terre (datées à l'Archéen), contenant des traces fossiles sont des dépôts volcaniques silicifiés par des fluides hydrothermaux. Cette activité hydrothermale a déjà été suggérée sur Mars, et pourrait avoir contribué à préserver des microorganismes. Pour cette sélection, nous avons choisi des sédiments volcaniques silicifiés provenant de Pilbara, Australie et datés de 3.45 Ga (00AU05). Nous avons

ajouté des chailles du même âge contenant ou non de la matière carbonée provenant de Barberton, Afrique du Sud ou encore de Pilbara (99SA01, 99SA05 et 00AU04). Pour compléter la sélection de roches siliceuses, j'ai ajouté une roche férrifère rubanée (BIF). Ces roches n'ont pas encore été observées sur Mars mais sont très riches en fer et y existent très probablement. Enfin, quelques carbonates sont visibles sur Mars, j'ai donc sélectionné deux échantillons de carbonates dont l'origine est plutôt hydrothermale et associée au volcanisme. Ces échantillons proviennent de Svalbard (09SV05) et de Chypre (11CY04). Le Tableau 3.1 présente la liste des échantillons étudiés dans ce chapitre. La deuxième partie de ce chapitre correspond à la description de chaque échantillon, qui ne sera pas reprise dans ce résumé. Cependant pour illustrer ce choix d'échantillons les Figs. 3.2 et 3.3 présentent des photos e macroscopiques et en microscopique de chaque échantillon.

La troisième partie de ce chapitre résume pour chaque échantillon le résultat de chaque analyse en utilisant les instruments de laboratoire. Le détail des analyses est accessible à partir du site internet et de la base de données associée : http://www.isar.cnrs-orleans.fr. Les Tableaux 3.2 et 3.3 présentent l'évaluation qualitative inhérente à l'identification de la structure, texture, minéralogie et composition pour chaque instrument et en les combinant. Cette étude montre que même en combinant les instruments de laboratoire, donc certainement encore plus avec les instruments de vols, les interprétations peuvent parfois être compliquées. Les premiers résultats démontrent la limite d'interprétation en utilisant des préparations en poudre. En effet, les textures et structures sont irrémédiablement perdues. Nous pensons qu'avec les futurs instruments d'ExoMars, seulement 50% des minéraux pourront être identifiés avec certitude. En effet, l'apport des caméras couleurs et du microscope binoculaire (loupe) sera essentiel pour aider à l'identification et l'interprétation des roches.

Finalement, nous avons sélectionné différents minéraux de bonnes qualités chimiques et cristallographiques. La liste des minéraux est proposée dans le Tableau 3.4 et la Fig. 3.4, ainsi que leurs analyses chimiques. Ces minéraux ont été identifiés sur Mars et sont les constituants principaux des roches. Nous avons sélectionné des carbonates de calcium (aragonite et calcite) de magnésium (magnesite) ; différents types de silicates : nésosilicate (olivine), sorosilicate (epidote), cyclosilicate (schorl), inosilicates (enstatite, wollastonite et diopside) et phyllosilicates (muscovite et nontronite). Notre sélection ne comporte pas de tectosilicates, qui peuvent être retrouvés dans le quartz des chailles sélectionnées précédemment. Nous avons sélectionné de l'opale, une silice hydratée. J'ai aussi ajouté un phosphate (apatite), des sulfates (gypse et barytine). Enfin j'ai sélectionné des oxydes de fer et de titane (goethite, magnétite et rutile). Une nontronite de synthèse a été fabriquée au laboratoire Hydrasa (Université de Poitiers).

Nous avons créé la collection de l'ISAR avec une large variété de roches et de minéraux afin de couvrir le plus largement possible les matériaux analogues de Mars. Cependant, il existe de nombreuses différences entre la Terre et Mars, les compositions chimiques ne sont pas exactement les mêmes. Par exemple, les basaltes martiens contiennent plus de Fe et Mg que leurs analogues terrestres. Mais les

conditions d'altération des roches sont aussi particulièrement différentes. Nous avons essayé d'établir le degré d'analogie de nos échantillons avec ceux de Mars en nous basant sur trois critères : la géochimie, la pétrologie et la géotechnique. Les échantillons, notés de 1 à 5 étoiles, sont de plus ou moins bons analogues. Le Tableau 3.5 présente les résultats. .

J'ai cherché un site analogue à Mars où il serait possible de trouver en un même endroit des basaltes et leurs produits d'altération obtenus dans des conditions similaires à celles de Mars. Le prochain chapitre va présenter les résultats de l'étude menée à Chypre qui semble être un site analogue.

Chapter IV
A new Mars analogue site in Cyprus

In this chapter, I describe a new Mars analogue site located in the *Skouriotissa* mine, in North West Cyprus, from which I collected samples in March and April 2011. Here the surfaces of outcropping ophiolitic basalts undergo various types of chemical alteration, in particular by acidic water, resulting in different mineralogies[12].

IV.1 Introduction

The previous chapter brought to light the difficulty of finding good analogues of Martian rocks and soils on Earth. I therefore searched for new terrestrial sites that are geologically more similar to the early and present Mars outcrops, *i.e.* a site where the main rocks are basalts (at least the basic body) that have been altered by the processes described in Chapter II part 2.2. However, it is obviously impossible to find similar atmospheric conditions (i.e., without oxygen) at the surface of the Earth. All the known analogue sites (e.g. Rio Tinto in Spain, *Amils et al., 2007*, or Utah Sandstone in USA, *Chan et al., 2004*) focus on present Martian conditions, and in particular on iron oxides, and are sometimes not very similar to Martian rocks from a geological point of view. The site of Rio Tinto in the Spanish pyrite belt, for instance, is used as an analogue site mainly in terms of the search for present life on Mars (extremophile life, NASA laboratory place), but the geological context is andesitic, i.e., made of

[12] A part of the content of this chapter is in review in *Geology* (*Bost et al., in review*).

more acidic volcanic rocks that are not very representative of the Martian surface. Moreover, these rocks are highly metamorphosed, at least to amphibolite facies, and are thus are unlike Martian rocks.

As noted in chapter II, habitable conditions for the appearance of life were possible during the Noachian period on Mars. With this in mind, the search for Noachian analogue sites on Earth is more relevant (*Westall et al., 2011a; Bibring et al., 2006*). At such a site, the alteration must occur under the effect of hydrothermal and meteoric or acidic water. Thus, mines are good objectives because they favour the production of acidic water. I therefore took advantage of an opportunity to join a field trip to Cyprus, organized by a team from the CNRS-ISTO-Orléans laboratory interested in epidotitisation processes in the deep oceanic crust close to the copper mines, in particular in the *Skouriotissa* mine.

IV.2. Location

Cyprus is a small elongated island (~ 10 000 km^2) located in the east of the Mediterranean Sea, to the south of the Turkish Anatolia (Fig. 4.1a). The *Skouriotissa* mine is located in the west of the island, south of the Morfou gulf, between Katydata to the south and Petra to the north. The GPS position of the open-pit is: N35.095364°; E32.887338°. The *Skouriotissa* mine is exploited essentially for copper by the *Hellenic copper Limited* company with 3 billion tons of proven ore reserves at a grade of 0.1 to 0.25 % of Cu (max: 2.35 % of Cu).

IV.3. Geological Background

The Troodos ophiolite (Fig. 4.1b) has been recognized for a long time as an uplifted slice of oceanic crust and mantle that was created through sea-floor spreading (*Gass, 1968* and *Moores and Vine, 1971*). Forming the central region of the eastern Mediterranean island of Cyprus, the ophiolite displays a dome-like structure centred on Mount Olympus (1952 m). The ophiolite formation dates back to the upper Cretaceous. Its stratigraphy includes a mantle sequence consisting of peridotites (harzburgites, dunites) and a serpentinite diapir exposed at the highest elevation. Along the north slope of the ophiolite, the mantle sequence is stratigraphically overlapped by a large gabbroic plutonic complex, a sheeted dyke complex, extrusive lavas (Pillow lavas) and oceanic sediments (Fig. 4.1c). The pillow lavas are divided into the Upper Pillow Lavas and the Lower

Pillow Lavas (respectively UPL and LPL) according to mineralogy, colour and dyke abundance (*Wilson and Ingham, 1959; Gass, 1960; in Grebby et al., 2010*). The thickness of the series is 1.5 km at the maximum. The study area is located on the northern flank of the Troodos ophiolite in the UPL formation (Fig. 4.1c). It consists of pillowed flows and sparse to abundant extrusive breccias, and is relatively free of intrusive rocks (*Moores and Vine, 1971* and references therein). Most of the pillow lavas contain olivine phenocrysts, commonly altered to brown calcite. The lavas have been altered by propylitization[13] to epidote-chlorite-albite and zeolite-facies assemblages. Olivine-free basalts are also present. The pillows are flattened and elongated. They are vesicular, the vesicules being infilled with calcite and zeolites (analcite and laumonite in order of abundance, e.g. *Dill et al., 2007*).

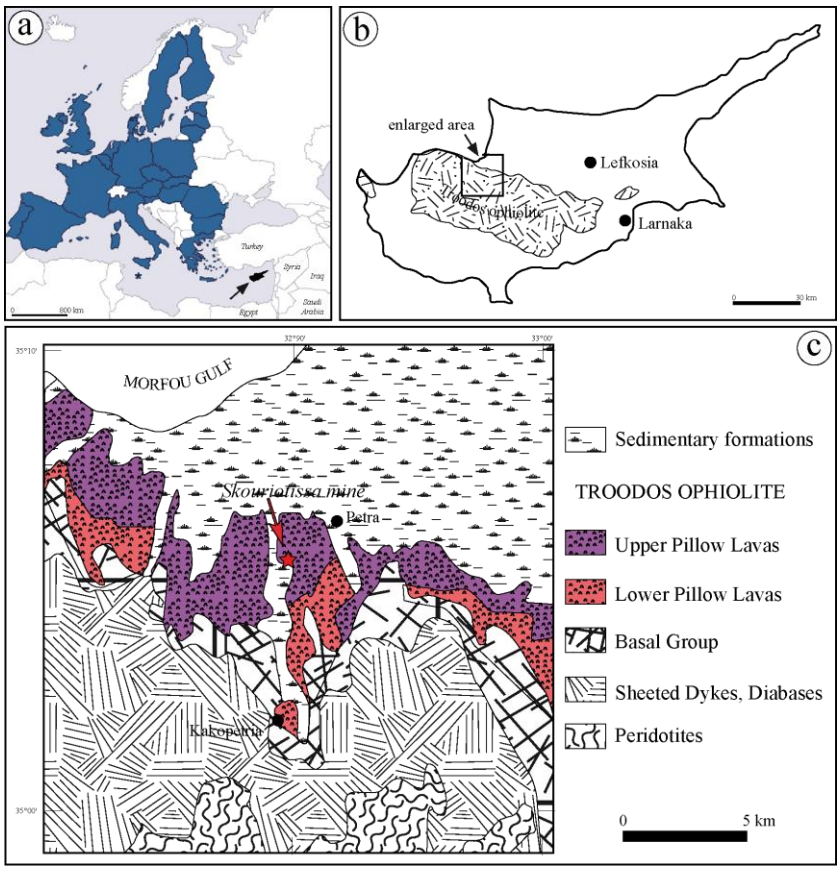

[13] Propylitic alteration is the chemical alteration of a rock, caused by iron and magnesium hydrothermal fluids. It typically results in epidote–chlorite–albite alteration (*Raoult and Foucault, 2010*)

◄Figure 4.1 a- Localization of Cyprus in the eastern Mediterranean Sea. b- Location of the Troodos ophiolite showing the position (square) of the enlarged area in c. c- simplified geological map of the study area showing the ophiolite formation in the south and the sediments in the north. The *Skouriotissa* mine is located in the Upper Pillow Lava formation (red star). After the Geological map of Cyprus, *Cyprus Geological Survey Department, 2007*.

◄*Figure 4.1 a- Localisation de Chypre à l'extrémité orientale de la mer Méditerranée. b- Localisation de l'ophiolite de Troodos avec en encadré la zone détaillée en c. c- Carte géologique simplifiée de la zone d'étude montrant une coupe nord-sud de l'ophiolite. La mine de* Skouriotissa *est localisée dans la formation Upper Pillow Lava (étoile rouge). D'après la carte géologique de Chypre, Cyprus Geological Survey Department, 2007*.

The *Skouritissa* mine itself is located in the UPL. It consists of an elliptical lens of massive sulphides (pyrite) trending east-west and capped by sedimentary deposits. This is a typical volcanogenic massive sulphide deposit (VMS) associated with mafic volcanism. Cyprus-type VMS are characterized by their small size, medium grade, and enrichment in Cu and Zn (*Jébrak and Marcoux, 2008*). The first sedimentary formation over the ophiolite is composed of umber (sienna) formation with grey tuff, orange and ochre-coloured hematite and sulfides in altered bands at the base, with a few layers of radiolarites (*Constantinou and Govett, 1972*). This formation is interpreted as being directly derived from submarine leaching of the sulphides, corresponding to the Trypa Group and was formed during the Jurassic (*Constantinou and Govett, 1972*). The formation overlying the Trypa Group consists of marls and argillites at the base overlain by reef limestones deposited in the upper Miocene (Fig. 4.2a). A post-Miocene 250° unmineralized normal fault, with a downthrow of about 30 meters to the east, divides it into a western and an eastern ore zone. This fault is unmapped by the Cyprus geological survey and not reported in the Figs. 4.1c and 4.2a.

My study focussed on the western part of the mine, named the *S-West Phoenix open pit*. An important gossan was developed on top of the sulphide deposit (Fig. 4.2a,b). There are significant formations of quartz and red jasper around the basalt pillows in some parts of the UPL formation. They were formed later than the sulphide deposits (Fig. 4.2c). *Richards and Boyle (1986)* showed that the jasper horizons are mudstone deposited interstitially with the pillow basalts that were converted into jasper when the enclosing lavas underwent low-temperature alteration unrelated to the sulphide mineralization. The latter is contemporaneous with the hydrothermal alteration of the UPL that resulted in a quartz-chlorite facies.

The second major phase of "weathering" of the pillow basalts is associated with the mining activities. The *Skouriotissa* mine, in particular the gossan, has been exploited for its copper since Roman times. The old workings are composed of mine galleries along the massive sulphide deposit. The galleries are largely drowned by meteoric water that has percolated into the sulphides. This acidic water is collected and transported by gravity to the *SW Phoenix* pit where it flows onto the pillow basalt lava formation (UPL) causing their alteration. I focussed my study around this modern hydrologic system.

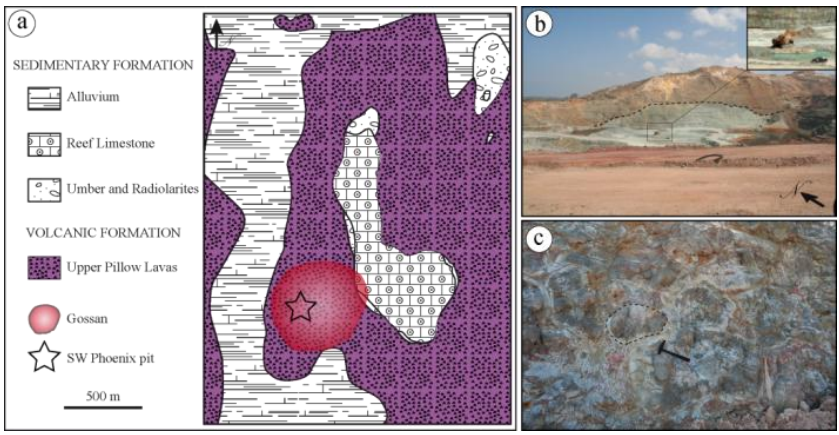

Figure 4.2: a- Detailed geological map of the *Skouriotissa* mine area. The gossan is located in the Upper Pillow Lavas formation. Faults are not mapped here. (After the Geological map of the Xeros-Troodos area, *Cyprus Geological Survey Department, 1969*). b- View of the SW Phoenix pit with the brown gossan at the top and the green quartz-chlorite pillow basalt formation (hydrothermally altered) at the bottom. Note the mechanical stripper for scale (in insert). The main massive ore deposit (main pit) is the darker lens to the right. The study area is on the right end of the picture. c- Detail of the pillow basalt formation. Note the presence of red jasper around the pillows. (The hammer in the centre is 33 cm-long).

Figure 4.2: a- Carte géologique des environs de la mine de Skouriotissa. Le chapeau de fer est localisé dans la formation Upper Pillow Lavas. Les failles ne sont pas cartées ici. (D'après la carte géologique de Xeros-Troodos, Cyprus Geological Survey Department, 1969). b- Vue de l'exploitation SW Phoenix avec le chapeau de fer en marron au sommet et à la base en vert la formation de basaltes en coussins à quartz-chlorite (altération hydrothermale). Notez la pelleteuse pour l'échelle (en insert). La zone de sulfures massifs est la lentille sombre sur la droite. La zone d'étude est juste à droite de l'image. c- Détail des basaltes en coussins. Notez la présence de jaspe autour des coussins. (Le marteau mesure 33 cm de long.)

IV.4. Sampling

The samples were collected following the flow of acidic water on the basaltic surface. The outcrop consists of a succession of lithological benches (~6-4 meters high and ~1 to 4 meters width) along which the water flows, making small grooves along the bench and creating small waterfalls between each bench. Samples were taken in five points at different elevations along the flowing water. The acidic water leaching from the VMS body results in a superficial iron oxide deposit but the sampled rocks are green. Five sites were thus defined from top to bottom (Fig. 4.3):

-**Site 1**, immediately adjacent to the acidic water of the mine drainage;

-**Site 2**, along the uppermost waterfall (Fig. 4.3). At this place the pillows are clearly visible in the outcrop. This level corresponds to the level shown in Figure 4.2c but without evidence of red jasper.

-**Site 3,** in the middle of the second large waterfall. The basalt at this level is slightly more massive.

-**Site 4**, at the bottom of the old pit, where the flow excavated ~40 centimetres into the basalt formation. A few inches of red mud occurs at the bottom of the waterfalls (Fig. 4.3), possibly the remains of a reserve of dirty water. To date, mining activity has led to the deepening of the pit and the creation of several levels.

-**Site 5**, exactly in the waterfall between the old and the new bottom of the pit. The basalt in the recently dug base of the pit is green and has not been altered by the acidic water but only by hydrothermal processes (quartz-chlorite facies).

At each site, the temperature, the pH and the conductivity were measured *in situ* (blue stars in Fig. 4.3). The rock samples were named 11CY08 to 11CY20 with respect to the ISAR nomenclature (cf. Chapter I). However, for more clarity, they were renamed as a function for their position in the field. To discriminate between natural chemical alteration due to the mining activity and the artificial acid weathering induced by the industrial lixiviation process used to concentrate the copper, , I sampled different parts of the waste dump that is regularly sprayed with acid in order to further release the copper. The samples were named 11CY05 to 11CY07. For these samples there is no precise location or information on the position in the geological levels since the samples were taken from all over the mine.

Finally, the samples are arranged along (1) a vertical line along the groove of flowing water: samples S1-1, S2-1, S3-1, S4-1 and S5-1, respectively 11CY16, 11CY13, 11CY09, 11CY08 and 11CY17 according to the ISAR nomenclature; and (2) horizontally in the pillow basalt formation: samples S2-1, S2-2 and S2-3, respectively 11CY13, 11CY14 and 11CY15; samples S3-1, S3-2,

S3-3 and S3-4, respectively 11CY09, 11CY10, 11CY11 and 11CY12; samples S5-1, S5-2, S5-3, respectively 11CY17, 11CY18 and 11CY19; the sample S4-2 (11CY20) corresponds to mud taken close to sample S4-1 (Fig. 4.3).

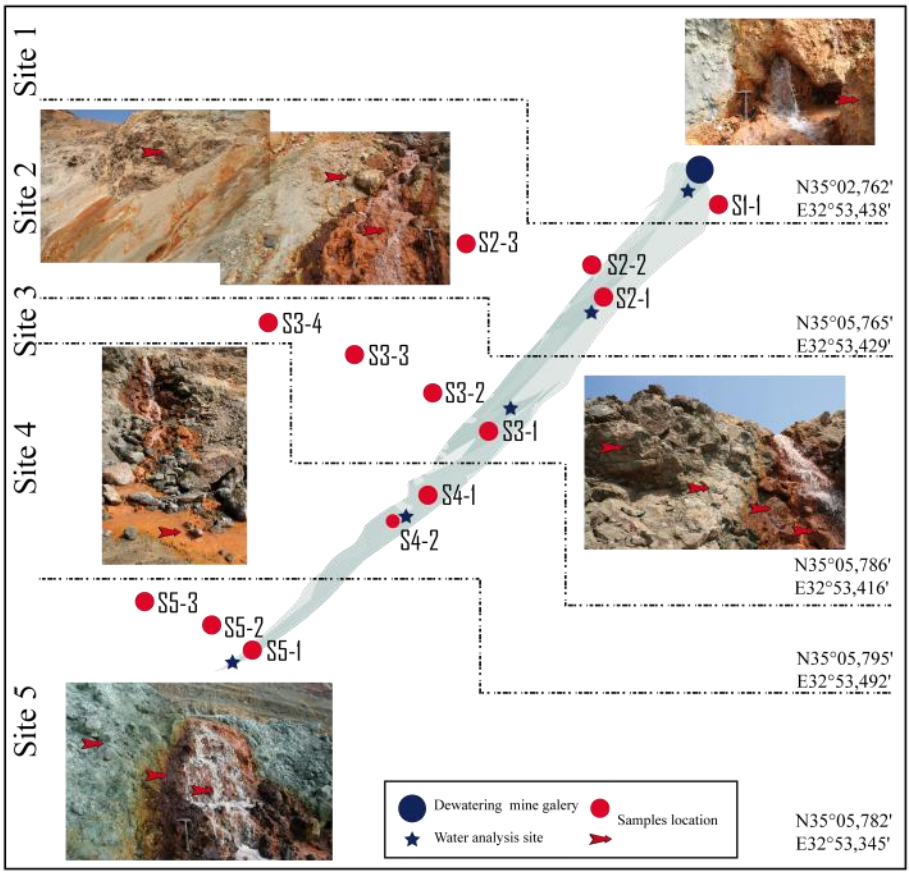

Figure 4.3: Location sketch of the different sampling sites along the groove of flowing water (in grey-blue) with associated field view. The red arrows show the samples location.

Figure 4.3: Schéma de localisation des différents sites d'échantillonnage le long du fossé (en gris-bleu) avec les photos de terrain associées. Les flèches rouges montrent la position des échantillons.

IV.5. Methods

Fifteen samples from the groove and from the waste dump were dried and crushed to a fine powder to make elemental analysis by ICP and mineralogical characterization by XRD. The elemental composition of 7 samples (S1-1, S2-1, S3-1 to S3-4 and S5-1) was determined by ICP-OES and ICP-MS for 10 major elements and 43 minor elements respectively. The XRD measurements were carried out in the Hydrasa Laboratory, with the help of Claude Fontaine and Alain Meunier. Before analysis the phyllosilicates were concentrated by suspending and settling the powders for 2 hours in de-ionised water and then they were sonicated. The phyllosilicates were then studied in oriented configuration after drying in the air, with ethyl-glycol vapour, and with heat treatment at 350°C and 550°C. Polished thin sections were made at the ISTO laboratory, but with difficulties due to the dominantly clayish composition. Mineralogy was investigated using optical microscopy and Raman spectroscopy.

IV.6. Results

IV.6.1: Water geochemistry measurements

The results of the water analyses are displayed in Table 4.1. The measurements were made *in situ* on the 30th Mars 2011.

	Site 1	Site 2	Site 3	Site 4	Site 5
Temperature (°C)	17.1	17.6	19.6	19.2	19.1
pH	5.85	5.21	4.03	4.13	3.96
Conductivity (µS/cm)	1689	1696	1855	1868	2966

Table 4.1: Parameters measured along the groove of flowing water. Sites are listed from the top to the bottom.

Tableau 4.1: Paramètres mesurés dans les eaux le long du fossé. Les sites sont classés de haut en bas.

Along the groove, the pH values fall from 5.85 to 3.96. The conductivity and the ion concentration increase in parallel with the pH decrease. The acid water produced by the mining activity and the iron core lixiviation induce acidic alteration of the basaltic materials. It is impossible to control the temporal chemical variability of water associated with rainfall and other climatic parameters. However, since it was in the very early spring time, the flow of water was relatively important and the pH was probably above annual average. Measured pH-values thus more or less correspond to maximum values, and *vice versa* for the conductivity. Finally, the water temperature is strongly influenced by climatic variability.

IV.6.2: Elemental analyses by ICP

Seven samples were selected to follow the chemical evolution (1) along the groove, with the samples S1-1, S2-1, S3-1 and S5-1, and (2) perpendicularly to the groove, with the samples S3-1 to S3-4 in site 3; the sample S3-1 is located at the intersection of the two series (Fig. 4.3). The geochemical analyses are reported in the Appendice C.

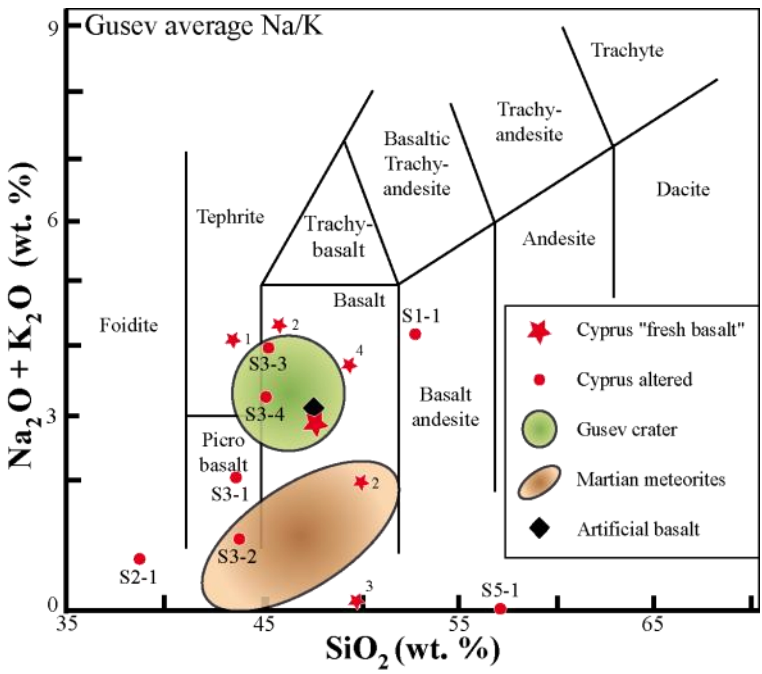

◄Figure 4.4: Total Alkali-Silica (TAS) diagram showing the compositions of fresh basalts from Cyprus ophiolite (red stars; after (1) *Bear, 1960*, (2) *Bear, 1961*, (3) *Moores and Vine, 1971*and (4) *Dill et al., 2007*. the large red star is mean composition of the fresh basalts. The red dots represent the samples taken along the groove of flowing water. Basalts from Gusev crater, meteorites (after *Mc Sween et al., 2009*) and artificial basalts are also reported for comparison (see Chapter V and *Bost et al., 2012*).

◄*Figure 4.4: Diagramme TAS montrant les basaltes frais de l'ophiolite de Chypre (étoiles rouges) d'après (1) Bear 1960, (2) Bear 1961, (3) Moores and Vine, 1971, (4) Dill et al., 2007., La grande étoile rouge représente la composition moyenne de ces basaltes, et les points rouges sont représentatifs des échantillons prélevés le long du fossé. Les basaltes ducratère de Gusev, les compositions mafiques des météorites (after Mc Sween et al., 2009) et les basaltes martiens artificiels sont reportés par comparaison (voir Chapitre V et Bost et al., 2012).*

No fresh basalt could be sampled in our sampling site to obtain the initial basaltic composition, but chemical analyses of these unaltered basalts in Cyprus are available (*Bear 1960, 1961* in *Moores et Vine, 1971*; *Dill et al., 2007*). These data are plotted in the TAS diagram in Figure. 4.4 (red stars), showing high variability in composition, in particular on the total alkali parameter Na_2O+K_2O. Thus, the average composition of the 6 analyses was chosen as a reference (large red star). This average composition is similar to that of the Martian Gusev basalts and to the artificial samples described later (*McSween et al., 2009; Bost et al., 2012* and Chapter V), although the Fe- and Mg-contents are very different.

As suggested by *Harnois (1988)*, the weathering corresponds to a depletion of the mobile components with respect to the immobile components. During basalt weathering, Si, Mg, Ca and Na are generally leached but Al and Ti remain essentially in the system and accumulate in the residue (e.g., laterites). Fe and K have more complicated behaviours. The proportion of Fe remaining in the residue is partially a function of the redox conditions of the system, and if K is generally leached during soil formation, clays particles absorb and retain K^+. The redox conditions for the host rock in the *NW Phoenix* pit are reducing (green colour) and become, at the surface, oxidising because of the acidic alteration as shown by the red-orange colour. The chemical index of weathering (CIW), proposed by *Harnois (1988)*, can be applied to soils and to silicate rocks of felsic to mafic composition. It is given by:

$$CIW = \left(\frac{Al_2O_3}{Al_2O_3 + CaO + Na_2O}\right).100 \qquad (1)$$

with an error margin given by:

$$\Delta CIW = CIW\left(\frac{\Delta Al_2O3}{Al_2O_3} + \frac{\Delta Al_2O_3 + \Delta CaO + \Delta Na_2O}{Al_2O_3 + CaO + Na_2O}\right) \quad (2)$$

with Al_2O_3, CaO, and Na_2O being the mole percent of the corresponding oxide in the material. In this index, Al_2O_3 represents the immobile component and CaO and Na_2O the mobile components. This index increases with weathering. For fresh basalts, the CIW varies around 40 mole% whereas the index of highly weathered basalt is below 80 mole%. Fresh basalts from Cyprus have a low CIW (36.70%; *Dill et al., 2007*) while altered samples have a CIW between 47 to 99 %, the most altered sample being S5-1 (Table 4.2).

There is no apparent correlation between the CIW and the position of the samples along the groove in Table 4.2. However, the elemental contents in mole% versus the CIW index plotted in Figure 4.5 show that SiO_2, CaO, Na_2O and K_2O decrease, Al_2O_3, TiO_2 and MnO are constant, and Fe_2O_3, MgO and Cu increase, with an increase in CIW. These results are in good accordance with the Goldschmidt classification (*Goldschmidt, 1926*) of insoluble precipitating elements (Fe^{3+}, Ti, Mn and Al) and soluble elements (K, Ca, Na, Fe^{2+}, Mg and Si). Even though Mg is a soluble cation, MgO shows a similar behaviour to that of TiO_2, which can be explained by its proximity to the insoluble field in the Goldschmidt diagram.

There is no correlation between the CIW with respect to the vertical sampling sequence (along the groove) but there is good correlation with the horizontal sequence: alteration increases closer to the groove. The geochemical analyses shows global alteration associated with tardi-magmatic/deuteritic processes but this does not allow any conclusion to be drawn regarding the different stages of the alteration process.Further mineralogical study is therefore necessary.

	Vertical Sampling				**Horizontal sampling**				
pH	5.84	5.21	4.03	3.95					
Sample	S1-1	S2-1	S3-1	S5-1	S3-1	S3-2	S3-3	S3-4	Fresh
CIW	71.57	91.76	74.42	98.98	74.42	59.87	57.82	55.97	36.70
ΔCIW	2.25	2.14	2.25	2.07	2.25	2.16	2.13	2.10	3.67

Table 4.2: Chemical index of weathering obtained using the *Harnois (1988)* method (with associated errors). Fresh sample data is from *Dill et al., (2007).*

Tableau 4.2. Index chimique d'altération obtenu avec la méthode de Harnois (1988), avec les incertitudes respectives. La donnée utilisée pour l'échantillon brut est celle de Dill et al., (2007).

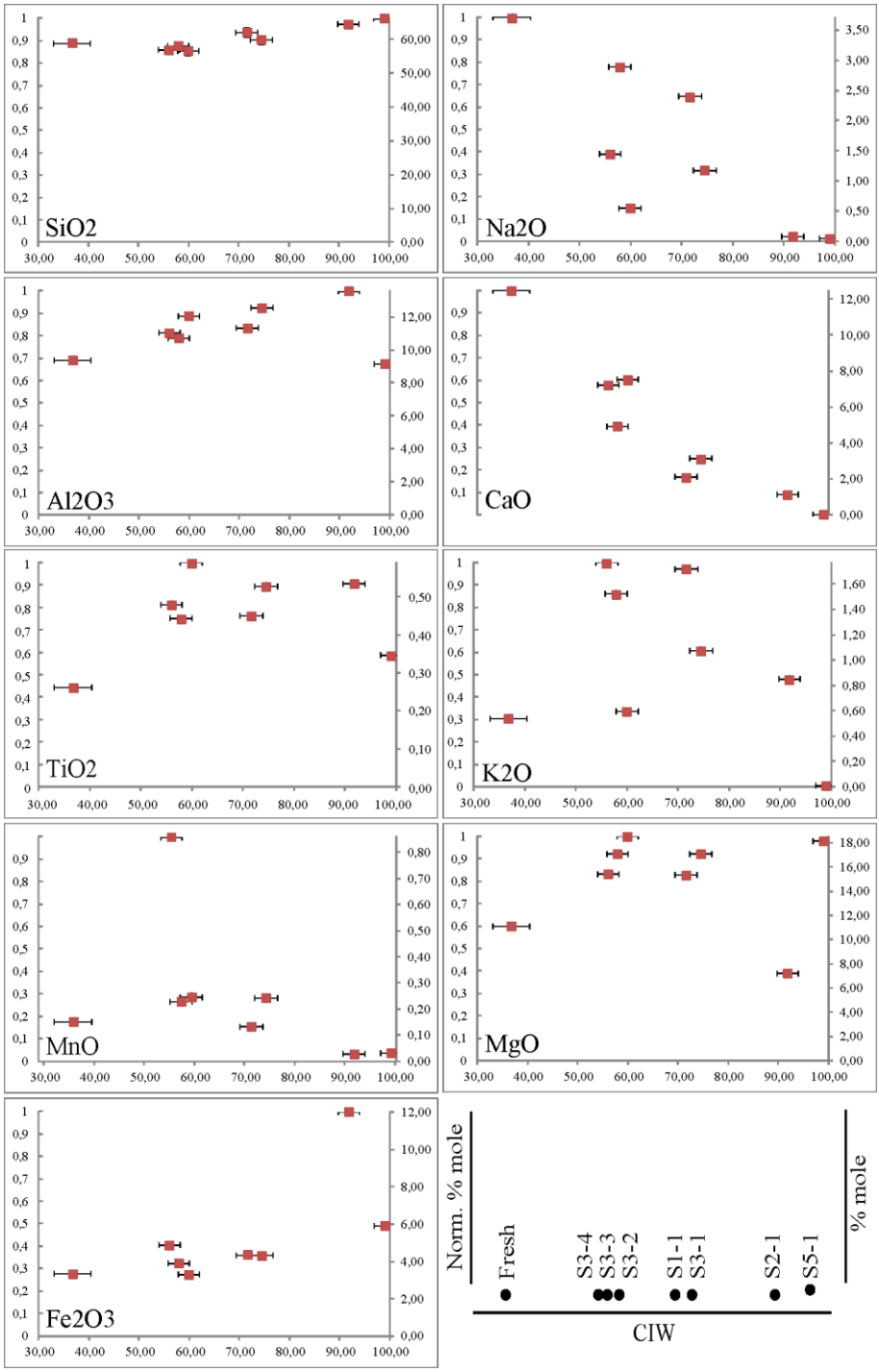
SiO2
Na2O
Al2O3
CaO
TiO2
K2O
MnO
MgO
Fe2O3
Norm. % mole
% mole
Fresh
S3-4
S3-3
S3-2
S1-1
S3-1
S2-1
S5-1
CIW

◄Figure 4.5: Concentrations in mole%of Al_2O_3, TiO_2, MnO, SiO_2, CaO, Na_20, K_2O, Fe_2O_3, and MgO versus the CIW index in Cyprus samples. Data on the left correspond to the unaltered basalt analysis from *Dill et al. (2007)*.

◄*Figure 4.5: Concentratiosn en pourcentages molaires de Al_2O_3, TiO_2, MnO, SiO_2, CaO, Na_20, K_2O, Fe_2O_3, and MgO en fonction de l'index CIW dans les échantillons de Chypre. La donnée la plus à gauche correspond à l'échantillon non altéré provenant de Dill et al. (2007).*

IV.6.2. Mineralogical characterisation

The mineralogy of the sampled rocks was characterized using XRD analysis, optical observation and Raman spectroscopy. The samples are described using the 3 main alteration facies observed: (1) quartz-chlorite facies, and intermediate facies, (2) smectite facies, and (3) smectite + sulphate facies. Finally, the waste dump mineralogy is also described.

IV.6.2.1. Quartz-chlorite facies.

The massive rocks were originally basalts from the upper pillow basalt lavas (UPL) described in part IV.4.3. The first alteration process which they were submitted to was the hydrothermal and deuteritic weathering, producing a typical quartz-chlorite facies. This mineralogy is observed in the lower level of the open pit (site 5) and corresponds to samples S5-1, S5-2 and S5-3 (locations and macroscopic views are displayed in Fig. 4.6).

XRD analyses (Fig. 4.7) indicates that clays are well organised, and could be chamosite, (Fe,Al,Mg)6(Si,Al)4O10(OH)8. Some traces of gypsum, natroalunite (zeolite) and feldspars are also observed.

►Figure 4.6: Location and photographs of samples S5-1, S5-2 and S5-3. The samples are blue-green with only a thin reddish surface.

►*Figure 4.6: Localisation et photos des échantillons S5-1, S5-2 et S5-3. Les échantillons sont bleu-vert avec seulement une fine surface rougeâtre.*

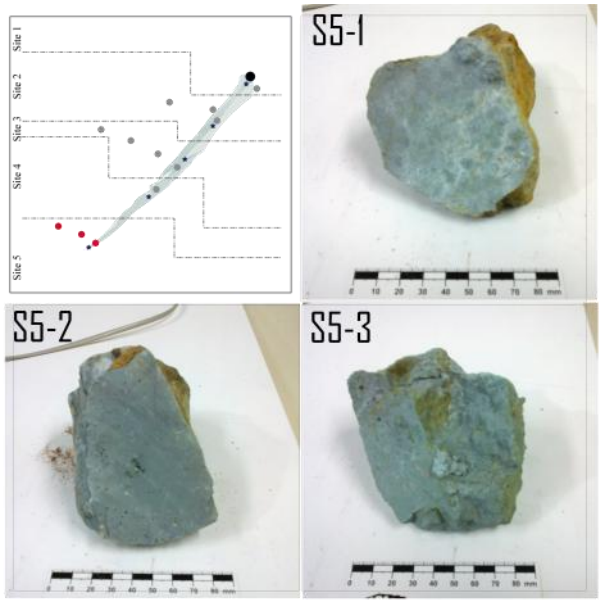
Site 1
Site 2
Site 3
Site 4
Site 5
S5-1
S5-2
S5-3

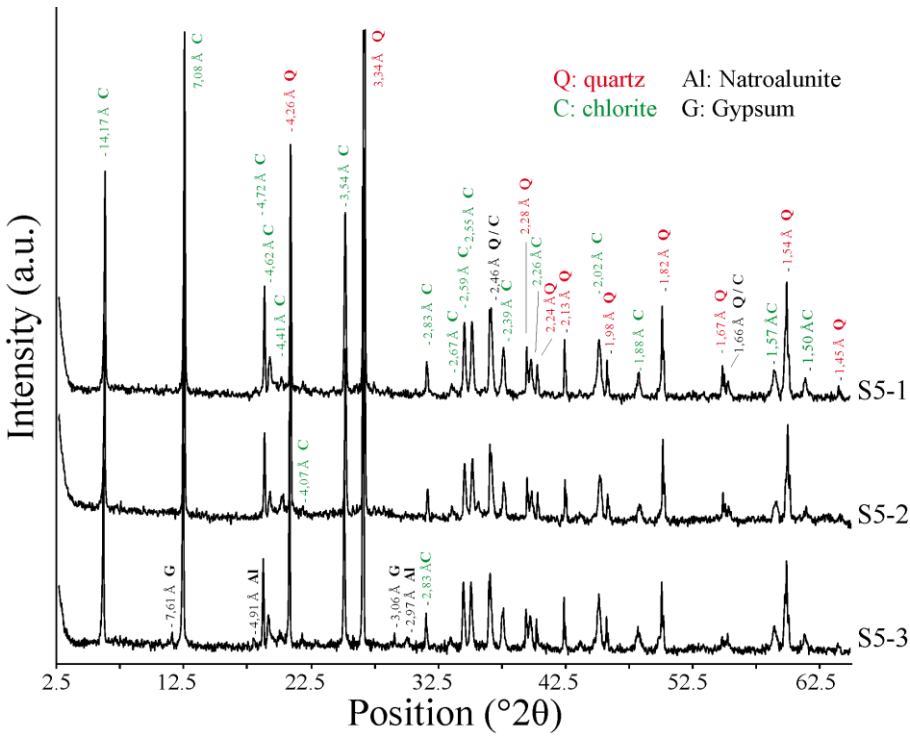
Q: quartz
C: chlorite
Al: Natroalunite
G: Gypsum
Intensity (a.u.)
Position (°2θ)
2.5
12.5
22.5
32.5
42.5
52.5
62.5
S5-1
S5-2
S5-3
-14,17 Å C
7,08 Å C
-4,72 Å C
-4,62 Å C
-4,41 Å C
-4,26 Å Q
-4,07 Å C
-3,54 Å C
3,34 Å Q
-2,83 Å C
-2,67 Å C
-2,59 Å C
-2,55 Å C
-2,46 Å Q / C
-2,39 Å C
-2,28 Å Q
-2,26 Å C
-2,24 Å Q
-2,13 Å Q
-2,02 Å C
-1,98 Å Q
-1,88 Å C
-1,82 Å Q
-1,67 Å Q
-1,66 Å Q / C
-1,57 Å C
-1,54 Å Q
-1,50 Å C
-1,45 Å Q
-7,61 Å G
-4,91 Å Al
-3,06 Å G
-2,97 Å Al
-2,83 Å C

◄Figure 4.7: Powder diffractogram pattern of S5-1, S5-2 et S5-3 samples. The observed mineralogical phases are quartz and chlorite. Traces of gypsum and natroalunite are also observed.

◄*Figure 4.7 : Spectres de diffraction X S5-1, S5-2 et S5-3. Les principaux minéraux observés sont le quartz et la chlorite, avec des traces de gypse et de natroalunite.*

Thin section observations and Raman mapping show that the quartz and chlorite are associated with some oxide grains, identified as Ti-oxides by Raman spectroscopy (Fig. 4.12). Small quartz grains occur in groups and in small cracks. Based on the elemental analysis, the chemical composition of the chlorite has been calculated, using *Dear et al., (1974)* as: $(Mg_{5.01}Al_{2.19}Fe_{3.27}Ti_{0.1})_{\Sigma=12}[(Si_{5.14}Al_{2.86})_8O_{20}](OH)_{16}$, which corresponds to a ripidolite.

IV.6.2.2 Intermediate facies

The intermediate facies corresponds to the sites 1 and 2; samples S1-1, S2-2 and S2-3 (Fig. 4.8). In this facies, quartz is the dominant mineral. The XRD analyses (Fig. 4.9) show that it is associated to subordinate phyllosilicate (interstratified chlorite/smectite). This mineral is associated with plagioclases, sometimes in equal proportion to that of quartz. Traces of K-feldspars are also observed.

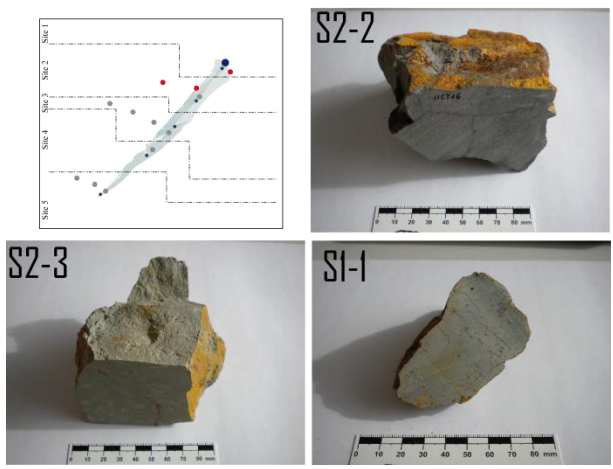

Figure 4.8: Location and photographs of samples S1-1, S2-2 and S2-3. The samples are blue-green with only thin reddish surface and veinelets.

Figure 4.8: Localisation et photos des échantillons S1-1, S2-2 et S2-3. Les échantillons sont decouleur turquoise, avec seulement une fine surface rougeâtre et quelques veinules.

In thin section, the chlorite/smectite clays are dark brown (Fig. 4.12f) and traces of pyrite were detected by Raman spectroscopy. From a mineralogical point of view, these samples are an intermediate facies, falling between the chlorite-quartz facies and the smectite facies.

►Figure 4.9: a- Powder diffractogram pattern of samples S1-1, S2-2 and S2-3. The observed mineralogical phases are quartz (Q) and interstratified clay: chlorite/smectite (ML). Plagioclases (P) and traces of K-feldspar (FK) were observed. b- X-Ray diffraction of oriented preparations of sample S2-2. The main mineral phase identified is a mixed-layer chlorite-smectite (CS) associated with very low amounts of plagioclases (P) and quartz (Q). Analyses made after the sample was air dried (AD), treated with ethylene glycol (EG), and heated to 350°C and 550°C.

►*Figure 4.9: a- Spectres de diffraction des rayons X des échantillons S1-1, S2-2 et S2-3. Les phases minéralogiques observées sont le quartz (Q) et une argile interstratifiée : chlorite/smectite (ML). Des traces de plagioclases (P) et de feldspaths potassiques sont aussi observées. b- Spectre de diffraction X de préparations orientées de l'échantillon S2-2. La principale phase identifiée est une chlorite-smectite (CS) associée avec un peu de plagioclase (P) et de quartz (Q). Séchage à l'air (AD), à l'éthylène glycol (EG) et chauffage à 350°C et 550°C.*

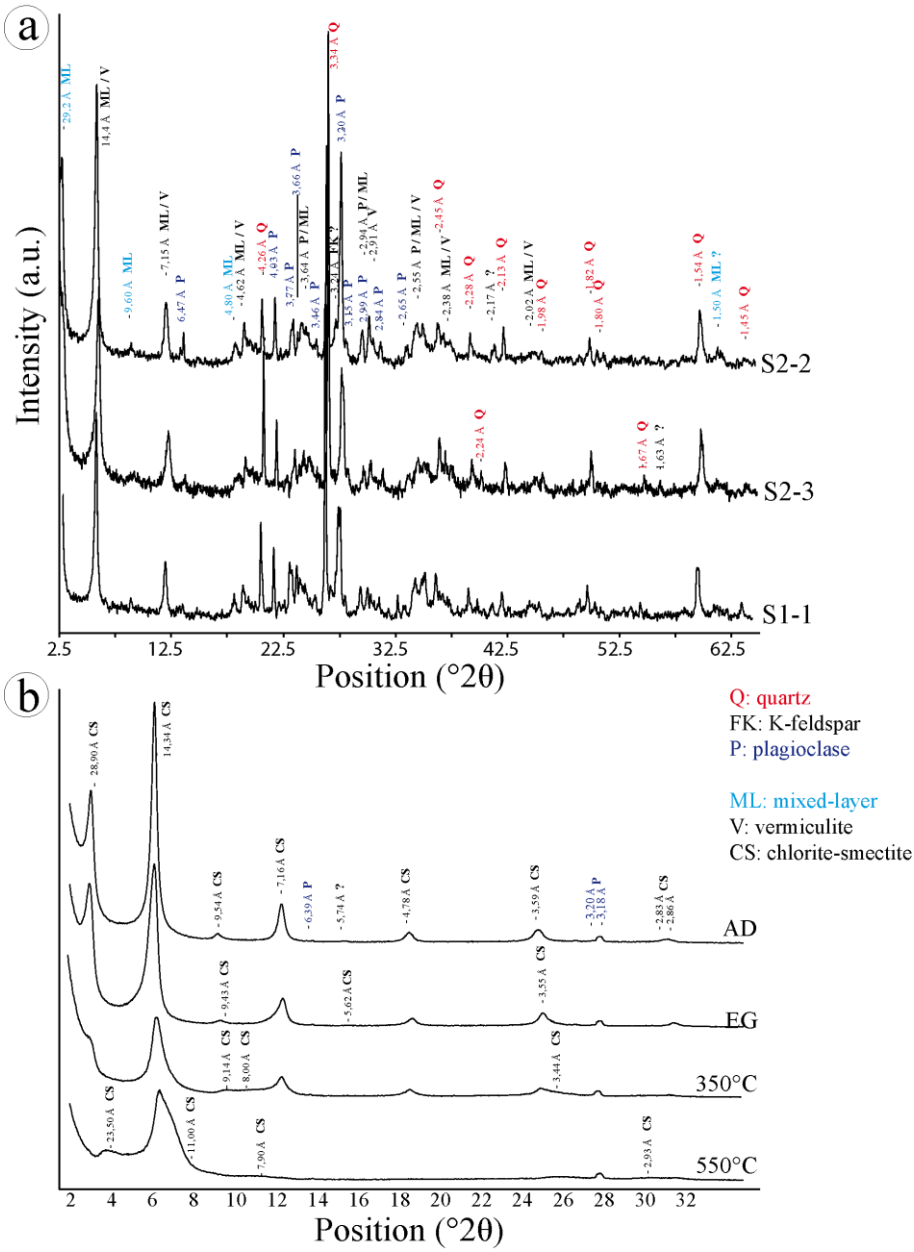
a
Intensity (a.u.)
S2-2
S2-3
S1-1
2.5
12.5
22.5
32.5
42.5
52.5
62.5
Position (°2θ)
b
Q: quartz
FK: K-feldspar
P: plagioclase
ML: mixed-layer
V: vermiculite
CS: chlorite-smectite
AD
EG
350°C
550°C
2
4
6
8
10
12
14
16
18
20
22
24
26
28
30
32
Position (°2θ)

IV.6.2.3. Smectite facies

This facies is observed in samples S3-2, S3-3 and S3-4 (Fig. 4.10).

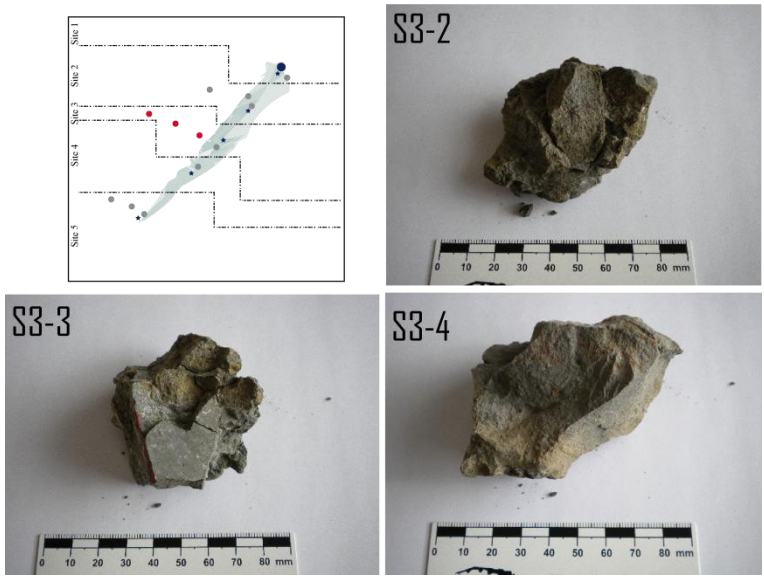

Figure 4.10: Location and photographs of the samples S3-2, S3-3 and S3-4. The samples are blue-green.

Figure 4.10: Localisation et photos des échantillons S3-2, S3-3 et S3-4. Les échantillons sont couleur turquoise.

This rock does not contain quartz or chlorite. XRD analyses (Fig. 4.11) show that the mineralogical assemblage essentially consists of smectite associated with pyroxene, plagioclase and small traces of zeolite. The pyroxene is augitic, $Ca(Mg,Fe)Si_2O_6$, and the zeolite has an analcime composition, $NaAlSi_2O_6,H_2O$. Locally, clinopyroxene and plagioclase may disappear while analcime increases. The clay is an interstratified smectite/chlorite with highsmectite-contents.

In thin section, the sample consists essentially of brown clay (probably smectite) associated with a very small amount of quartz and some feldspars (Fig. 4.12c, 12d). The initial paragenesis represented by large sub-euhedral diopside-augite crystals (Fig. 4.12d,e) and elongated plagioclases is still visible. Carbon nanophases were observed by Raman spectroscopy. Small oxides are present but

could not be identified by Raman due to their very small size (< 1µm). It was also impossible to identify the black clay phase (Fig. 4.12e). The same facies is also observed in sample S2-1. The identified minerals are essentially composed by smectite clays materials associated with very small amounts of quartz and pyrite (Fig. 4.11). Oriented analyses show corrensite as the only clay phase (somewhat different from sample S2-3).

►Figure 4.11: a- Powder diffractogram pattern of samples S3-2, S3-3 and S3-4. The observed mineralogical phases are smectite (Sm), plagioclase (P), clinopyroxene (Cpx) and traces of zeolites (Z, Z1 and Z2). b- X-ray diffraction of oriented preparations of sample S3-3. The main mineral phases identified are smectite (Sm) and chlorite (C) with very low amounts of plagioclase (P). Analyses made on preparations that were either air dried (AD), or treated with ethylene glycol (EG), and by heating at 350°C and 550°C.

►*Figure 4.11 : a- Spectres de diffraction X des échantillons S3-2, S3-3 et S3-4. Les phases minéralogiques observées sont la smectite (Sm), le plagioclase (P) et le clinopyroxène (Cpx) avec des traces de zeolites (Z, Z1 et Z2). b- Spectre de diffraction X de préparations orientées de l'échantillon S3-3. Les principales phases identifiées sont une smectite (Sm) et une chlorite (C), associées avec un peu de plagioclases (P). Séchage à l'air (AD), traitement à l'éthylène glycol (EG) et par chauffage à 350°C et 550°C.*

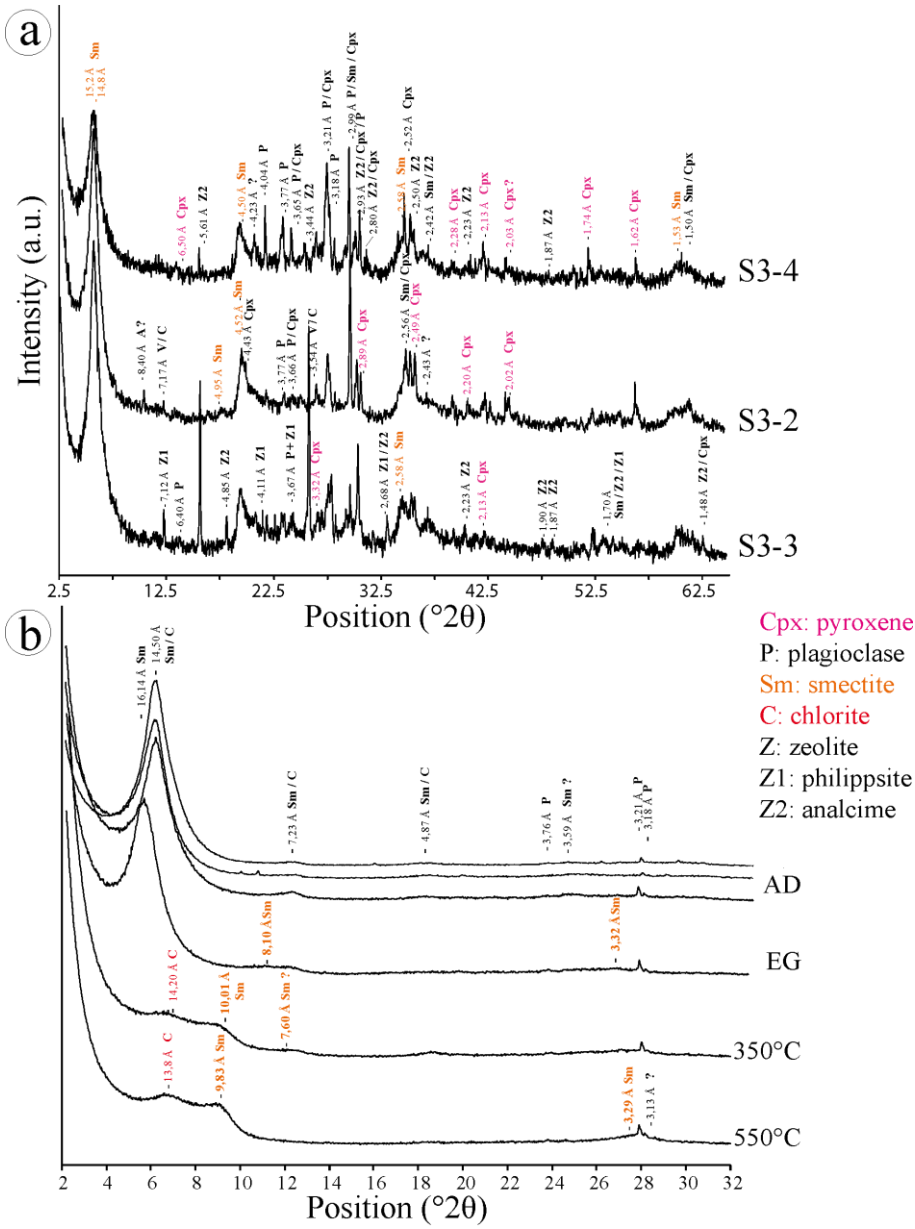
a
Intensity (a.u.)
S3-4
S3-2
S3-3
2.5
12.5
22.5
32.5
42.5
52.5
62.5
Position (°2θ)
b
Cpx: pyroxene
P: plagioclase
Sm: smectite
C: chlorite
Z: zeolite
Z1: philippsite
Z2: analcime
AD
EG
350°C
550°C
2
4
6
8
10
12
14
16
18
20
22
24
26
28
30
32
Position (°2θ)

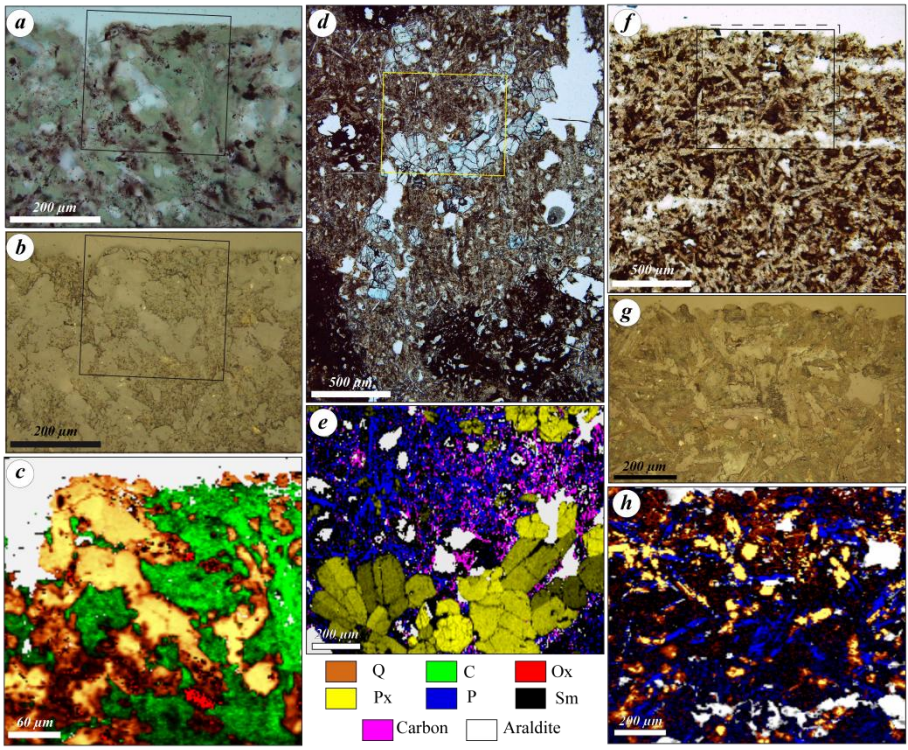

Figure 4.12: Optical views of the different mineral facies and associated Raman maps. *(a to c) :* The quartz-chlorite facies (S5-1). (a):transmitted light, (bin reflected light. (c) Raman map corresponding to the black square in (a) and (b). *(d to e):* The smectite facies (S3-4).(d): transmitted light. (e): Associated Raman map corresponding to the yellow box in (d). *(f to h):* The intermediate level (S2-2). (f) : Transmitted light. (g): Reflected light image of the box in (f). (h): Raman map of the box shown in (f). (Q: quartz, C: chlorite, Ox: oxide, Px: pyroxene, P: plagioclase, and Sm: smectite)

Figure 4.12: Images optiques des différents facies minéralogiques et cartographies Raman associées. (a à c) : Le facies à quartz-chlorite (S5-1) en lumière transmise (a), en lumière réfléchie (b).(c) : Cartographie Raman du carré noir indiqué en (a) et (b). (d et e) Le facies smectite (S3-. (d) : Lumière transmise. (e): Cartographie Raman du carré jaune indiqué en (d). (f à h) Le facies intermédiaire (S2-2. (f) : lumière transmise ;(g) :vue en lumière réfléchie de la zone indiquée en pointillés sur (f). (h)Carte Raman de la zone photographiée en (f).(Q: quartz, C: chlorite, Ox: oxide, Px: pyroxene, P: plagioclase, et Sm: smectite)

IV.6.2.4. Smectite, zeolite and sulphate facies

This facies is observed in samples S3-1, S4-1 and S4-2 taken along the groove of flowing water (Fig. 4.13). This system has been strongly leached by the circulation of acidic water.

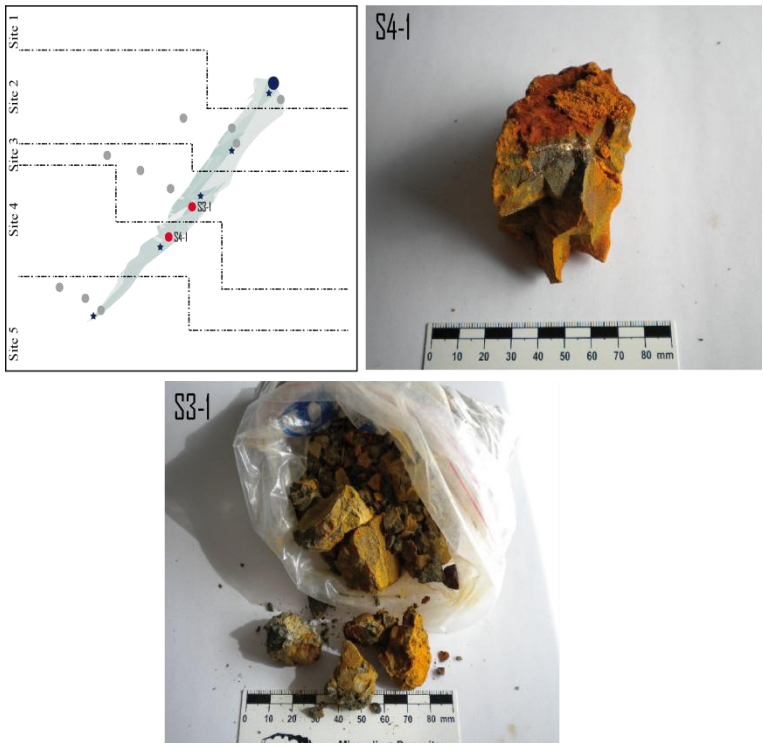

Figure 4.13: Location and photographs of samples S3-1 and S4-1. Sample S4-2 is mud taken near sample S4-1 and is thus not represented in the figure. The samples have a blue-green core with a reddish weathered surface.

Figure 4.13: Localisation et photos des échantillons S3-1 et S4-1. L'échantillon S4-2 est de la boue prélevée à proximité de l'échantillon S4-1 et n'est pas représentésur la figure. Les échantillons ont un cœur bleu-vert et une surface altérée dans les rouges.

The rocks are essentially composed of smectite associated with low amounts of the zeolites analcime and philippsite (respectively $Na_{16}(Al_{16}Si_{22}O_{96}),16H_2O$ and $K_2(Ca_{0.}5Na)_4(Al_6Si_{10}O_{32}),12H_2O$) and traces of

plagioclase. Although the proportions of smectite and analcime can be locally reversed, the philippsite and analcime ratio remains unchanged. This sample also contains a small amount of hydrated sulphates, gypsum and natrojarosite ($CaSO_4$, $2H_2O$ and $NaFe_3(SO_4)_2(OH)_6$, respectively). In the mud sample (S4-2) the smectite- and natrojarosite-contents is comparable to those in other samples (Fig. 4.14). The oriented analyses show smectite associated with trace amounts ofchlorite.

IV.6.2.5 Waste dump mineralogy

The waste dump, resulting from enhanced acid leaching to extract residual Cu, was also sampled in order to be compared with materials outcropping along the groove. . Three samples were collected: 11CY05, 11CY06 and 11CY07. Sample 11CY07 contains only a quartz-chlorite assemblage, whereas sample 11CY06 contains only gypsum associated with small quartz grains, natrojarosite and traces of hexahydrite, alunogene and chlorite. At the top of the waste dump, the materials are essentially composed of sulphates. The most abundant one is a hydrated sulphate with a chemical composition falling in the wupatkiite-pickeringite solid solution: $((Co,Mg)Al_2(SO_4)_4,22H_2O$ and $MgAl_2(SO_4)_4,22H_2O$, respectively). Hexahydrite ($MgSO_4$, $6H_2O$) is the second most abundant hydrated sulphate is . The only phyllosilicates present in the waste dump are highly crystallized chlorite and chamosite.

►Figure 4.14: a- X-ray diffractograms of samples S3-1, S4-1 and S4-2. b- X-ray diffraction patterns of an oriented preparation of sample S3-1. The main mineral phase identified is smectite (Sm) with very low amount of F-feldspar (FK) and quartz (Q). Analyses made on preparation that were air dried(AD), treated with ethylene glycol (EG), and heatied to 350°C and 550°C.

►*Figure 4.14: a- Clichés de diffraction X des échantillons S3-1, S4-1 et S4-2. b- Diffractogrammes des préparations orientées de S3-1. La phase minérale principale identifiée dans cet échantillon est la smectite (Sm) associée à un peu de feldspath potassique (FK) et de quartz (Q). Séchage à l'air (AD), à l'éthylène glycol (EG) et après chauffage à 350°C et 550°C.*

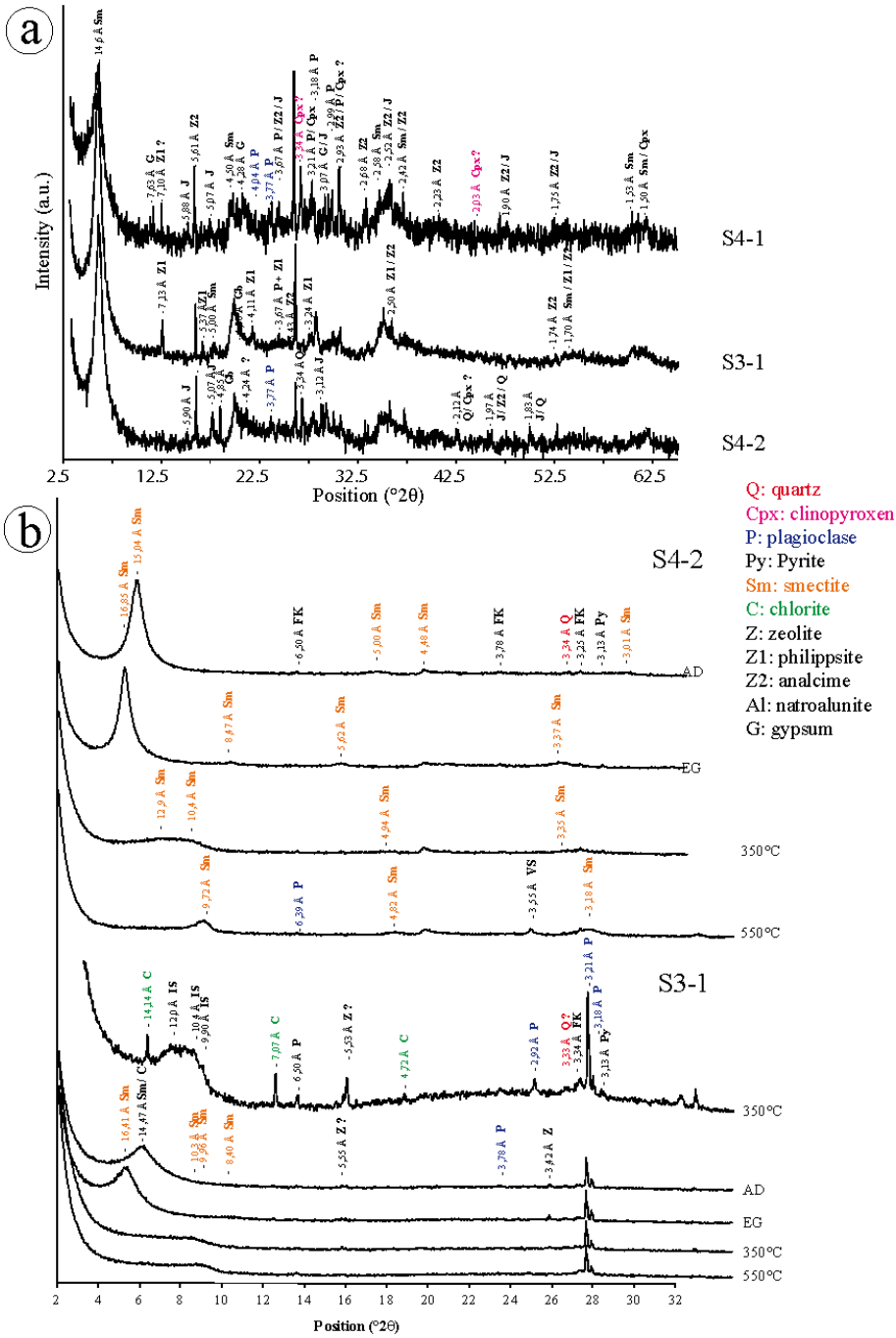
a
Intensity (a.u.)
Position (°2θ)
S4-1
S3-1
S4-2
b
S4-2
S3-1
AD
EG
350°C
550°C
Position (°2θ)
Q: quartz
Cpx: clinopyroxen
P: plagioclase
Py: Pyrite
Sm: smectite
C: chlorite
Z: zeolite
Z1: philippsite
Z2: analcime
Al: natroalunite
G: gypsum

IV.7. Discussion

IV.7.1 Mineralogy

The mineralogical observations are summarized in Table 4.3. The massive host-rock consists of three types of mineral associations (paragenesis):

- (1) quartz + chlorite;

- (2) smectite (+ pyroxene + plagioclase);

- (3a) smectites + zeolites and (3b) smectites + zeolites + sulphates.

The intermediate facies is a mixture of the first and second facies. Hematite was not observed in the studied area.

Paragenesis (1) corresponds to the quartz-chlorite facies typical of the Upper Pillow Lava formation. It is associated with primary hydrothermal alteration (*Richards et al., 1989*), which suggests formation by deuteritic processes.

Paragenesis (2) corresponds to a further evolution of paragenesis (1), especially with the transformation of interstratified primary chlorite to a mixed chlorite/smectite, such as corrensite. This paragenesis is related to further metasomatic alteration in low temperature conditions operating during the aging of the Troodos extrusive sequences (*Richards et al., 1989*).

Indeed, the presence of fairly abundant pyroxene, a primary mineral, attests to the basaltic origin of the material, although the main phase is smectite. This paragenesis is similar to the smectite facies described in the Pitherokhoma mine by *Richards et al. (1989)*, and can also be compared to the facies (3a) described by *Alt and Honnorez (1984)* in the DSDP site 417. This mineralogy is associated to the circulation of oxygenated seawater.

Paragenesis (3) (a) and (b) are the evolution of paragenesis (2) in more acidic conditions. The first alteration step is lixiviation. Figure 4.5 (samples S3-1 and S3-3) shows a sudden variation of the elemental composition, in particular a decrease in Fe, which, from a mineralogical point of view, corresponds to the precipitation of Fe-free zeolites . Moreover, the presence of zeolites can be explained by the destabilization of pyroxene (i.e. clinopyroxene + fluid = analcime + albite, and volcanic glass + fluid = phillipsite). Zeolites can be

formed by interaction of seawater-derived fluids with basalts (*Alt and Honnorez, 1984*).

However, the increase in acidic conditions is associated with the appearance of sulphate minerals (gypsum and natrojarosite). It is for this reason that the study of materials in the acid-weathered waste dump is important.

The waste dump mineralogy is typical of that associated with acidic leaching whereby acidic water attacks the primary minerals, such as chlorite and albite, and releases Mg, Fe, Al, Ca and Na. Thus we observe the following sequence of increasingly less soluble salts with decreasing pH: wupatkiite-pickeringite [$(Co,Mg,Ni)Al_2(SO_4)_4 \bullet 22H_2O$ and $MgAl_2(SO_4)_4 \bullet 22H_2O$] → hexahydrite [$MgSO_4 \bullet 6H_2O$] → alunogens [$Al_2(SO_4)_3 \bullet 17H_2O$] → natrojarosite [$NaFe_3(SO_4)(OH)_6$] → gypsum [$CaSO_4 \bullet 2H_2O$].

Geochemical analyses confirm the mineralogical evolution suggested by Table 4.3 . Samples S3-1 and S3-2 show a geochemical composition with a very important decrease in Fe associated an important variation of the mineralogy. It underlines the fact that the evolution (superimposition) of hydrothermal and metasomatic alteration to an alteration with acidic water in rock-buffered reduced conditions promotes the precipitation of sulphates. Complementary mineralogical and geochemical characterization (e.g., chemical analyses of mine waste waters, elemental analysis of minerals using electron microprobe), and a more detailed sampling in the outcrop will be necessary to refine this interpretation. Finally, it is possible to characterize the different mineralogical facies in the *Skouriotissa* mine (Fig. 4.15).

►Table 4.3: Mineralogical composition of the different facies. From top to bottom of the Table: (1) chlorite-quartz facies, (2a) intermediate facies, (2b) smectite facies, (3a) smectite + zeolite facies, then (3b) smectite + zeolite+ sulphate. tr.: traces, *: samples with geochemical analysis.

►*Tableau 4.3: Composition minéralogique des différents faciès. De haut en bas du Tableau : (1) faciès à chlorite-quartz, (2a) faciès intermédiaire, (2b) faciès à smectite, (3a) faciès à smectite + zeolite, (3b) faciès à smectite + zeolite + sulphate. tr.: traces, *: échantillons avec des analyses géochimiques.*

Table 4.3 : Mineralogical composition of the different facies

Localisation		Phyllosilicates			Zéolites		Quartz	Feldspars		Pyroxene	Pyrite	Sulphates	
Site	Sample	Interstratify	Chlorite	Smectite	Philippsite (Z1)	Analcime (Z2)		KFeldspars	Plagioclase			Gypse	Natrojarosite
Site 5	S5-1*		+++++				+++++	tr (?)					
	S5-2		++++				++++++	tr (?)					
	S5-3		++++				++++++	tr (?)					
Site 2	S2-2	+++ +					+++	tr	+++				
	S2-3	+++					+++++	tr	++				
Site 1	S1-1*	+++					++++	+	++		tr		
Site 2	S2-1*			++++++			tr				tr		
Site 3	S3-1			++++++	+	+			tr				
	S3-2*			++++++		tr			+	+++			
	S3-3*			++++	+	+++			tr	+			
	S3-4*			+++(+)		+			++	+++			
Site 4	S4-1			+++	+	+++			tr			+	+
	S4-2			++++++		+	+		tr (?)	tr (?)			++

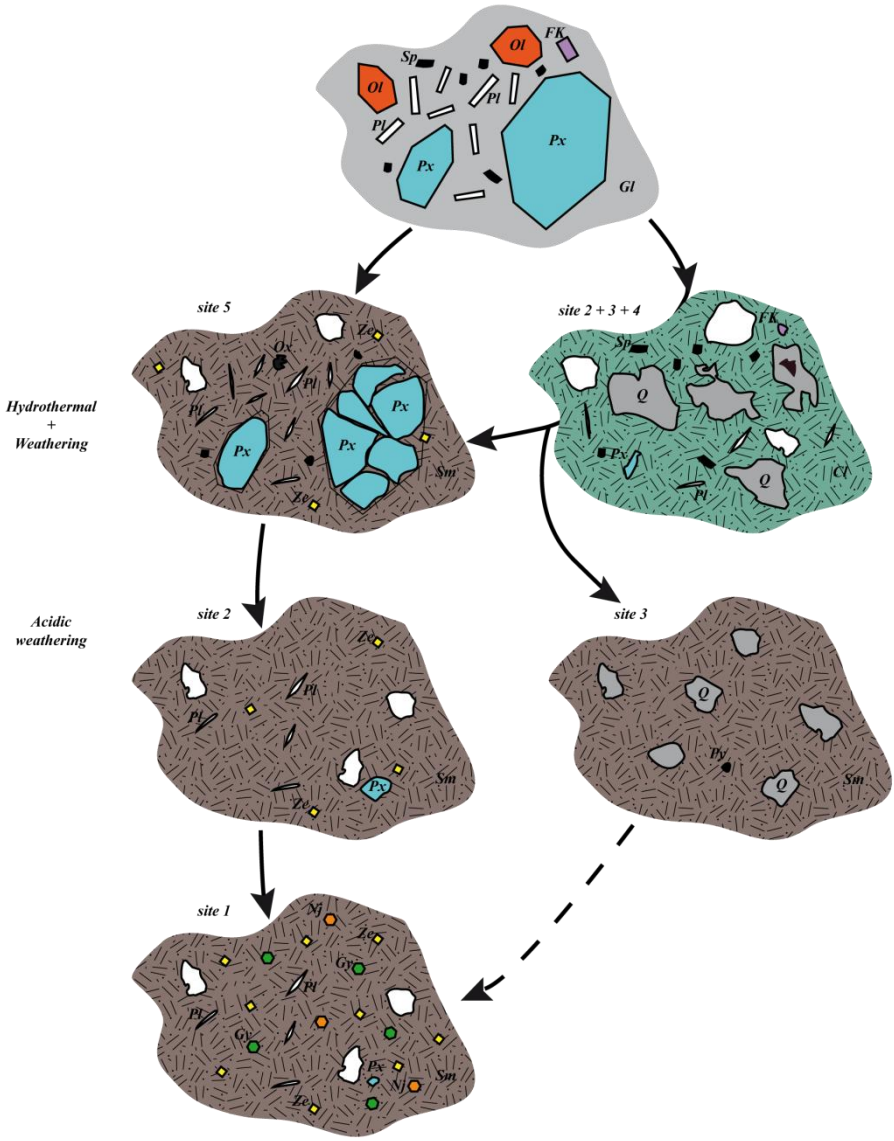
Ol
FK
Sp
Ol
Pl
Pl
Px
Px
Gl
site 5
site 2 + 3 + 4
Hydrothermal
+
Weathering
Ox
Zc
Pl
Pl
Px
Px
Px
Sm
Zc
FK
Sp
Q
Px
Q
Cl
Pl
Acidic
weathering
site 2
site 3
Zc
Pl
Pl
Px
Sm
Zc
Q
Ply
Q
Sm
site 1
Nj
Zc
Gy
Pl
Pl
Gy
Px
Nj
Sm
Zc

◄Figure 4.15: Mineralogical evolution of the *Skouriotissa* basalt during hydrothermal and acidic weathering. The horizontal exchanges are only suggestions for which there is no evidence in thin sections. Sp : spinel (black), FK: K-feldspar (purple), Px : pyroxene (blue), Ol : olivine (dark orange), Pl: plagioclase (white), Gl : glass (grey), Ox : oxide, Sm :smectite, Cl: chlorite, Nj : natrojarosite, Ze : zeolite, Gy : gypsum (green), Q: quartz (dark grey), Py: pyrite (black). White spots are vacuoles.

◄*Figure 4.15: Evolution minéralogique des basaltes de* Skouriotissa *pendant l'altération hydrothermale et acide. Les échanges horizontaux sont seulement suggérés en l'abscence de preuves en lames minces. Sp : spinelle (noir), FK: feldsphath potassique (violet), Px : pyroxene (bleu), Ol : olivine (orange foncé), Pl: plagioclase (blanc), Gl : verre (gris), Ox : oxyde, Sm : smectite, Cl: chlorite, Nj : natrojarosite, Ze : zeolite, Gy : gypse (vert), Q: quartz (gris foncé), Py: pyrite (noir).Les plages blanches sont des vacuoles.*

IV.7.2. Relevance for Mars exploration

Martian basalts have been altered by different acidic processes during the Noachian and Hesperian periods. Acid-sulphate weathering of basalts is a likely explanation for the sulphate-rich outcrops observed by the MERs Spirit and Opportunity (*Golden et al., 2005*). For example, the jarosite occurrence (associated with other hydrated sulphates) in Eagle, Fram and Endurance crateroutcrops in Meridiani Planum (*Squyres et al., 2004; Clark et al., 2005*) could only have been formed by aqueous processes under very acidic conditions (*van Breeman, 1980* and *Bigham and Nordstron, 2000* in *Golden et al., 2005*). Phyllosilicates (clays) have been interpreted to be the result of aqueous weathering (e.g. *Bibring et al., 2006*) but some of them may also be associated with deuteritic processes (*Ehlman et al., 2011* and *Meunier et al., 2012*). The latter phenomenon corresponds to deep-seated alteration of magmatic rocks during the later stages of their formation and is the direct result of magma consolidation. The phyllosilicates precipitate from fluids representing the residual liquid present at the end of the crystallization. Thus the precipitation of phyllosilicates in these conditions can be considered as a sort of hydrothermal phenomenon.

The rocks in the *Skouriotissa* mine exhibit alteration that is due to both natural processes and human activity. Two types of alteration have occurred. First, a pseudo-deuteritic alteration that resulted in the quartz-chlorite facies, followed by a second weathering process (smectite facies) that is associated with alteration by acidic waters flowing down the groove from the sulphide ore deposit and resulting in the formation of zeolites and sulphates.

IV.7.3. Mg enrichment

The Mg-content of the basalts is the discrimant parameter between Martian and terrestrial basalts (cf. Chapters II and III). The Upper Pillow basalt series in the Troodos ophiolite has Mg- and Fe-contents typical of terrestrial basalts and therefore strongly depleted in Mg and Fe with respect to Martian basalts.

The ternary diagram in Fig. 4.16 shows the evolution of the composition of basaltic rocks during weathering. Itcompares typical terrestrial basaltic weathering (*Nesbitt and Wilson, 1992*), Martian basalt weathering (as suggested by *Hurowitz et al., 2006* and *Ehlmann et al., 2011*), and the weathering observed in Cyprus. The classical terrestrial weathering is associated with an increase in Al and a decrease in Ca, Na, K, and especially in Fe and Mg. The Martian weathering sequence is more difficult to explain. The measurements in Gusev Crater (yellow and green squares) show different evolutions: increase of Ca, Na, K, Al and decrease of Fe and Mg, as well as the contrary.

►Figure 4.16: FM-A-CNK ternary diagram (mole %). FM= total Fe as FeO* + MgO ; A = Al_2O_3; CNK=CaO + Na_2O + K_2O (). The diagram shows the chemical evolution of basaltic rocks during terrestrial weathering (grey arrows: Baynton basalt, Australia, described by *Nesbitt and Wilson, 1992*) compared to the clays analyzed on Mars (white hexagons after *Ehlmann et al., 2011*). Note the different directions of alteration of the rocks in Gusev crater (green squares for RAT and brown squares for surface; after *Hurowitz et al., 2006*). The samples from this study correspond to the red dots and exhibit typical terrestrial weathering sequences. This alteration favours the concentration in Fe and Mg, in particular in sample S5-1, shown by the dotted line, and could be similar to a Martian process.

►*Figure 4.16: Diagramme ternaire (en mole %) FeO* + MgO (FM), Al_2O_3 (A), CaO + Na_2O + K_2O (CNK) montrant l'évolution géochimique des basaltes durant l'altération terrestre (flèche grise, basaltes de Baynton, Australie, décrits par Nesbitt and Wilson, 1992) comparée avec l'analyse d'argiles de Mars (hexagones blancs d'après Ehlmann et al., 2011). On notera les différentes directions prisest pendant l'altération des roches provenant du crater Gusev (carré vert pour le RAT et marron pour la surface, d'après Hurowitz et al., 2006). Les échantillons de cette étude correspondent aux points rouges et sont typiques d'une altération terrestre. Cependant, cette altération semble favoriser la concentration en Fe et Mg, en particulier dans l'échantillon S5-1, montrée au bout de la ligne en pointillés, et pourrait représenter un processus comparable à un processus martien.*

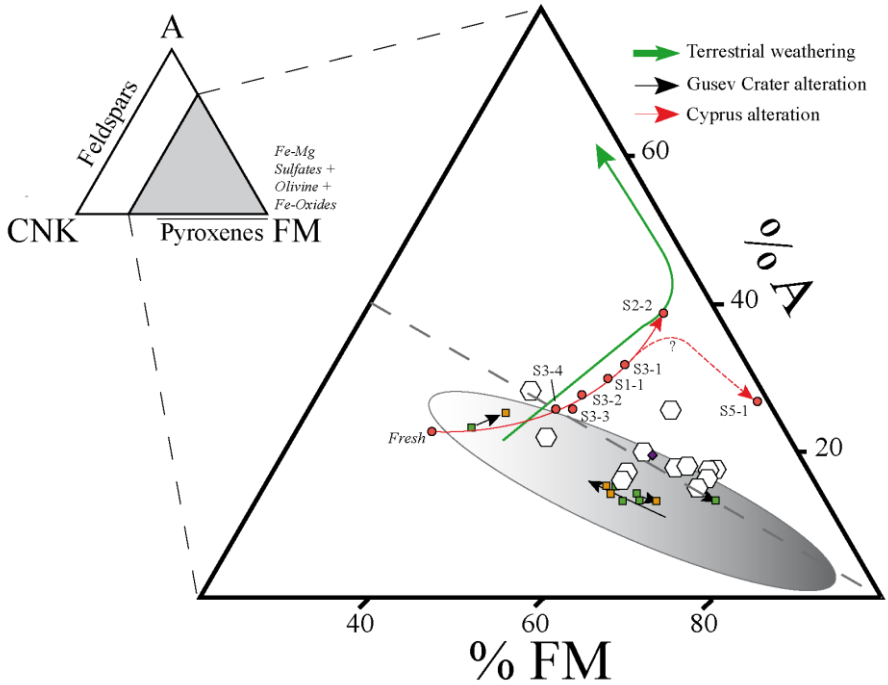

Clays can be considered as the ultimate weathering products and are displayed in Fig. 4.16 as white hexagons (*Ehlmann et al., 2011*). The basaltic weathering in the *Skouriotissa* mine is associated with a decrease in Ca, Na and K, and an increase in Al. However, it seems that the alteration favours the concentration of Fe and Mg (shown by the sample S5-1 and dotted arrow in Fig. 4.16). This is in contrast to the conventional terrestrial alteration and can be explained by the fact that the circulation of acidic fluids hinders the migration of Fe and Mg and promotes the formation of Fe-Mg rich clays. Similar phenomena may have taken place on Mars, suggesting that the natural enrichment in Fe and Mg basalts may be lower than previously expected.

IV.8 Conclusion

Study of the alteration of terrestrial basalts under subaqueous (seawater and/or hydrothermal) acidic and superficial conditions may reveal similarities with surface and subsurface processes occurring on early Mars. A suitable

terrestrial analogue site should therefore consists of non-metamorphosed basalt, *i.e.* a relatively young environment (*Tosca et al., 2004; Hurrowitz et al., 2006*) that has undergone acidic alteration. On Earth, typical acidic environments are found in sulphide-rich quarries and mine tailings in volcanogenic massive sulphide (VMS) ore deposits. VMS deposits are widespread in the oceanic basaltic crust (*Jebrak and Marcoux, 2008*) and are related to high to medium temperature hydrothermalism at ridge crests. Primary alteration of the VMS (Cyprus type) and associated basalts by seawater and/or hydrothermal fluids occurs at the seafloor whereas secondary alteration occurs when these formations are subaerially exposed as ophiolites. The *Skouriotissa* mine corresponds to a massive sulphide ore deposit associated with basaltic volcanism (VMS-Cyprus type). These environments are very good analogue sites for understanding alteration that has taken place on the Noachian Martian surface.

However, more work is necessary in the *Skouriotissa* open pit in order to confirm these preliminary observations and interpretations of the geochemical and petrological data. For example, it would be useful to make more detailed and regular sampling along the outcrop in order to identify changes in the mineralogical phases in three dimensions.

The samples from Cyprus have been included in the ISAR collection. The relevance of the samples as Mars analogues is detailed in the Table 4.4. The analogy is based on the different characteristics studied: geochemistry, petrology (including texture and structure) and geotechnical properties. They are evaluated using stars: 1 to5 stars indicating respectively poor to excellent correspondance. However, the geotechnical properties of these samples have not been measured and therefore a value of 3 stars was attributed, based on knowledge of the Martian surface materials.

►Table 4.4. Analogy of the samples from Cyprus with the surface of early Mars surface; between 1 to 5, respectively bad to very good (n/a is not applicable).

►*Tableau 4.4. Analogie des échantillons de Chypre avec la surface primitive de Mars ; de 1 à 5 étoiles, du plus mauvais au meilleur respectivement (n/a pour non applicable).*

	Samples		Geochemistry	Petrology	Geotechnics	Total
Along the groove	S1-1	*11CY16*	****	****	***	11/15
	S2-1	*11CY13*	***	****	***	10/15
	S2-2	*11CY14*	n/a	****	***	*7/10*
	S2-3	*11CY15*	n/a	****	***	*7/10*
	S3-1	*11CY09*	****	****	***	11/15
	S3-2	*11CY10*	****	****	***	11/15
	S3-3	*11CY11*	*****	****	***	12/15
	S3-4	*11CY12*	*****	****	***	12/15
	S4-1	*11CY08*	n/a	****	***	*7/10*
	S5-1	*11CY17*	****	****	***	11/15
	S5-2	*11CY18*	n/a	****	***	*7/10*
	S5-3	*11CY19*	n/a	****	***	*7/10*
waste		11CY05	n/a	****	***	*7/10*
		11CY06	n/a	****	***	*7/10*
		11CY07	n/a	****	***	*7/10*

The previous chapters brought to light the difficulty of finding very good analogues of Martian basalts on Earth, in particular with respect to the Fe- and Mg- contents. The only way to obtain perfect analogues is thus to make synthetic samples in the laboratory. In the following chapter, I describe an experiment to synthesize a geochemical analogue of the Gusev Crater basalts.

Chypre, un nouveau site analogue (Résumé Français)

Ce chapitre décrit un nouveau site analogue de Mars situé dans la mine de Skouriotissa au nord-ouest de l'île de Chypre. Ce travail fait suite à ma mission de terrain à Chypre au printemps 2011. Dans la mine, les basaltes ophiolitiques subissent différentes altérations chimiques. En particulier avec l'interaction d'eau d'exhaure acide, ce qui produit différentes minéralogies. Dans le chapitre précédent nous avons montré qu'il était difficile de trouver de bons analogues de roches et de sols martiens. Afin d'avoir des échantillons plus pertinents, il est intéressant de chercher des échantillons géologiquement similaires à ceux de Mars primitive à actuelle et qui ont été altérés par les processus décrits dans le Chapitre II partie 2.2. : des basaltes altérés dans des conditions hydrothermales et par la circulation d'eaux d'exhaure acides. Des sites analogues ont déjà été proposés (Rio Tinto en Espagne ou les calcaires de l'Utah aux USA). Ces derniers étaient focalisés sur l'analogie à des conditions martiennes actuelles mais pas toujours avec un point de vue géologique. Par exemple, le site de RioTinto est particulièrement intéressant pour la recherche de vie extrêmophile, mais le contexte géologique n'est pas comparable à celui de Mars. Les roches sont andésitiques et ont subi un métamorphisme très important, ce qui n'est pas le cas sur Mars. Les environnements miniers sont particulièrement intéressants car ils sont souvent associés à la production d'eau acide. J'ai eu l'opportunité de faire une mission de terrain à Chypre, où il était possible de visiter une mine de cuivre en environnement basaltique.

Chypre est une petite île allongée à l'extrémité orientale de la mer Méditerranée au sud de la péninsule anatolienne (Fig. 4.1). La mine de Skouriotissa est localisée à l'ouest de l'île, au sud du golfe de Morfou et au sud de la ville de Petra. Cette mine est exploitée pour le cuivre par la Hellenic copper Limited.

Le site est situé dans l'ophiolite de Troodos, datés du Crétacé supérieur, qui forme un dôme centré sur le Mont Olympus. Stratigraphiquement l'ophiolite est composée, du cœur vers le centre, de peridotites, de serpentines, de gabbros, d'un complexe de dyke et de laves extrusives (en coussins), l'ensemble étant couvert par des sédiments océaniques (Fig. 4.1c). Les laves en coussins sont divisées en deux parties : inférieure (LPL) et supérieure (UPL), d'une épaisseur maximum de 1,5 km. La mine est située dans la partie supérieure des basaltes en coussin. Elle consiste en une lentille de sulfures massifs associés au volcanisme mafique (Fig. 2). On parle de « Volcanogenic massive sulphide » (VMS) de type Chypre (Jébrak et Marcoux, 2008). Ma zone d'étude est focalisée sur la partie ouest de la mine appelée 'S-West Phoenix open pit'. Un important chapeau de fer s'est développé au sommet du dépôt de sulfures (Fig 4.2a,b). Des formations de quartz et de jaspes rouges sont visibles autour des basaltes en coussins dans quelques endroits de la formation UPL. Ces objets se sont formés à basse température après la mise en place des minéralisations sulfurées. L'altération de l'ensemble de l'UPL par des fluides hydrothermaux a pour résultat de transformer la roche en un faciès à quartz-chlorite. La seconde phase majeure d'altération des basaltes en coussins est associée aux activités minières. De nombreuses galeries recoupent les sulfures massifs, elles collectent les eaux de météoritiques qui sont ensuite rejetées par une exhaure acide qui se déverse dans un fossé. La formation des basaltes en coussins

subit une altération acide en surface au contact des eaux d'exhaure. J'ai focalisé mon étude sur ce système.

Les échantillons ont été prélevés au niveau du fossé et autour de celui-ci en 5 points (Fig. 4.3) de haut en bas : le site 1 directement au niveau de l'exhaure ; le site 2 le long d'une grande cascade, à un niveau où les basaltes en coussins sont bien visibles ; le site 3 au milieu de l'affleurement, là où les basaltes sont plus massifs ; le site 4 au bas de l'ancien carreau de mine et le site 5 au pied de la falaise où les eaux se déversent dans un petit lac, à un niveau mis récemment en exploitation (Fig. 4.3). Au niveau de chaque site, la température, le pH et la conductivité ont été mesurés. Les échantillons sont nommés d'après la nomenclature de l'ISAR de 11CY08 à 11CY20. Cependant pour plus de clarté, nous avons utilisé une nomenclature reprenant le numéro de site et l'avons précisée sur la figure 4.3. Sept échantillons ont été analysés par ICP-OES et ICP-MS. L'ensemble des échantillons a été étudié en diffraction des rayons X, en microscopie optique et en spectrométrie Raman.

Les mesures de température, de pH et de conductivité sont reportées dans le Tableau 4.1. Le long du fossé, le pH baisse et la conductivité augmente, en accord avec la lixiviation des roches le long du fossé par des eaux acides. Les mesures ont été faites au début du printemps, où les eaux sont abondantes, les valeurs de pH doivent être plus faibles l'été lorsque l'eau est plus rare. Les échantillons analysés ont été placés dans le graphique TAS (Fig 4.4), les basaltes frais sont assez proches des basaltes martiens, et l'altération provoque une chute du Na_2O et du K_2O. L'indice d'altération (ou CIW) permet d'évaluer le taux d'altération d'une roche à partir de sa composition chimique. L'index est reporté pour chaque échantillon dans le Tableau 4.2. Une relation existe entre l'index et l'échantillonnage vertical : le taux d'altération augmente plus l'échantillon est proche du fossé. Les analyses géochimiques ne sont pas suffisantes pour comprendre les différentes phases d'altération, c'est pour cela que la suite du chapitre est dédiée à l'étude minéralogique. Différents facies ont été mis à jour : le premier est un mélange quartz-chlorite (Fig.4.6-4.7) avec quelques traces de sulfates et d'oxydes de titane. Le deuxième est un facies intermédiaire (Fig. 4.8-4.9) où le quartz est dominant, associé à une argile interstratifiée de type chlorite/smectite. Ces minéraux sont associés avec du plagioclase et quelques traces de feldspaths potassiques. Le troisième type est un facies à smectite (Fig. 4.10-4.11). Cette roche ne contient ni quartz ni chlorite mais est composée essentiellement de smectite associée à du pyroxène, du plagioclase et quelques traces de zéolites. Le quatrième type est un facies à smectite, zéolite et sulfates. Il est présent dans le fossé aux niveaux 3 et 4 (Fig. 4.13). La roche est essentiellement composée de smectites avec de l'analcime et de la philippsite (zeolites) et quelques traces de plagioclases. Lorsque l'altération augmente, des sulfates hydratés apparaissent, ce sont du gypse et de la natrojarosite. Enfin l'étude des échantillons provenant des haldes, arrosées régulièrement d'eau très acide, sont composées soit de quartz-chlorite (échantillon non alteré), soit d'un mélange ou uniquement de sulfates (gypse, natrojarosite) avec des traces d'hexahydrite et d'alunogènes. Le sulfate le plus présent est un mélange wupatkiite-pickeringite.

La minéralogie du site est donc constituée de trois paragenèses principales : (1) quartz-chlorite associées à une altération hydrothermale primaire, deuteritique.

(2) smectite (+ pyroxènes et plagioclases), correspondant à l'évolution de la paragenèse (1) associée à une altération metasomatique de basse température, pendant l'extrusion de l'ophiolite. Enfin, la paragenèse (3) découpée en deux, se déroule dans des conditions d'eaux plus acides. (3a) correspond à la lixiviation des roches avec une baisse de le teneur en Fe. Puis l'évolution plus acide de l'eau favorise la précipitation de sulfates, paragenèse (3b) comparable à celle ultime observée dans les haldes. Le Tableau 4.3 et la Fig. 4.15 reprennent les différentes paragenèses observées.

Sur Mars, les basaltes ont été altérés suivant différents processus acides pendant le Noachien et l'Hesperien. L'altération par des eaux acides explique la présence d'affleurements riches en sulfates. Les phyllosilicates se forment aussi dans des conditions aqueuses, et certains auteurs proposent même une relation avec des phénomènes deuteritiques. Les altérations observées dans la mine de Skouritissa présentent des résultats minéralogiques similaires. Ce site est intéressant pour comprendre les phénomènes martiens.

Comme nous l'avons vu dans les précédents chapitres la teneur en Mg des basaltes est un paramètre permettant de discriminer les basaltes martiens et terrestres. Les basaltes de l'ophiolite de Troodos ne dérogent pas à la règle. L'altération des échantillons chypriotes (Fig. 4.16) est très similaire à celle terrestre, mais il semble que sur la fin la concentration en Fe+Mg augmente fortement, un peu comme il est observé sur Mars.

L'étude de l'altération de basaltes terrestres sous l'effet de l'eau (de mer ou hydrothermale) dans des conditions acides révèle des similarités avec les processus de surface et de subsurface présents sur Mars. Un bon site analogue terrestre est composé des basaltes non métamorphisés qui ont subi des altérations acides. Ce type d'environnement peut être trouvé dans des VMS associés aux roches basaltiques du type Chypre. La mine de Skouriotissa correspond à ce type d'environnement et semble être un bon site analogue de Mars. Une nouvelle mission de terrain et des analyses complémentaires seraient intéressantes pour confirmer l'analogie et regarder les évolutions géochimiques et pétrologiques à plus petite échelle (minéraux).

Enfin, les échantillons provenant de Chypre ont été intégrés dans la collection de l'ISAR. J'ai évalué leur pertinance pour l'exploration martienne avec des étoiles (de 1 à 5), de mauvais à bien. Les résultats sont portés dans le Tableau 4.4.

Les précédents chapitres montrent la difficulté de trouver de parfaits basaltes analogues de Mars sur Terre, en particulier en raison des teneurs en Fe et Mg très différentes. La seule possibilité pour obtenir des échantillons analogues parfaits est de faire des échantillons synthétiques en laboratoire. Dans le prochain chapitre, je vais présenter les résultats de la synthèse expérimentale de basaltes analogues des basaltes du cratère Gusev, Mars.

Chapter V
Synthesis of basalts analogue to Gusev crater

The MER rover Spirit made several analyses of basalts in Gusev Crater showing that they are chemically very different from terrestrial basalts. In particular they are characterized by higher Mg- and Fe- contents. Thus, in order to complete the Mars analogue samples collection for the ISAR, it appeared pertinent to synthesize good chemical analogue basalts in laboratory, based on the geochemical data from Spirit. In this chapter, I present the results of two experiments that I made to make a glassy basalt produced by quench cooling (<1 hour) and a more slowly-cooled basalt (1 day). This study is in *Meteoritics and Planetary Science* (*Bost et al., 2012*).

V.1 Introduction

Based on analyses of SNC Martian meteorites and on *in situ* analyses on Mars during the Pathfinder and MER missions, the composition of Martian basalts varies depending upon the materials and/or the analytical methods used. In Figure 5.1, the total alkali-content (TAS) and FeO*/MgO ratios of Martian basaltic rocks are plotted as a function of wt.% SiO_2 (Figs. 5.1a and 5.1b, respectively; *Economou 2001*, *Gellert et al., 2006*, *Ming et al., 2008* and *McSween et al., 2009*). The Figures 5.1a and 5.1b show that most of the *in situ* measurements plot within the basaltic field whereas the SNC meteorites plot outside it, within the komatiite field (hatched area, Fig. 5.1a). Shergottites have

lower alkali- and lower Fe- and Mg- contents than basaltic rocks and nakhlites are richer in SiO_2 than basalts. This is probably due to the fact that the SNC meteorites are cumulate-type facies rather than basalt melts (*McSween et al., 2009*). Terrestrial basalts are notably Fe-Mg poorer than Martian rocks (*McSween et al. 2009*).

►Figure 5.1 : $Na_2O + K_2O$ oxides and FeO*/MgO ratios versus SiO_2 plots (in wt. %; 5.1a and 5.1b, respectively): composition of our synthetic basalt (red star) as compared to that of *in situ* Martian basalts and SNC Martian meteorites (after *McSween et al., 2009* and *Le Bas et al., 2000*). The terrestrial volcanic samples presently included in the ISAR lithotheque are also shown (black circles). The synthetic Pathfinder rock (1) and soil (2) from *Tosca et al., (2004)* and the synthetic Los Angeles sample (3) from *Hurowitz et al., (2005)* are also shown for comparison. The Bounce rock is the only sample of basaltic origin that was analysed in the Meridiani Planum by the Opportunity rover (*Rieder et al., 2004 and Zipfel et al., 2004*). The FeO*/MgO-silica diagram is used for distinguishing dry tholeiitic (TH) and wet calc-alkaline (CA) rocks. All Martian samples are tholeiitic.

►*Figure 5.1: Diagrammes $Na_2O + K_2O$ et FeO*/MgO en fonction de SiO_2 (en % poids figures 5.1a et 5.1b respectivement) représentant la composition des basaltes synthétisés (étoile rouge) comparée aux analyses in situ des basaltes martiens et des météorites SNC (d'après McSween et al., 2009 et Le Bas et al., 2000). Les échantillons volcaniques terrestres sont ceux inclus dans l'ISAR (cercles noirs). Les échantillons synthétiques analogues des roches (1) et sols (2) de Pathfinder (d'après Tosca et al., 2004) et l'échantillons synthetic de la météorite Los Angeles d'après Hurowitz et al., (2005) sont reportées pour comparaison. La « Bounce rock » est le seul échantillon d'origine volcanic analysé sur Meridiani Planum par Opportunity (Rieder et al., 2004 and Zipfel et al., 2004). Le diagramme FeO*/MgO-silice est utilisé pour distinguer la série tholeiitique (TH) de la série calc-alkaline (CA). L'ensemble des échantillons martiens est tholeiitique.*

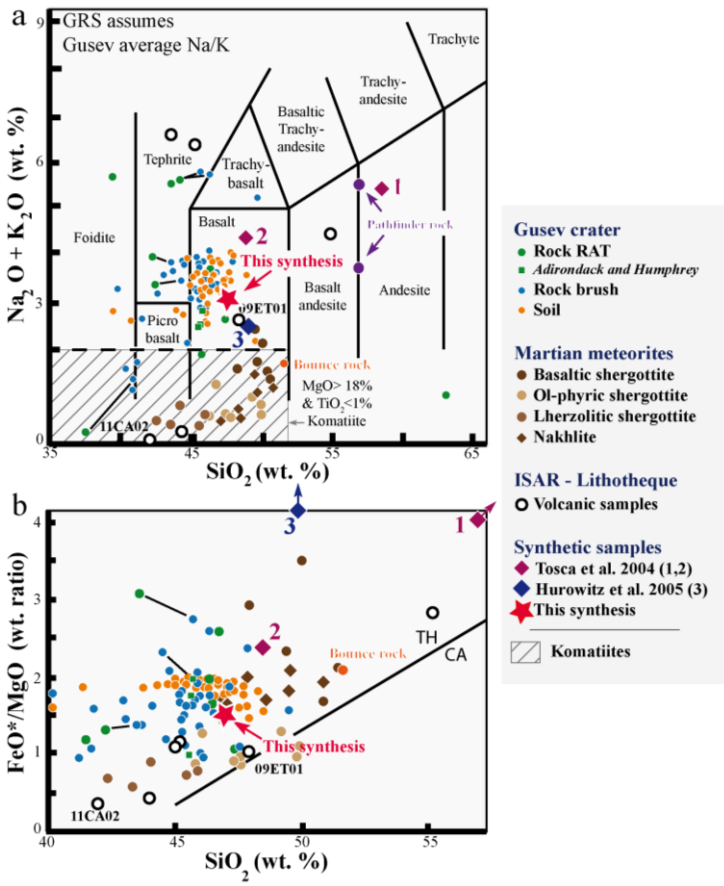

Previous attempts have been made to create artificial Martian basalts. *Tosca et al., (2004)* based their synthesis on data from the APX Spectrometer on the *Sojourner* rover reported by *Economou (2001)* and *Wanke et al., (2001).* Plotted in the TAS diagram in Figure 5.1a, these latter *in situ* analyses are richer in silica and have a more andesitic composition than those made by the rover Spirit. This is due to the fact that the Pathfinder rock surfaces were not cleaned before analysis and what was analyzed was a silica-rich weathered rind (*McSween et al., 2009*). Recent measurements obtained *in situ* by Spirit (*Gellert et al., 2006*) show that the volcanic rocks are closer to basalts or picro-basalts (Fig. 5.1a). The soil sample synthesized by *Tosca al. (2004)* has a chemical composition that is more representative of Martian basalts. A second attempt to synthesize Martian rocks was made by *Hurowitz et al. (2005),* using the Martian meteorite Los Angeles (described by *Rubin et al., 2000*) as a reference. Although

this synthetic Martian basalt falls within the basalt field of the TAS diagram (Fig. 5.1a), its Fe and Mg composition is much higher than that of the Martian basalts analyzed *in situ*.

For this study I wanted to synthesize fresh Martian basalts. Thus, I used an average composition of the basalts analyzed *in situ* by Spirit, corrected in order to take the alteration into account.

V.2 Materials and Methods

V.2.1 Reference data

Gusev crater is located at 14° 35S, 175° 25E and has a diameter of 166 km. The age of its volcanic rocks has been estimated to be older than 3.5 Gy (Late Noachian/Early Hesperian; *Squyres et al., 2004*). Gusev data from Spirit were chosen rather than Meridiani Planum data from Opportunity because the materials in this site are too altered to be considered as primary basalts, excepte for the Bounce Rock which is a shergottite-like rock (*Rieder et al., 2004 and Zipfel et al., 2004;* Fig. 5.1).

V.2.2 Reconstruction of a pristine basaltic composition

The geochemical Martian basalt analyses plotted in Fig. 5.1 are taken from *Gellert et al., (2006)*. These authors analysed the data obtained from rough, brushed, and abraded (RAT) rock surfaces. My goal was to determine a chemical composition similar to that of a fresh, unaltered Martian basalt. I therefore narrowed my choice to rock analyses obtained from surfaces that had been abraded by the RAT (Table 5.1). However, even in the case of surfaces abraded to a depth of a few millimetres, alteration is still present, as indicated by their friability and the presence of secondary minerals (cf. *McAdam et al., 2008; Viles et al., 2010* and citations therein). In order to correct this alteration, I used the results of previous experimental alteration of Martian analogue basalts made by *Tosca et al., (2004)* and *Hurowitz et al., (2005)* (Fig. 5.2a). As noted above, *Hurowitz et al., (2005)* synthesized a shergottite with a gabbroic texture using the Los Angeles meteorite as a starting composition. The alteration of the material under Martian conditions resulted in a large decrease in Al_2O_3 and a slight increase in FeO and MgO (Fig. 5.2b). This type of alteration was probably

favoured by the holocrystalline texture of the rock characterised by a porphyritic texture dominated by large, easily alterable plagioclase laths. On the other hand, the basaltic (olivine-rich) soil used by *Tosca et al. (2004)* documented a significant decrease in the FeO- and MgO- contents with alteration, a slight increase in CaO, Na_2O and K_2O, but more or less stable Al_2O_3 contents (Figs. 2a and 2b).

Oxides, wt%	Adirondack	Humphrey		Mazatzal Brooklyn	Pot of Gold	Wooly Patch		Clovis Plano	Ebenezer	Uchben Koolik
		RAT1	*RAT2*	*RAT2*		*Sabre RAT*	*Mastodon RAT*			
Soil n°	34	59	60	86 (84)	172 (171)	197 (198)	199 (200)	218	232 (233)	287
SiO_2	45.7	46.3	45.9	45.8	42.9	46.8	46.4	42.2	47.4	45.6
TiO_2	0.48	0.58	0.55	0.59	0.77	0.94	0.91	0.84	0.79	0.8
Al_2O_3	10.87	10.78	10.68	10.7	10.32	12.6	10.34	8.95	9.28	9.52
MnO	0.41	0.41	0.41	0.42	0.24	0.1	0.13	0.3	0.16	0.25
MgO	10.83	9.49	10.41	9.72	9.91	10.92	11.62	11.52	14.82	14.28
CaO	7.75	8.19	7.84	8.02	5.86	3.64	3.44	6.04	3.44	4.48
Na_2O	2.4	2.8	2.5	2.8	3	3.3	2.9	3.6	2.3	2.4
K_2O	0.07	0.13	0.1	0.16	0.2	0.07	0.04	0.35	0.33	0.35
P_2O_5	0.52	0.57	0.56	0.65	1.08	1.24	1.2	1.05	0.97	0.94
Cr_2O_3	0.61	0.68	0.6	0.54	0.27	0.27	0.18	0.17	0.16	0.15
Cl	0.2	0.32	0.26	0.23	0.57	0.78	1.03	1.63	1.46	1.85
SO_3	1.23	1.09	1.28	1.48	7.96	2.87	2.41	7.53	3.2	5.26
FeOb	18.8	18.6	18.8	18.9	16.7	16.3	19.2	15.6	15.6	13.9
Total	99.87	99.94	99.89	100.01	99.78	99.83	99.8	99.78	99.91	99.78
Fe^{3+}/Fe_T	0.16	0.19	0.15	0.10	0.51	0.59	0.61	0.84	0.83	0.79

Table 5.1: Chemical analyses of rough and abraded surfaces using the RAT tool obtained from rocks in Gusev Crater by Spirit (after *Gellert et al., 2006*). The ration Fe3+/FeT is from soil (*Morris et al., 2006*).

Tableau 5.1 : Analyses chimiques faites sur la surface brute et abrasée avec l'instrument RAT, obtenues par Spirit sur Gusev Crater (after Gellert et al., 2006). Le ratio Fe3+/Fe T est d'après le sol ((Morris et al., 2006).

►Figure 5.2: a-Ternary diagram total (mole%) FeO* + MgO (FM), Al_2O_3 (A), CaO + Na_2O + K_2O (CNK) showing the chemical evolution of basaltic rocks during terrestrial weathering (dotted arrows: Baynton basalt, Australia (1) and basaltic samples described by *Nesbitt and Wilson (1992),* plus Deccan basalt weathering products by *Greenberger et al., (2011)* (2); compared to the rocks analyzed in the Gusev crater on Mars by Spirit and two synthetic samples (square, *Tosca et al., 2004*, hexagon, *Hurowitz et al., 2005*). Note the two directions of alteration of rocks in Gusev crater (circles and stars). I considered that Wishstone, Champagne and Watchtower (stars) were marginal and that Adirondach, Humphrey, Ebenezer and Clovis (circles; Table 5.1; by *Hurowitz et al., 2006*) were representative samples. The samples from this study correspond to the red stars. b- Enlarged plot of the box in a showing the Martian weathering effect (full arrow). Whatever the composition of the basalt, weathering induces a drastic loss of MgO and FeO with a slight variation of Al_2O_3 and CaO + Na_2O + K_2O. *Hurowitz et al., (2006)* show that the effects of weathering are different on Earth and on Mars (Fig. 5.2a and 5.2b, respectively).

►*Figure 5.2: a- Diagramme ternaire total (en mole%) FeO* + MgO (FM), Al2O3 (A), CaO + Na2O + K2O (CNK) montrant l'évolution des roches basaltiques pendant l'altération terrestre (flèches pointillées : basalte de Baynton, Australie (1) et échantillons des basaltes décrits par Nesbitt and Wilson (1992), plus produits d'altération des basaltes du Deccan (2) d'après Greenberger et al., (2011); comparé aux roches analysées sur Mars dans le cratère Gusev (cercles et étoiles). Les échantillons de cette étude correspondent aux étoiles rouges. b- Zoom de la zone grisé en a montrant l'effet de l'altération des basaltes martiens (flèches grises). Suivant la composition des basaltes, l'altération induit une forte perte en MgO and FeO associée à une faible variation de Al_2O_3 et CaO + Na_2O + K_2O. Hurowitz et al., (2006) montrant que l'effet de l'altération est différent sur la Terre et sur Mars (Fig. 5.2a et 5.2b, respectivement).*

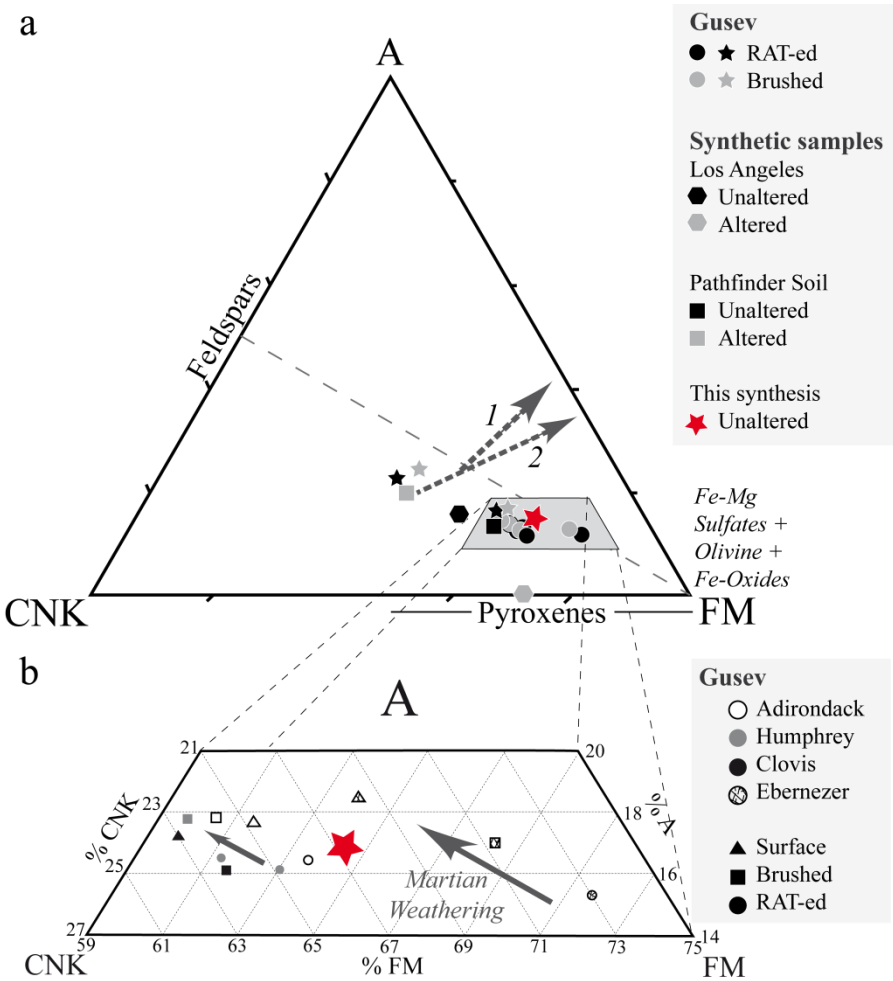

Another study based on the MER analyses by *Hurowitz et al. (2006)* shows an alteration process that follows the trend experimentally produced by *Tosca et al. (2004)* with the preferential dissolution of olivine in low pH conditions.

V.2.3 Geochemical composition of the samples

The ten selected analyses from Spirit show little variability in their weight percentages of oxides (Table 5.2). I chose Adirondack, Humphrey and Mazatzal Brooklyn because they are certainly the least altered basalts. The other basalts show varying degrees of alteration, even on the RAT surfaces. Pot-of-Gold and Woolly Patch are less altered than Clovis, Ebernezer and Uchben (*Morris et al., 2006*). I therefore corrected for the alteration by choosing a basalt composition that has no volatiles (also because fluid basalts extruded at the surface of Mars were more likely to be degassed). Thus, I did not include volatile elements, such as Cl, S, C, or water for this synthesis even though *Gaillard and Scaillet (2009)* have shown that degassed Martian basalts can retain ca. 0.1 wt% S. I also increased the Fe and Mg contents. Al was also not increased in order to take into account of the Al_2O_3 reaction.

Oxides, wt%	SiO_2	TiO_2	P_2O_5	Al_2O_3	Cr_2O_3	MnO	FeO	MgO	CaO	Na_2O	K_2O	NiO
PFS	48.68	1.16	1.19	10.29	–	0.49	19.23	7.66	7.07	3.56	1.02	–
SLA	49.8	1.27	0.77	10.9	–	0.43	20.4	3.34	9.7	2.32	0.26	–
09ET01	48.09	1.02	0.29	11.29	–	0.18	10.43	12.06	12.67	1.82	0.95	–
Mean (Target)	47.58	0.76	0.92	10.87	0.37	0.29	18.00	11.90	6.12	2.94	0.19	0.05

Table 5.2: Compared analyses of synthetic Martian basalts (PFS: *Tosca et al., 2004*; SLA: *Hurowitz et al., 2005*), a picritic basalt from Etna (sample 09ET01 see chapter III) and the composition targeted for my synthetic basalt.

Tableau 5.2: Comparaison chimique entre les différents basaltes synthétiques (PFS: Tosca et al., 2004; SLA: Hurowitz et al., 2005), un basalte picritique de l'Etna (09ET01, voir chapitre III) et la composition cible de mes basaltes artificiels

The composition used is shown in Fig. 5.1. It is very similar to that used in the previous studies of *Filiberto et al., (2008)* or *Stanley et al., (2011)* for instance. It was assumed that the magma was extruded at the surface and was therefore completely degassed. No viscous rhyolitic-type lavas have yet been unambiguously observed at the surface of Mars. In our experiment, the high concentrations of Mg produce a very fluid magma. Similar Mg-rich melts that were common on the early Earth produced very thin, fluid, degassed lavas called komatiites.

V.2.4 Methods

The samples were made at the CNRS-ISTO laboratory with the collaboration Fabrice Gaillard. The basic ingredients were provided as powdered oxides (SiO_2, TiO_2, P_2O_5, Al_2O_3, Cr_2O_3, MnO, FeO, MgO, K_2O, and NiO) except for CaO and Na_2O that were present as carbonates. The total amount of material used was 2g. The weight percent of each ingredient is reported in Table 5.2. Note that we used ferrous iron (FeO) at 99.5% purity in this experiment. The oxides were mixed together in an agate mortar and then placed in an open alumina crucible that was positioned in a circular vertical oven (Adamel^{TM}) at atmospheric pressure (10^5 Pa). We assumed that the surface pressure on Early Mars was more or less similar to that of the Earth's surface today (*Halevy et al., 2007*). In order to obtain reducing conditions, an atmosphere of 80% CO_2 and 20% CO was used in the chamber. Such a gas mixture imposes oxygen fugacity near FMQ -1 (i.e. 1 log unit more reducing that the oxygen fugacity buffered by the fayalite-magnetite-quartz redox buffer), which corresponds to oxidizing conditions recorded in Shergottite rocks (*Herd et al., 2002*). Note that higher FMQ values of FMQ-3 were determined for the later crystallization stage of NWA 1068/1110 by *Herd (2006)*, whereas *Schmitt et al., (2011)* determined an FMQ between -4 to +3 for a Gusev basalt. On Mars, the average melting conditions are estimated to be between 1.0 GPa to 1.2 GPa and 1320°C to 1550°C (*Monders et al., 2007; Musselwhite et al., 2006*). In this study, the samples were heated to 1350 °C and exposed to the CO-CO_2 atmosphere for 3 hours. We used Al_20_3 containers to avoid iron loss from the metal containers normally used for such high temperature experiments (*Gaillard et al., 2003*). Previous experiments on basaltic melts at similar temperatures have shown that interactions between melt and alumina container are negligible and only a narrow region (100µm) at the melt – alumina interface is affected (*Pommier et al., 2010*).

Once the melts were homogenized, the two samples were cooled at different rates. One sample was slowly cooled in the oven for one day (we estimate that the cooling rate was ~ 110°C/hour). This sample has the ISAR code 11AR01. The second sample, ISAR code 11AR02, was drop quenched in the CO-CO_2 atmosphere from 1350°C to room temperature. Calculation of the cooling rate in this sample shows that it reached a temperature of less than 400°C in the core of the sample after 8 minutes (cooling rate >> 1400°C/hour at the surface). We obtained a "crystalline" basalt (11AR01) and a glass-rich basalt (11AR02). We did not use longer cooling times because this would have produced a gabbro-like texture. Experimental study of the formation of spinifex textures in komatiites gives cooling rates between 10°C/h and 1428°C/h (review in *Faure et al., 2006*).

Once the crucibles were cold, polished sections were made. The two polished sections were then investigated in reflected light microscopy, in scanning electron microscopy equipped with EDX and by Raman spectroscopy. Powdered preparations of the samples were also investigated by IR spectroscopy. Finally, elemental analyses were made on the polished sections using electron microprobe.

V.3 Results

V.3.1 Al-crucible interactions

Al-rich oxides with a normative chemical formula of $(Fe^{2+}_{0.24}Mg_{0.76})(Fe^{3+}_{0.30}Cr_{0.03}Al_{1.67})O_4$, measured using the electron microprobe, occur at the edge of the crucible to within 45 µm of the crucible walls (Fig. 5.3). These spinels obviously resulted from reaction with the alumina crucible. Thus, in the following study, these reactive phases were not taken into account and only the mineralogy and texture in the sample cores are described.

V.3.2 Structure and texture

Both samples exhibited a homogeneous texture in polished section. Some cracks appeared due to the retraction of the magma during cooling and crystallization. The slowly cooled basalt 11AR01 contains some rare vesicles, whereas the rapidly-cooled sample 11AR02 contains many of them due to the drop quenching which prevented out-gassing of carbonate-derived CO_2.

►Figure 5.3: a- SEM backscattered image of the border part of 11AR01 sample at 20 kV and 10 nA. In light grey, the olivine with dentritic texture and in darker grey, the elongate pyroxene, with the spinel grains in white and the basaltic glass in black. b- Associated Raman map (red square) with the Al crucible in yellow, enstatite (pyroxene) in green, olivine in red, and the reactive phase, spinel, in blue.

►*Figure 5.3: Image MEB en électrons rétrodiffusés de la partie centrale de 11AR01 (refroidissement lent) à 20 kV et 10 nA. En gris clair, l'olivine avec des textures dentritiques et en gris foncé, des pyroxènes allongés, avec des grains de spinels (en blanc dans un verre basaltique en noir. b- Cartographie Raman associée (rectangle rouge sur a) avec en jaune le creuset, en vert l'enstatite, en rouge l'olivine et en bleu le spinel de reaction.*

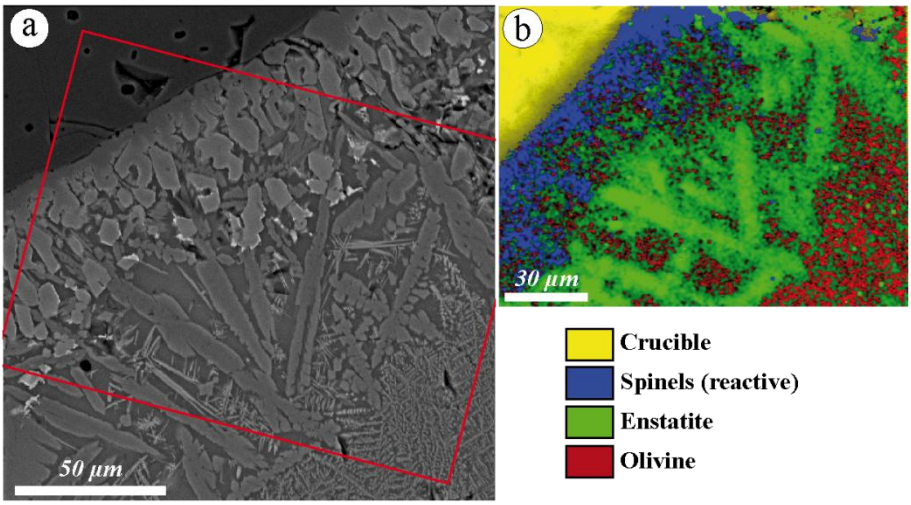

The drop quenched basalt displays an aphanitic microlithic texture consisting of spinels, olivine crystals and small dendritic to microlitic pyroxene crystals in a dominant glassy matrix (Fig. 5.4). The slowly-cooled basalt presents different textures (Fig. 5.5 and Fig. 5.6). The pyroxenes are skeletal and very elongated and are associated with acicular olivine. This dendritic texture is similar to the spinifex texture observed in very rare terrestrial basalts (sample 11CA02 described in Chapter III for example). The spinifex texture of this komatiite was attributed to very rapid cooling (around 1000°C/h; *Faure et al., 2006*) of a melt containing very low water (only few hundred ppm H_2O; *Arndt et al., 2004*). The melt conditions of our basalt were similar to those of the Dundonald Township komatiite from Ontario described by *Arndt et al., (2004)* in terms of very low water-content, high Mg-content, and relatively rapid cooling, although bulk chemical compositions are different (basalt versus komatiite, Fig. 5.1). The acicular textures observed in sample 11AR01 differ from hopper or swallow-tail-like textures observed in olivines in terrestrial submarine basalts, such as MORBs. The latter are associated with highly viscous magmas extruded at high pressure that were subjected to undercooling (*Bryan, 1972*), a situation very different to the conditions of formation of our basalts. Our melts were cooled at a relatively rapid rate that precludes metastability (undercooling).

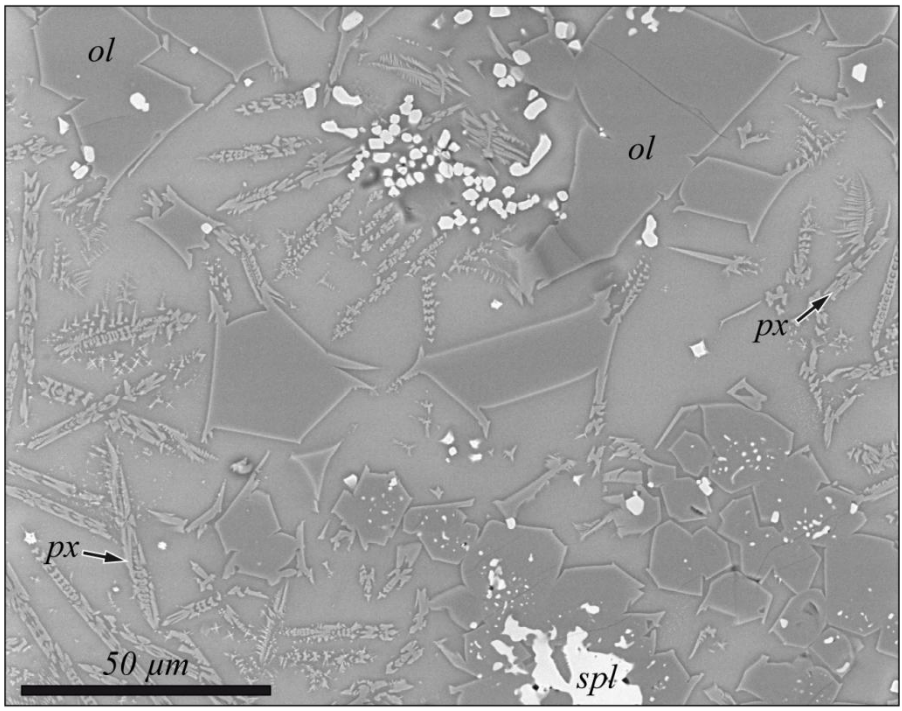

Figure 5.4: Backscattered image of the inner part of sample 11AR02 (drop quenched) in polished section. Spinels (*spl*) are in white and are associated with blocky olivine crystal (*ol- dark grey*) in a grey basaltic glass containing very small dendrite crystals of pyroxenes (*px- light grey*).

Figure 5.4: Image MEB en électrons rétrodiffusés de la partie centrale de 11AR02 (refroidissement rapide). Les spinels (spl) sont en blanc associés à des cristaux massifs d'olivine (ol - gris foncé) dans un verre basaltique (gris) contenant de toutes petites dendrites de pyroxènes (px- gris clair).

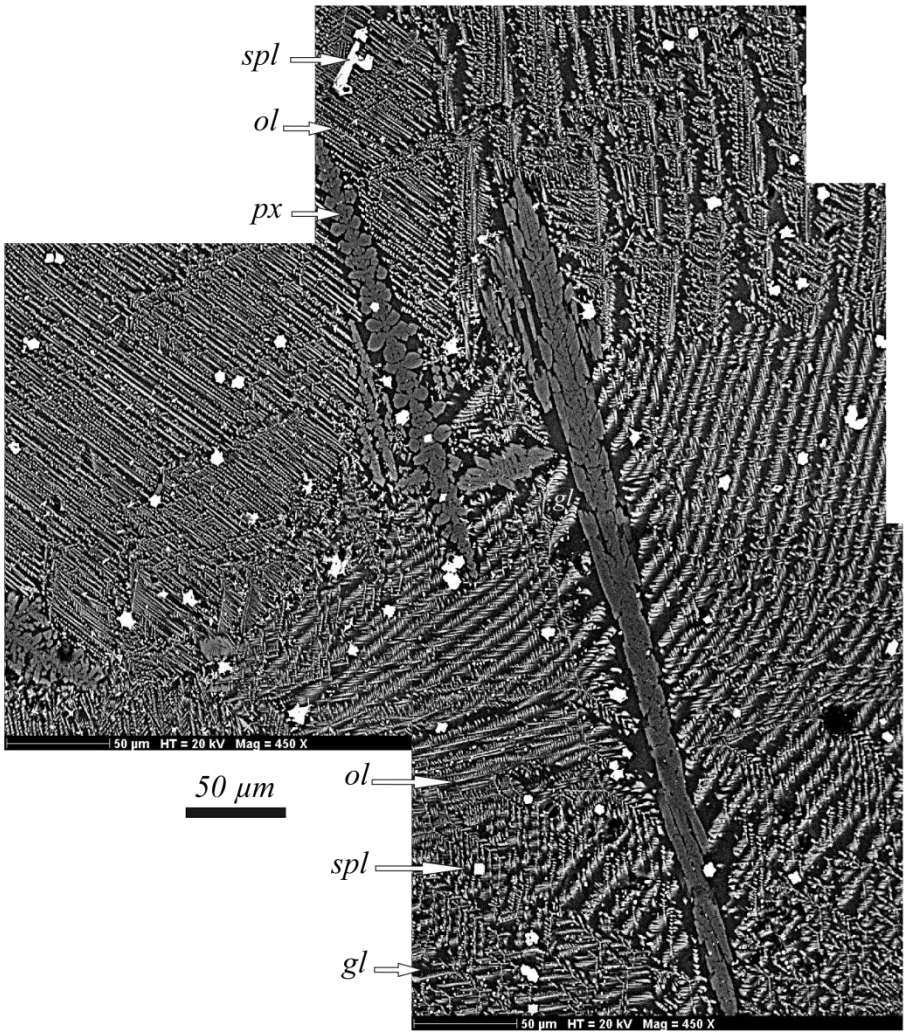

Figure 5.5: SEM backscattered image of the inner part of 11AR01 sample (slowly-cooled) at 20 kV and 10 nA. In light grey, olivine (*ol*) with a dentritic texture and in darker grey; an elongated pyroxene with a calcic augite to Mg-pigeonite composition (*px*); spinel grains (*spl*) in white and the basaltic glass in black (*gl*). The pyroxenes have a skeletal appearance.

Figure 5.5. Image MEB en électrons rétrodiffusés de la partie centrale de 11AR01 (refroidissement lent) à 20 kV et 10nA. En gris clair, l'olivine (ol) avec des textures dentritiques et en gris foncé, des pyroxènes allongés, ayant une composition Ca-augite à Mg-pigeonite (px), avec des grains de spinels (spl) en blanc dans un verre basaltique en noir (gl). Les pyroxènes sont squelettiques.

V.3.3 Mineralogy

V.3.3.1 Slowly-cooled basalt- Sample 11AR01

The major mineralogical phases in this slowly cooled sample are large elongated clinopyroxene crystals (100 x 10 µm²) and small olivines (10 x <1 µm²) associated with spinels in a glass (Fig. 5.5). The probable crystallization sequence is spinel, clinopyroxene, olivine and glass. These phases were confirmed by Raman and IR spectrometry. Microprobe analyses (Table 5.3) permitted more precise characterization of the large pyroxene crystals, having an average chemical formula of $(Ca_{0.21}Na_{0.07})_{\Sigma=1-p}$ $(Fe_{0.57}Mg_{1.02}Al_{0.12}Ti_{0.02})_{\Sigma=1+p}$ $(Si_{1.92}Al_{0.08})$ O_6 . Their compositions range from subcalcic-augite to Mg-pigeonite class. The Al-poor spinels within the basalt contrast with the Al-rich spinels formed close to the crucible walls. The average chemical composition of the basaltic spinels is $(Fe^{2+}_{0.51}Mg_{0.55})_{\Sigma=1}$ $(Fe^{3+}_{0.63}Cr_{0.49}Al_{0.89}Ti_{0.03})$ $_{\Sigma=2}$ O_4. The olivine crystals were too fine-grained (< 1µm) to be analyzed using the microprobe (spot size: ~1µm²), but they were identified as forsteritic olivine by Raman spectrometry (Fig. 5.6). These minerals are embedded in a Mn- and P-enriched basaltic glass having a plagioclase-like chemical composition, given in Table 5.3.

The IR spectra shown in Fig. 5.7, made on a bulk powder, confirm the pyroxene and olivine composition. Since this basalt was produced from a dry, degassed melt, it does not contain any hydrous minerals (e.g. amphibole, clay). This sample is very similar to the samples produce by *Faure et al., 2006* (Figures 14a and 14b in *Faure et al., 2006*).

►Figure 5.6: 11AR01 (slowly-cooled sample). a-Reflected light optical view showing large elongate augitic crystals (*px*), dentritic crystals forsterite (*ol, white arrow*), and small spinels (*spl*). b- Raman map of (a); augite is in yellow and forsterite in green, and the spinels do not give any spectrum. The identification of forsterite is indicated by Raman measurements only because the crystals are too small to be measured by microprobe. c- Raman spectra used for mapping (Analytical conditions: laser power ~ 10 mW; obj. x 100).

►*Figure 5.6: 11AR01. a- image en lumière réfléchie montrant des cristaux d'augite allongés (px), des cristaux de forsterite dendritiques (ol, flèche blanche) et des petits spinels (spl). b- Cartographie Raman de a, l'augite est en jaune, la forsterite en vert, les spinels n'ont pas donné de spectre. La composition forsteritique est obtenue par analyse Raman. c- Spectres Raman utilisés pour faire l'image (Conditions d'analyses : puissance laser ~ 10 mW; obj. x 100)*

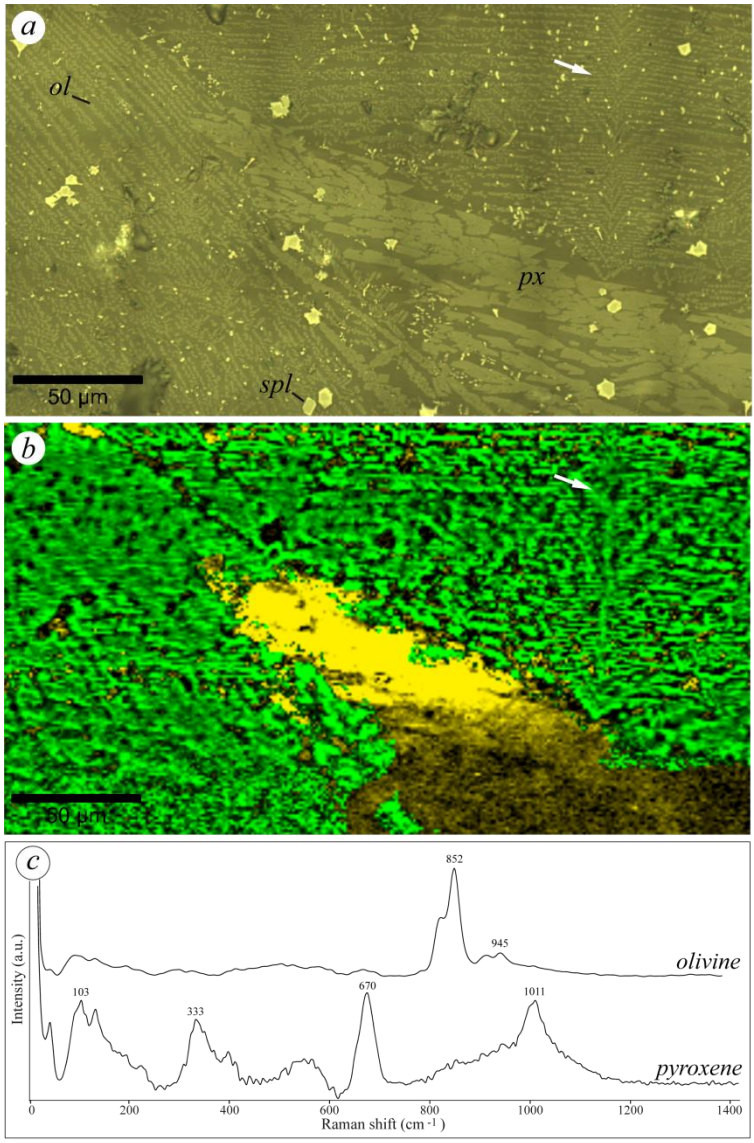
a
ol
px
spl
50 µm
b
50 µm
c
852
945
olivine
103
333
670
1011
pyroxene
Intensity (a.u.)
0
200
400
600
800
1000
1200
1400
Raman shift (cm -1)

Oxides, wt%	K_2O	SiO_2	FeO	CaO	Na_2O	TiO_2	Al_2O_3	MnO	Cr_2O_3	MgO	NiO	P_2O_5	Total
11AR01													
Pyroxene	0.059	47.543	16.821	4.835	0.865	0.631	11.028	0.387	0.021	17.022	0.134	0.904	100.249
2σ	0.093	1.526	2.252	1.580	1.250	0.046	3.966	0.067	0.036	5.830	0.095	0.197	–
Spinel	0.006	1.294	42.586	0.261	0.061	1.069	17.240	0.289	21.815	9.599	0.484	0.053	94.755
2σ	0.013	1.446	0.857	0.127	0.052	0.080	3.399	0.065	2.928	0.795	0.134	0.043	–
Glass	0.330	50.633	11.519	8.180	3.988	0.708	18.574	0.230	0.016	3.392	0.005	1.579	99.153
2σ	0.034	1.612	0.652	1.338	0.360	0.161	1.472	0.094	0.025	1.833	0.013	0.278	–
11AR02													
Olivine	0.014	33.599	24.758	0.251	0.032	1.434	1.332	0.301	0.181	39.032	0.093	0.073	101.100
2σ	0.011	14.745	19.264	0.078	0.030	2.348	3.089	0.106	0.144	13.762	0.076	0.047	–
Spinel	0.009	0.137	73.114	0.058	0.049	3.613	6.208	0.330	0.065	7.268	0.000	0.024	90.873
2σ	0.004	0.012	4.601	0.028	0.041	1.762	1.292	0.053	0.092	0.483	0.000	0.008	–
Glass	0.212	46.438	15.888	7.225	2.914	1.706	13.555	0.285	0.135	9.927	0.009	0.299	98.594
2σ	0.054	6.068	2.118	2.669	0.760	1.055	4.892	0.104	0.296	6.950	0.015	0.111	–

Table 5.3: Average chemical composition in weight percent of minerals and glass measured by electronic microprobe in the sample 11AR01 (slow cooling) and associated 2σ error.

Table 5.3: Composition chimique moyenne en pourcentage poids des minéraux et verre (par microsonde électronique) de 11AR01 et 11AR02 avec l'erreur 2 σ associée.

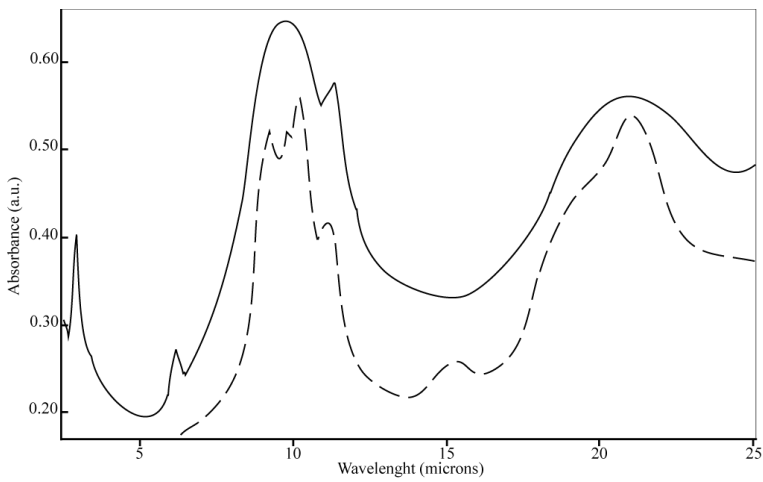

Figure 5.7: IR spectrum in absorbance of 11AR01. Pyroxene is identified by its spectrum (dotted line) by comparison with data data base of the Research Branch of Agriculture Canada.

Figure 5.7: Spectre d'absorbance IR de 11AR01. Le pyroxène est identifié par comparaison avec le spectre provenant de la base de données de la « Research Branch of Agriculture Canada », (ligne pointillée).

V.3.3.2 Quenched basalt- Sample 11AR02

This drop quenched sample shows a similar mineralogy and crystallization sequence to that of the slowly cooled basalt 11AR01. However, it is characterized by a different crystal size and texture (Fig. 5.4). Early spinels have a structural formula of $(Fe^{2+}_{0.65}Mg_{0.25})_{\Sigma=1}$ $(Fe^{3+}_{1.67}Al_{0.23}Ti_{0.06})_{\Sigma=2}$ O_4 . They are Cr-free, Fe^{3+}-richer and Al-poorer than spinels formed in the more slowly cooled sample. They are surrounded by later, polyhedral olivine crystals, with a near-forsteritic chemical composition of $(Fe_{0.50}Mg_{1.50})_{\Sigma=2}$ (SiO_4) with traces of Ti and Al (Fo_{75}; Table 5.3). Based on their habits (see Fig. 5.4), they can be interpreted as sub-liquidus olivines (*Faure et al., 2007*). Very fine skeletal to feathery dendritic pyroxene crystals were observed in a glass. These crystals were too small to be localised and analysed with the electron microprobe but were revealed by Raman spectroscopy. The glassy matrix predominates in this basalt compared to the slowly cooled sample 11AR01. Its chemical composition in weight oxide percent is given in Table 5.3. The glass is not enriched in P_2O_5 and we presume that this component was segregated in the pyroxenes crystals.

V.4 Discussion

V.4.1 Komatiites on Mars?

There are some differences between our artificial basalts and those on Mars. Compared to the ten Gusev basalts ranging from unaltered to slightly altered that were chosen as the baseline for this study, the silica composition in our basalts is slightly lower than the very fresh basalts (Adirondack, Humphrey and Mazatzal brooklyn). However, the high Fe and Mg contents are similar. Some basalts observed on Mars contain euhedral olivine (*McSween et al., 2004*), whereas olivines in our samples are both small and acicular (slow cooling, 11AR01) or quasi-euhedral (drop quenched basalt, 11AR02). The absence of plagioclase feldspar in these samples is due to the low Ca and Al contents compensated by high Mg and Fe content; a phenomenon already known in primitive melts. One of the most interesting results of this study is that the more slowly cooled basalt has a texture and mineralogy similar to terrestrial komatiites (Fig. 5.8).

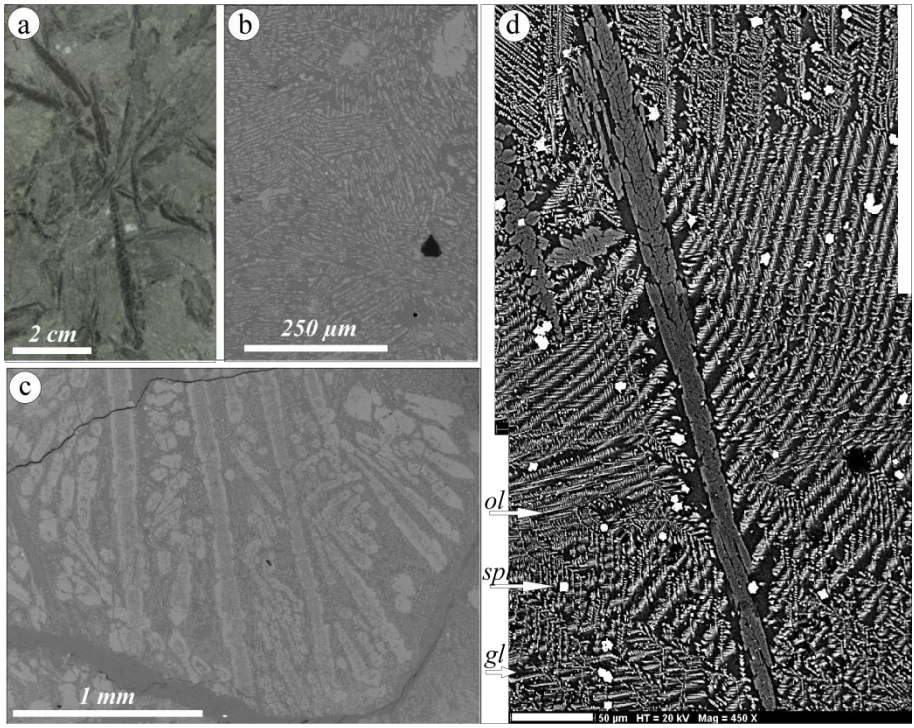

Figure 5.8: Terrestrial komatiite sample from Dundonald: a- macroscopic image; b, c- backscattered images showing spinifex textures. d- Sample 11AR01 (see Fig.5.5). Theses textures are very similar to those of the komatiite.

Figure 5.8: Komatiites terrestres de Dundonald. a- vue macroscopique ; b et c- images MEB rétrodiffusées montrant des textures spinifex. d- échantillon 11AR01 (voir Fig. 5.5). Ces textures sont très similaires.

These rocks were very common on the Early Earth during the Archaean epoch, which corresponds to the Noachian on Mars. They are Mg-rich rocks produced by very thin, fluid lavas extruded at the surface (and not at depth in the ocean). Indeed, it has been suggested that komatiites could be present on Mars (*Reyes and Christensen 1994; Nna-Mvondo and Martinez-Frias 2007*). There is evidence of very fluid lava flows in Gusev crater and on Tharsis (e. g. *Greeley et al., 2005* and *Mangold et al., 2009*), comparable to komatiite lava flows on the Early Earth. However, to date, spinifex textures have not yet been observed by the MI imager of Spirit and Opportunity, perhaps because of the rapid alteration of this kind of rocks. Our study, however, supports the suggestion that spinifex-textured basaltic rocks (similar to 11AR01) or true komatiites could occur on Mars. Although komatiites have a higher Mg-content than the basalts in this

study (Mg ~12 wt%), we suggest that the lower Mg-content could be compensated by a high content of Fe. Our samples contain 29.90 wt% of MgO + FeO, which is similar to an average composition of a Barberton-type komatiite (30 wt% of MgO + FeO; *Arndt, 2003*).

V.4.2 Comparison with previous studies

Our synthetic basalts differ from those previously produced by *Tosca et al., (2004)* and *Hurowitz et al., (2005)* because both melt compositions and experimental P-T melting conditions were different. The synthesis pressure conditions used by *Tosca et al., (2004)* are comparable to ours, ~10^5 Pa, but we used 1350°C whereas these authors used ~ 1120°C. The chemical composition of the melt thus produced from the Pathfinder soil by *Tosca et al., (2004)* was close to the melt we produced, but was different from the silica-rich Pathfinder rock (Fig. 5.1). Moreover, because *Tosca et al., (2004)* immediately ground their sample to a powder for the alteration experiment it is not possible to compare their mineralogy and texture to those of our synthetic basalts. The artificial rock produced by *Hurowitz et al., 2005* was obtained at ~1135°C and at ~0.1 Pa (~1 mbar). The rock was cooled very slowly (~6°C/hour) and a "holocrystalline basalt with aphanitic-porphyritic texture" without glass was produced, a texture which is more similar to a gabbro than to a basalt. A further difference is that the chemical composition of the melt synthesized by *Hurowitz et al., (2005)* was a shergottite analogue of the Los Angeles meteorite. It's very low Mg-content is different from the Gusev crater basaltic rocks (Fig. 5.1b).

V.4.3 Implication for Early Life on Mars

The volcanics in Gusev crater are of Noachian age (*Soderblom and Bell, 2008*). This is the period when Mars had somewhat similar environmental conditions to those of the Early Earth and was potentially habitable (*Westall, 2005; Bibring et al., 2006; Jakosky et al., 2007; Southam et al., 2007; Westall et al., 2011*). As noted above, Fe-Mg-rich basalts and komatiite-type basalts were common on the Early Earth. Such rocks are favourable habitats for chemolithotrophic microorganisms that obtain their energy and nutrients from chemical reactions on rocks surface (cf. *Furnes et al., 2008*). Furthermore, alteration of these rocks would have produced Fe-Mg clays, such as nontronite and chlorite-saponite, that could have been implicated in the concentration of prebiotic organics and thus in various scenarios for the origin of life (*Meunier et*

al., 2010). Given the interpretations of such materials associated with Noachian terrains on the surface of Mars (*Poulet et al., 2005; Bibring et al., 2006; Mustard et al., 2008; Ehlmann et al., 2009*), we can extend the analogy with the Early Earth to hypothesize the potential importance of this kind of rocks and their alteration products for not only an origin of Martian life, but also as habitats for possible Martian microorganisms. Both samples could be weathered by glass alteration. The drop quenched sample contains more glass and would be rapidly altered, whereas the spinifex texture could be used as a site of preferential development of clays (such as nontronite) along specific surfaces (elongates grain surfaces). This could favour the colonization of volcanic rocks by microorganisms, in particular chemolithotrophs. For example, traces of the activities of such organisms have been preserved in basalts and derivatives of volcanic rocks from the Early Archaean terrains of Barberton and the Pilbara (review in *Furnes et al., 2007; Westall et al., 2006; Westall et al., 2011*) as well as in amygdales in pillow basalts (*Cavalazzi et al., 2011*). Moreover, typical alteration of the mafic rocks, such as komatiites, in aqueous conditions, a high pH and low $aSi0_2$ leads to serpentinization (this reaction produces H_2, which can serve as an important source of energy for chemosynthetic organisms, *Schulte et al., 2006*). Note that biological activity is associated with serpentinization process in hydrated mantle (*Ménez et al., 2012*). Furthermore, serpentine deposits have been observed on the Martian surface (*Ehlmann et al., 2010*) and could be a possible habitat for early life on Mars. Thus, if life ever appeared on Mars, it is possible that traces of its existence could be found directly in the surfaces, cracks and vesicles of this volcanic type of rocks. *In situ* missions to Mars should examine such rocks if there is evidence that they have been associated with water.

V.5 Conclusion

We produced experimental Fe-Mg-rich basalts based on the geochemical data from Gusev basalts. The slowly cooled basalt present specific spinifex textures that are very similar to those of Early Earth basalts and komatiites that were formed in an equivalent period to the Noachian and Hesperian on Mars. Fe-Mg-rich basalts and their alteration products are also highly relevant for the appearance and habitability of life. Nontronite and chloritic clays could have concentrated prebiotic organic molecules that were the building bricks of life, whereas surfaces, cracks and vesicles in such lavas were ideal habitats for primitive anaerobic life forms, such as chemolithotrophic microorganisms (*Furnes et al., 2007; Cavalazzi et al., 2011*).

This study concludes my thesis project by adding basalt analogues to the ISAR that are good chemical and textural analogues of Martian basalts.

Basaltes martiens artificiels (Résumé Francais)

Les analyses chimiques des basaltes du cratère Gusev par Spirit ont montré qu'ils étaient chimiquement différents des basaltes terrestres. Cette variation se traduit particulièrement par une teneur en Mg et Fe beaucoup plus forte pour les basaltes martiens. Pour compléter la collection de l'ISAR, il apparaît pertinent de fabriquer en laboratoire des basaltes analogues. Ce chapitre présente les résultats de deux synthèses, l'une avec un refroidissement lent et l'autre avec un refroidissement rapide (respectivement 1 jour et 1 heure).

Des études précédentes avaient déjà fabriqué des basaltes martiens artificiels mais en se basant sur des données de la mission Pathfinder ou depuis la météorite martienne Los Angeles. La Fig.5.1, montre que ces échantillons ne sont pas en adéquation avec les résultats récents. Il semble particulièrement pertinent de fabriquer des échantillons avec une composition chimique proche de celle des basaltes du cratère Gusev. Nous avons choisi une composition chimique moyenne basée sur les analyses in-situ des dix échantillons les moins altérés (Tableau 5.1). En effet nous voulons fabriquer un basalte artificiel ayant une composition initiale, avant toute altération. Les basaltes sur Gusev sont assez altérés. La Fig. 5.2 montre l'altération des basaltes terrestres et martiens. On note que sur Mars lors de l'altération c'est principalement la teneur en Fe et Mg qui baisse. La composition chimique des basaltes sera donc corrigée de l'altération et ne comportera pas de volatils, considérant une mise en place à la surface ou le magma est totalement dégazé. Le Tableau 5.2 reporte la composition chimique utilisée et comparée aux deux précédentes expériences et à l'échantillon 09ET01.

Les échantillons ont été préparés au CNRS-ISTO avec la collaboration de Fabrice Gaillard. Les ingrédients chimiques sont fournis en poids d'oxyde ou en carbonates. L'échantillon final représentera 2 grammes de roche. La poudre est mélangée dans un mortier avant d'être mise dans un creuset en alumine et placée dans un four Adamel vertical à pression atmosphérique, à une température de 1350°c et sous une atmosphère de CO-CO_2. Lorsque les échantillons sont liquides, le premier est refroidi lentement (une journée, 11AR01) et le deuxième est trempé (refroidissement rapide, 11AR02). Une fois les creusets froids une section polie est préparée, ainsi que des poudres.

Les deux échantillons présentent une texture homogène, seule une bordure de réaction est visible entre le creuset et l'échantillon (Fig. 5.3). L'échantillon trempé présente une texture aphanitique microlithique (Fig. 5.4). L'échantillon au refroidissement lent présente des cristaux de pyroxène très allongées, squelettiques et des olivines aciculaire, similaire aux textures spinifex des komatiites (Fig. 5.5 ; voir chapitre III).

L'échantillon 11AR01 est constitué de clinopyroxènes allongés, de petites olivines associées à des spinelles dans un verre. Les compositions chimiques de chaque minéral sont calculées à partir des analyses microsonde (cf. Tableau 5.3), sauf pour l'olivine qui est trop petite pour analyse. Le spectre IR de la Fig. 5.7, faite sur poudre,

confirme la présence de pyroxène et d'olivines. L'olivine est aussi identifiée au Raman (fig. 5.6).

L'échantillon 11AR02 est constitué de la même minéralogie que l'échantillon 11AR01. Cependant les cristaux n'ont ni la même taille ni la même morphologie. De nouveau les analyses chimiques de chaque minéral sont consignées dans le Tableau 5.3, sauf pour les pyroxènes qui sont trop petits.

L'échantillon 11AR01 présente une texture semblable aux spinifex (Fig. 5.8). Pouvons-nous trouver des komatiites sur Mars ? Il y a quelques différences entre nos échantillons de synthèse et les échantillons martiens. La composition chimique en silice est un peu supérieure aux basaltes vraiment frais (Adirondack, Humphrey et Mazatzal brooklyn), bien que les teneurs en Fe et Mg soient similaires. Des basaltes martiens présentent des olivines automorphes alors que dans ces échantillons elles sont petites et aciculaires (11AR01) ou quasi-automorphes (11AR02). L'absence de feldspaths dans les échantillons est due à la faible teneur en Ca et Al, compensée par une forte teneur en Mg et Fe: un phénomène déjà connu dans les mélanges primitifs. Le plus intéressant est donc la présence d'une texture et d'une minéralogie similaires à celle des komatiites. Ces roches sont très communes à l'Archéen. Ces roches riches en Mg forment des laves très fluides à la surface et des coulées très fines. Des komatiites ont déjà été décrites à la surface de Mars. De plus, des preuves d'épanchement de magma très fluides en surface sont un autre argument. Cependant, aucune texture spinifex n'a encore été révélée par le microscope des MER, peut être à cause de l'altération rapide des ces roches. Cette étude suggère que des roches basaltiques, ou de vraies komatiites peuvent être présentes à la surface de Mars. Nos basaltes synthétiques sont différents de ceux des précédentes études, puisque les compositions chimiques initiales et les paramètres de pression et de température sont différents. Par exemple nous utilisons une température de 1350°C comparée à 1120°C; ou encore une deuxième étude a proposé des basaltes holocristallins avec des textures aphanitiques porphyriques sans verre qui évoque plus un gabbro qu'un basalte.

Ce travail a aussi une implication dans la recherche de vie passée sur Mars. En effet, les échantillons synthétisés sont analogues de roches martiennes du Noachien, une période où la vie est possiblement apparue sur Mars. Ces roches riches en Fe et Mg sont des habitats favorables pour des organismes chemiolithotrophes. De plus, l'altération de ces roches produit des argiles riches en Fe et Mg comme la nontronite ou les argiles de la famille chlorite-saponite, qui peuvent être impliquées dans la concentration des organismes prébiotiques. Finalement, l'altération en conditions aqueuses de roches mafiquescomme les komatiites, favorise la serpentinisation. Ce processus est souvent associé à une importante activité biologique. Des preuves de la présence de serpentinites ont déjà été observées sur Mars et peuvent constituer de possibles habitats pour une vie primitive.

Nous avons produit des basaltes synthétiques riches en Fe et Mg fondés sur les données provenant du cratère Gusev. L'échantillon refroidi lentement présente des textures spinifex, très similaires aux komatiites typiques de la Terre primitive formées à une époque contemporaine du Noachien martien. Ces produits et leurs altérations

semblent être pertinents pour la recherche d'environnement ayant pu abriter la vie. Ce travail conclut mon projet de thèse et permet d'ajouter des basaltes analogues, ayant une composition chimique et texturale analogue aux basaltes martiens, à la collection de l'ISAR.

Conclusions

The main objective of this thesis was to follow a scientific approach for creating a collection of rocks for testing and calibrating space instrumentation for on-going and future space missions. For this purpose, it was first necessary to establish a logical classification of the samples and to develop an interface allowing scientists and engineers implicated in space missions to obtain information on relevant samples and to be able to borrow the samples. This was accomplished with the ISAR website. Because of the emphasis is presently laid on Mars missions, I concentrated my efforts on the collection of Mars analogue samples. The choice of samples was based on the data available about the mineralogical and geochemical composition of the Martian surface. The analogue samples were fully characterized using several techniques relevant to space missions but using laboratory instrumentation that allowed higher spatial resolution and accuracy. This first set of rocks is already being used by different scientific teams working on the ExoMars project. In December 2010, smalls slab of the ISAR samples exhibiting both weathered and fresh surfaces were provided to Derek Pullan, University of Leicester, for the calibration board of the PanCam system. I participated in the ExoMars-XRD meeting with Lucia Marinageli (ExoMars-XRD PI, International Research School of Planetary Sciences, Pescara – Italy) where I gave her a selection of 12 samples from the ISAR to calibrate the XRD instrument. Unfortunately, this calibration could not be completed in time for this report. In November 2011, a number of samples were used by the Raman team, directed by Fernando Rull (Raman PI; Universidad Asociada - Centro de Astrobiologia, Valladolid). Samples have been sent to the MicrOmega team to test and calibrate the instrument (Jean-Pierre Bibring, PI - F. Westall, co-PI -, and his PhD student, Cedric Pilorget, IAS, Orsay, France). They have also been provided to the group of Paul Mahaffy (Goddard Space Center) for

testing the SAM instrument for MSL and the GC-MS part of the MOMA instrument for ExoMars-2018, as well as to Fred Goesmann (Max Planck Institute, Mainz) for testing the LD-MS part of MOMA. The final implementation of ISAR is the proposal of a blind test to the different teams involved in ExoMars. The objective is to determine the level of expertise accessible with the different instruments, separately and then alltogether. The test is thus composed of two stages:

1. Two unlabelled samples were sent to the teams that accepted to participate in the test (Raman, MicrOmega and MOMA) as <250 µm grains size powders. Each team will send back the result of their analyses and their first interpretation.
2. The results obtained from each instrument will be grouped together and sent to the participants with complementary data, e.g. photography, to help them to refine their interpretation.

The aim of this experiment is not to put the instruments in competition but to bring out their complementarity. This test will thus help to develop the interaction between the ExoMars teams and with the ISAR team in order to improve the level of expertise accessible during the mission (ability to identify a rock or to detect past traces of life for instance).

The first sample (A) is the 00AU05, the Kitty's Gap chert from Australia containing the oldest remains of microbial colonies. The second sample (B) is a komatiite from the Komatii river in South Africa (10SA09). The first stage is still in progress. The available results are displayed in the Table 6.1.

Samples :	**Chert - 00AU05**	**Komatiite - 10SA09**
ISAR Characterization :	**Minerals:** Quartz, hydromuscovite and anatase. **Organic molecules:** Only carbon as kerogen.	**Minerals:** Quartz, amphiboles, clays, talc, iron oxide, hematite and dolomite. **Organic molecules:** Some
ExoMars Raman	**Minerals:** quartz, calcite, anatase, muscovite. carbonaceous material	**Minerals:** amphibole (Pargasite), carbonaceous material
MicrOmega	?	?
MOMA	?	?

◄Table 6.1: Comparison of minerals and organic molecules observed in the two blind test samples using ISAR instrumentation and with some of the ExoMars instruments.

◄*Tableau 6.1: Comparaison des minéraux et des molécules organiques observées dans les deux échantillons du test à l'aveugle en utilisant les instruments de l'ISAR et quelques uns des instruments d'ExoMars.*

During the first part of my project, I had to evaluate the degree of analogy and the pertinence of each Mars analogue sample. It was clear that the perfect analogue sample does not exist on Earth, in particular because of enrichment in Fe and Mg in Martian volcanics and because of the different alteration processes. This conclusion led me to search for an area where basaltic samples were altered by acidic fluids. Thus, in the second part of my thesis, I suggested the *Skouriotissa* copper mining open pit in Cyprus as a possible good Martian analogue site. This is a very massive sulphides deposit (VMS) in a basaltic environment that has been altered by natural meteoric water and acid mine runoff. I therefore sampled altered and unaltered rocks in order to obtain mineralogical information along an alteration profile and to study the weathering effect. I was thus able to document mineral associations similar to those found on Noachian/early Hesperian Mars terrains and to correlate them with specific subaqueous/subaerial and pH conditions of alteration. This terrestrial analogue site has rock and weathering characteristics that help to improve our understanding of geological subsurface phenomena on Mars. It is therefore pertinent to continue the investigation of this site and to sample it in finer detail in order to trace the past and present physico-chemical processes, which are certainly comparable to those taking place on Mars. The search for other analogue sites must also be made, taking into account the new geological data coming from Mars.

The most relevant Mars analogue samples are obviously basalts. However, the perfect chemical analogue basalt cannot exist on Earth where basalts are depleted in Fe-Mg with respect to Martian basalts. The last part of my project was thus dedicated to the fabrication of a Martian basalt with a chemical composition based on the data collected in Gusev crater by Spirit. The two synthesized samples show very interesting textures and structures. This study increases our understanding of the geological processes taking place on Mars (e.g. textures provide information about the cooling rate conditions).

The ISAR collection is far from complete and it will be necessary to add new Mars analogue rocks and minerals, such as evaporite minerals

(sulfates, chlorates or carbonates) that have been identified on the surface of Mars (e.g. *McLennan et al., 2005; Gendrin et al., 2005*) and which, on Earth, are often associated with traces of life (e.g. *Barbieri and Stivaletta, 2011*). These kinds of samples have been collected in a variety of terrestrial environments, such as the Atacama desert, in playas lakes (e.g. Morocco), or around areas showing mining activity such as the *Skouriotissa* mine in Cyprus. They will be analysed and characterized in the same way as the first set of ISAR samples. Analogue samples from other solar system bodies, such as the Moon and asteroids, will also be added to the collection.

Artificial weathering of the synthesized basalts, in comparison with that of samples from natural environments (e.g. Cyprus) could be very interesting. In order to mimic the weathering effect occurring during the Noachian period, this alteration could be made with acid water (pH<4) circulating on the surface of the sample. The results could thus be compared with the "natural" processes observed in Cyprus. A second experiment carried out under simulated Martian atmosphere and high UV irradiation, in order to study the alteration of the surface of Mars over the last 3 Gy would also be interesting. For astrobiological purposes, the alteration of the artificial Martian basalt synthesized in the course of my project by lithotrophic or photo-litotrophic microorganisms under simulated early Mars conditions would be also very pertinent and will be undertaken in the near future. This experiment could give important information about the interaction between life and rocks and may, above all, be very helpful for the detection of past or present traces of life on Mars.

Conclusion (résumé Francais)

L'objectif principal de cette thèse est d'avoir une approche scientifique afin de créer une collection de roches pour tester et calibrer les instruments de vols des futures missions spatiales. Pour cela, il a été nécessaire d'établir une classification logique des échantillons et de développer une interface adaptée aux scientifiques et ingénieurs impliqués dans les missions spatiales dans le but d'obtenir des informations pertinentes sur les échantillons et pourvoir, le cas échéant, les emprunter. Cet objectif est réalisé à travers le site web de l'ISAR. Puisque les missions sont actuellement tournées vers Mars, j'ai concentré mon travail sur la collection d'échantillons analogues de Mars. Les analogues sont intégralement caractérisés en utilisant de nombreuses techniques pertinentes pour les missions spatiales ; tout en utilisant des instruments de laboratoire qui permettent d'avoir de bonnes résolutions et de la précision. Le premier lot d'échantillons a d'ores et déjà été utilisé par différentes équipes du projet ExoMars (PanCam, ExoMars-XRD, MicrOmega, Raman et MOMA) ; dernièrement lors de la réalisation d'un test à l'aveugle avec les futurs instruments de vol. L'objectif est de déterminer le degré d'expertise de chaque instrument ainsi qu'avec l'ensemble des instruments. Le test se fait en deux étapes : 2 échantillons en poudre, ont été envoyés aux équipes participantes (Raman, MicrOmega et MOMA) pour analyse sans aucune autre information. Dans une deuxième étape les résultats obtenus sont regroupés et échangés entre les équipes pour faire une deuxième itération d'interprétation. L'objectif de l'exercice n'est pas de mettre les instruments en compétition mais de mettre en évidence leur complémentarité. Les deux échantillons A et B sont respectivement un chert de Kitty's Gap (00AU05) et une komatiite d'Afrique du Sud (10SA09). Les résultats d'analyse disponibles sont reportés dans le tableau 6.1.

Pendant la première partie de mon projet, j'ai évalué le degré d'analogie et de pertinence de chaque échantillon analogue de Mars. Il est évidement que le parfait échantillon analogue de Mars n'existe pas. En particulier à cause de l'enrichissement en Fe Mg des basaltes, ou des processus d'altération différents. Cette première conclusion m'a incité à chercher un lieu où des basaltes sont altérés par des fluides acides. C'est pourquoi j'ai suggéré l'étude de la mine de Skouriotissa. Les basaltes y sont altérés par des processus hydrothermaux, météoriques et acides. La minéralogie résultante semble similaire aux observations martiennes, et ce site semble être un bon site analogue de la Mars du Noachien – Amazonien.

Les meilleurs analogues de Mars sont sans aucun doute les basaltes. Néanmoins des basaltes parfaitement analogues chimiquement de Mars n'existent pas sur Terre, en particulier à cause de leur faible teneur en Fe et Mg. La dernière partie de ma thèse a donc été dédiée à la fabrication de basaltes martiens avec une composition chimique fondée sur les données collectées dans le cratère Gusev par Spirit. Les deux échantillons synthétisés présentent de très intéressantes textures et structures. Cette étude augmente la compréhension des processus géologiques qui ont pris place sur Mars.

La collection de l'ISAR est loin d'être complète, et il est nécessaire d'ajouter de nouvelles roches et de nouveaux minéraux analogues de Mars, comme des évaporites.

Enfin l'altération des basaltes artificiels et la comparaison avec des échantillons provenant d'environnements naturels (comme Chypre) peut être très intéressant. Il serait intéressant de reproduire les conditions chimiques d'altération, mais aussi d'essayer avec uniquement un rayonnement UV. Dans un contexte exobiologique, faire altérer les échantillons par des microorganismes lithotrophes ou photolitotrophes, dans des conditions simulant la Mars primitive, semble vraiment pertinent pour mieux comprendre les interactions entre la vie et la roche, et pourrait aider à la détection d'une vie passée ou présente sur Mars.

References

A

Ablay G. J., and Marti J., 2000. Stratigraphy, Structure, and Volcanic Evolution of the Pico Teide-Pico Viejo Formation, Tenerife, Canary Islands. *Journal of Volcanology and Geothermal Research* 103:175-208.

Alt J. C., and Honnorez J., 1984. Alteration of the upper oceanic crust, DSDP site 417: mineralogy and chemistry. *Contributions to Mineralogy and petrology* 87:149-169.

Amils R., Gonzalez-Toril E., Fernandez-Remolar D., Gomez F., Aquilera A., Rodriguez N., Malki M., Garcia-Moyano A., Fairen A. G., de la Fuente V., and Sanz J. L., 2007. Extreme environments as mars terrestrial analogs : The Rio Tinto case. *Planetary and Space Science* 55:370-381. Doi:10.1013/j.pss.2006.02.006.

Amundsen H. E. F., Benning L., Blake D. F., Fogel M., Ming D., Skidmore M., Steele A., and the AMASE team, 2011. Cryogenic origin for Mars analogue carbonates in the Bockfjord volcanic complex, Svalbard (Norway), *42nd Lunar and Planetary Conference, The Woodland Texas*, Abstract # 2223.

Armstrong R. A., Compston W., De Wit M. J., and Willians I. S., 1990. The stratigraphy of the 3.5-3.5 GA Barberton greenstone belt revisited: a single zircon ion microprobe study. *Earth and Planetary Science Letters* 101:90-106.

Arndt N. T., 2003. Komatiites, kimberlites, and boninites. *Journal of Geophysical Research* 108 B6-2293. doi:10.1029/2002JB00215.

Arndt N. T., Lesher C. M., Houlé M. C., Lewin E., and Lacaze Y., 2004. Intrusion and Crystallization of a Spinifex-Textured Komatiite Sill in Dundonald Township, Ontario. *Journal of Petrology* 45:2555-2571.

Arvidson, R. E., Poulet F., Morris R. V., Bibring J.-P., Bell III J. F., Squyres S. W., Christensen P. R., Bellucci G., Gondet B., Ehlmann B. L., Farrand W. H., Fergason R. L., Golombek M., Griffes J. L., Grotzinger J., Guinness E. A., Herkenhoff K. E., Johnson J. R., Klingelhöfer G., Langevin Y., Ming D., Seelos K., Sullivan R. J., Ward J. G., Wiseman S. M., and Wolffet M., 2006. Nature and origin of the hematite-bearing plains of Terra Meridiani based on

analyses of orbital and Mars Exploration rover data sets, *Journal of Geophysical Research* 111:E12S08. doi:10.1029/2006JE002728.

B

Bandfield J. L., 2002. Global mineral distributions on Mars. *Journal of Geophysical Research* 107:5042. Doi:10.1029/2001je001510

Bandfield J. L., Glotch T. D., and Christensen P. R., 2003. Spectroscopic Identification of Carbonate Minerals in the Martian Dust. *Science* 301:1084-1087.

Bandfield J. L., Hamilton V. E., Christensen P. R., and McSween H. Y., 2004. Identification of quartzofeldspathic materials on Mars. *Journal of Geophysical Research* 109:E10009. Doi:10.1029/2004JE002290.

Barbieri R., and Stivaletta N., 2011. Continental evaporites and the search for evidence of life on Mars. *Geological Journal*, 46: 513–524.

Barbin V., Blanc P., Klossa B., Lorin C., and Thomas R., 1999. Cathodoluminescence: a new approach to the in situ study of martian surface mineralogy. Symposium International: Programme d'exploration de Mars & mission de retour d'échantillons (Paris). Resumé, *CNES.Edit*.

Bear L.M., 1960. Geol. Surv. Cyprus Mem. 3:1-122.

Bear L.M, 1961 (?) only reference in Moores and Vine 1971

Bibring J. -P., Langevin Y., Mustard J. F., Poulet F., Arvidson R., Gendrin A., Gondet B., Mangold N., Pinet P., Forget F., and the OMEGA Team, 2006. Global Mineralogical and Aqueous Mars History Derived from OMEGA/Mars Express Data. *Science* 312:400-404. Doi: 10.1126/science.1122659.

Bigham J. M., and Nordstrom D. K., 2000. Iron and aluminum hydroxysulfates from acid sulfate waters, in *Sulfate Minerals: Crystallography, Geochemistry, and Environmental Significance*, Rev. Mineral. Geochem., vol. 40, edited by Alpers C. N., Jambor J. L., and Nordstom D. K., pp. 351–403, Mineral. Soc. of Am., Washington, D. C

Bonin B., 2011. Granites extra-terrestres. in *Granites et granitoïdes*, Geochronique 120 : p.39.

Bonin B., 2012. Extra-terrestrial igneous granites and related rocks : a reviw of their occurrence and petrogenesis. *Lithos*, in press.

Borg L. E., Connelly J. N., Nyquist L. E, Chih C.-Y., Weismann H., and Reese Y., 1999. The age of carbonates in martian meteorite ALH84001. *Science* 186:90-94.

Bost N., Westall F., Gaillard F., Ramboz C., and Foucher F., 2012. Synthesis of a spinifex-textured Basalt as an analogu to Gusev Crater basalts, Mars. *Meteoritics & planetary Science*, 47: 820-831.

Bost N., Westall F., Ramboz C., Foucher F., Pullan D., Meunier A., Petit S., Fleischer I., Klingelhöfer G., and Vago J. L., in review. Missions to Mars: Characterization of Mars analogue rocks for the International Space Analogue Rockstore (ISAR). *Planetary Space Science;* submitted.

Bost N., Ramboz C., Westall F., Fontaine C., Foucher F., and Pilorget C., The Skouriotissa mine: A new terrestrial analogue for mineral formation on early Mars, *Geology;* submitted.

Boynton W. V., Ming D. W., Kounaves S. P., Young S. M. M., Arvidson R. E., Hecht M. H., Hoffman J., Niles P. B., Hamara D. K., Quinn R. C., Smith P. H., Sutter B., Catling D. C., and Morris R. V., 2009. Evidence for Calcium Carbonates at the Mars Phoenix Landing site. *Science*, 325:61-64. Doi: 10.1126/science.1172768.

Brack A., 2000. The exobiology exploration of Mars: a survey of the European approaches. *Planetary and Space Science* 48:1023-1026.

Bryan W. B., 1972. Morphology of Quench Crystals in Submarine Basalts. *Journal of Geophysical Research* 77:5812-5819.

C

Carter J., Poulet F., Bibring J.-P., and Murchie S., 2010. Detection of Hydrated Silicates in Crustal Outcrops in the Northern Plains of Mars. *Science* 328:1682-1686.

Carr M. H., and Head J. W., 2009. Geologic history of Mars, *Earth and Planetary Science Letters* 294:185-203. Doi:10.1016/j.epsl.2009.06.042.

Cavalazzi B., Westall F., Cady S. L., Barbieri R., and Foucher F., 2011. Potential fossil endoliths in vesicular pillow basalt, Coral Patch Seamount, eastern North Atlantic Ocean. *Astrobiology* 11:619-632.

Chan M. A., Beitler B., Parry W. T., Ormö J., and Komatsu G., 2004. A possible terrestrial analogue for haematite concretions on Mars. *Nature* 439:731-734.

Christensen P. R., Morris R. V., Lane M. D., Bandfield J. L., and Malin M. C. , 2001. Global mapping of Martian hematite mineral deposits: Remnants of water-driven processes on early Mars, *Journal of Geophysical Research* 106:23,873–23,885. doi:10.1029/2000JE001415.

Christensen P. R., McSween H. Y., Bandfield J. L., Ruff J. L., Rogers A. D., Hamilton V .E., Gorelick N., Wyatt M. B., Jakosky B. M., Kieffer H. H., Malin M. C., and Moersch J. E., 2005. Evidence for magmatic evolution and diversity on Mars from infrared observations. *Nature* 436:504-509. Doi:10.1038/nature03639.

Ciobanu M.-C., Rabineau M., Droz L., Révillon S., Ghiglione J.-F., Dennielou B., Jorry S.-J., Kallmeyer J., Etoubleau J., Pignet P., Crassous P., Vandenabeele-Trambouze O., Laugier J., Guégan M., Godfroy A., and Alain K., 2012. Paleoenvironmental imprint on subseafloor microbial communities inWestern Mediterranean Sea Quaternary sediments. *Biogeosciences Discussion* 9:253–310. Doi:10.5194/bgd-9-253-2012.

Clark B. C., Morris R. V., McLennan S. M., Gellert R., Jolliff B., Knoll A. H., Squyres S. W., Lowenstein T. K., Ming D. W., Tosca N. J., Yeni A., Christensen P. R., Gorevank S., Brücknerd J., Calvin W., Dreibus G., Farrand W., Klingelhoefer G., Waenke H., Zipfel J., Bell III J.F., Grotzinger J., McSween H.Y., and Rieder R., 2005. Chemistry and mineralogy of outcrops at Meridiani Planum. *Earth and Planetary Science Letters* 240:73-94. Doi:10.1016/j.epsl.2005.09.040.

Clifford S. M., and Parker T. J., 2001. The evolution of the Martian hydrosphere: Implications for the fate of a primordial ocean and the current state of the northern plains, *Icarus* 154, 40, doi:10.1006/icar.2001.6671.

Coltelli M., Del Carlo P., and Vezzoli, L., 2000. Stratigraphic constraints for explosive activity in the past 100 ka at Etna Volcano, Italy, *International Journal of Earth Sciences* 89:665-677, doi: 10.1007/s005310000117.

Coltelli M., Del Carlo P., Pompilio M., and Vezzoli L., 2005. Explosive eruption of a picrite: The 3930 BP subplinian eruption of Etna volcano (Italy), *Geophysical Research Letters, 32*, L23307, doi: 10.1029/2005GL024271.

Constantinou G., and Govett G. J. S., 1972. Genesis of sulphide deposits, ochre and umber of Cyprus. Transactions of the institution of mining and metallurgy. Section B. *Applied Earth Science* 81:B34-B46.

Cyprus Geological Survey Department, 1969. *Geological Map of the Xeros-Trodos Area*.

Cyprus Geological Survey Department, 2007. *Geological Map of cyprus*.

D

Dear W. A., Howie R. A., and Zussman J., 1966. *An introduction to the rock-forming minerals*. ed by Longman Group Limited .

Decarreau A., Petit S., Martin F., Farges F., Vieillard P., and Joussein E., 2008. Hydrothermal synthesis, between 75 and 150°C, of high-charge, ferric nontronites, *Clays and Clay Minerals* 56:322-327, Doi: 10.1346/CCMN.2008.0560303.

Dehant V., 2010. Mars Interior: Part 1: Structure and Activity. Communication in ESA-Les Houches III *Mars Workshop 2010*.

Dehouck E., Mangold N., Le Mouélic S., Ansan V., and Poulet F., 2010. Ismenius Cavus, Mars : A deep paleolake with phyllosilicates deposits. *Planetary and Space Science* 58:941-946. Doi:10.1016/j.pss.2010.02.005.

Dill H. G., Füssl M., and Botz R., 2007. Mineralogy and (economic) geology of zeolite-carbonate mineralization in basic igneous rocks of the Troodos complex, Cyprus. *N. Jb. Miner. Abh*. 183/3:251-268.

DoCouto D., 2009. *Signification géologique des datations chimiques sur monazite. Application à la série polymétamorphique de la Sioule (Nord du Massif Central)*, Mémoire Master 2, Université d'Orléans.

E

Economou T. E., 2001. Chemical analyses of Martian soil and rocks obtained by the Pathfinder alpha proton x-ray spectrometer. *Radiation Physics and Chemistry* 61:191– 197.

European Space Agency, 2010. ExoMars Science Management Plan. *EXM-MS-PL-ESA-00002*, Issue 5, Rev. 4. ESA-ESTEC, Norrdwijk, 60 pp.

Ehlmann B. L., Mustard J. F., Murchie S. L., Poulet F., Bishop J. L., Brown A. J., Calvin W.M., Clark R. N., Des Marais D. J., Milliken R. E., Roach L. H., Roush T. L., Swayze G. A., and Wray J. J., 2008. Orbital Identification of Carbonates-Bearing Rocks on Mars. *Science* 322:1828-1832. Doi: 10.1126/science.1164759

Ehlmann B. L., Mustard J. F., Swayze G. A., Clark R. N., Bishop J. L., Poulet F., Des Marais D. J., Roach L. H., Milliken R. E., Wray J. J., Barnouin-Jha O., and Murchie S., 2009. Identification of hydrated silicate minerals on Mars using MRO-CRISM: Geologic context near Nili Fossae and implications for

aqueous alteration. *Journal of Geophysical Research* 114:E00D08. Doi:10.1029/2009JE003339.

Ehlmann B. L., Mustard J. F., and Murchie S.L., 2010. Geologic setting of serpentine deposits on Mars, *Geophysical Research Letter* 37:L06201. Doi:10.1029/2010GL042596.

Ehlmann B. L., Mustard J. F., Murchie S. L., Bibring J. -P., Meunier A., Fraeman A. A., and Langevin Y., 2011. Subsurface water and clay mineral formation during the early history of Mars. *Nature* 479:53-60. Doi:10.1038/nature10582.

F

Fassett C. I., and Head J. W., 2007. Valley formation on martian volcanoes in the Hesperian: Evidence for melting of summit snowpack, caldera lake formation, drainage and erosion on Ceraunius Tholus. *Icarus* 189: 118-135. Doi: 10.1016/j.icarus.2006.12.021

Faure F., Arndt N., and Libourel G., 2006. Formation of Spinifex Texture in Komatiites: an Experimental Study. *Journal of Petrology* 47:1591-1610. Doi:10.1093/petrology/egl1021.

Faure F., Schiano P., Trolliard G., Nicollet C., and Soulestin B., 2007. Textural evolution of polyhedral olivine experiencing rapid cooling rates. *Contribution to Mineralogy and Petrology* 153:405-416.

Filiberto J., Treiman A. H., and Le L., 2008. Crystallization experiments on a Gusev Adirondack basalt composition. *Meteoritics & Planetary Science* 43:1137–1146.

Fookes P. G., 2008. Some aspects of the geology of Svalbard. *Geology Today* 24:146-152

Foucault A. and Raoult J.-F., 2010. *Dictionnaire de géologie*. Universcience, Dunod editor.416 p.

Foucher F., Bost N., Rüßman P., and Westall F., 2011. Effect of grain size distribution on Raman analyses: consequences for ExoMars-C measurements. *EPSC-DPS joint meeting*, Nantes, France, October 2011

Foucher F., López Reyes G. , Bost N., Rull F., Rüßmann P., and Westall F., 2012. ☻ Effect of the crushing process on Raman analyses: consequences for the Mars 2018 mission. EGU General Assembly, Vienne, Austria, April 2012.

Furnes H., Banerjee N. R., Staudigel H., Muehlenbachs K., NMcLoughlin N., de Wit M., and Van Kranendonk M., 2007. Comparing petrographic signatures of bioalteration in recent to Mesoarchean pillow lavas: Tracing subsurface life in oceanic igneous rocks. Precambrian Research 158:156-176. doi:10.1016/j.precamres.2007.04.012.

G

Gaillard F., Pichavant M., and Scaillet B., 2003. Experimental determination of activities of FeO and Fe2O3 components in hydrous silica melts under oxidizing conditions. Geochimica et Cosmochimica Acta 67:4389-4409.

Gaillard F., and Scaillet B., 2009. The sulfur content of volcanic gases on Mars. *Earth and Planetary Science Letters* 279:34-43.

Gass I. G., 1960. *The geology and mineral resources of the Dhali area*: Cyprus Geological Survey Department Memoire 4.

Gass I. G., 1968. Is the Troodos massif of Cyprus a fragment of Mesozoic ocean crust? *Nature* 220:39–42.

Gellert R., Rieder R., Anderson R. C., Brückner J., Clark B. C., Dreibus G., Economou T., Klingelhöfer G, Lugmair G. W., Ming D. W., Squyres S. W., d'Uston C., Wänke H., Yen A., and Zipfel J., 2004. Chemistry of Rocks and Soils in Gusev Crater from the Alpha Particle X-ray Spectrometer. *Science* 305:829-832. Doi: 10.1126/science.1099913.

Gellert R., Rieder R., Brückner J., Clark B. C., Dreibus G. , Klingelhöfer G., Lugmair G., Ming D. W., Wänke H., Yen A., Zipfel J., and Squyres S. W., 2006. Alpha Particle X-Ray Spectrometer (APXS): Results from Gusev crater and calibration report. *Journal of Geophysical Research* 111:E02S05. doi:10.1029/2005JE002555.

Gendrin A., Mangold N., Bibring J.-P., Langevin Y., Gondet B., Poulet F., Bonello G., Quantin C., Mustard J., Arvidson R., and Le Mouélic S., 2005. Sulfates in Martian Layered Terrains: The OMEGA/Mars Express View. *Science* 307:1587-1591. Doi: 10.1126/science.1109087.

Goldschmidt V. M., 1926. *Geochemische Verteilungsgesetze der Elemente*. Skrifter Norske Videnskaps—Akad. Oslo

Golden D. C., Ming D. W., Morris R. V., and Mertzman S. A., 2005. Laboratory-simulates acid-sulfate weathering of basaltic materials: Implications for formation of sulfates at Meridiani Planum and Gusev crater, Mars. *Journal of Geophysical Research* 110:E12S07. Doi:10.1029/2005JE002451.

Gooding J. L., 1992. Soil Mineralogy and Chemistry on Mars: Possible Clues from Salts and Clays in SNC Meteorites. *Icarus* 99:28-41.

Götze J., Krbetschek M. R., Habermann D., and Wolf D., 2000. High resolution CL studies of feldspars minerals, in *Cathodoluminescence in geosciences* edited by Pagel M., Barbin, V., Blanc, P.,and Ohnenstetter, D . Springer, Berlin Heidelberg New York Tokyo, pp 246–270

Grebby S., Cunningham D., Naden J., and Tansey K., 2010. Lithological mapping of the Troodos ophiolite, Cyprus, using airborne LiDAR topographic data. *Remote Sensing of Environment* 114:713–724.

Greeley R., Foing B. H., McSween H. Y., Neukum G., Pinet P., van Kan M., Werner S. C., Williams D. A., and Zegers T. E., 2005. Fluid lava flows in Gusev crater, Mars. *Journal of Geophysical Research* 110:E05008. Doi:10.1029/2005JE002401.

Greenberger R. N., Mustard J. F., Kumar P. S., Dyar M. D., Speicher E. A., and Skulte E. C., 2011. Weathering products of Deccan basalts and implications for Mars. *42nd Lunar and Planetary Science Conference*, abstract 2548.

H

Habermann D., Neuser R. D., and Richter D. K., 2000. Quantitative high resolution spectral analysis of Mn2þ in sedimentary calcite. in

Cathodoluminescence in geosciences edited by Pagel M., Barbin, V., Blanc, P.,and Ohnenstetter, D . Springer, Berlin Heidelberg New York Tokyo, pp 331–358

Halevy I., Zuber M. T., and Schrag D. P., 2007. A sulfur dioxide climate feedback on early Mars. *Science* 318:1903–1907. doi: 10.1126/science.1147039.

Harnois L., 1988. The CIW index: A new chemical index of weathering. *Sedimentary Geology*, 55:319-322.

Hartman W. K., and Neukum G., 2001. Cratering Chronology and the Evolution of Mars. *Space Science Review* 96: 165-194. doi: 10.1023/A:1011945222010

Herd C. D. K., 2006. Insights into the redox history of the NWA 1068/1110 martian basalt from mineral equilibria and vanadium oxybarometry. *American Mineralogist* 91:1616-1627. Doi:10.2138/am.2006.2104.

Herd C. D. K., Borg L. E., Jones J. H., and Papike, J. J., 2002. Oxygen fugacity and geochemical variations in the martian basalts: Implications for martian basalt petrogenesis and the oxidation state of the upper mantle of Mars. *Geochimica et Cosmochimica Acta* 66:2025-2036.

Hoelhler T. M., and Westall, F., 2010. Mars Exploration Program Analysis Group Goal One: Determine if life ever arose on Mars. *Astrobiology* 10:859-867.

Hofmann A., and Bolhar R., 2007. Carbonaceous Cherts in the Barberton Greenstone Belt and Their Siginifiance for the Study of Early Life in the Archean Record. *Astrobiology*, 7:355-388. doi:10.1089/ast.2005.0288.

Hurowitz J . A., McLennan S. C., Lindsley D. H., and Schoonen M. A., 2005. Experimental epithermal alteration of synthetic Los Angeles meteorite: Implication for the origin of Martian soils and identification of hydrothermal sites on Mars. *Journal of Geophysical Research* 110:E07002. doi:10.1029/2004JE002391.

Hurowitz J. A., McLennan S. M. , Tosca N. J., Arvidson R. E., Michalski J. R., Ming D. W., Schröder C., and Squyres S. W., 2006. In situ and experimental evidence for acidic weathering of rocks and soils on Mars. Journal of Geophysical Research 111:E02S19. doi:10.1029/2005JE002515.

Hynek B. M., Arvidson R. E., and Phillips R. J., 2002. Geologic setting and origin of Terra meridian hematite deposit on Mars. *Journal of Geophysical Research* 10:E10.

J

Jakosky B. M., and Shock E. L., 1998. The Biological Potential of Mars, the Early Earth, and Europa. American Astronomical Society, DPS meeting #30, #11.05; *Bulletin of the American Astronomical Society* 30:1031.

Jakosky B. M., Westall F., and Brack A., 2007. Mars. In Planets and Life: The Emerging Science of Astrobiology, edited by Sullivan W.T. and Baross J.A., Cambridge, Cambridge University Press. pp. 357-387.

Jébrak M., and Marcoux E., 2008. *Géologie des ressources minérales*. Géologie Quebec.

K

Kamenestsky V. S., Pompilio M., Métrich N., Sobolev A. V., Kuzim D. V., and Thomas R., 2007. Arrival of extremely volatile-rich high-Mg magmas changes explosivity of Mount Etna, *Geological Society of America, 35*, 255-258, doi: 10.1130/G23163A.1.

Kleinhans M. G., van de Kasteele H.E., and Hauber E., 2010. Palaeoflow reconstruction from fan delta morphology on Mars. *Earth and Planetary Science Letters* 294:378–392. Doi:10.1016/j.epsl.2009.11.025.

Klingelhöefer G., Morris R. V., Bernhardt B., Rodionov D., de Souza Jr. P. A., Squyres S. W., Foh J., Kankeleit E., Bonnes U., Gellert R., Schröder Ch., Linkin S., Evlanov E., Zubkov B., and Prilutski O., 2003. Athena MIMOS II Mössbauer spectrometer investigation, *Journal of Geophysical Research*, 108:8067. doi: 10.1029/2003JE002138.

Kminek G., and Bada J. L., 2006. The effect of ionizing radiation on the preservation of amino acids on Mars. *Earth and Planetary Science Letters* 245:1-5. doi: 10.1016/j.epsl.2006.03.008.

L

Le Bas M. J., 2000. IUGS Reclassification of the High-Mg and Picritic Volcanic Rocks. *Journal of Petrology* 41:1467-1470.

Le Deit L., Hauber E., Fueten F., Pondrelli M., Rossi A., Mangold N., van Gasselet S., Massé M., and Jaumann R., 2011. Geological analysis of Gale Crater on Mars. *EPSC-DPS Joint Meeting 2011*. Vol.6, EPSC-DPS2011-966.

Lefèvre F., and Forget F., 2009. Observed variations of methane on Mars unexplained by known atmospheric chemistry and physics. *Nature* 460:720-723. Doi:10.1038/nature08228.

Loizeau D., Mangold N., Poulet F., Bibring J.-P., Gendrin A., Ansan V., Gomez C., Gondet B., Langevin Y., Masson P., and Neukum G., 2007, Phyllosilicates in the Mawrth Vallis region of Mars, *Journal of Geophysical Research*, 112, E08S08, Doi:10.1029/2006JE002877.

Loizeau D., Mangold N., Poulet F., Ansan V., Hauber E., Bibring J.-P., Gondet B., Langevin Y., Masson P., and Neukum G., 2010. Stratigraphy in the Mawrth Vallis region through OMEGA, HRSC color imagery and DTM. *Icarus* 205:396-418. Doi: 10.1016/j.icarus.2009.04.018.

M

Mangold N., Poulet F., Mustard J. F., Bibring J.-P., Gondet B., Langevin Y., Ansan V., Masson Ph., Fassett C., Head III J. W., Hoffmann H., and Neukum G., 2007. Mineralogy of the Nili Fossae region with OMEGA/Mars Express data: 2. Aqueous alteration of the crust. *Journal of Geophysical Research* 112:E08S04, Doi:10.1029/2006JE002835.

Mangold N., Loizeau D., Poulet F., Ansan V., Baratoux D., LeMouelic S., Bardintzeff J. -M., Platevoet B., Toplis M., Pinet P., Masson P., Bibring J. – P., Gondet B., Langevin Y., and Neukum G., 2009. Mineralogy of recent volcanic plains in the Tharsis region, Mars, and implications for platy-ridged flow composition. *Earth and Planetary Science Letters* 294:440-450. Doi:10.1016/j.epsl.2009.07.36.

Marzo G. A., Davila A. F., Tornabene L. L., Dohm J. M., Fairén A. G., Gross C., Kneissl T., Bishop J. L., Roush T. L., and McKay C. P., 2010. Evidence for Hesperian impact-induced hydrothermalism on Mars. *Icarus* 208:667-683. Doi: 10.1016/j.icarus.2010.03.013.

McAdam A. C., Zolotov M. Y., Sharp T. G., and Leshin L. A., 2008. Preferential low-pH dissolution of pyroxene in plagioclase-pyroxene mixtures: Implication for martian surface materials. *Icarus* 196:90-96. Doi:10.1016/j.icarus.2008.01.008.

McKay D. S., 1996. the search for Life on Mars.*Origins of Life and Evolution of the Biosphere* 27:263–289.

McKay D. S., Gibson Jr. E. K., Thomas-Keprta K. L., Vali H., Romanek C. S., Clemett S. J., Chillier X. D. F., Maechling C. R., and Zareet R. N., 1996. Search for Past Life on Mars: Possible Relic Biogenic Activity in Martian Meteorite ALH84001. *Science* 273:924-930. Doi:10.1126/science.273.5277.924

McLennan S. M., Bell III J. F., Calvin W. M., Christensen P. R., Clark B. C., de Souza P. A., Farmer J., Farrand W. H., Fike D. A., Gellert R., Ghosh A., Glotch T. D., Grotzinger J. P., Hahn B., Herkenhoff K. E., Hurowitz J. A., Johnson J. R., Johnson S. S., Jolliff B., Klingelhöfer G., Knoll A. H., Learner Z., Malin M. C., McSween Jr. H. Y., Pocock J., Ruff S. W., Soderblom L. A., Squyres S. W., Tosca N. J., Watters W. A., Wyatt M. B., and Yen A., 2005. Provenance and diagenesis of the evaporite-bearing Burns formation, Meridiani Planum, Mars. *Earth and Planetary Science Letters* 240:95-121. Doi:10.1016/j.epsl.2005.09.041

McSween H. Y., Arvidson R. E., Bell III J. F., Blaney D., Cabrol N. A., Christensen P. R., Clark B. C, Crisp J. A., Crumpler L. S., Des Marais D. J., Farmer J. D., Gellert R., Ghosh A., Gorevan S., Graff T., Grant J., Haskin L. A., Herkenhoff K. E., Johnson J. R., Jolliff B. L., Klingelhoefer G., Knudson A. T., McLennan S., Milam K. A., Moersch J. E., Morris R. V., Rieder R., Ruff S. W., de Souza P. A., Squyres S. W., Wänke H., Wang A., Wyatt M. B., Yen A., and Zipfel J., 2004. Basaltic Rocks Analyzed by the Spirit Rover in Gusev Crater. *Science* 305:842-845. Doi: 10.1126/science.3050842.

McSween H. Y., Taylor G. J., and Wyatt M. B., 2009. Elemental Composition of the Martian Crust. *Science* 324:736-739. Doi: 10.1126/science.1165871. Ménez B., Pasini V., and Brunelli D., 2012. Life in the hydrated suboceanis mantle. *Nature Geoscience* 5:133-137. Doi:10.1038/NGEO1359.

Meunier A., Petit S., Cockell C. S., El Albani A., and Beaufort D., 2010. The Fe-Rich Clay Microsystems in Basalt-Komatiite Lavas: Importance of Fe-Smectites for Pre-Biotic Molecules Catalysis During the Adean Eon. *Origins of Life and Evolution of Biospheres* 40:253-272. doi:10.1007/s11084-010-9205-2.

Meunier A., Petit S., Ehlmann B. L., Dudoignon P., Westall, F., Mas A., El Albani A., and Ferrage E., 2012. Magmatic precipitation as a possible origin of Noachian clays on Mars. *Nature Geoscience.* Doi:10.1038/ngeo1572.

Michalski, J. R., and Niles, P. B., 2010. Deep crustal carbonate rocks exposed by meteor impact on Mars. *Nature Geoscience*. Doi:10.1038/ngeo971.

Miliken R. E., Swayze G.A., Arvidson R. E., Bishop J. L., Clark R. N., Ehlmann B. L., Green R. O., Grotzinger J. P., Morris R. V., Murchie S. L., Mustard J. F., and Weitz, C., 2008. Opaline silica in young deposits on Mars. *Geology* 36:847-850.

Ministry of Agriculture, natural resources and environment, government of Cyprus, 1995. *Mineral Ressource Map of Cyprus*. Cyprus Geological Survey.

Ming D. W., Gellert R., Morris R. V., Arvidson R. E., Brückner J., Clark B. C., Cohen B. A., d'Uston C., Economou T., Fleischer I., Klingelhöfer G., McCoy T. J., Mittlefehldt D. W., Schmidt M. E., Schröder C., Squyres S. W., Tréguier E., Yen A. S., and Zipfel J., 2008. Geochemical properties of rocks and soils in Gusev Crater, Mars: Results of the Alpha Particle X-Ray Spectrometer from Cumberland Ridge to Home Plate. *Journal of Geophysical Research* 113:E12S39. Doi:10.1029/2008JE003195.

Monders A. G., Médard E., and Grove T. L., 2007. Phase equilibrium investigations of the Adirondack class basalts from the Gusev plains, Gusev crater, Mars. *Meteoritics & Planetary Science* 42:131-148.

Moores E. M., and Vine F. J., 1971. Troodos Massif, Cyprus and other ophiolites as oceanic crust: Evaluation and implications. *Philosophical Transactions of the Royal Society of London A* 268:443–467.

Morris R. V., Klingelhöfer G., Schröder C., Rodionov D. S., Yen A., Ming D. W., de Souza Jr. P. A., Fleischer I., Wdowiak T., Gellert R., Bernhardt B., Evlanov E. N., Zubkov B., Foh J., Bonnes U., Kankeleit E., Gütlich P., Renz F., Squyres S. W., and Arvidson R. E., 2006. Mössbauer mineralogy of rock, soil, and dust at Gusev crater, Mars: Spirit's journey through weakly altered olivine basalt on the plains and pervasively altered in the Columbia Hills. *Journal of Geophysical Research* 111: E02S13. Doi:10.1029/2005JE002584.

Morris R.V., Ruff S. W., Gellert R., Ming D. W., Arvidson R. E., Clark B. C., Golden D. C., Siebach K., Klingelhöfer G., Schröder C., Fleischer I., Yen A. S., and Squyres S. W., 2010. Identification of Carbonate-Rich Outcrops on Mars by the Spirit Rover. *Science* 329:421-424. Doi: 10.1126/science.1189667.

Mumma M. J., Villanueva G. L., Novak R.E., Hewagama T., Bonev B. P., DiSanti M. A., Mandell A. M. and Smith M. D., 2009. Strong Release of Methane on Mars in Northern Summer 2003. *Science* 323: 1041-1045. Doi: 10.1126/science.1165243.

Musselwhite D. S., Dalton H. A., Kiefer W. S., and Treiman A. H., 2006. Experimental petrology of the basaltic shergottites Yamato-980459: Implications for the structure of the Martian mantle. *Meteoritics & Planetary Science* 41:1271-1290.

Mustard J. F., Murchie S. L., Pelkey S. M., Ehlmann B. L., Milliken R. E., Grant J. A., Bibring J.-P., Poulet F., Bishop J., Noe Dobrea E., Roach L., Seelos F., Arvidson R. E., Wiseman S., Green R., Hash C., Humm D., Malaret E., McGovern J. A., Seelos K., Clancy T., Clark R., Des Marais D., Izenberg N., Knudson A., Langevin Y., Martin T., McGuire P., Morris R., Robinson M., Roush T., Smith M., Swayze G., Taylor H., Titus T., and Wolff M., 2008. Hydrated silicate minerals on Mars observed by the Mars Reconnaissance Orbiter CRISM instrument. *Nature* 454:305-309. Doi:10.1038/nature07097.

Mustard J. F., Ehlmann B. L., Murchie S. L., Poulet F., Mangold N., Head J. W., Bibring J.-P., and Roach L. H., 2009. Composition, Morphology, and Stratigraphy of Noachian Crust around the Isidis basin. *Journal of Geophysical Research* 114:E00D12. Doi:10.1029/2009JE003349.

N

Nesbit H. W., and Wilson R. E., 1992. Recent chemical weathering of basalts. *American Journal of Science* 292:740-777.

Nna-Mvondo D., and Martinez-Frias J., 2007. Review komatiites: from Earth's geological settings to planetary and astrobiological contexts. *Earth Moon Planet* 100:157-179.

O

Orberger B., Rouchon V., Westall F., de Vries S. T., Pinti D. L., Wagner C., Wirth R., and Hashizume K., 2006. *Microfacies and origin of some Archean cherts (Pilbara, Australia)*, in Processes on the Early Earth, edited by Reimold, W. U., and R. L.Gibson, Geological Society of America Special Paper 405, 133–156, Geological Society of America, doi:10.1130/2006.2405(08).

P

Poilblanc R., and Crasnier F., 2006. *Spectroscopies infrarouge et Raman, Collection Grenoble Science*, EDP Science. ISBN 2-86883-744-1.

Pommier A., Gaillard F., and Pichavant M., 2010. Time-dependent changes of the electrical conductivity of basaltic melts with redox state. *Geochimica et Cosmochimica Acta* 74:1653–1671.

Posth N. R., Huelin S., Konhauser K. O., and Kappler A., 2010. Size, density and composition of cell–mineral aggregates formed during anoxygenic phototrophic Fe(II) oxidation: Impact on modern and ancient environments. *Geochimica et Cosmochimica Acta* 74:3476–3493. Doi:10.1016/j.gca.2010.02.036

Poulet F., Bibring J.-P., Mustard J. F., Gendrin A., Mangold N., Langevin Y., Arvidson R. E., Gondet B., Gomez C., and the Omega Team, 2005. Phyllosilicates on Mars and implications for early martian climate. *Nature* 438:623-627. Doi:10.1038/nature04274.

Poulet F., Mangold N., Loizeau D., Bibring J.-P., Langevin Y., Michalski J., and Gondet B., 2008. Abundance of minerals in the phyllosilicate-rich units on Mars. *Astronomy and Astrophysics*, 487:L41-L44. Doi: 10.1051/0004-6361:200810150.

Pullan D., 2008. *Analogue Studies for In Situ Surface Planetary Exploration*. PhD Thesis, University of Leicester.

R

Rasmussen B., Fletcher I. R., Brocks J. J., and Kilburn M. R., 2008. Reassessing the first appearance of eukaryotes and cyanobacteria. *Nature* 455:1101-1104. Doi:10.1038/nature07381.

Reyes D. P., and Christensen P. R., 1994. Evidence for Komatiite-type lavas on Mars from Phobos ISM data and other observations. *Geophysical Research Letters* 21:887-890.

Richards H. G., Cann J. R., and Jensenius J., 1989. Mineralogical zonation and Metasomatism of the Alteration Pipes of Cyprus Sulfide Deposits. *Economic Geology* 84:91-115.

Richards H. G., and Boyle J. F., 1986. Origin, alteration and mineralization of inter-lava metalliferous sediments of the Troodos ophiolite, Cyprus, in Gallagher M. J., Ixer R. A., Neary C. R., and Prichard H. M. eds., *Metallogeny of basic and ultrabasic rocks*. London, Inst. Mining Metallurgy:21-31.

Rieder R., Gellert R., Anderson, R. C., Brückner J., Clark B. C., Dreibus G., Economou T., Klingelhöfer G., Lugmair G. W., Ming D. W., Squyres S. W., d'Uston C., Wänke H.,Yen A., and Zipfel J., 2004. Chemistry of Rocks and Soils at Meridiani Planum from the Alpha Particle X-ray Spectrometer. *Science* 306:1746-1749. Doi: 10.1126/science.1104358.

Rosing M. T., 2011. Isua Supracrustal Belt. in *Encyclopedia of Astrobiology*, edited by Gargaud M., et al., vol. 2, pp 868-874.

Rubin A., Warren P., Greenwood J., Verish R., Leshin L., Hervig R., Clayton R., and Mayeda T., 2000. Los Angeles: The most differentiated basaltic Martian meteorite. *Geology* 28:1011-1015.

Ruff S., Farmer J. D., Calvin W. M., Herkenhoff K. E., Johnson J. R., Morris R. V., Rice M. S., Arvidson R. E., Bell III J. F., Christensen P. R., and Squyres S. W., 2011. Characteristics, distribution, origin, and siginificance of opaline silica observed by the Spirit rover in Gusev crater, Mars. *Journal of Geophysical Research* 116:E00F23. Doi:10.1029/2010JE003767.

Ruiz-Mirazo K., and Moreno A., 2011. Life. in Encyclopedia of Astrobiology, edited by Gargaud M., t al., vol. 2, pp 919-921.

Rull-Pérez F., and Martinez-Frias J., 2006. Raman Spectroscopy goes to Mars, *Spectroscopy Europe* 18:18-21.

Rusk B. G., Lowers, H. A., Reed M. H., 2008. Trace elements in hydrothermal quartz: Relationships to cathodoluminescent textures and insights into vein formation. *Geology* 36:547-550. Doi:10.1130/G24580A.1.

S

Schertl H.-P., Neuser R. D., Sobolev N. V., Shatsky V. S., 2004. UHP-metamorphic rocks from Dora Maira/Western Alps and Kokchetav/Kazakhstan: New insights using cathodoluminescence petrography. *Eur. J. Mineral*. 16:49-57.

Schmidt M. E., Schrader C. M., and McCoy T. J., 2011. How oxidized are the Gusev basalts? 42nd Lunar and Planetary Science Conference, abstract 2277.

Schulte M., Blake D., Hoehler T., and McCollom T., 2006. Serpentinization and its implications for life on the early Earth and Mars, *Astrobiology* 6:364-376. Doi:10.1089/ast.2006.6.364.

Skjelkvåle B., Amundsen H. E. F., O'Reilly S. Y., Griffin W. L., and Gjelsvik T., 1989. A primitive alakali basaltic stratovolcano and associated eruptive

centres, northwestern spitsbergen: Volcanology and tectonic significance. *Journal of Volcanology and Geothermal Research*. 37:1-19.

Soderblom L.A., and Bell III J.F., 2008. *Exploration of the Martian surface: 1992-2007*. The Martian Surface: Composition, Mineralogy, and Physical Properties, edited by Bell III J.F..Cambridge. Published by Cambridge University Press.

Song Y., and Yuan X., 2009. New Method for Identification of Blue Topaz—An Application of Cathodoluminescence(CL). *Journal of Geography and Geology* 1:13-19.

Southam G., and Westall F., 2007. *Geology, life and habitability*. in T. Spohn (Ed.), Treatise On Geophysics - Vol. 10 Planets and Moons, Elsevier, Amsterdam, 421-438.

Southam G., Rothschild L. J., and Westall F., 2007. The Geology and Habitability of Terrestrial Planets: Fundamental Requirements for Life. *Space Science Review* 129:7-34.

Stanley B. D., Hirschmann M. M., and Withers A. C., 2011. CO2 solubility in Martian basalts and Martian atmospheric evolution. *Geochimica et Cosmochimica Acta* 75:5987-6003. Doi:10.1016/j.gca.2011.07.027.

Steele, A., Fries M. D., Amundsen H. E. F., Mysen B. O., Fogel M. L., Schweizer M., and Boctor N. Z., 2007. Comprehensive imaging and Raman spectroscopy of carbonates globules from Martian meteorite ALH 84001 and a terrestrial analogue from Svalbard, *Meteoritics & Planetary Science*, 42:1549-1566.

Summons R. E., Amend J. P., Bish D., Buick R., Cody G. D., Des Marais D. J., Dromart G., Eigenbrode J. L., Knoll A. H., and Sumner D.Y., 2011. Preservation of martian organic and environmental records: final report of the Mars biosignature working group. Astrobiology 11:157-181. Squyres S. W., Arvidson R. E., Bell III J. F., Brückner J., Cabrol N. A., Calvin W., Carr M. H., Christensen P. R., Clark B. C., Crumpler L., Des Marais D. J., d'Uston C., Economou T., Farmer J., Farrand W., Folkner W., Golombek M., Gorevan S., Grant J. A., Greeley R., Grotzinger J., Haskin L., Herkenhoff K. E., Hviid S., Johnson J., Klingelhöfer G., Knoll A., Landis G., Lemmon M., Li R., Madsen M. B., Malin M. C., McLennan S. M., McSween H. Y., Ming D. W., Moersch J., Morris R. V., Parker T., Rice Jr. J. W., Richter L., Rieder R., Sims M., Smith M., Smith P., Soderblom L. A., Sullivan R., Wänke H., Wdowiak T., Wolff M., and Yen A., 2004. The Spirit Rover's Athena Science Investigation at Gusev Crater, Mars. *Science* 305:794-799. Doi: 10.1126/science.3050794.

Squyres S. W., Arvidson R. E., Ruff S., Gellert R., Morris R. V., Ming D. W., Crumpler L., Farmer J. D., Des Marais D. J., Yen A., McLennan S. M., Calvin W., Bell III J. F., Clark B. C., Wang A., McCoy T. J., Schmidt M. E., and de Souza Jr. P. A., 2008. Detection of Silica-Rich Deposits on Mars. *Science* 320:1063-1067. Doi: 10.1126/science.1155429.

T

Taylor G. J., McLennan S. M., McSween H. Y., Wyatt M. B., and Lentz R. C. F., 2008. *Implications of observed primary lithologies*. In The Martian Surface:

composition, Mineralogy, and Physical Properties, edited by Bell, J. F., pp. 501-518, Cambridge University Press.

Thomas R., Barbin V., Ramboz C., Thierkel L., Gille P., Leveille R., and Ramseyer K., 2009. Cathodoluminescence instrumentation for analysis of Martian sediments. *In Cathodoluminescence and its Application in the Planetary Science*, Ed. By Pagel M., Barbin V., Blanc P., and Ohnenstetter D., Springer Verlag. 111-126. doi:10.1007/978-3-540-87529-1_6.

Thomas-Keprta K. L., Clemett S. J., McKay D. S., Gibson E. K., and Wentworth S. J., 2009. Origins of magnetite nanocrystals in martian meteorite ALH84001, *Geochimica et Cosmochimica Acta.* 73-6631-6677.

Tice M., and Lowe D. R., 2004. Photosynthetic microbial mats in the 3416-Mys-old ocean, *Nature* 431:549-552.

Tice M., and Lowe D. R., 2006. The origin of carbonaceous matter in pre-3.0 Ga greenstone terrains: A review and new evidence from the 3.42 Ga Buck Reef Chert. *Earth-Science Reviews* 76:259-300.

Tice M., 2009. Environmental controls on photosynthetic microbial mat distribution and morphogenesis on a 3.42 Ga clastic- starved platform, *Astrobiology 9*:989-1000.

Tonarini S., Armienti P., d'Orazion M., Innocenti F., 2001. Subduction-like fuids in the genesis of Mt. Etna magmas:evidence from boron isotopes and fluid mobile elements, *Earth and Planetary Science Letters* 192:471-483.

Tosca N. J., McLennan, S. M., Lindsley, D. H., Schoonen, M. A. A., 2004. Acid-sulfate weathering of synthetic Martian basalt: The acid fog model revisited. *Journal of Geophysical Research* 109:E05003, Doi:10.1029/2003JE002218.

Treiman A. H., Amundsen H. E. F., Blake D. F., and Bunch T., 2002. Hydrothermal origin for carbonate globules in Martina meteorite ALH84001: terrestrial analogue from Spitsbergen (Norway), *Earth and Planetary Science Letters* 204:323-332.

V

Van Breeman N., 1980. Acid sulfate soils, in *Land Reclamation and Water Management, ILRI Publ*. 27:53– 57, Int. Inst. for Land Reclam. And Impr., Wegeningan, Netherlands.

Viles H., Ehlmann B., Wilson C. F., Cebula T., Page M., and Bourke M., 2010. Simulating weathering of basalt on Mars and Earth by thermal cycling. *Geophysical Research Letters* 37:L18201. doi: 10.1029/2010GL043522.

W

Wänke H. J., Bruckner G., Dreibus R., Rieder R., and Ryabchikov I., 2001. Chemical composition of rocks at the Pathfinder site. *Space Science Revue* 96:317–330.

Westall F., 1999.The nature of fossil bacteria: A guide to the search for extraterrestrial life. *Journal of Geophysical Research-Planets* 104 (E7):16437-16451.

Westall F., Steele A ., Toporski J., Walsh M., Allen C., Guidry S., McKay D., Gibson E., and Chafetz H., 2000. Polymeric substances and biofilms as biomarkers in terrestrial materials: Implications for extraterrestrial samples. *Journal of Geophysical Research-Planets* 105 (E10):24511-24527.

Westall F., and Folk R. L., 2003. Exogenous carbonaceous microstructures in Early Archaean cherts and BIFs from the Isua Greenstone Belt : implications for the search for life in ancient rocks. *Precambrian Research* 126:313-330.

Westall F., 2005. Early life on Earth and Analogies to Mars. In *Water on Mars and Life*, edited by Tokano T.: Advances in Astrobiology and Biogeophysics, Springer Berlin Heidelberg. pp.45-64. doi: 10.1007/b12040.

Westall F., de Vries S. T., Nijman W., Rouchon V., Orberger B., Pearson V., Watson J., Verchovsky A., Wright I., Rouzaud J. -N., Marchesini D., and Anne S., 2006a. The 3.466 Ga Kitty's Gap Chert, an Early Archaean microbial ecosystem In Processes on the Early Earth, edited by W.U. Reimold W.U. and R. Gibson. *Geol. Soc. Amer. Spec Pub.* 405:105-131.

Westall F., de Ronde, C. E. J., Southam G., Grassineau N., Colas M., Cockell C., and Lammer H., 2006b. Implications of a 3.472-3.333 Ga-old subaerial microbial mat from the Barberton greenstone belt, South Africa for the UV environmental conditions on the early Earth. *Phil. Trans. Roy. Soc. Lond*. Series B., 361:1857–1875.

Westall F., 2010. Early life : nature, distribution and evolution. In "Origins and evolution of life an astrobiological perspective" M. Gargaud, P. López-Garcìa, H. Martin (Eds.) Cambridge University Press, 391-413

Westall F., Foucher F., Cavalazzi B., de Vries S. T., Nijman W., Pearson V., Watson J., Verchovsky A., Wright I., Rouzaud J. –N., Marchesini D., and Anne S., 2011a. Volcaniclastic habitats for early life on Earth and Mars: A case study from ~ 3.5 Ga-old rocks from the Pilbara Australia. *Planetary and Space Science* 59:1093-1106. Doi:10.1016/j.pss.2010.09.006.

Westall F., Cavalazzi B., Lemelle L., Marrocchi Y., Rouzaud J. –N., Simionovici A., Salomé M., Mostefaoui S., Andreazza C., Foucher F., Toporski J., Jauss A., Thiel V., Southam G., MacLean L., Wirick S., Hofmann A., Meibom A., Robert F., and Défarge C., 2011b. Implications of in situ calcification for photosynthesis in a ~3.3 Ga-old microbial biofilm from the Barberton greenstone belt, South Africa. *Earth and Planetary Science Letters* 310:468-479. Doi:10.1016/j.epsl.2011.08.029.

Westall F., and Cavalazzi B., 2011. *Biosignatures in rocks.* In "Encyclopedia of Geobiology" Reitner Joachim, Thiel Volker (Eds.) XXVIII, 928 p., University of Göttingen, Berlin

Westall F., Loizeau D., Foucher F., Bost N., Bertrand M., Vago J. L., Kminek G., ans Zegers T., Scenarios for the search for life on a habitable Mars, in prep.

Wilson R. A. M., and Ingham F. T., 1959. *The geology of the Xeros-Troodos area, with an account of the mineral resources: Cyprus Geological Survey Department*. Memoire 1, 184 p.

Z

Zipfel J., Anderson R., Brückner J., Clark B. C., Dreibus. G., Economou T., Gellert R., Klingelhöfer G., Lugmair G. W., Ming D., Reider R., Squyres S. W., d'Uston C., Wänke H, and Yen A., 2004. APXS analyses of bounce rock - The first shergottites on Mars. *Meteoritics & Planetary Science* 39 Suppl.:A118.

Scientific production

Publications:

- "Synthesis of a spinifex-textured Basalt as an analogue to Gusev crater basalts, Mars."
N. Bost, F. Westall, F. Gaillard, C. Ramboz, and F. Foucher
Meteoritics & Planetary Science, Vol. 47, pp. 820-831.
doi:10.1111/j.1945-5100.2012.01355.x.

- "Missions to Mars: Characterization of Mars analogue rocks for the International Space Analogue Rockstore (ISAR)"
N. Bost, F. Westall, C. Ramboz, F. Foucher, D. Pullan, G. Klingelhöfer, I. Fleischer, and J. L. Vago
Planetary and Space Science, submitted fro publication.

- "The Skouriotissa mine: A new terrestrial analogue for mineral formation on early Mars"
N. Bost, C. Ramboz, F. Westall, C. Fontaine, F. Foucher and C. Pilorget
Geology, submitted for publication.

Oral communications:

- "The International Space Analogue Rock Store (ISAR): A key tool for future planetary exploration."

N. Bost, F. Westall, C. Ramboz, F. Foucher, and the ISAR Team
EGU General Assembly, Vienne, Austria, April 2012.

- "Hydrothermal, deuteric and acidic basalt alteration at the *Skouriotissa* Mine, Cyprus: relevance for Mars."
N. Bost, F. Westall, C. Ramboz, C. Fontaine, A. Meunier, and F. Foucher
EGU General Assembly, Vienne, Austria, April 2012.

- "New Synthetic Martian Basalts from Spirit data, Gusev crater"
N. Bost, F. Westall, F. Gaillard, C. Ramboz, and F. Foucher
EPSC-DPS joint meeting, Nantes, France, October 2011.

- "The European Space Analogue Rock Collection (ESAR) at the OSUC-Orleans for *in situ* planetary missions"
F.Westall, D. Pullan, N. Bost, C. Ramboz, *et al.*
EPSC-DPS joint meeting, Nantes, France, October 2011.

- "ExoMars: Mars analogue rocks in the European Space Analogue Rockstore (ESAR)."
N. Bost, F. Westall, C. Ramboz, F. Foucher, and the ESAR Team
EGU General Assembly, Vienne, Austria, April 2011.

- "ExoMars et La lithothèque Orléanaise: une banque de roches analogues pour des missions in-situ."
N. Bost, F. Westall, C. Ramboz, F. Foucher, *et al*..,
Reunion des Sciences de la Terre 2010, Bordeaux, France, October 2010.

- "La lithothèque Orléanaise: une banque de roches analogues pour des missions in-situ."
N. Bost, F. Westall, C. Ramboz, F. Foucher, *et al*..,
Congrès de la Société Francaise d'Exobiologie 2010, Biarritz, France, September 2010.

- "ExoMars: Mars analogue rocks in the European lithotheque at Orleans."
N. Bost, F. Westall, C. Ramboz, F. Foucher, *et al.*
Archaemat Workshop 2010, Barberton, South Africa, August 2010.

- "Cathodoluminescence imagery as a complementary tool for developing Martian geology and searching for early life on Mars."
C. Ramboz, Y. Rubert, N. Bost, L. Thirkell, V. Barbin, P. Gautret, and F. Westall
Archaemat Workshop 2010, Barberton, South Africa, August 2010.

- "ExoMars: Mars analogue rocks in the European lithotheque at Orleans"
N. Bost, F. Westall, C. Ramboz, F. Foucher, *et al.*
Cospar 2010, Bremen, Germany, July 2010.

Posters:

- "Cathodoluminescence: an imaging technique for the search of extraterrestrial life."
C. Ramboz, Y. Rubert, N. Bost, F. Westall, and C. Lerouge
EGU General Assembly, Vienne, Austria, April 2012.

- "The European Space Analogue Rockstore: a key tool for supporting in-situ missions on Mars."
N. Bost, F. Westall, C. Ramboz, F. Foucher, *et al.*
Exploring Mars Habitability Conference 2011, Lisboa, Portugal, June 2011.

- "Raman and cathodoluminescence imagery: complementary tools for Martian Geology and the search for Early Life on Mars."
N. Bost, F. Westall, C. Ramboz, F. Foucher, *et al.*
EGU General Assembly, Vienne, Austria, April 2011.

- "2018 MAX-C/ExoMars mission: the Orleans mars-analogue rock collection for instrument testing."
N. Bost, F. Westall, C. Ramboz, F. Foucher, *et al.*
Lunar and Planetary Science Conference 42nd, The Woodlands, Texas, USA, March 2011.

- "Mars exobiology mission 2018 (MAX-C/ExoMars) and the mars analogue rock collection at the OSUC Orleans."

F. Westall, D. Pullan, N. Bost, C. Ramboz, F. Foucher, *et al.*
Lunar and Planetary Science Conference 42nd, The Woodlands, Texas, USA, March 2011.

- "The Orléans-Lithothèque – an analogue rockstore for *in situ* missions."
N. Bost, F. Westall, C. Ramboz, and the Orléans-Lithothèque Team
EGU General Assembly, Vienne, Austria, May 2010.

- "Early archaean shallow water sediments as analogues for Noachian sediments on Mars"

N. Bost, F. Westall, C. Ramboz, and M. Viso
First International conference on Mars Sedimentology and Stratigraphy, El Paso, Texas, USA, April 2010.

- "The Orléans lithothèque: a Mars analogue rock store and data base for space missions - and the key role of Raman spectroscopy."
N. Bost, F. Foucher, F. Westall, C. Ramboz, and the Orléans-Lithothèque Team
Workshop Mars III, Les Houches, France, March/April 2010.

Other works:
Publications:

- "Scenarios for the search for life on a habitable Mars"
F. Westall, D. Loizeau, F. Foucher, N. Bost, M. Bertrand, J. L. Vago, G. Kminek, and T. Zegers
in preparation

- "Effect of grain size distribution on Raman analyses: consequences for the future missions to Mars"
F. Foucher, G. Lopez-Reyes, N. Bost, F. Rull-Perez, P. Rüßmann, and F. Westall
Submitted to *Journal of Raman Spectroscopy*.

Poster:

- "Effect of the crushing process on Raman analyses: consequences for the Mars 2018 mission."

F. Foucher, G. López Reyes, N. Bost, F. Rull, P. Rüßmann, and F. Westall
EGU General Assembly, Vienne, Austria, April 2012.

- "Effect of grain size distribution on Raman analyses: consequences for ExoMars-C measurements."
F. Foucher, N. Bost, P. Rüßman, and F. Westall, F.
EPSC-DPS joint meeting, Nantes, France, October 2011

Appendices

Appendice A
The Cathodoluminescence Instrument

This annex describes the development of a cathodoluminescence (CL) instrument to which I participated during my thesis. My contribution was the continuation of two Research and Technological (R&T projects (2004-2006 then 2007-2009) financed by CNES in Orléans (at the LPC2E under the responsibility of R. Thomas firstly, then at ISTO coordinated by C. Ramboz). They were mainly focused on developing the application of cathodoluminescence in the search for life on Mars. The main part of this study was the optimization of the instrument and imaging tests.

A.1. Physical principle.

Cathodoluminescence is the visible optical response of a material subjected to an electronic bombardment (Fig. A.1). The most common example is the cathode ray tube of television.

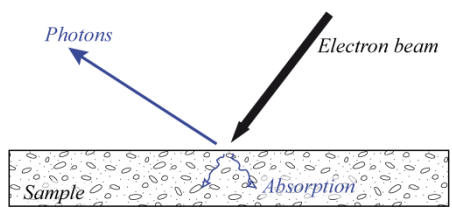

Figure A.1. Scheme of the cathodoluminescence phenomenon.

Figure A.1: Schéma de principe de la cathodoluminescence.

This technique is used in geosciences for studying mineral growth (e.g. in quartz, *Rusk et al., 2008*) and for detecting trace elements and mineral defects. It is thus very useful for a deeper understanding of rock formation.

A.2 Instrument optimization

When I started my work, the conventional cold cathode CL apparatus was not well isolated from mechanical vibrations induced by other instruments (e.g. computer fan). This noise was enhanced by the significant overhang of the assembly (Fig. A.2a). My first objective was thus to improve the stability of the system. An anti-vibration mat was placed below the system (in black in photo Fig. A.2b), and the associated monitoring system were isolated (e.g. the spectrometer was fixed on the wall). The mount of the analysis chamber and the optical device were improved using aluminum rods in order to increase its rigidity.

►Figure A.2: The cathodoluminescence system such as it was specifically developed at the end of the first R&T CNES "electron lamp" project (2004-2006) (a)9 and in April 2010 at the end of the second "electron lamp" CNES project (b) . Note in (b) the simplified optical mount. The system is equipped with a turret with 3 objectives x4, x10 and x20 and with a cooled Retiga 4000 camera. The plate is centered on a flat surface and illuminated by an optical fiber integrated below the analysis chamber. The Zeiss MM1 spectrometer is coupled to the microscope via an optical fiber and it is placed on a dedicated mount to the right of the camera. The instrument is placed on an anti-vibration mat (black in photo b).

►Figure A.2: *Appareil de cathodoluminescence développé à l'issu des 2 R&T CNES « Lampe à électrons 2004-2010 », a- en septembre 2009 et b- en avril 2010. En b, on notera la présence du statif optique simplifié, comportant une tourelle équipée de 3 objectifs x4, x10 et x20 et d' une caméra refroidie Retiga 4000. La platine est centrée sur un support plan et éclairée par une fibre optique intégrée sous la chambre d'analyse. Le spectromètre Zeiss MM1 avec sa fibre optique sont placés sur un support dédié à droite de la camera, l'alimentation du spectromètre est fixée au mur (en haut à gauche sur b.). L'instrument est posé sur un tapis anti-vibrations (en noir sur la photo b.).*

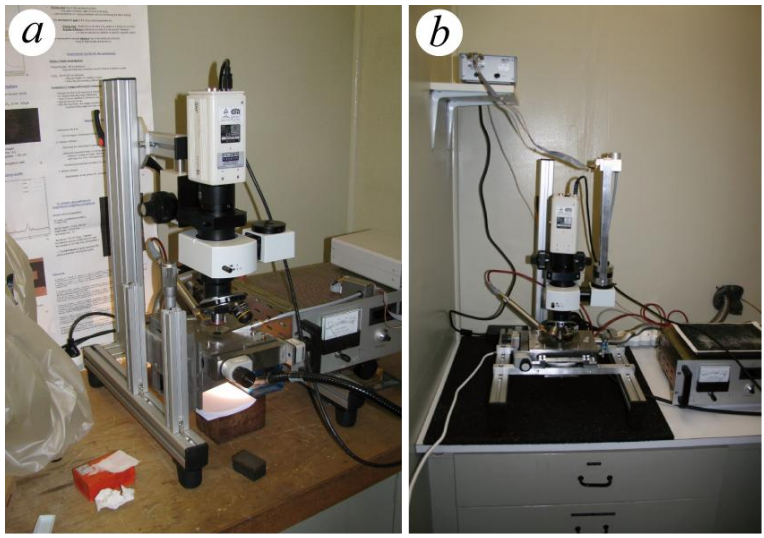

The CL chamber is illuminated uniformly from below using an optical fiber allowing observation of the sample in transmitted light. A Retiga 4000 CCD camera, cooled by Pelletier effect, was bought thanks to an extra funding from the CNES. This low-noise CCD camera, which can acquire images with exposure times of up to 17 mn,replaced the JVC KY-F75U tri-CCD camera that did not allow longer exposure times than 20 seconds. Finally, a specific sample holder for standard thin sections was made.

A.3 Cathodoluminescence imagery test

The instrument was tested using standards and ISAR samples. Here I present the results obtained on a micaschist thin section from La Sioule Valley, France, on a topaz lent by Prof. J. Götze from Germany and already studied by *Götze et al. (2000)* and, finally on two ISAR samples originating from Svalbard (see Chapter 3). Microscopic observations were carried out on thin sections.

A.3.1 Kyanit-garnet micaschist from La Sioule Valley (France)

The major rock-forming phases can usually be identified by optical observation in transmitted light microscopy (for identification of the various silicates phases in the micaschist, see *Do Couto, 2009*). However, whereas

phlogopite (Ph) can easily be identified (in brown in Fig. A.3a), the other transparent minerals are difficult to distinguish and to identify unambiguously. Some of these phases are less transparent and were cleaved. On the other hand, the CL image reveals that there are three sorts of transparent minerals (Fig. A.3b). Kyanite can be identified by its bright red luminescence and corresponds to the cleaved white mineral observed in optical microscopy. The more transparent areas consist of two phases: orthoclase with bright blue luminescence and non-luminescent quartz. The comparison between Figures A.3d and A.3e (it shows CL images of the same area acquired with both experimental setups) provides evidence of the CL intensity gain provided by the optimized apparatus, including the low-noise cooled camera. Finally, the CL image of kyanite obtained with our laboratory setup is of better quality than the images taken by *Schertl et al. (2004)* in a SEM chamber (Figs. A.3b and A3.e, respectively).

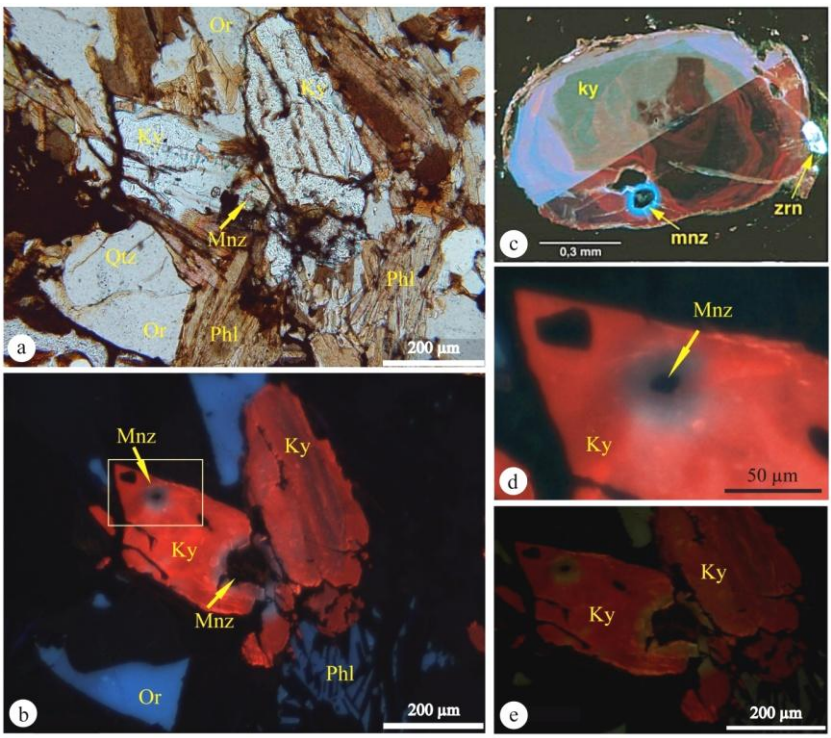

◄Figure A.3: Photomicrographs of a thin section of a mica-garnet-kyanite micaschist from La Sioule Valley, France. a- Optical micrograph in transmitted light. b- CL image of the same area as in (a). (c-to d) Focused CL image of a kyanite crystal with a monazite inclusion. (c) CL image taken in a SEM chamber by *Schertl et al. (2004)*. (d) CL image taken with our optimized cold cathode CL apparatus(e) Same as (e) with our equipment, before optimization. Ky = kyanite, Phl = phlogopite, Qtz = quartz, Or = orthoclase and Mnz = monazite. Analysis conditions (b, d, e): ~15 kV, ~110 µA, PAr = 50 mTorr.

◄*Figure A.3 : Phots o d'une lame mince de micaschiste à grenat-disthène (série de la Sioule). a- lumière naturelle. b- vue en cathodoluminescence de la même zone que (a). (c- e) images en cathodoluminescence d'un cristal de disthène avec monazite en inclusion. On peut comparer une image de CL sur MEB d'après Schertl et al. (2004 (c),) avec l'image de CL acquise avec notre appareil de CL à cathode froide optimisé (d) (la chambre est la Cathodyne commercialisée par OPEA).et enfin (e) avec notre équpement non optimisé iLégende : Ky=disthène, Phl=phlogopite, Qtz= quartz, Or= orthoclase, Mnz=monazite. Conditions d'analyse (b,d,e) : ~15 kV, ~ 110 µA,* P_{Ar}*=50 mTorr.*

Figure A.3 also shows the presence of a small accessory monazite mineral, a Th-U-bearing phosphate, rich in rare earth elements (here Ce)). Although the monazite itself is non luminescent, it is indirectly revealed on the CL image by crystal lattice defects that are created in the disthène crystal by the radioactive decay of Th and U, yielding the bluish pleochroïc halo (provoked

A.3.2. Topaz from Euba

This sample from Euba, Germany, was provided by Prof. Jens Götze. It consists of euhedral crystals of topaz ($Al_2SiO_4(F,OH)_2$). Figure A.4a shows an optical view of the three crystals (Fig. A.4-a) and the associated Raman map of the upper crystal (Fig. A.4-b). The CL image (c) was obtained and published by *Götze et al., 2000*, and image (d) was obtained using the instrument developed in Orléans. The green grains observed by CL could be a dickite ($Al_2Si_2O_5(OH)_4$) as suggested by Raman spectroscopy. Feldspars are also associated in the paragenesis.

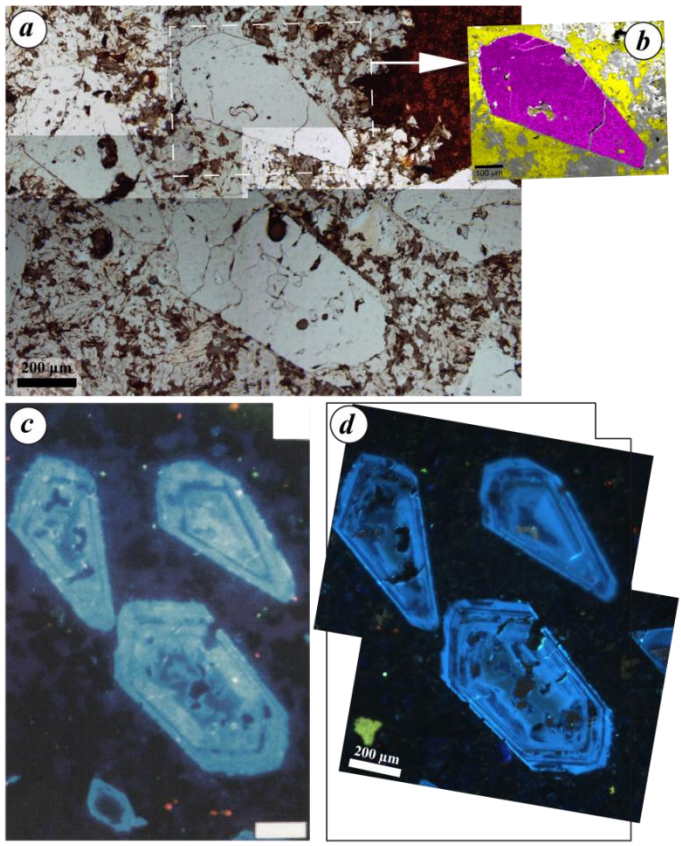

Figure A.4: Photomicrographs of Topaz monocrystals from Euba, Germany. a- natural light. b- Raman mapping of the top topaz grain with in pink topaz, in yellow quartz, and in grey araldite. c- CL image of the three topaz grains (in blue) from *Götze et al., (2000)*. d- CL image of the same three topaz grains (in blue) with our equipment. The green grains may be dickite (suggested by Raman measurement). Analysis conditions (d): ~ 15 kV, ~ 70 µA, PAr = 50 mTorr, Obj. : x 20, 8.17 seconds exposure.

Figure A.4: Microphotographies de monocristaux de topaze provenant d'Euba, Allemagne. a- lumière naturelle; b- cartographie Raman du grain de topaze en haut, avec la topaze en rose, le quartz en jaune et l'araldite en gris. c- Image CL des trois grains de topaze (en bleu) d'après Götze et al. (2000). d- Image CL des mêmes grains de topaze (en bleu) avec notre instrument. Les grains verts sont certainement de la dickite (d'après les analyses Raman). Conditions d'analyses (d) ~ 15 kV, ~ 70 µA, PAr = 50 mTorr, Obj. : x 20, 8.17 secondes de temps de pause.

A.3.3 Basalt from Svalbard, ISAR samples 09SV15 and 09SV05.

This ultramafic basalt formed during the eruption of the Sverrefjell volcano, northeast of Spitsbergen, 60,000 years ago. It contains 20% in volume of enclaves of mantle (dunite) and crustal rocks (gneisses and granulites). Many carbonate globules permeate the rock, either the basalt or its enclaves. For more details see Chapter III, *Sklelkvåle et al. (1989)* and *Treiman et al. (2002)*.

The CL image reveals the presence of numerous microliths of oligoclase (feldpath Ca-Na) in a non luminescent vitreous matrix (Fig. A.5). Vesicles contained in the glass and filled with glue are have a very subtle light grey luminescence (white arrows in Fig. A.5). Many luminescent orange spots in the glass and phenocrysts are secondary carbonates associated with plagioclase; carbonate concretions are observed on the surface of the sample (Figs. A.5b and A.5c).

The analyses carried out on the different samples have validated the system performance and allow to consider it as operational for low to high luminescence imagery. This is all the more true as the presented microphotographs were acquired with exposure time <20s, ~ 30 000 time shorter than the maximum exposure time compatible with our camera.

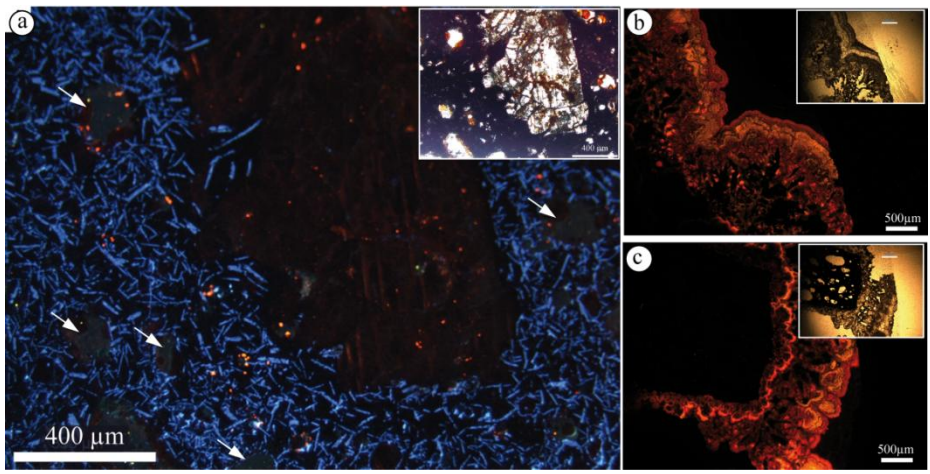

◄Figure A.5: Cathodoluminescence photomicrographs of a thin section of basalt from the Sverrefjell stratovolcano, Svalbard, Norway. a- The CL image reveals the presence of numerous microliths of feldspar in blue located in the basaltic glass. The plagioclase phenocryst visible in natural light (see inset) is not luminescent. The many orange points suggest a contamination of the basalt by carbonates. Analysis conditions: 12.4 kV, 130 µA, PAr = 50 mTorr. b- and c- CL images of carbonate concretions precipitated on the surface of the sample (see the optical image in insert). Analysis conditions: 10.2 kV, 120 uA, PAr = 50 mTorr.

◄*Figure A.5 : Images en cathodoluminescence d'un échantillon de basalte provenant du stratovolcan Sverrefjell sur l'île de Svalbard (Norvège). a- L'image de CL révèle la présence de nombreux microlithes de feldspath potassique qui luminescent en bleu dans le verre basaltique vésiculé. Le phénocristal de plagioclase visible en lumière naturelle (voir insert) est non luminescent. Les nombreux points fortement luminescents en orange traduisent sans doute une contamination du basalte par des carbonates. Conditions d'analyse : 12.4 kV, 130 µA, P_{Ar}=50 mTorr. b- et c- : Microphotographie de CL des concrétions carbonatées précipitées sur la surface de l'échantillon de basalte (vue optique en insert). Conditions d'analyses: 10,2 kV, 120 µA, P_{Ar}=50 mTorr.*

A.4 Cathodoluminescence spectrometry

Spectral analysis of the luminescence of minerals is a necessary complement to tCL imaging. A Zeiss MMS 1 spectrometer and its associated optical system were coupled to the CL equipment via the microscope. A mirror is put on the optical axis in order to deflect 80% of the light emitted by the sample onto the lens of the optical fiber driving the collected light to the spectrometer (Fig. A.2b). The Retiga 4000 camera and the fiber-spectrometer can be interchanged in order to collect the total light emitted by the sample. I have made several tests during my thesis, in particular, on the large hexagonal topaz crystal from Euba in Fig. A.6a. The obtained spectrum is in good accordance with a previous study on artificially tinted topaz jewel, showing a peak around 450-500 nm (Fig. A.6b, after *Song and Yuan, 2009*).

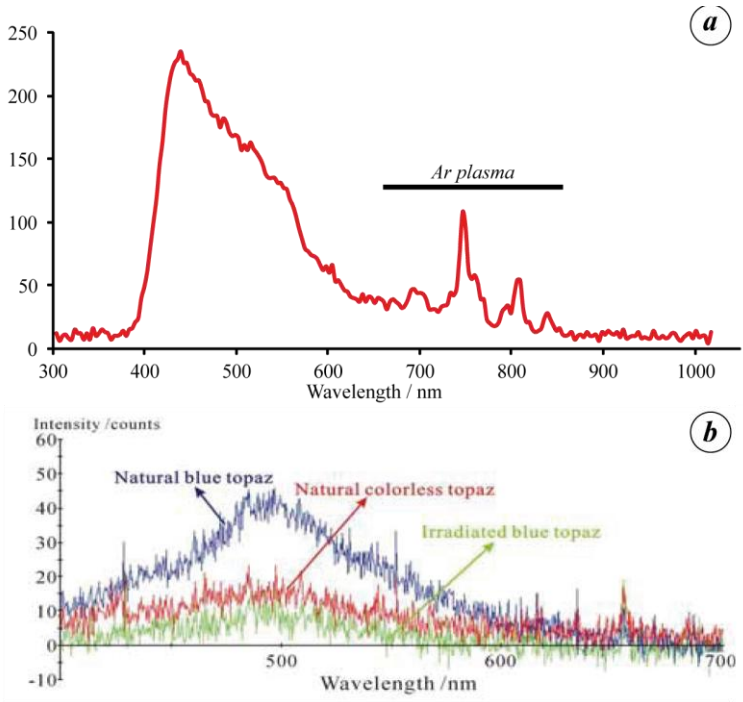

Figure A.6: a- CL spectrum of the large hexagonal crystal of topaz from Euba obtained with the Zeiss MMS1 spectrometer. Note the argon plasma emission peaks between 700 nm and 850 nm. (Integration time: 6 seconds). b- CL spectra characteristics of natural blue, natural colorless and irradiated topaz crystals (after *Song and Yuan, 2009*).

Figure A.6: a- Spectres de CL du grand cristal hexagonal de topaze d'Euba obtenue avec le spectromètre Zeiss MMS1. Notez les pics de diffusion du plasma d'argon entre 700 nm et 850 nm (temps d'intégration de 6 secondes). b- Spectres de CL caractéristiques de topazes naturelles bleues, incolores et irradiées (d'après Song and Yuan, 2009).

I tried to test the spectrometer with others samples, such as cherts. However, no spectrum was obtained with the Zeiss MM1 spectrometer because of an imperfect coupling of the spectrometer with the microscope.

A.5. Conclusions

During this thesis, I have participated in the development and optimization of the cathodoluminescence system on different types of rocks. CL imagery is a very helpful technique for detecting microstructures in rocks: fractures, alteration phases, vesicles, accessory minerals, irradiation haloes etc…. For instance, the microliths in the basalt from Svalbard revealed by CL are difficult to detect with optical microscopy. The observation of monazite *in situ* in space missions (suche as in the micaschist from La Sioule) could be very interesting for a Sample Return Mission since this mineral rich in uranium and thorium is adequate for dating. Finally, CL could be relevant for the search for life (e.g. specific mineralogy or traces elements, *Barbin et al., 1999*). According to *Thomas et al., 2009*, it could be a useful complement for characterizing rock mineralogy during exploration of the Martian surface. In particular, it can help to the search for evidence of past biological activity and the identification of ancient geochemical conditions.

Appendice B
Example of detailed samples characterization for the ISAR: samples from Svalbard

In this annex, I present the full characterization of a volcanic sample (09SV15) associated with a carbonate cemented breccia- (09SV05). These samples have been chosen as examples to describe the typical geological and mineralogical information stored in the ISAR database. A résumé of these data can be downloaded as a pdf file directly from the website (www.isar.cnrs-orleans.fr).

B.1. Geological Background

The two samples 09SV15 and 09SV05 were obtained from the quaternary strato-volcano (≈100 Ky) Sverrefjell (N79°26,255; E013°20,486) located on the island of Svarlbard, north of Norway, during the NASA-AMASE[14] mission (*Artic Mars Analog Svalbard Expedition*). The Sverrefjell formed by off-ridge alkali basaltic volcanism induced by the opening of the Artic Basin and the Greenland Sea (*Skelkvåle et al., 1989*). Volcanoes are aligned along the Bockfjord, parallel to an important fault which defines the contact between a major Devonian (416 to 374.5 My) graben, filled with

[14] http://www.nasa.gov/mission_pages/mars/news/amase; http://astrobiology.nasa.gov/articles/nasa-participates-in-the-arctic-mars-analogue-svalbard-expedition-amase-2009/

Devonian red-beds (molasse), and Caledonian basement rocks of the Heckla Hoek formation (Fig. B.1a). Quaternary volcanism is subactive and associated with hot springs.

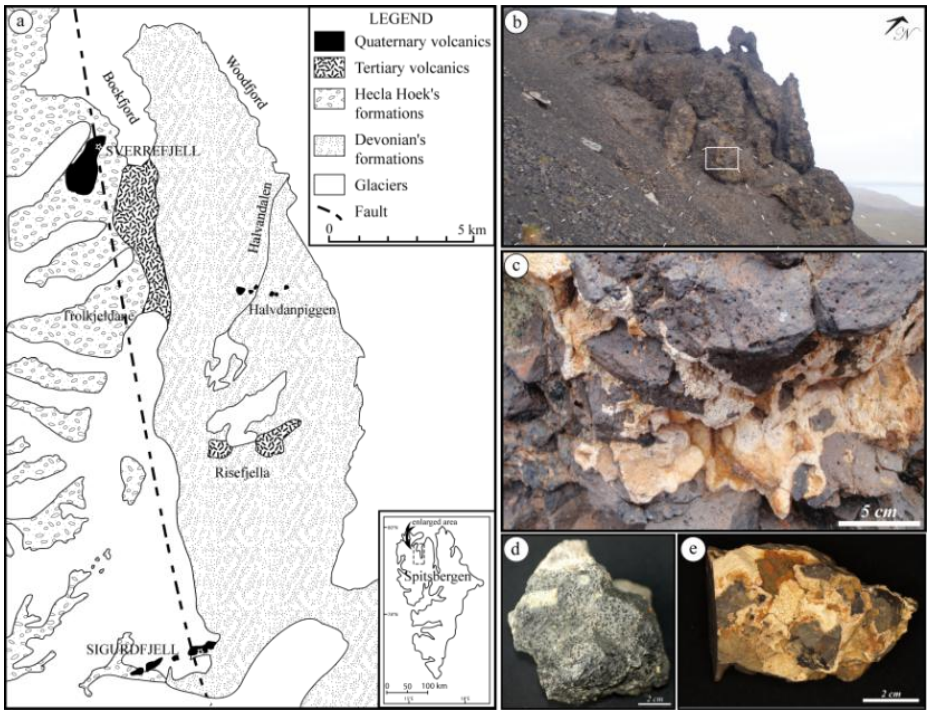

Figure B.1: a- Simplified geological map of the N-W of the Svalbard Island along the quaternary volcanoes Sverrefjell and Sigurdfjell; modified after *Skelkvåle et al., 1989*. b- Outcrop in the north-east of the Sverrefjell volcano showing basalt associated with breccias and carbonates. c- Detail of the outcrop showing the relationship between basalt and carbonates. d- The basaltic sample 09SV15. e- The carbonate sample 09SV05.

Figure B.1: a- Carte géologique simplifiée du nord-ouest de l'ile de Svalbard (Spitzberg) le long des volcans Quaternaires Sverrefjell et Sigurdfjell, modifié d'après Skelkvåle et al., 1989. b- Affleurement au nord-est du volcan Sverrefjell avec des basaltes associés à des brèches et des carbonates. c- Détail de l'affleurement montrant les relations entre le basalte et les carbonates. d- Vue de l'échantillon 09SV15. e- Vue de l'échantillon de carbonates 09SV05.

- 09SV15 is a primitive and ultramafic basalt (Fig. B.1b-d) containing approximately 20% of xenoliths (mantle dunites, sample 09SV02, and some gneissic crustal elements).

- 09SV05 is a zoned carbonate (Fig. B.1c,e) that was deposited by hydrothermal exhalation or possibly by aqueous alteration during eruption under an ice cap (*Steele et al., 2007; Amundsen et al., 2011*).

B.2 : 09SV15 analysis

B.2.1: Global description

09SV15 is a massive and highly vesicular basalt (fig. B.1d), with vesicle sizes ranging between 1 and 5 mm. The outer surface of the hand specimen shows some brownish grey bleaching, indicating very minor weathering. The fresh basalt surface is dark grey. Dunite xenoliths up to 2 cm in size and some macroscopic olivine grains (0.5-1 mm size) can be observed (Fig. B.1b-d). The mineralogy of the basalt is olivine (Fo_{90}) occurring as phenocrysts with pyroxenes ($Mg\#_{57}$) associated with plagioclase microlites and minor glass. The basalt is brechified and cemented by different carbonates layers and globules (09SV05).

B.2.2: Optical microscopy and cathodoluminescence

Optical and cathodoluminescence observations permit identification of the typical basaltic mineralogy: olivine (Fo_{90}) occurring as phenocrysts, pyroxenes ($Mg_{\#57}$) associated with plagioclase microlites, and minor glass (Fig. B.2). Secondary minerals include amphibole, oxides and spinels. This sample has the particularity of containing quartz grains, possibly a xenolithic contribution. The CL image reveals the presence of numerous microliths of oligoclase (feldpath Ca-Na) in a non luminescent vitreous matrix (Fig. B.2). Vesicles contained in the glass and filled with glue show very subtle light grey luminescence (white arrows in Fig. B.2). Many orange luminescent spots in the glass and phenocrysts are secondary carbonates associated with plagioclase; carbonate concretions are observed at the surface of the sample (09SV05).

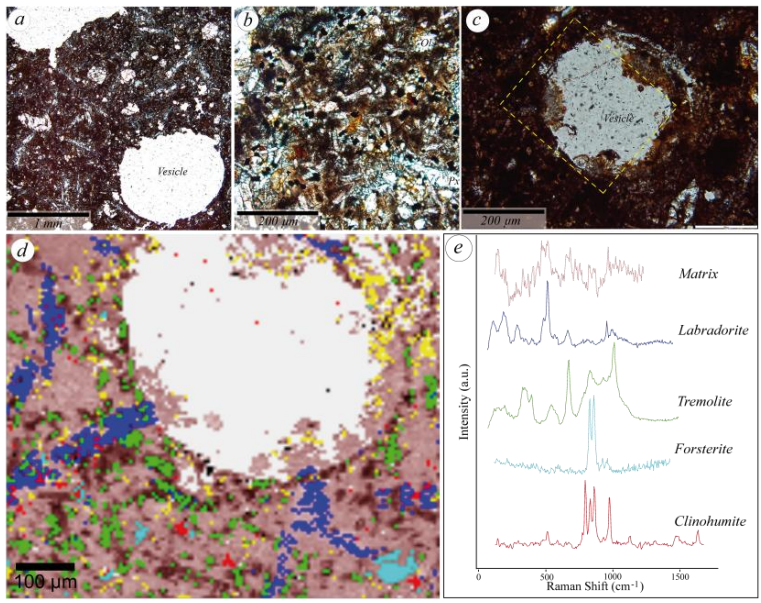

Figure B.2: a- Optical view of sample 09SV15 in thin section. Olivine and pyroxene crystals are associated with elongated plagioclases. b- Detailed optical view of sample 09SV15 showing the microliths associated with small oxide in a glassy matrix. c- Optical view showing in yellow field imaged by Raman in (d). d- Raman map of the yellow square in (c), with the matrix in salmon, labradorite in blue, tremolite in green: tremolite, forsterite in light blue, and clinohumite in red. e- Raman spectrum used for making the Raman map in (d).

Figure B.2: a-Image optique de l'échantillon 09SV15 en lame mince. Les cristaux d'olivine et pyroxène sont visibles, associés avec des plagioclases alongés. b-Détail de l'échantillon 09SV15, montrant des microlithes associés avec des petits oxydes dans un verre. c- Vue optique de la zone cartographiée en Raman en (d). d- Cartographie Raman du carré jaune sur (c), avec en saumon: matrice, bleu: labradorite, vert: trémolite, bleu ciel: forsterite et rouge: clinohumite. c- spectres Raman utilisés pour faire la carte (d).

B.2.3: Electron microprobe

The chemical composition obtained by microprobe measurements of these three major silicate phases is given in Table B.1.

Mineral	Elements wt.%											
	K_2O	SiO_2	FeO	CaO	Na_2O	TiO2	Al_2O_3	MnO	Cr_2O_3	MgO	Cl	P_2O_5
Olivine	0.028	40.071	15.094	0.242	0.003	0.003	0.06	0.08	0.092	46.088	0	0.105
Pyroxene	4.667	49.478	6.984	4.628	7.19	2.198	19.025	0.182	0.026	2.225	0.205	1.015
Plagioclase	0.088	42.159	8.459	22.751	0.627	5.286	9.87	0.128	0.056	10.744	0	0.330

Table B.1: Elemental electron microprobe analyses of major minerals in the sample 09SV15. The measurements were obtained with the Cameca SX50 from ISTO-BRGM at Orléans.

Tableau B.1 : Analyses élémentaires réalisées sur les minéraux majeurs de l'échantillon 09SV15 à l'aide de la microsonde électronique Cameca SX50 de l'ISTO-BRGM, Orléans.

B.2.3: Raman spectroscopy

The average Raman spectra of the different phases were obtained from mapping the thin section (Fig. B.2). The mapping was made around a vesicle (in grey), where elongated feldspars (labradorite) associated with globular olivine (forsterite) and small spinels (clinohumite) in a basaltic glass with microlites of felspath (matrix in salmon) were observed. All the major phases were detected: augite (pyroxene), forsterite (olivine), and labradorite (feldspath). Minor magnesiochromite (spinel) and quartz phases were also observed, the latter probably associated with a xenolithic contribution. Raman spectra are also providing on powder samples of the rock. The spectra of each of the minerals identified are shown in Fig. B.3. Mineral identification by Raman spectroscopy documents the same minerals as identified by Raman mapping with some variation; the tremolite spectrum may be an augite and the clinohumite is a magnesiochromite. Tremolite and ugite have similar spectra but the geological context favours augite.

B.2.4: IR spectroscopy

The IR analyses were carried out on pellet made of 0,506 mg of powdered sample mixed with KBr and pressed at 8 tons. The spectral acquisition was made in transmission. The two major elements in the basalt (Fig. B.4a) were detected with this method: olivine (in large dotted line, Fig. B.4a) and pigeonite (in dotted line, Fig. B.4a). The IR pigeonite identification can be correlated to the augite identification made by Raman spectroscopy and microprobe elemental analysis. The small peak at 749.26 cm^{-1} is labradorite.

B.2.5: Mössbauer analyses

Mössbauer analyses were made on both the weathered (in grey in Fig. B.5c,d) and unweathered (in black on Fig. B.5c,d) surfaces of the basalt.The two analyses are very similar and show olivine and pyroxenes, thus confirming the lack of significant weathering of the sample. However the intensity of the olivine peak from the inner, cut rock surface is greater than that of the surface, indicating that the olivine on surface is more altered (Fig. B.5c). The "npOx" correspond to microcrystalline oxides.

B.2.6: XRD analyses

The XRD analyses show the major mineral phases: forsterite, augite, nepheline and anorthite (Fig. B.5e). Identification of anorthite is in good accordance with the detection of labradorite by Raman spectroscopy since these two minerals are in the plagioclase-feldspar solid solution. The presence of nepheline, a feldspathoid, is intriguing because it indicates a lack of SiO_2 in the melt, although Raman and microprobe analysis show the presence of quartz grains. The coexistence of these two phases is unlikely, although *Skjelkåle et al. (1989)* also observed this mineral in the basalt (xenocrystals).

B.3: 09SV05 analysis

B.3.1: Global description

The 09SV05 carbonate globules are compositionally layered and were compared by *Treiman et al. (2002)* to the Martian meteorite ALH 84001. The first layer closest to the host rock is composed by a fine size carbonate grain with carbonated cement. The second level is composed of clusters of magnetite and dolomite with a nebulitic, porous texture suggesting a rapid crystallization. The penultimate layer is composed of large globules of dolomite (in dark brown) included in a fine radiate-fibrous matrix of dolomite and magnesite. The external layer of the crust consists of a massive layer of radiating magnesite crystals. This layer is sometimes weathered in the surface.

B.3.2: Optical microscopy and cathodoluminescence

Optical and cathodoluminescence (CL) observations document different carbonate phases: the external rings are formed first by magnesite and secondly by dolomite (Fig. B.3). The absence of luminescence in the CL image demonstrates the lack of Mn and Fe. CL confirms the nebulitic, porous texture of the small carbonates grains in the second layer. These carbonates contain Mn (demonstrated by orange-red colour in CL associated to the luminance of the ion Mn^{2+} in the carbonate crystalline lattice, *Haberman et al., 2000*). The interface between the carbonates and the basalt is outlined by the presence of small pyrite grains. Texture and structure are clearly observed in CL and the different layers are distinguishable except the external layer that does not contain luminescent elements.

B.3.4: Electron microprobe

The electron microprobe analyses demonstrate that the highly luminescent spots observed in CL are associated with a high content of Mg and Mn.

B.3.5 Raman spectroscopy

Raman spectroscopy confirms the different mineral phases: magnesite, dolomite, ankerite and siderite (Fig. B.4). Raman mapping carried out on the thin section documents the laminated nature of the different carbonates in the crust (Fig. B.3). A very fine zonation of dolomite in the magnesite layers is observed. This weak variation corresponds to a change of chemical composition of the environment.

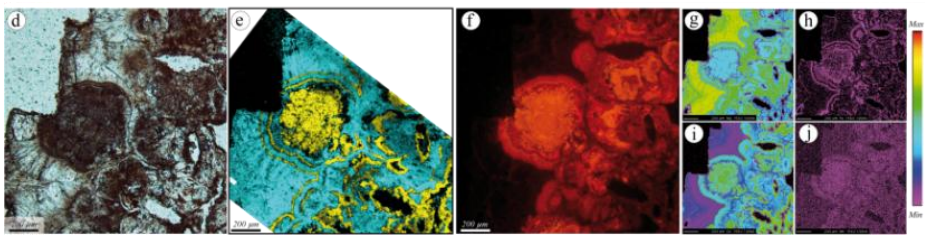

Figure B.3: Optical observations, Raman maps and analyses of the Svarlbard carbonates. d- Optical view in transmitted light of layered carbonates from Svalbard, Norway. e- Raman map of (d) with in magnesite light blue and dolomite in yellow (laser power: 5 mW, obj. x100). f- Cathodoluminescence image, this image reveals the low content of Mn and Mg in the sample and, in particular, the zoned structure of the crust. g to j- Microprobe elemental maps of Mg, Ca, Fe and Mn. Note the detail of the magnesite deposit and the relation between the Ca-Mg and Fe maps and the cathodoluminescence image: The content of Mn and CL activation are correlated. (For the four maps, low contents are in purple and high contents in red).

Figure B.3 : Observations optiques, image Raman et analyses des carbonates de Svalbard, Norvège. d-Image optique en lumière transmise. e- cartographie Raman de (d) avec en bleu ciel magnesite et en jaune dolomite (puissance laser : 5mW, obj. x100). f- Image en cathodoluminescence, cette image révèle une faible teneur en Mn et Mg de l'échantillon et des zonations. g-j Cartographies élémentaires de Mg, Ca, Fe, Mn, par microsonde éléctronique.

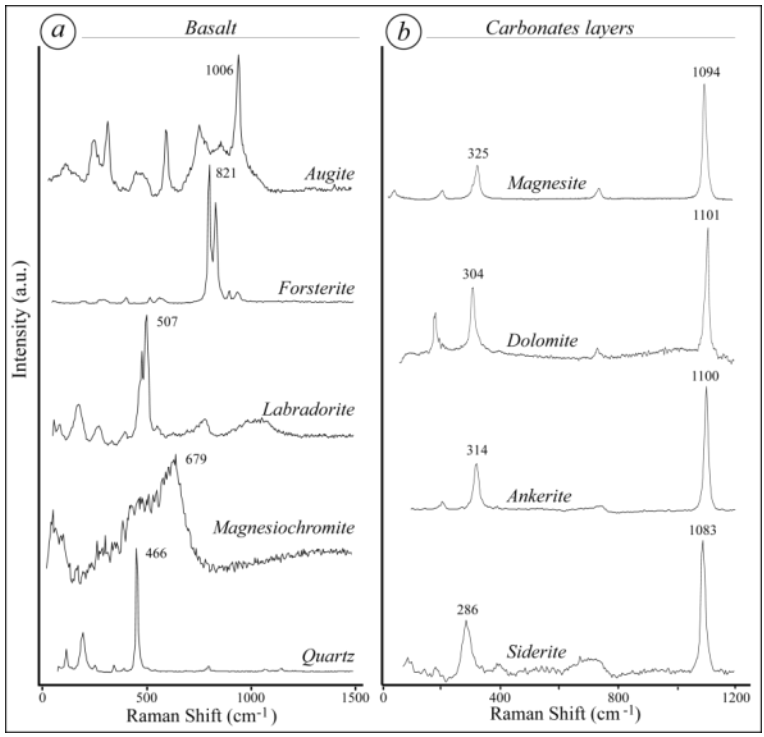

Figure B.4*:* Raman spectra from the Svalbard samples. a- Basalt and b- carbonates made on a polished thin section. (Experimental conditions: obj. x100, ~1mW).

Figure B.4: Spectre Raman des échantillons de Svalbard. a- basaltes et b- carbonates réalisées sur des sections polies. (Conditions experimentales: obj. x100, ~1mW).

B.3.6: IR spectroscopy

The IR analyses were carried out on a pellet made of 0,498 mg of powder mixed with KBr and pressed at 8 tons, in transmission mode. The dolomite spectrum associated with the magnesite and ankerite spectra is displayed in Fig. B.5b. The signal corresponds to a mixture of the 3 carbonates. The components were identified using the data base of the research branch of agriculture in Canada.

B.3.7: Mössbauer analyses

Carbonates in Mössbauer can be easily be confused with pyroxene (*Morris et al., 2010*). Since this technique is very sensitive to iron, it is particularly suited for analyzing F- containing carbonates (fig. B.5d). However, it is not possible to differentiate the pure Fe carbonate siderite from other carbonates containing some iron (e.g. ankerite). The other analyses show that these carbonates phases were partially mixed.

B.3.8: XRD analyses

The XRD analyses on the carbonate powder bring to light the presence of at least 3 carbonates (Fig. B.5f). The first one is crystalline dolomite. The two other carbonates always present peaks shifted to the right with respect to the dolomite meaning that they contain smaller ions in their crystalline lattice. Based on the previous analyses, it is possible to say that these atoms are probably magnesium, iron or manganese. These two carbonates could thus be siderite and magnesite, or a mix of poorly to moderaly crystalline carbonates.

►Figure B.5: a, b- IR spectra (black line) made on the powdered basalt and carbonates layers, respectively, measured in the 1400-400 cm^{-1} wavelength range with a 4 cm^{-1} resolution. The spectrum is compared with IR spectra for pigeonite (a, dot-dashed line) and olivine (a, dashed lined). Thick dotted line - the IR spectra of dolomite, thin dotted line - the IR spectra of magnesite and ankerite. The reference spectra were obtained from the Research Branch Agriculture, Canada. c, d- Mössbauer spectra made on the core and altered surface of the Svalbard basalt and carbonates layers, respectively. The carbonates in the core (d, in grey) is less altered than at the surface and provide better analyses than at the surface. Some microcrystals of iron oxide can be observed (npOx). e, f- X-ray diffraction spectra of the powdered basalt and carbonates layers, respectively. This analysis shows the presence of a peak for the three major minerals in the basalt with forsterite, enstatite, spinel, in particular chromite (e). The carbonate analysis shows the presence of a peak for the three carbonates in the sample, primarily dolomite with two other carbonates, possibly magnesite and/or siderite (f).

►*Figure B.5: a,b- specters IR (ligne noire) faite sur la poudre de basalte et de carbonates resperctivement et mesurée entre 1400-400cm^{-1} avec une résultion de 4 cm^{-1}. Les spectres sont comparés avec le spectre IT de la pigeonite (a, ligne tiretée) et l'olivine (a, ligne pointillée). En pointillé large, le spectre IR de la dolomite, in petit pointillée, le spectre IR de la magnesitie et l'ankerite. Les spectres de référence sont obtenus dans Research Branch Agriculture Canada. c, d- spectres Mössbauer réalisée au cœur et sur la surface altérée de l'échantillon de basalte de Svalbard et sur les couches de carbonates, respectivement. Le cœur de carbonates (d, en gris) est plus alteré que la surface et permet d'obtenir une meilleur analyse. Quelques cristaux d'oxydes de fer sont observés (npOx). e, f- Spectre de diffraction des rayons C de la poudre de basalte et des carbonates, repsectivement. Cette analyse montre la présence de trois mineraux principaux : forsterite, enstatite et spinel (chromite, e). L'analyse des carbonates montre la présence de 3 pics correspondant à des la dolomite et deux autres carbonates possiblement de la magnesite et/ou sidérite.*

Appendice B: Example of detailed samples characterization for the ISAR

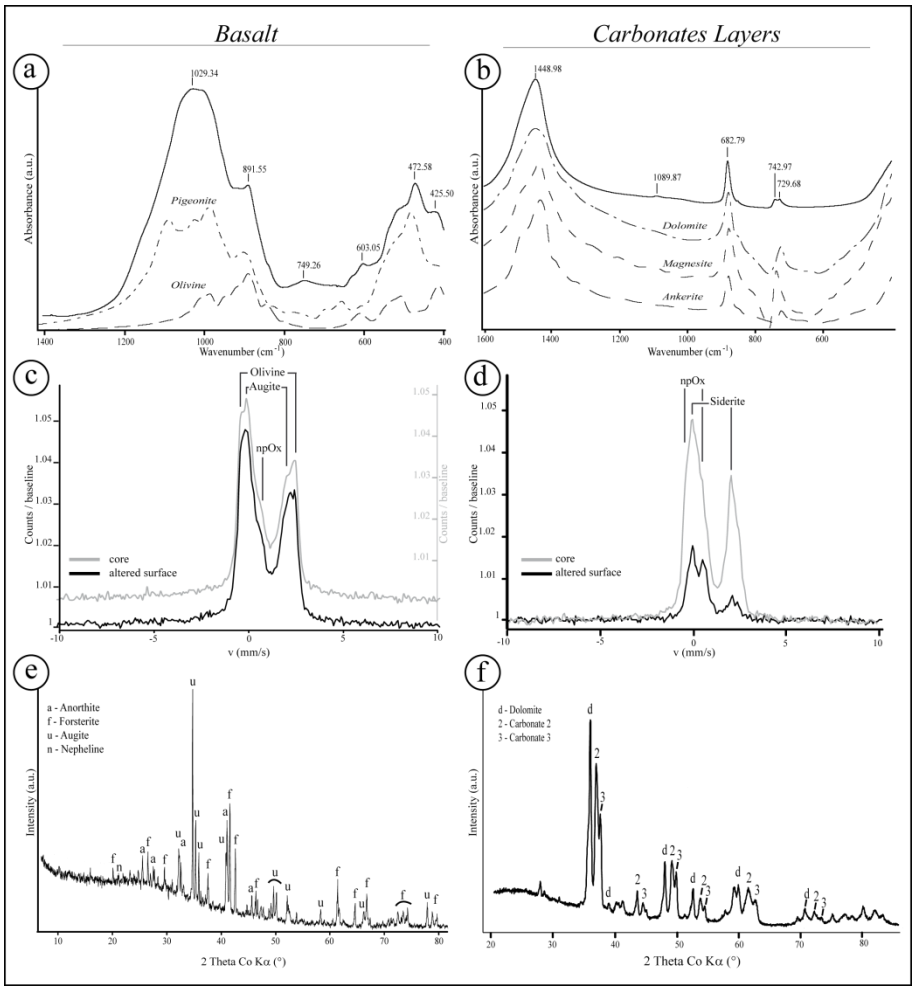

Appendice C:
Geochemical data

	09ET01	09SV15	09SV02	09TE08	07SA20	11CA02	10SA09	09SV02
SiO_2 (wt%)	48.092	45.161	44.126	60.174	55.237	42,89	44.685	43.65
Al_2O_3	11.297	13.984	13.911	19.118	13.635	6,64	3.875	3.513
Fe_2O_3	10.43	11.25	10.726	3.639	10.382	10,27	11.997	9.892
MnO	0.1752	0.1539	0.1463	0.1556	0.1767	0,17	0.1578	0.1371
MgO	12.061	10.232	9.846	0.487	3.704	23,59	24.103	37.837
CaO	12.671	8.214	10.442	1.096	7.227	7,83	4.732	3.326
Na_2O	1.817	4.574	4.636	8.201	4.507	0,07	0.333	0.353
K_2O	0.949	2.075	2.004	5.247	0.151	0,02	0.03	0.043
TiO_2	1.016	2.559	2.199	0.761	1.324	0,34	0.338	0.143
P_2O_5	0.291	0.764	0.872	0.12	0.159	0,05	< L.D.	0.051
FL	1.473	1.291	0.767	0.648	3.747	7,52	8.538	0.224
Total	100.271	100.258	99.677	99.646	100.249	99.39	98.7888	99.169
As (ppm)	1.109	1.141	1.66	5.369	< L.D.	< L.D.	< L.D.	< L.D.
Ba	333.5	759.8	916	927.6	21.73	3,325	32.43	18.1
Be	1	2.032	2.193	6.957	0.577	< L.D.	< L.D.	< L.D.
Bi	< L.D.	< L.D.	< L.D.	0.286	< L.D.	< L.D.	< L.D.	< L.D.
Cd	0.154	0.251	0.201	0.601	< L.D.	< L.D.	< L.D.	< L.D.
Ce	51.63	86.15	108.6	144.4	18.42	1,325	4.348	1.725
Co	47.27	46.38	42.73	0.911	30.69	87,08	85.62	99.72
Cr	820	368.7	343.3	12.16	21.09	2787	2288	3164
Cs	0.58	0.827	1.189	1.788	0.299	1,245	0.243	< L.D.
Cu	90.46	34.58	36.77	7.424	106.7	25,36	14.69	1422
Dy	3.445	4.805	4.879	4.411	5.502	1,173	1.266	0.542
Er	1.672	1.833	1.898	2.431	3.447	0,759	0.728	0.333
Eu	1.507	2.62	2.632	1.77	1.203	0,23	0.376	0.138
Ga	13.81	23.7	22.81	27.72	17.85	7,455	5.184	3.715
Gd	4.326	6.852	6.815	4.757	4.812	0,896	1.169	0.459
Ge	1.634	1.24	1.318	1.569	1.252	1,354	1.246	1.053
Hf	2.227	5.258	4.913	14.87	2.437	0,497	0.614	0.238
Ho	0.62	0.774	0.789	0.822	1.178	0,26	0.256	0.117
In	< L.D.	< L.D.	< L.D.	< L.D.	< L.D.	< L.D.	< L.D.	< L.D.
La	26.01	47.57	66.1	86.6	7.151	0,47	1.672	0.874
Lu	0.232	0.18	0.201	0.416	0.533	0,127	0.106	0.055
Mo	1.505	4.078	3.908	11.94	0.449	< L.D.	< L.D.	1.146
Nb	15.64	63.05	63.7	166.2	3.871	0,336	1.225	0.983
Nd	24.07	37.55	40.22	40.89	12.27	1,388	3.312	1.135
Ni	144.2	291	266.1	6.076	37.1	1051	1483	2170
Pb	4.4093	3.801	5.6397	16.1729	1.1065	< L.D.	< L.D.	< L.D.
Pr	6.102	9.673	10.97	13.56	2.594	0,251	0.689	0.232
Rb	21.52	48.95	50.28	144	2.976	3,349	0.955	1.321
Sb	0.111	0.112	0.172	0.806	< L.D.	0,136	0.186	0.265
Sm	5.071	7.877	7.743	6.358	3.617	27,94	1.017	0.345
Sn	0.945	2.143	2.037	3.667	1.044	0,635	0.581	1.072
Sr	612.8	970.6	1098	65.62	132.6	0,46	14.79	27.43
Ta	0.992	3.923	3.56	11.51	0.315	7,236	0.103	0.053
Tb	0.621	0.941	0.953	0.759	0.826	0,028	0.198	0.08
Th	4.134	5.965	8.545	23.91	0.584	0,173	0.177	0.097
Tm	0.234	0.222	0.243	0.392	0.525	< L.D.	0.108	0.053
U	1.241	1.581	2.159	6.313	0.165	0,119	0.043	0.041
V	225.4	167.7	139.1	13.74	431.6	< L.D.	103.7	68.17
W	0.458	1.044	1.508	4.811	< L.D.	137,5	< L.D.	0.313
Y	17.67	21.77	22.63	25.15	36.29	< L.D.	6.967	3.247
Yb	1.496	1.27	1.444	2.71	3.488	7,454	0.724	0.348
Zn	84.69	116.5	112.9	107.9	95.34	0,778	73.09	60.79
Zr	92.22	221.7	215.3	855.3	89.31	60,59	21.72	8.108

Notes: Analyses make by Service d'Analyse des Roches et Minéraux- Centre de Recherches Pétrographiques et Géochimiques (SARM-CRPG). Nancy. France. Abbrevation: F.L. - fire loss ignition loss; L.D.- lower limit of detection. Major element data in wt%. trace element data in ppm.

	09SV05	11CY04	99SA01	99SA05	06AU01		00AU05		00AU04
					with layers	*red layers*	*with layers*	*black layers*	
SiO_2 (wt%)	7.765	22,22	99,49	95,48	85.127	85.191	92.36	96.28	97,37
Al_2O_3	2.175	5,67	0,24	1,79	0.182	0.174	5.51	2.63	1,35
Fe_2O_3	3.054	3,18	< L.D.	0,83	12.497	12.61	1.59	0.78	< L.D.
MnO	0.0613	0,03	< L.D.	0,01	0.2761	0.2784	< L.D.	< L.D.	< L.D.
MgO	28.457	7,76	< L.D.	0,38	< L.D.	< L.D.	< L.D.	< L.D.	0,06
CaO	14.41	26,09	0,03	0,08	< L.D.	< L.D.	< L.D.	< L.D.	0,07
Na_2O	0.498	0,97	0,02	0,03	< L.D.	< L.D.	< L.D.	< L.D.	0,02
K_2O	0.225	0,43	0,07	0,35	< L.D.	< L.D.	1.59	0.78	0,33
TiO_2	0.397	0,21	0,03	0,08	0.005	0.004	0.28	0.09	0,06
P_2O_5	0.172	0,04	0,03	< L.D.	0.082	0.077	< L.D.	< L.D.	0,03
FL	42.324	32,66	0,48	0,82	0.897	0.803	< L.D.	< L.D.	0,59
Total	99.537	99.26	100.38	99.85	99.0661	99.13741	99.74	99.78	99.87
As (ppm)	5.734	< L.D.	8,596	18,69	3.02	3.865	1.29	1.647	1,129
Ba	128.3	8,129	16,61	40,66	44.82	43.87	61.04	47.75	24,22
Be	0.658	< L.D.	< L.D.	< L.D.	< L.D.	< L.D.	< L.D.	< L.D.	< L.D.
Bi	< L.D.	< L.D.	< L.D.	< L.D.	0.111	< L.D.	< L.D.	< L.D.	< L.D.
Cd	< L.D.	< L.D.	< L.D.	< L.D.	< L.D.	< L.D.	< L.D.	< L.D.	< L.D.
Ce	13.75	2,219	0,718	0,751	3.195	3.112	14.6	12.95	5,004
Co	9.85	9,257	0,83	2,731	8.842	8.577	0.34	0.55	1,026
Cr	83.37	81,05	11,53	106,8	38.84	27.05	14.25	14.79	15,54
Cs	0.626	0,144	0,088	0,214	< L.D.	< L.D.	0.971	0.56	0,13
Cu	234.2	32,6	6,209	5,813	7.205	8.618	8.03	69.36	11,67
Dy	0.787	1,047	0,039	0,094	0.407	0.414	1.46	0.97	0,185
Er	0.311	0,677	0,013	0,08	0.32	0.299	0.87	0.52	0,088
Eu	0.422	0,235	0,022	0,05	0.154	0.155	0.49	0.38	0,116
Ga	3.682	5,706	0,384	2,713	0.425	0.374	9.01	4.33	3,012
Gd	1.097	0,847	0,042	0,096	0.383	0.359	1.44	1.08	0,316
Ge	1.293	0,449	0,825	0,92	1.043	1.168	2.08	2.09	0,68
Hf	0.86	0,534	0,042	0,213	0.057	0.047	1.65	1.01	0,323
Ho	0.132	0,228	0,005	0,025	0.098	0.103	0.29	0.18	0,031
In	< L.D.	< L.D.	< L.D.	< L.D.	0.138	< L.D.	< L.D.	< L.D.	< L.D.
La	7.497	0,948	0,548	0,395	1.827	1.781	7.37	6.27	2,838
Lu	0.033	0,119	0,003	0,018	0.058	0.059	0.13	0.07	0,015
Mo	0.859	< L.D.	< L.D.	< L.D.	1.594	1.144	< L.D.	< L.D.	< L.D.
Nb	9.824	0,48	< L.D.	0,592	0.178	0.183	3.73	1.51	0,636
Nd	5.861	1,794	0,299	0,38	1.575	1.479	6.84	6.09	2,344
Ni	151.3	19,87	7,632	29,34	37.73	30.64	< L.D.	7.42	5,493
Pb	1.4079	1,004	2,6779	0,7153	80.3334	1.8322	4.08	5.6	3,1089
Pr	1.527	0,349	0,084	0,103	0.372	0.375	1.79	1.56	0,625
Rb	6.561	6,298	1,381	9,18	0.399	< L.D.	30.31	15.46	6,609
Sb	0.447	< L.D.	0,306	0,814	0.921	0.933	2.31	2.257	0,729
Sm	1.192	12,82	< L.D.	< L.D.	0.292	0.306	1.46	1.255	< L.D.
Sn	2.431	0,643	0,067	0,106	< L.D.	< L.D.	2.57	9.48	0,42
Sr	580.2	0,67	0,593	0,543	6.15	5.761	11.32	7.12	0,523
Ta	0.598	628,6	3,104	2,053	0.018	0.033	0.35	0.15	3,108
Tb	0.155	0,04	< L.D.	0,05	0.058	0.061	0.23	0.17	0,078
Th	0.908	0,153	0,005	0,015	0.046	0.026	2.19	1.37	0,041
Tm	0.04	0,156	0,107	0,172	0.051	0.049	0.14	0.07	0,456
U	0.27	0,112	0,003	0,015	0.226	0.177	0.57	0.4	0,012
V	27.99	0,534	0,125	0,168	5.643	5.256	42.89	23.69	0,141
W	2.074	63,02	2,266	40,88	0.571	0.264	2.36	1.34	11,36
Y	3.746	< L.D.	< L.D.	0,772	4.391	4.443	9.02	5.33	0,148
Yb	0.235	6,523	< L.D.	0,702	0.315	0.321	0.89	0.48	0,923
Zn	26.33	0,745	0,022	0,097	< L.D.	< L.D.	< L.D.	49.69	0,085
Zr	38.17	32,49	< L.D.	< L.D.	2.652	2.384	68.81	56.94	< L.D.

Notes: Analyses make by Service d'Analyse des Roches et Minéraux- Centre de Recherches Pétrographiques et Géochimiques (SARM-CRPG). Nancy. France. Abbrevation: F.L. - fire loss ignition loss; L.D.- lower limit of detection. Major element data in wt%. trace element data in ppm.

	11CY10	11CY11	11CY12	11CY13	11CY16	11CY17	11CY09
SiO_2 (wt%)	43,78	45,21	45,09	38,70	52,63	56,93	43,57
Al_2O_3	15,83	14,17	14,85	13,82	16,29	13,37	15,47
Fe_2O_3	6,80	8,08	10,26	19,21	9,83	13,53	8,36
MnO	0,23	0,21	0,80	0,02	0,13	0,03	0,21
MgO	9,61	8,92	8,22	2,92	8,72	10,48	8,35
CaO	5,44	3,59	5,35	0,63	1,66	0,04	2,12
Na_2O	0,45	2,32	1,19	0,06	2,10	0,05	0,89
K_2O	0,73	1,86	2,19	0,80	2,29	0,02	1,23
TiO_2	0,61	0,46	0,51	0,43	0,51	0,40	0,51
P_2O_5	< L.D.	0,13	0,03	0,05	0,04	< L.D.	< L.D.
FL	17,08	15,59	12,50	24,70	7,13	5,91	20,14
Total	100,54	100,53	100,98	101,32	101,30	100,75	100,84
As (ppm)	< L.D.	< L.D.	3,984	21,9	< L.D.	< L.D.	1,358
Ba	123,4	280,6	223,9	58,14	56,31	2,739	387,9
Be	< L.D.	< L.D.	< L.D.	< L.D.	< L.D.	< L.D.	< L.D.
Bi	< L.D.	< L.D.	< L.D.	0,164	< L.D.	< L.D.	< L.D.
Cd	0,264	< L.D.	< L.D.	0,63	< L.D.	< L.D.	0,378
Ce	1,469	4,816	2,795	0,978	2,207	0,369	1,544
Co	39,04	24,73	34,04	31,7	37,2	70,11	37,37
Cr	448,4	300	402,1	214,1	86,3	177	332,9
Cs	0,138	0,846	0,624	0,281	< L.D.	< L.D.	0,53
Cu	215,7	36,07	50,36	482,8	423,8	808,7	281,1
Dy	1,451	2,942	1,372	0,594	1,569	0,18	0,878
Er	0,949	1,83	0,84	0,377	1,015	0,179	0,614
Eu	0,291	0,663	0,332	0,155	0,355	0,012	0,188
Ga	11,01	11,01	13,4	12,46	14,19	9,83	10,46
Gd	0,967	2,587	1,068	0,509	1,217	0,129	0,607
Ge	8,325	2,376	3,124	0,958	0,702	0,524	5,149
Hf	1,031	0,8	0,889	0,712	0,87	0,661	0,89
Ho	0,31	0,641	0,29	0,126	0,344	0,048	0,192
In	0,072	< L.D.	< L.D.	0,098	< L.D.	< L.D.	< L.D.
La	0,446	2,273	1,459	0,871	1,107	0,135	0,757
Lu	0,206	0,284	0,146	0,066	0,169	0,068	0,126
Mo	< L.D.	< L.D.	< L.D.	22,09	< L.D.	< L.D.	0,686
Nb	0,583	0,502	0,529	0,401	0,465	0,382	0,475
Nd	1,541	4,863	2,198	1,684	2,232	0,401	1,302
Ni	77,48	67,46	80,55	44,33	49,37	42,72	68,12
Pb	0,7412	0,8619	0,8846	8,5542	0,903	< L.D.	0,8478
Pr	0,25	0,833	0,412	0,316	0,399	0,08	0,253
Rb	8,45	24,67	24,6	8,375	9,16	< L.D.	25,1
Sc	52,01	36,97	42,62	33,94	35,8	32,05	40,57
Sb	< L.D.	< L.D.	0,156	2,095	0,125	< L.D.	0,128
Sm	0,652	1,722	0,767	0,463	0,836	0,092	0,454
Sn	0,362	0,31	0,326	< L.D.	0,341	< L.D.	0,314
Sr	34,98	50,69	62,06	6,093	61,44	< L.D.	24,39
Ta	0,052	0,04	0,043	0,031	0,035	0,032	0,047
Tb	0,199	0,439	0,198	0,088	0,227	0,026	0,124
Th	0,178	0,148	0,149	0,104	0,141	0,112	0,146
Tm	0,169	0,273	0,132	0,059	0,158	0,036	0,105
U	0,128	0,122	0,106	0,236	0,115	0,089	0,145
V	194,2	184,6	116,5	171,4	228,9	128,9	153,4
W	< L.D.	0,114	0,416	0,691	0,13	0,132	0,119
Y	7,807	19,73	7,159	3,575	9,341	1,25	4,879
Yb	1,3	1,795	0,911	0,416	1,103	0,314	0,799
Zn	153	74,86	67,33	420,8	365,3	< L.D.	238,4
Zr	30,82	24,3	27,29	21,86	26,93	20,61	27,45

Notes: Analyses make by Service d'Analyse des Roches et Minéraux- Centre de Recherches Pétrographiques et Géochimiques (SARM-CRPG). Nancy. France. Abbrevation: F.L. - fire loss ignition loss; L.D.- lower limit of detection. Major element data in wt%. trace element data in ppm.

Nicolas BOST

L'analyse géochimique et minéralogique de matériaux analogues de Mars et la création de l'International Space Analogue Rock Store

L'objectif de la thèse est de créer une collection de roches et minéraux analogues pour calibrer et tester les futurs (et existants) instruments de vol, en accord avec la géologie de Mars afin de préparer les futures missions *in situ* (MSL-2011 et ExoMars-2018). Les échantillons sont caractérisés avec des instruments de laboratoire (microscope, Raman, IR, DRX, MEB, microsonde électronique, et ICP-MS), mais aussi avec des instruments de vol en développement (Mössbauer MIMOS II, les spectromètres ExoMars Raman et IR (MicroOmega)). L'ensemble des échantillons sont décrits sur une base de données en ligne à l'adresse : www.isar.cnrs-orleans.fr. Une partie de cette thèse est dédiée au développement d'un instrument de cathodoluminescence, qui peut être adapté au spatial.

L'étude des processus d'altération des basaltes sur Terre montrant des similarités avec les processus de surface et de subsurface présent sur Mars, permet d'aider à mieux comprendre et interpréter les objets sur Mars. Pour cela, et pour compléter la collection, des basaltes altérés dans des conditions hydrothermales et acides ont été collecté dans la mine de *Skouriotissa* à Chypre. L'évolution minéralogique des basaltes à travers les différents facies d'altération a été étudiée.

Parce que les basaltes terrestres sont plus pauvres en Fe et Mg que les basaltes martiens, deux basaltes artificiels ont été synthétisé. Ces deux échantillons sont différents en terme de refroidissement (~110°C/h et trempé). On note que le basalte refroidi lentement montre des textures spinifex similaires aux komatiites. Si ce type de basalte est présent sur Mars, et altéré en présence d'eau, ceci peut avoir d'importantes implications exobiologiques.

Mots clés: Mars, lithothèque, ISAR, analogues, basalte, sédiments volcaniques, phyllosilicate, silice hydrothermale, échantillons artificiels, processus d'altérations, exobiologie, Chypre.

Geochemical and mineralogical analysis of Mars analogue materials and the creation of the International Space Analogue Rock Store (ISAR)

In order to prepare for the next *in situ* missions to Mars (MSL-2011 and ExoMars-2018), the objective of my thesis is to create a collection of relevant analogue rocks and minerals for calibrating and testing future (and existing) space flight instruments, in accordance with the geology of Mars. They were characterized using standard laboratory instrumentation (optical microscopy, Raman, IR, XRD, SEM, electron microprobe and ICP-MS), as well as by flight instrumentation in development (Mössbauer MIMOSII, ExoMars Raman and IR (MicrOmega) spectrometers). All the samples are described in an online database in the following web site: *www.isar.cnrs-orleans.fr*. A part of this thesis is dedicated to the development of a cathodoluminescence (CL) instrument that could potentially be adapted for space flight.

Study of alteration processes of basalts on Earth that show some similarities to surface and subsurface processes occurring on Mars may help understand and interpret martian features. Therefore, to complete the collection, samples of hydrothermal and acidic weathered basalts were collected from the *Skouriotissa* mine in Cyprus. The mineralogical evolution of the basalt through different alteration facies was studied.

Because terrestrial basalts are poorer in Fe and Mg than martian basalts, I synthesized two artificial martian basalts. The two artificial basalts are different in terms of cooling rate (~110°C/h and drop-quenched, >1200°C/h). Interestingly, the more slowly-cooled sample exhibits a spinifex texture, similar to that of komatiites. If similar basalts occur on Mars, such rocks when altered by aqueous processes may have astrobiological implications.

Key-words: Mars, rockstore, ISAR, analogues, basalt, volcanic sediment, phyllosilicate, hydrothermal silica, artificial samples, weathering processes, astrobiology, Cyprus.

Centre de Biophysique Moléculaire
Rue Charles Sadron, 45071 ORLEANS Cedex2
Institut des Sciences de la Terre d'Orléans
1A rue de la Férollerie, 45071 ORLEANS Cedex2